DECEMBER 1991
ENVIRONMENTAL SCIENCE & TECHNOLOGY

ES&T

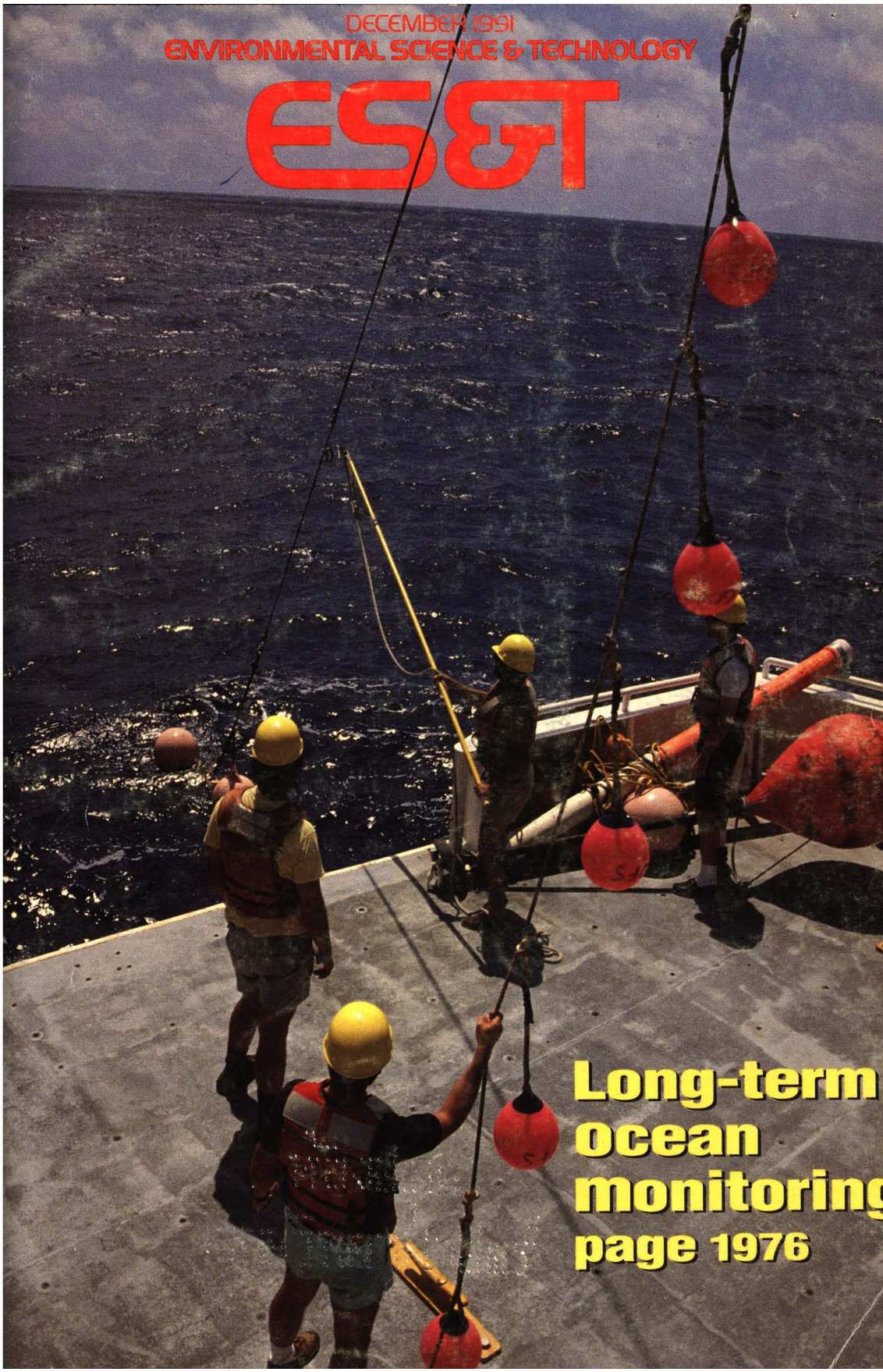

Long-term ocean monitoring

page 1976

Master Difficult Environmental Samples

If you are in the business of monitoring the land we use, the water we drink and the air we breathe, you should be in business with Varian.

Varian analytical instruments have superb sensitivity, down to parts-per-trillion levels, and can master even the most difficult samples. You'll discover new techniques that ensure easy sample handling, enhanced laboratory productivity, and reliable analytical results.

And instrumentation is only the beginning. We're committed to working with our customers, so when you buy from Varian, you'll buy more than just a single instrument or system. We deliver a whole package. A package that includes technical support and superior service. Details? Call 1-800-926-3000. In Canada, call 1-800-387-2216.

GC • GC/MS • HPLC • AA • ICP • UV-Vis-NIR • NMR • Sample Preparation

varian

CIRCLE 4 ON READER SERVICE CARD

D I F I C E™

from test tube to report . . . error free

Never Touched by Human Hands

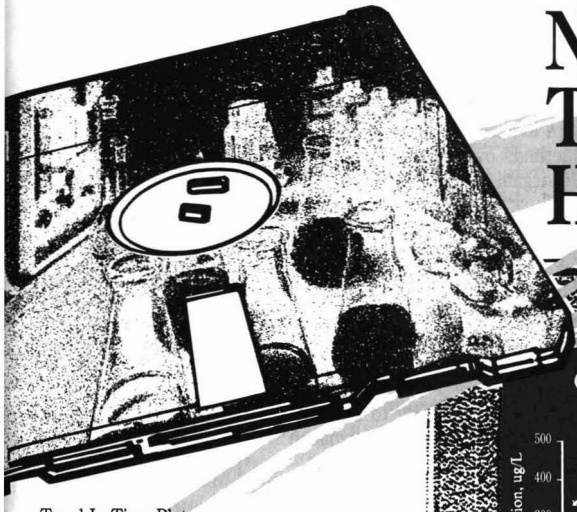

Trend In Time Plot . . .
Edifice™ Graphically Shows Trends In Your Data

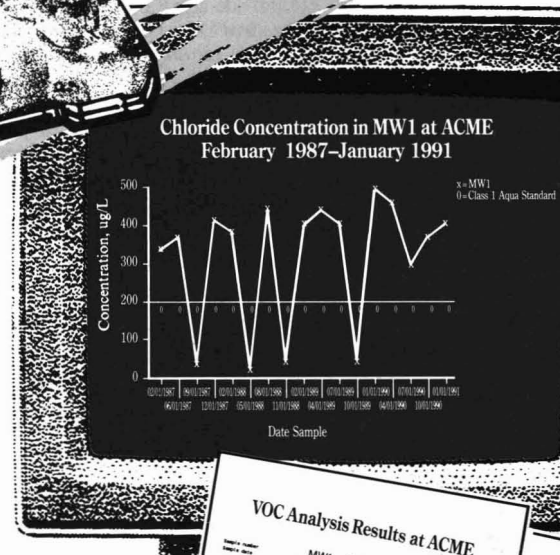

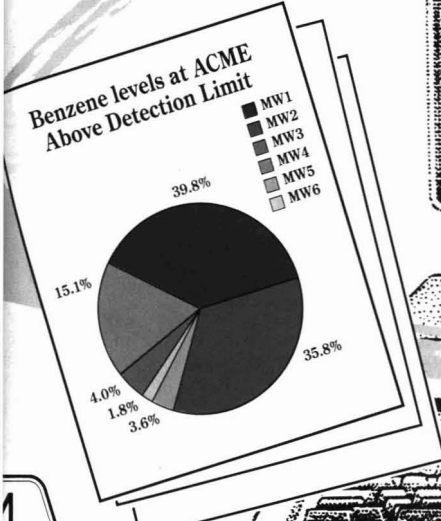

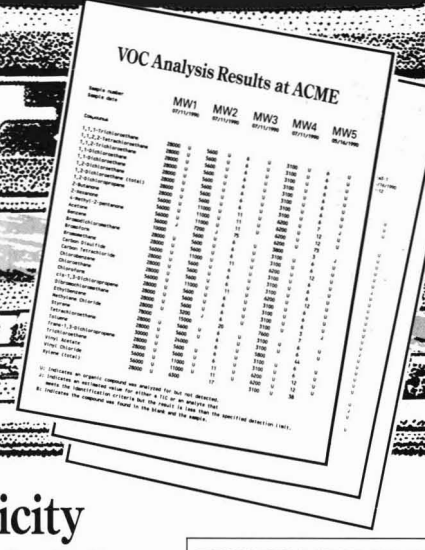

fice™ . . . the essence of simplicity

- ads Lab Data Error Free
- re Transcription Errors
- ul Graphing Capabilities . . . Views Two
- ndent Graphs Simultaneously
- ing Your Analytical Lab Data is a Breeze
- DIFICE™
- User Friendly Reporting:
- ible/User Definable Table Reports
- ible/User Definable Free Form Reports
- Unlimited Data Sorting Capability
- Basic Statistical Analysis of Data Sets (Custom Statistical Packages Can Be Added)
- Works on Whole Database or Any Subset (ex: Choose Only Benzene via Filter Mechanism)
- Easy To Use . . . Context Sensitive Help at The Touch of F1 Key
- EDIFICE™ Manuals Are Online
- No Programming Necessary
- Up to 14,000,000 records per file . . . and 24 indices
- For IBM and Compatibles

DEMO DISC AVAILABLE FOR $10.00
(refundable upon purchase of EDIFICE™)

MITTELHAUSER corporation

Mittelhauser Corporation
Software Development Group
1240 Iroquois Drive
Naperville, Illinois 60563 (708) 369-0201

lhauser Corporation . . . Environmental Consulting and Remediation Services

CIRCLE 5 ON READER SERVICE CARD

ES&T CONTENTS

Volume 25, Number 12, December 1991

FEATURE

PRÉCIS

VIEWS

REGULATORY FOCUS

ESTHAG 25(12) 1943–2120 (1991)
ISSN 0013 936X

Cover: and p. 1976, Dale Helzel, University of Hawaii
Credits: pp. 1954, 1964, Comstock Stock Photography; p. 1972, Exxon Co., U.S.A.

DEPARTMENTS

UPCOMING

Algal microfossil-based chemical models

Environmental crisis in Czechoslovakia

RESEARCH

Please send *research* manuscripts to Manuscript Reviewing, *feature* manuscripts to Managing Editor. For editorial policy, author's guide, and peer review policy, see the January 1991 issue, page 45, or write Yvonne D. Curry, Manuscript Reviewing Office, *ES&T*. A sample copyright transfer form, which may be copied, appears on the inside back cover of the January 1991 issue.

Environmental Science & Technology, *ES&T* (ISSN 0013-936X), is published monthly by the American Chemical Society at 1155 16th Street, N.W., Washington, D.C. 20036. Second-class postage paid at Washington, D.C., and at additional mailing offices. POSTMASTER: Send address changes to *Environmental Science & Technology*, Membership & Subscription Services, P.O. Box 3337, Columbus, Ohio 43210.
Canadian GST Reg. No. R127571347.

SUBSCRIPTION PRICES 1991: Members, $39 per year; nonmembers (for personal use), $73 per year; institutions, $329 per year. Foreign postage, $16 additional for Canada and Mexico, $36 additional for Europe including air service, and $45 additional for all other countries including air service. Single issues, $28 for current year; $31 for prior years. Back volumes, $367 each. For foreign rates add $4 for single issues and $16 for back volumes. Rates above do not apply to nonmember subscribers in Japan, who must enter subscription orders with Maruzen Company Ltd., 3–10 Nihon bashi 2 chome, Chuoku, Tokyo 103, Japan. Tel: (03) 272-7211.

SUBSCRIPTION SERVICE: Orders for new subscriptions, single issues, back volumes, and microform editions should be sent with payment to American Chemical Society, Dept. L-0011, Columbus, OH 43268-0011. Phone orders may be placed, using VISA, MasterCard, or American Express, by calling the ACS Sales Office at (614) 447-3776 or toll free (800) 333-9511 from anywhere in the continental U.S. (For general information, in the Washington, D.C., area call 872-4363 or toll free 800-227-5558.) Changes of address, subscription renewals, claims for missing issues, and inquiries concerning records and accounts should be directed to Manager, Membership and Subscription Services, ACS, P.O. Box 3337, Columbus, Ohio 43210. Changes of address should allow six weeks and be accompanied by old and new addresses and a recent mailing label. Claims for missing issues will not be allowed if loss was due to insufficient notice of change of address, if claim is dated more than 90 days after the issue date for North American subscribers or more than one year for foreign subscribers, or if the reason given is "missing from files."

The paper used in this publication meets the minimum requirements of American National Standard for Information Sciences—Permanence of Paper for Printed Library Materials, ANSI Z39.48-1984.

CORRESPONDENCE

*To whom correspondence should be addressed.

This issue contains no papers for which there is supplementary material in microform.

Environmental protection: Form or substance?

It was recently pointed out in *Chemical and Engineering News* (Oct. 21, 1991) that 1991 was the first year since 1948 that no U.S. scientist won a Nobel prize. In the same issue, it was noted that Dow Chemical has appointed a panel of environmental advisors which included one academic from the United States. The issue contained two other reports. In one, cooperation among Japan and the state of Tennessee, the Tennessee Valley Authority, and Oak Ridge National Laboratory on high-tech developments was analyzed in terms of the benefits and potential encumbrances to U.S. institutions. The other report critically reviewed the new efforts by the World Bank to shed its environmentally checkered past.

At first reading, these reports seem to be unrelated, but the overall impression I get is that none of them bodes well for this country or for the world in general. Some people might say that the shutout in Nobel prizes is a statistical fluke, reflecting only the emergence of western European science after World War II, not the demise of our own. What does it matter if the basic science of complex chemical systems is first elucidated in France rather than the United States, or if fundamental advancements in NMR spectroscopy are first made in Switzerland? The results of the research are readily assimilated by the world community, and all benefit. Besides, many would say, much of this research is done in parallel fashion in the United States, which by any measure continues to be a world leader in essentially every major field of scientific inquiry.

Moreover, it is increasingly clear that we are approaching a new economic order where science, business, and industry transcend national governments. What does it matter then if Japan funds projects in Tennessee, or if Hewlett-Packard decides, as it has, to fund a chair in environmental chemistry at a university in Germany rather than in its home country? Indeed, the concept of "home" is challenged continually, even for individuals, as our means of communication and travel make the distances between us and our world neighbors shorter and shorter.

Those who travel to Europe regularly, however, know that support there for fundamental science is yielding important results, and that in some fields we are simply not keeping up. Many people in this country feel that the cause is a lack of will in government and the private sector to devote major resources to new science. Why else, these cynics say, would scientists from Tennessee be so eager to "relate, exchange people, start programs" with the Japanese, if not to "receive research funds?" (*C&EN*, Oct. 21, 1991, p. 18).

Dow's group of environmental advisors symbolizes a rather recent commitment of major industries to bring environmental stewardship into the board room, rather than the back lot. Other large companies are responding similarly, as the pages of *C&EN* and this journal regularly report. The World Bank's environmental efforts signify a similar realization by the world financial community that the environment and economics are now inextricably intertwined. Both institutions' moves are healthy signs.

However, the nagging doubt remains: Are we addressing environmental protection with glitz or substance? How well do the managers of the financial and business institutions of this world appreciate the need for new research in environmental science and technology? Are they being advised at the highest level by scientists and engineers who are devoted to the research process? Given how much we do not know about how natural systems work, and how humans affect them, are we responding to the cry for environmental protection with public relations gimmicks, or programs of real merit? Will the Dow group, when finally constituted, contain more representatives from the scientific and engineering community; and will the World Bank and USAID [United States Aid for International Development] define environmental research in terms that are compatible with their own internal objectives and preferences, or in terms of the real needs in the developing world?

Will the nation with the largest GNP of all contribute its fair share to unraveling the secrets of the natural world and to solving the problems caused by humanity's impact on nature?

0013-936X/91/0925-1949$02.50/0

Recommended Reading!

ACS Books on Environmental Chemistry and Chemical Health and Safety

Pesticide Transformation Products

Fate and Significance in the Environment

Here is the first available resource on the fate, effects, and significance of pesticide transformation products, highlighting the awareness that pesticides are transformed to other chemicals that are often still biologically active. Covers pesticide degradation mechanisms and products, the fate of transformation products in the physical and biological environment, and the significance of transformation products in crop protection and environmental contamination.

L. Somasundaram and Joel R. Coats, Editors
ACS Symposium Series No. 459
320 pages (1991) Clothbound
ISBN 0-8412-1994-X
$64.95

Immunoassays for Trace Chemical Analysis

Monitoring Toxic Chemicals in Humans, Food, & the Environment

This text clearly brings together a broad range of the applications of analytical immunochemistry, including immunoassays for chemical residues in food and the environment, natural toxins, and monitoring human exposure to toxic chemicals. Also included are three appendixes that provide up-to-date compilations of references organized according to applications: environmental monitoring, mycotoxin analysis, and DNA- and protein-adduct analyses.

Martin Vanderlaan, Larry H. Stanker, Bruce E. Watkins, and Dean W. Roberts, Editors
ACS Symposium Series No. 451
362 pages (1991) Clothbound
ISBN 0-8412-1905-2
$79.95

Immunochemical Methods for Environmental Analysis

This valuable reference focuses on the use of immunoassays in environmental monitoring and quality control, including regulatory aspects. Its 18 chapters are divided into three sections covering immunoassay evaluation guidelines, academic advances in immunoassay technology, and immunoassay activities in industry. Recommended reading for agricultural, pesticide, and environmental scientists; analytical chemists; and biotechnologists.

Jeanette M. Van Emon and Ralph O. Mumma, Editors
ACS Symposium Series No. 442
239 pages (1990) Clothbound
ISBN 0-8412-1875-7
$49.95

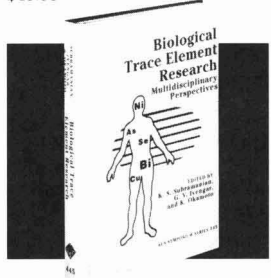

Biological Trace Element Research

Multidisciplinary Perspectives

Planning considerations, quality assurance, and analytical methods (e.g., furnace atomic absorption spectrometry, neutron activation analysis, and HPLC-fluorometry) are just some of the topics adressed here. The text is multidisciplinary in scope and examines problems of speciation in trace element research, the need for biological reference materials, and factors affecting element bioavailability.

K. S. Subramanian, G. V. Iyengar, and K. Okamoto, Editors
ACS Symposium Series No. 445
376 pages (1991) Clothbound
ISBN 0-8412-1888-9
$84.95

Developing a Chemical Hygiene Plan

This essential "how-to" book tells you what you need to know to comply with the federal regulation known as the "OSHA Laboratory Standard". Developed by the ACS Committee on Chemical Safety, the guide presents hygiene plans

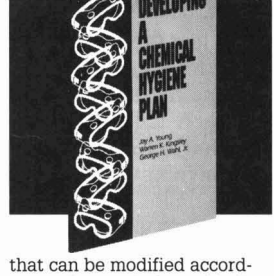

that can be modified according to the particulars of individual laboratories. Several appendices are provided, including employee information and training techniques, exposure assessment procedures, the elements of an emergency procedure plan, the OSHA Laboratory Standard, a list of contacts for states that have OSHA-approved state plans, and a list of acronyms.

Jay A. Young, Warren K. Kingsley, and George H. Wahl, Jr.
72 pages (1990) Paperbound
ISBN 0-8412-1876-5
$18.95

Emerging Technologies in Hazardous Waste Management II

In this sequel to ACS Symposium Series No. 422 the editors expand their coverage with contributions on air treatment, as well as a greater examination of computer applications and modeling. Of special interest is a presentation on the use of internal radiant energy within a gas-fired combustion chamber to maintain high combustion temperatures, a technique that appears important for the thermal destruction of many chlorinated species.

D. William Tedder and Frederick G. Pohland, Editors
ACS Symposium Series No. 468
446 pages (1991) Clothbound
ISBN 0-8412-2102-2
$89.95

The Green Flame

Surviving Government Secrecy

Written for the general reader, this lively and entertaining volume provides a first-hand account of secret defense research being performed in the years following the Korean War. Dequasie shares his memories from the start of his work on the government-sponsored boron fuels project to the final government decision to kill the project. Backed up with documentation that has only recently been declassified, this volume paints a vivid and intriguing picture of the chemical and engineering challenges involved in the work, explores the worlds of sabotage, explosions, and possible spy activity, and explains why this billion dollar effort ultimately failed.

Andrew Dequasie
250 pages (1991) Clothbound
ISBN 0-8412-1857-9
$22.95

Order from:

American Chemical Society
Distribution Office, Dept. 163
1155 Sixteenth St., N.W.
Washington, DC 20036
or CALL TOLL FREE
800-227-5558
or in Washington DC
(202) 872-4363
and use your credit card!
Or FAX your order to
(202) 872-6067

INTERNATIONAL

The Antarctic is a protected continent, according to a treaty signed Oct. 4 in Madrid. Under the treaty, oil and mineral exploration would be banned until at least 2041, when a two-thirds majority of all 26 signatories would be needed to lift the ban. The agreement provides for monitoring of the Antarctic, as well as protection of wildlife and control of waste disposal and marine pollution. The treaty almost foundered in June when the United States rejected a provision that required a unanimous vote to lift the ban on oil and mineral exploration. The change to the requirement for a two-thirds majority removed the United States' objection. To date, 26 nations have signed the Antarctic Treaty; 24 signed this revision, but Japan and South Korea will sign on after their domestic legal procedures are completed.

The Eighth Conference of Directors of Water Research Organizations was held in Juan-les-Pins, France, the first week in October. Participants from 17 countries, including Eastern European nations, focused on the directives of the European Community and their influence on the ecology of aquatic systems. Emphasis was on environmental impacts on the Mediterranean, Baltic, and North Seas and on costs for necessary corrective actions against pollution of those waters. In addition, research strategies, project management, and general trends were discussed, as was the environmental situation in the Eastern European countries. For information contact Fritz Frimmel, Engler-Bunte-Institut der Universität Karlsruhe, Postfach 6980, D-7500 Karlsruhe, Germany.

FEDERAL

The U.S. Senate Commerce Committee vehemently protested a decision by the General Agreement on Tariffs and Trade (GATT) that U.S. environmental protection laws and regulations may not be used as a barrier to trade. At issue was a ban on imports of tuna from Mexico, Vanuatu, and Venezuela because of those countries' failure to comply with the U.S. Marine Mammal Protection Act (MMPA) that requires the protection of dolphins by tuna fishermen. In January 1991, Mexico had challenged MMPA as a trade barrier under GATT. Led by Sen. Ernest Hollings (D-SC), 59 senators called on the Bush administration to block implementation of the GATT report for now and to modify GATT to balance environmental protection against economic provisions of free trade. "We cannot ignore our responsibility to conserve world resources in an effort to appease our trading partners," said Sen. Hollings.

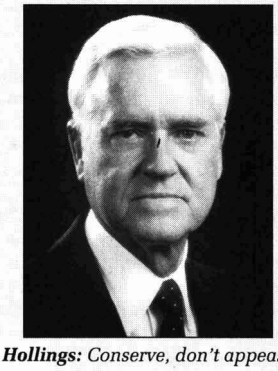

Hollings: *Conserve, don't appease*

EPA plans to remove 358 active ingredients of pesticides from registration lists, thereby effectively canceling licenses to distribute or sell 1053 pesticides that contain these active ingredients. The agency's reason is that "registrants of these active ingredients failed to support or have withdrawn support for the registration of their product(s)." To provide time to find alternative products, EPA will allow registrants to continue selling the "deregistered" products for six months after the effective date of cancellation. Existing stocks in the hands of dealers and users generally may be used until those stocks are exhausted. To report commitments to support any reregistration, or for more information, contact Virginia Dietrich, Office of Pesticide Programs (H7508C), EPA, 401 M St. S.W., Washington, DC 20460.

Rainwater runoff is a pollutant, according to Clean Water Act Amendments of 1987 that are now taking effect. This means that EPA likely will require local jurisdictions to ensure that rainwater and stormwater will be cleaned up before they are discharged to navigable waterways. The cost of building or refurbishing systems to handle rain runoff will be passed on to homeowners and condominium owners, and probably will be passed on to renters through rent increases. For example, in Montgomery County, MD, in suburban Washington, DC, homeowners may expect to be assessed $33 a year for stormwater treatment, and condominium owners may pay $17 a year. These assessments probably will increase with, or somewhat ahead of, the rate of inflation.

EPA has acted against 23 facilities that allegedly imported or exported hazardous chemicals in violation of various environmental laws. On behalf of the agency, the Department of Justice has filed 21 administrative actions that seek a total of $9.8 million in fines. Fifteen of these actions involve shipments of hazardous wastes or chemicals into Mexico and shipments of hazardous wastes or chemicals to and from Canada.

President Bush has announced the elevation of the Solar Energy Research Institute (Golden, CO) to national laboratory status and renamed the facility the National Renewable Energy Laboratory. The change of status was announced in late September.

STATES

Alaska and the U.S. Department of Justice settled their *Exxon Valdez* oil spill dispute a second time. Exxon will plead guilty to criminal violations of environmental law and pay a fine of $150 million plus $100 million in restitution. Moreover, Exxon will pay $900 million over 10 years to reimburse the state and federal governments for their share of cleanup costs. Of the criminal fine, $125 million will be forgiven be-

0013-936X/91/0925-1951$02.50/0

cause of the $2.5 billion Exxon said it paid to help clean up the Prince William Sound spill. Native corporations and villages may go forward with suits against Exxon. Critics characterize the new agreement as an insignificant increase in the fine. Also, because of the tax deductibility of the restitution and effects of inflation, the new settlement actually could cost Exxon less than the first one over the long term. A federal judge had thrown out the first settlement of $1 billion [*Environ. Sci. Technol.* 1991, *25*(5), 813] as inadequate.

Georgia's No-Tillage Farm Assistance Program has been awarded a $100,000 Ford Foundation Innovations Grant. The program, locally known as "Rent-A-Drill," provides small-scale farmers with specialized equipment, including a drill that in one trip cuts a shallow incision in the field, deposits seeds, fertilizes, and covers the row. This approach reduces the use of commercial fertilizers, saves fuel, and diminishes soil erosion. The Foundation grant will be used for education and outreach efforts to promote no-tillage farming, especially among minority and low-income farmers. For more information contact Paul Burks, Governor's Office of Energy Resources, 254 Washington St., Suite 401, Atlanta, GA 30334.

New York has released its 1990 Toxic Release Inventory report. State Environmental Conservation Commissioner Thomas Jorling notes "substantial progress" in the state's efforts to reduce toxic discharges. He said that releases in 1990 totaled 110.1 million lb, 16% less than releases reported for 1989 and 42% less than releases in 1988. Volumes of fugitive emissions in 1990 were 19% lower than those of 1989 and 38% lower than those of 1988. Benzene emissions of 1990 were down by 65% as compared with those of 1989. Moreover, facilities in New York "have already nearly achieved EPA's nationwide goal of cutting in half by 1995 the amounts of 17 groups of toxic chemicals released or discharged," according to Jorling.

SCIENCE

The deep ozone hole over the Antarctic is back for the third year in a row. It is the first time that a "deep" hole has been observed for three years in a row, according to Tom Clarkson, a scientist with the New Zealand Meteorological Service. The hole allowed a loss of 50–60% of overall stratospheric ozone over the Antarctic, with essentially total depletion between 5.7 and 12 mi altitude. Stratospheric ozone over the Arctic also will be under study by scientists from the National Center for Atmospheric Research (Boulder, CO), who will monitor this ozone through the Arctic winter and spring. Chlorofluorocarbons and certain other nonnatural air contaminants are suspected of playing a major role in the depletion of the Arctic and Antarctic ozone layers. Depletion over the Antarctic is exacerbated because of extreme cold and resultant airflow patterns during the Southern Hemisphere's spring.

If greenhouse gas emissions continue at their current rate, their concentrations in 2025 will be double those of 1985, according to data from the new ECHAM atmospheric model developed at the University of Hamburg (Germany). ECHAM subdivides the ocean and atmosphere into 500 × 500-km sections. In addition, ECHAM divides the ocean and atmosphere vertically into 19 layers and allocates four to six of those layers to the stratosphere. Data have been fed into a supercomputer to calculate a 100-year scenario. One interesting indication is that with a sustained rise in carbon dioxide concentration at current rates, sea levels would rise an average of only 16 cm by 2085. Projected temperature increases also are more modest than those forecast by previous models; nevertheless, the continents would warm much faster than the oceans, and some polar oceanic areas actually may cool. For more detail, contact the Max Planck Institut für Meteorologie, Bundestraße 55, W-2000 Hamburg 13, Germany.

TECHNOLOGY

Can dredged material in containment areas be used for aquaculture? To answer this question, the U.S. Army Corps of Engineers (Vicksburg, MS) has set up a demonstration aquaculture site next to the Brownsville (TX) Ship Channel. Its main components will be a 4-acre nursery pond, mainly for hatching shrimp, and two grow-out ponds totaling about 220 acres. A total of 30,000 gal/min of water, with predators filtered out, will be supplied. If the demonstration succeeds, it could ease the Corps' problem of finding new sites for dredged material containment. Currently, sites are difficult to acquire because of high real estate costs and objections by owners of surrounding properties. Potential profits from shrimp farming, for example, could mitigate these difficulties.

Electromigration may be useful as an in situ method for removing sulfate and other contaminants from groundwater, according to Donald Runnells of the University of Colorado (Boulder, CO). Runnells tells *ES&T* that results of his studies indicate that SO_4^{2-}, Cl^-, and other soluble anions tend to concentrate around the anode. If that result is verifiable, sulfate and other species that are difficult to remove by conventional methods may be removable. The same may hold true for cations, such as metals, if they comprise a significant proportion of the dissolved ionic species in the groundwater. Potential problems include corrosion of the anode, determining optimum electrode numbers and spacing, and contaminant removal efficiency. Runnells and his group are planning a test of anion removal from groundwater under a contract from the Electric Power Research Institute.

Freeze-crystallization, the same process that produces freeze-dried coffee, is being studied as a wastewater treatment method. Freeze Technologies Corporation (Raleigh, NC), in conjunction with Westinghouse Hanford Company (Richland, WA), is developing the technique for cleaning up water contaminated with organic compounds, salts, and heavy metals. A volatile liquid refrigerant is injected into wastewater, generating ice crystals of relatively clean water. The ice is then removed and washed. A separate, concentrated fraction containing the waste materials is left.

A novel scheme for generating electricity with compressed air produced by ocean wave action is being patented by Eberle Energy Enterprises, Inc. (Dallas, TX). The

system, named MOTO (Motion of the Ocean), might also be engineered to produce hydrogen from water or potable water. MOTO consists of a network of 30-foot-diameter toroids riding up and down on eight-foot-diameter pilasters (see illustration). Each toroid can store up to 4500 cubic feet of compressed gas at 500 psi. According to the company, a system of three toroids could provide enough compressed air for turbines to generate 3 MW of electricity.

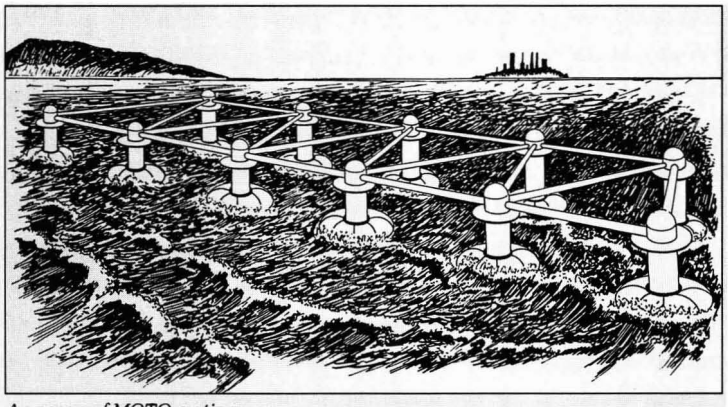

An ocean of MOTO motion

BUSINESS

Dow Chemical Company will be the first U.S. firm to set up a board of outside advisers with environmental professional backgrounds. Members of this board will have access to senior executives and to confidential data. Among the members are a former EPA administrator, two academics, one environmental journalist, the head of a research organization, and a former deputy director from the French Ministry of the Environment. Ultimately, there will be 10–14 members. The board normally will meet three or four times a year and set its own agenda, according to David Buzzelli, Dow's vice president for environment, health, and safety.

The Newspaper Enterprise Association (NEA) has engaged Jay Hair, president of the National Wildlife Federation, to write a weekly syndicated column on environmental issues for NEA's papers. The column made its debut Oct. 7 and is distributed to more than 600 newspapers nationwide, including the *Rocky Mountain News* (Denver, CO) and the *Memphis Commercial-Appeal* (Memphis, TN). "I plan to give readers fresh information that will help them understand current environmental events, and help them feel they have enough knowledge to be able to make a difference in protecting the Earth," Hair says. He believes the column is needed because "In today's world, the average citizen is bombarded by a deluge of complicated and often confusing environmental news." Hair holds a doctorate in zoology from the University of Alberta, Canada, and he helped develop the national fish and wildlife policy for the Department of the Interior.

The Alabama Electric Cooperative dedicated the nation's first compressed air energy storage (CAES) power plant Sept. 27. The $65 million plant stores compressed air in a cavern during periods when electricity is least expensive and use is low. During periods of peak demand, the compressed air is heated and expanded in a combustion turbine to generate electricity. One full charge from the 110-MW, 26-hour CAES plant can supply the power demand of 11,000 homes. The Electric Power Research Institute and the National Rural Electric Cooperative Association provided a total of $8,660,000 in funding, plus technical assistance. How well might the facility work? Perhaps a forecast can be made based on the operating experience of the world's first CAES facility (290 MW) in Huntorf, Germany, which has operated since 1978. The Huntorf plant has a 99% starting reliability and 90% availability.

Procter & Gamble (Cincinnati, OH) has awarded $5000 grants to 20 local Keep America Beautiful (KAB, Boston) affiliates in 10 states. This prize money will enable these KAB affiliates to expand environmental education programs in their own communities. The prizes were awarded to winners of the "Let's Not Waste the 90s" program, Procter & Gamble's first national environmental education contest that it sponsored in partnership with KAB.

Four government scientists will earn royalties if their patented method for scrubbing NO_x from coal combustion is commercialized. An exclusive licensing agreement between the Department of Energy and NOXSO Corp. (Pittsburgh, PA) guarantees that researchers from the Pittsburgh Energy Technology Center will divide 15% of future royalties. Under the 1986 Federal Technology Transfer Act, federal researchers can receive such payments. The patented method, which improves the efficiency of an advanced scrubbing system invented by NOXSO, involves destruction of NO_x captured on beads coated with sodium carbonate. Heating to regenerate the beads removes trapped NO_x which is then fed back into the boiler and destroyed. The DOE scientists discovered that by adding methane the efficiency of NO_x reduction jumped from 60% to 90%. DOE will fund scale-up tests of the new system at a Babcock & Wilcox small boiler simulator in Alliance, OH.

To lower the cost of wind-generated electricity, the National Renewable Energy Laboratory (formerly the Solar Energy Research Institute), the Department of Energy, and eight U.S. wind power companies are negotiating a joint program to improve the operation of wind power facilities. Half of the $5 million cost for this program will be funded by the electric companies. Monies will support projects such as a new power processing system, an improved hybrid wind–diesel power system, and new blades for advanced airfoils. DOE's goal is to reduce the cost of wind-generated electricity from the current 8 cents per kilowatt-hour to 5 cents per kilowatt-hour by the mid-1990s.

HEALTH EFFECTS of tropospheric OZONE

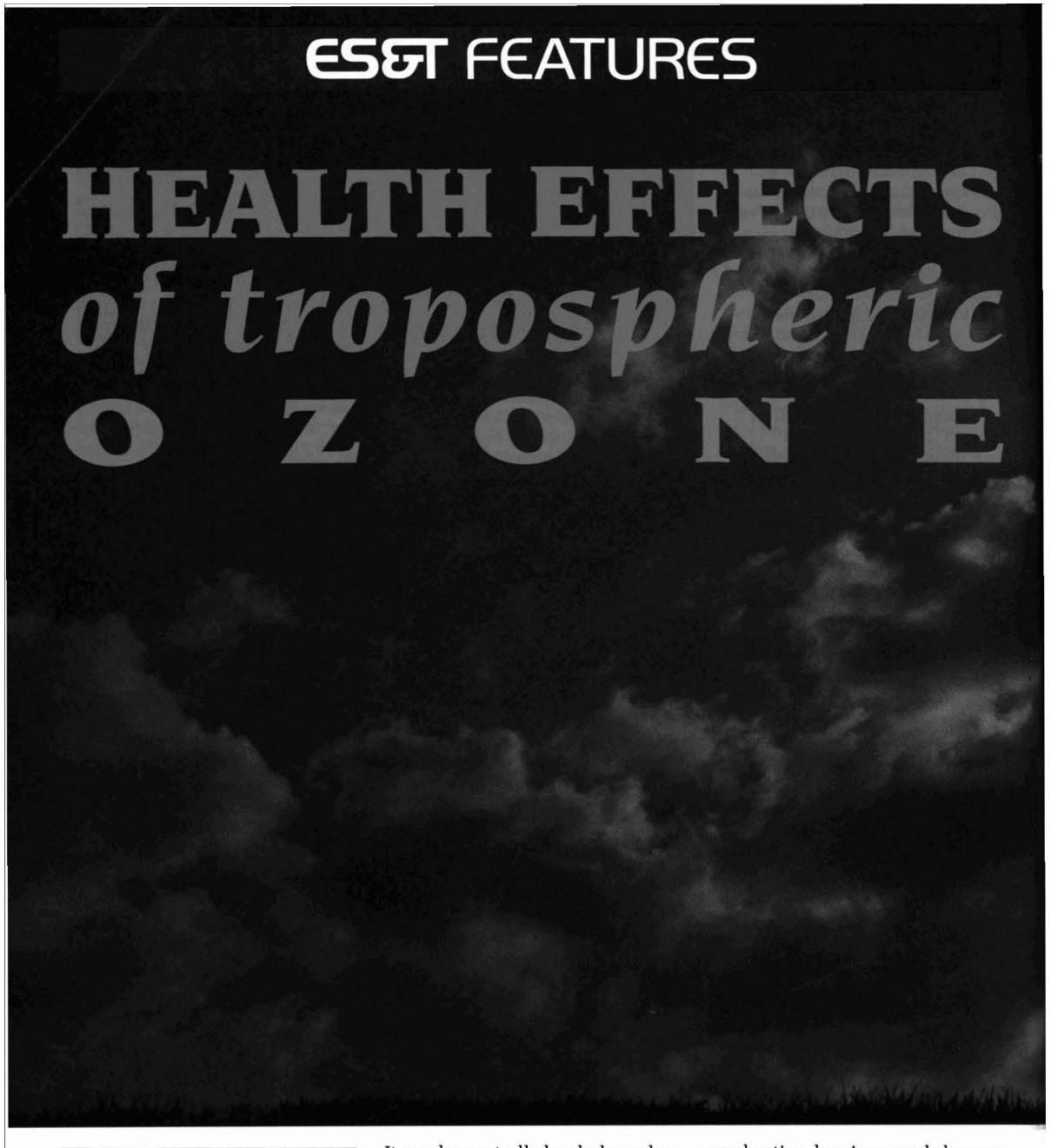

Morton Lippmann
Institute of Environmental Medicine
New York University Medical Center
New York, NY 10016

Ozone (O_3) in the troposphere is almost entirely a secondary air pollutant, formed through a complex photochemical reaction sequence that requires reactive hydrocarbons, nitrogen dioxide (NO_2), and sunlight. It can be controlled only by reducing ambient air concentrations of hydrocarbons, NO_2, or both. Nitric oxide (NO) and NO_2 are primary pollutants, known collectively as NO_x. In the atmosphere, NO is gradually converted to NO_2. Motor vehicles, one of the major sources of hydrocarbons and NO_x, have been the primary target of control efforts, and major reductions in hydrocarbon emissions per vehicle (> 90%) have been achieved over the past two decades. NO_x from stationary source combustion has increased, however, and there also have been large increases in vehicle miles driven. The net reduction in exposure, therefore, has been modest, at best. For example, in 1986–1988, exceedances of the current National Ambient Air Quality Standards (NAAQS) were recorded in 101 communities with a combined population of 112 million persons.

O_3 was recognized as a powerful lung irritant soon after its initial synthesis in 1851 (*1*). It was first

0013-936X/91/0925-1954$02.50/0

placed on the American Conference of Governmental Industrial Hygienists (ACGIH) list of threshold limit values (TLVs) for occupational exposure in 1946, with an eight-hour time weighted average concentration limit of 1 ppm. In 1954, the TLV was reduced to 0.1 ppm time weighted average. The current ACGIH TLV of 0.1 ppm, as a ceiling value, was adopted in 1989 (*2*).

Health effects among the general community were first reported in 1967 among high school athletes in California, in terms of lowered performance on high-exposure days (*3*). In 1971, the initial NAAQS was set at 0.08 ppm of *total oxidant*. The NAAQS was revised in 1979 to 0.12 ppm of O_3, on the basis of clinical studies by DeLucia and Adams (*4*) that showed that asthmatic adults who were exercising and were exposed for 1 h to 0.15 ppm O_3 in a test chamber had increased cough, dyspnea, and wheezing, and experienced small but nonsignificant reductions in pulmonary function (*5*). A small margin of safety was applied to protect against adverse effects not yet uncovered by research and against effects whose medical significance remains controversial.

On May 1, 1989, the Clean Air Scientific Advisory Committee sent a closure letter to the EPA administrator on its reviews of the 1986 O_3 Criteria Document, the 1988 Criteria Document Supplement, and the Agency Staff Paper of 1988, reporting a split recommendation concerning a scientifically supportable

upper bound to the range for a revised 1-h NAAQS. Half of the members advocated accepting the 0.12 standard, whereas the other half recommended a reduced upper bound (*6*). The EPA administrator has not yet proposed a revised O_3 NAAQS.

The acute response effects in the population at large are reductions in lung function and increases in respiratory symptoms, airway reactivity, permeability, and inflammation. For asthmatics, additional effects include increased rates of medication usage and restricted activities. With respect to chronic exposures, it is suggested that repetitive elicitation of acute responses will lead to chronic damage to the human lung of the kinds seen after chronic exposure studies in rats and monkeys.

Exposures and dosimetry

The only significant exposure route for O_3 is inhalation, and exposure can be defined as the concentration at the nose and mouth. There have been few measurements of personal exposure to O_3, and the common assumption that the concentrations we breathe are the same as those measured at central monitoring sites has limited validity. Local concentrations outdoors are reduced in the vicinity of heavy vehicular traffic as a result of O_3 scavenging by NO. On the other hand, areas with less traffic, downwind of a monitor, may have higher O_3 concentrations because of active photochemistry in an air mass enriched with precursor chemicals from motor vehicle exhaust. Thus, outdoor O_3 concentrations may be either higher or lower than those measured at central monitoring sites.

Indoor concentrations of O_3 almost always are substantially lower than those outdoors because of efficient scavenging by indoor surfaces and the lack of indoor sources. The only major indoor sources are copying machines and electrostatic air cleaners. Because most individuals spend more than 80% of their time indoors, their total O_3 exposures are much lower than those estimated from outdoor concentrations. According to a model developed by Hayes (*7*), O_3 peak-concentration indoor-outdoor ratios range as follows:

- home—0.65 (windows open), 0.36 (air conditioned), 0.23 (typical construction, windows closed);
- office—0.82 [heating, ventilation, and air conditioning (HVAC) systems supplying 100% outdoor air], 0.60 (typical HVAC), and 0.32 (energy-efficient HVAC); and
- vehicle—0.41 (85 mph), 0.33 (55 mph), and 0.21 (10 mph).

O_3 exposures are only one determinant of O_3 dose. Dose also is determined by the volumes of air inhaled and the pattern of uptake of O_3 molecules along the respiratory tract. When persons work or exercise outdoors and increase their rate of ventilation, the contribution of outdoor exposure to total dose of O_3 becomes a greater determinant of total daily O_3 dose. The dose to target tissues in the respiratory acini (the region from the terminal bronchioles through the alveolar ducts) increases more with exercise than does total respiratory tract dose, because O_3 penetration increases with tidal volume and flow rate. Gerrity et al. (*8*) reported that the mean extrathoracic removal efficiency for all measurements was 39.6 ± 0.7%, and the mean intrathoracic removal efficiency was 91.0 ± 0.5% in 18 healthy, nonsmoking, young male volunteers. The effects of concentration, breathing frequency, and mode of breathing on removal efficiency were relatively small.

"The acute response effects [of ozone] in the population at large are reductions in lung function and increases in respiratory symptoms . . . and inflammation."

Tissues in the respiratory acini of humans, rabbits, guinea pigs, and rats receive the highest local dose from inhaled O_3, according to models developed by Miller et al. (*9–11*); the dose in humans is about twice that in rats for the same exposure (*12*). Children receive somewhat greater doses than do adult humans (*13*). This comparative dosimetry is consistent with the greater effects of O_3 on lung function seen in humans than in rats (*14*).

Human clinical studies

The major focus has been on the extensive body of data on the health effects of a single day's maximum hourly exposure to ambient O_3. The 1971 and 1979 NAAQS for photochemical oxidants were based on the maximum 1-h concentrations as the relevant index of exposure, and this, in turn, has focused most of the clinical research on exposure protocols involving either 1 or 2 h of exposure. Recent research has shown, however, that effects can be produced with exposures as short as 5 min (*15*), and that various effects become progressively larger as exposures at a given concentration are extended to 6.6 h (*16–18*).

There are more data on respiratory function responses than on any other coincident responses to short-term O_3 inhalation. The major debate about very small, but statistically significant, decrements in function from such studies is how to interpret their health significance (*19*).

The inhalation of O_3 causes concentration-dependent mean decrements in exhaled volumes and flow rates during forced expiratory maneuvers, and these decrements increase with depth of breathing (*20*). There is a wide range of reproducible responsiveness among healthy subjects (*21*), and functional responsiveness to O_3 is no greater, and usually lower, among cigarette smokers (*22, 23*), older adults (*24, 25*), asthmatics (*26, 27*), and patients with chronic obstructive pulmonary disease (*28, 29*). The only exception is that patients with allergic rhinitis had greater changes in airway resistance (*30*).

The effects of O_3 on respiratory function accumulate over time. Folinsbee et al. (*16*) exposed 10 adult male volunteers to 6.6 h of O_3 exposure at 120 parts per billion (ppb).

Moderate exercise was performed for 50 min/h for 3 h in the morning, and again in the afternoon. The functional decrements become progressively greater after each hour of exposure, reaching average values of about 400 mL for forced vital capacity (FVC) and approximately 540 mL for forced expiratory volume in one second (FEV_1) by the end of the exposure. Follow-up studies by Horstman et al. (*17*) done on 21 adult males with 6.6-h exposures at 80, 100, and 120 ppb produced similar responses at 120 ppb—that is, a mean FEV_1 decline of 12.3%—whereas those men exposed at 80 and 100 ppb showed lesser changes which also became progressively greater after each hour of exposure. McDonnell et al. conducted a further follow-up study using the same exposure protocol by exposing 38 additional healthy young men (*18*) to 80 ppb. As shown in Figure 1, there was a mean FEV_1 decline of 8.4% at the end of the sixth hour of exposure, which was similar to that seen by Horstman et al. (*17*) for the same exposures.

The time scale for the biological integration of O_3 exposure also can be deduced from the rate at which the effects dissipate. Folinsbee and Hazucha (*31*) studied 18 young adult females exposed to 350 ppb O_3 for 70 min, including two 30-min periods of treadmill exercise at 40 L/min. Their mean decrement in FEV_1 at the end of the exposure was 21%; at 18 h thereafter, it was 4%, and at 42 hours it was 2%.

In summary, it is now clear that the respiratory function effects of ozone can accumulate for many hours, and that an appropriate averaging time for transient functional decrements caused by O_3 is ≥ 6 h. Thus, there is less scientific basis for the current health-based exposure limit with an averaging time of 1 h than previously believed. As shown in Figure 2, O_3 exposures in ambient air now can have broad peaks with 8-h averages of about 90% of the peak 1-h averages (*32*); the functional decrements among active people out of doors exposed during the summer to ambient concentrations are likely to be much greater than those predicted on the basis of the responses in the chamber studies following 1- to 2-h exposures.

Mean respiratory symptom scores have been closely associated with group mean pulmonary function changes in adults acutely exposed in controlled exposures to O_3. Hayes et al. (*33*), however, found only a weak to moderate correlation between FEV_1 changes and symptom severity in an analysis conducted using data from individual subjects.

Exposure to O_3 also can alter the responsiveness of the airways to other bronchoconstrictive challenges, as measured by changes in respiratory mechanics. For example, Folinsbee et al. (*16*) reported that airway reactivity to the bronchoconstrictive drug methacholine for the whole group of subjects was approximately doubled following 6.6-h exposures to 120 ppb O_3. On an individual basis, however, they found no apparent relationship between the O_3-associated changes in methacholine reactivity and those

FIGURE 1
Means[a] for the differences between clean air and 80-ppb ozone exposures[b]

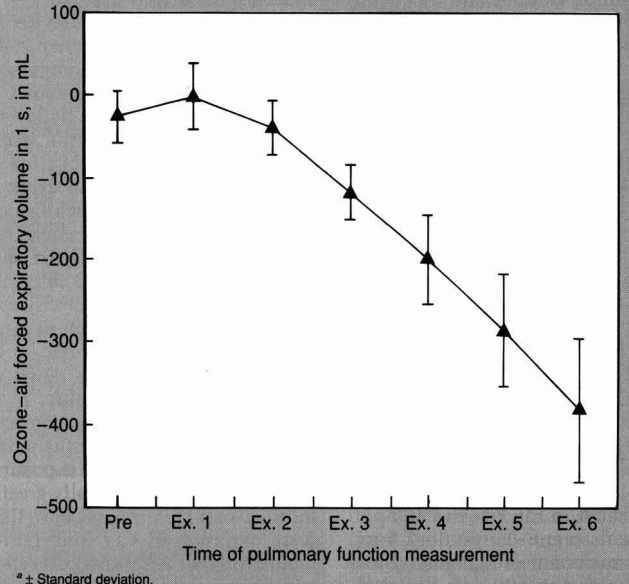

[a] ± Standard deviation.
[b] At pre-exposure and at the end of each hour of exposure with moderate exercise for 38 healthy young men.
Source: Reference 18. ©1991; used by permission *Arch. Environ. Health.*

FIGURE 2
Profile of daily ozone concentrations[a]

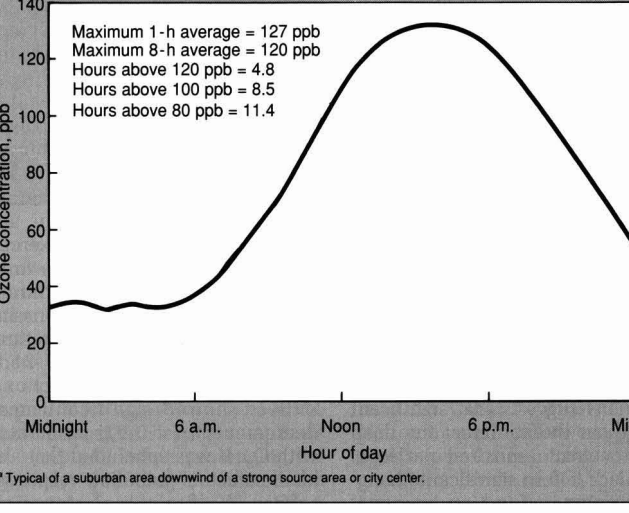

[a] Typical of a suburban area downwind of a strong source area or city center.

in FVC or FEV_1. The follow-up tests by Horstman et al. (*17*), involving 6.6-h exposures to 80, 100, and 120 ppb, indicated 56%, 89%, and 121% mean increases in methacholine responsiveness, respectively.

Reports of Koren et al. (*34*) and Devlin et al. (*35*) also described inflammatory and biochemical changes in the airways following O_3 exposure. In the initial studies, subjects were exposed to 400 ppb for 2 h while performing intermittent exercise at a ventilation rate of 70 L/min to examine cellular and biochemical responses in the airways. Broncho-alveolar lavage (BAL) was performed 18 h after the O_3 exposure. (Lavage is instillation of sterile saline solution and subsequent recovery of most of the saline, cells, and secretions contained therein.) An 8.2-fold increase in polymorphonuclear leukocytes (PMNs or neutrophils) was observed after exposure to O_3. Devlin et al. (*35*) reported that a significant inflammatory response, as indicated by increased levels of PMNs, also was observed in BAL fluid from subjects exposed to either 80 or 100 ppb O_3 for 6.6 h. The 6.6-h exposure to 100 ppb O_3 produced a 3.8-fold increase in PMNs at 18 h after exposure, whereas the 6.6 h at 80 ppb produced a 2.1-fold increase. The amounts of O_3 inhaled in the 80- and 100-ppb protocols were ~2.0 and ~2.5 μg, and the amount of O_3 inhaled was ~3.6 μg in the 400-ppb protocol. Thus, the effect of concentration apparently was somewhat greater than that of exposure duration. The significant increase in PMNs at a concentration as low as 80 ppb suggests that lung inflammation from inhaled O_3 has no threshold down to ambient background O_3 levels.

Foster et al. (*36*) studied the effect of 2-h exposures to 200 or 400 ppb O_3 with intermittent light exercise on the rates of tracheobronchial mucociliary particle clearance in healthy adult males. The 400-ppb O_3 exposure produced a marked acceleration in particle clearance from central and peripheral airways, as well as a 12% drop in FVC. It is of interest that the 200-ppb O_3 exposure produced a significant acceleration of particle clearance in peripheral airways, but failed to produce a significant reduction in FVC. This suggests that significant changes in the ability of the deep lung to clear deposited particles take place before significant changes in respiratory function.

Table 1 summarizes the nature of the various human responses to single exposures to O_3. The weight of the evidence from these results, showing functional and biochemical responses, which accumulate over multiple hours and persist for many hours or days after exposures at levels commonly encountered in ambient air, is clear and compelling.

Human epidemiology

Acute effects. Spektor et al. (*37*) found that children at summer camps with active outdoor recreation programs had greater decrements in lung function than children exposed to O_3 at comparable concentrations in chambers for 1 or 2 h. Furthermore, their activity levels, although not measured, were known to be considerably lower than those of the children exposed in the chamber studies while performing very vigorous exercise. Because it is well established that functional responses to O_3 increase with levels of physical activity and ventilation (*20*), the greater responses in the camp children had to be caused by other factors, such as greater cumulative exposure, or to the potentiation of the response to O_3 by other pollutants in the ambient air. Cumulative daily exposures to O_3 were, in fact, generally greater for the camp children, because they were exposed all day long rather than for a 1- or 2-h period preceded and followed by exposure to clean air.

A follow-up study (*38*) addressed the issue of the potentiation of the characteristic functional response to inhaled O_3 by other environmental cofactors. It involved healthy adult nonsmokers engaged in a daily program of outdoor exercise with exposures to an ambient mixture containing low concentrations of acidic aerosols and NO_2, as well as O_3. Each subject did the same exercise each day, but exercise intensity and duration varied widely between subjects, with an average breathing volume of 79 L/min, and with the duration of daily exercise averaging 29 min. Respiratory function measurements were performed immediately before and after each exercise period. O_3 concentrations during exercise ranged from 21 to 124 ppb. All measured functional indices showed significant mean decrements ($p < 0.01$) associated with O_3. It was concluded that ambient cofactors potentiate responses to O_3. The functional responses seen in these studies are summarized in Table 2 in terms of the percentage changes at an extrapolated concentration of 120 ppb for the mean of the groups, and for the individuals at the 90th percentiles of the groups.

Kinney et al. (*39*) studied school children in Kingston and Harriman, TN, whose lung function was measured in school on as many as six occasions during a 2-month period in the late winter and early spring. Child-specific regressions of function versus maximum 1-h O_3 exposure during the previous day indicated significant associations between O_3 and function, with coefficients similar to those seen in the summer camp studies by Lippmann et al. (*40*) and Spektor et al. (*37*). Children in school may be expected to have relatively low activity levels; therefore, the relatively high response coefficients may be attributed to potentiation by other pollutants, or to a low level of seasonal adaptation.

Kingston-Harriman is notable for its relatively high levels of aerosol acidity. As shown by Spengler et al. (*41*), Kingston-Harriman has higher annual average and higher peak acid aerosol concentrations than other cities studied, such as Steubenville, OH; St. Louis, MO; and Portage, WI. Alternatively, the relatively high response coefficients could have been ascribed to the fact that the measurements were made in the late winter and early spring. Linn et al. (*42*) have shown evidence for a seasonal adaptation, and children studied during the summer may not be as responsive as children examined earlier in the year.

Several epidemiology studies have provided evidence of qualitative associations between ambient oxidant levels > 100 ppb and symptoms in children and young adults, such as throat irritation, chest discomfort, cough, and headache (*43, 44*). Thus, symptoms reported for individuals exposed to O_3 in purified air are similar to those found for exposures in ambient air; an exception is eye irritation, a symptom commonly associated with exposure to photochemical oxidants, which has not been reported for controlled exposures to O_3 alone. Other oxidants, such as aldehydes and peroxyacetyl nitrate, are primarily responsible for eye irritation, and generally are found in atmospheres containing higher ambient O_3 levels (*45, 46*).

TABLE 1
Human responses to single O_3 exposures

Response	Subjects	Exposure conditions	Reference
5–10% mean decrement in forced expiratory volume in 1 s	Healthy young men	180 ppb, intermittent heavy exercise, 2 h, O_3 in purified air	68
		80 ppb, moderate exercise, 6.6 h, O_3 in purified air	17
		100 ppb, very heavy exercise, 0.5 h, O_3 in ambient air	38
	Healthy children	100 ppb, normal summer camp program, O_3 in ambient air	37
Increased cough	Healthy young men	120 ppb, intermittent heavy exercise, 2 h, O_3 in purified air	68
	Healthy young men	80 ppb, moderate exercise, 6.6 h, O_3 in purified air	17
	Healthy young men and women	120–130 ppb, heavy exercise, 16–28 min, O_3 in purified air	69
Reduced athletic performance	Healthy young men	180 ppb, exercise, $\dot{V}_E$[a] of 54 L/min for 30 min; 120 L/min for 30 min; O_3 in purified air	70
	Healthy young men and women	120–130 ppb, exercise, $\dot{V}_E$ of 30–120 L/min, 16–28 min, O_3 in purified air	69
Increased airway reactivity	Healthy young men	80 ppb, moderate exercise, 6.6 h, O_3 in purified air	17
	Young men with allergic rhinitis	100 ppb, heavy exercise, 2 h, O_3 in purified air	30
Increased airway permeability	Healthy young men	400 ppb, intermittent heavy exercise, 2 h, O_3 in purified air	71
Increased airway inflammation	Healthy young men	80 ppb, moderate exercise, 6.6 h, O_3 in purified air	35
Accelerated tracheobronchial particle clearance	Healthy young men	200 ppb, intermittent light exercise, 2 h, O_3 in purified air	36

[a] Total volume of air exhaled per minute.

TABLE 2
Population-based decrements in respiratory function associated with exposure to ozone in *ambient* air

	Percent decrement at 120 ppb O_3			
	Camp children[a]		Adult exercisers[b]	
Functional index	Mean	90th percentile	Mean	90th percentile
Forced vital capacity	5	14	5	16
Forced expiratory volume in 1 s	8	19	4	12
FEF_{25-75}[c]	11	33	16	39
PEFR[d]	17	42	13	36

[a] 93 children at Fairview Lake, NJ, YMCA summer camp, 1984. Source: Reference 37.
[b] 30 nonsmoking healthy adults at Tuxedo, NY, 1985. Source: Reference 38.
[c] Forced expiratory flow rate between 25% and 75% of vital capacity.
[d] Peak expiratory flow rate.

Several studies have reported associations between ambient photochemical oxidant pollution and exacerbation of asthma (*47–49*), but the role of O_3 specifically and the nature of the exposure–response relationships remain poorly defined. Hammer et al. (*43*) found associations between photochemical oxidants and respiratory symptoms in healthy young adult females (100 student nurses) in Los Angeles, in proportion to ambient ozone levels. However, they ignored smoking and serial correlation in the data and other potentially colinear air pollutants, and used linear regression to model the probability of a respiratory incident. Moreover, they assumed a pollutant would have the same impact on starting an episode of symptoms as on prolonging the episode; and they collapsed the data on individuals to rates per day.

Schwartz and Zeger (*50*) reexamined the original diaries from this study and modeled incidence and duration of a symptom separately. They reported that photochemical oxidants (at 74 ppb) were associated with increased chest discomfort ($p < 0.001$) and eye irritation (also $p < 0.001$).

Ostro and Rothschild (*51*) used the Health Interview Survey, a large cross-sectional data base collected by the National Center for Health Statistics, to examine associations between ambient air pollutants and respiratory morbidity. They reported an association between fine particulates and minor restrictions in activity and respiratory conditions severe enough to result in lost work time and confinement to bed for adults. O_3 was associated only with more minor restrictions.

Bates and Sizto (*52*) examined associations between ambient air pollutants and hospital admissions for respiratory disease in Southern Ontario. They found a consistent association in summer between hospital admissions for respiratory disease and daily levels of SO_4^{2-}, O_3, and temperature, but no association for

hospital admissions for a group of nonrespiratory conditions such as bone fractures. Multiple regression analyses showed that all environmental variables together accounted for 5.6% of the variability in respiratory admissions, and that when temperature was forced into the analysis first, it accounted for only 0.9% of the variability.

Ozkaynak et al. (*53*) studied hospital admissions in relation to O_3 for Boston, Springfield, Worcester, New Bedford, and Fall River, MA. They reported positive associations between 1-h maximum O_3 levels in the summer months and the daily admissions for pneumonia and influenza.

Kinney and Ozkaynak (*54*) examined a 10-year record of daily mortality data from Los Angeles County. Controlling for temperature, they demonstrated associations between short-term variations in total mortality (excluding accidents and suicides) and pollution. Similar results were detected for cardiovascular mortality. Temperature and O_3 had the strongest association with mortality, and annual regressions demonstrated the consistency of the results over time.

Human epidemiology

Chronic effects. The chronic effects data base includes a quite limited amount of information on human effects and a more substantial volume of data on effects seen in laboratory animals undergoing chronic exposures. A study by Linn et al. (*42*) in Southern California provided evidence for a seasonal adaptation of lung function. In this study, a group of subjects selected for their relatively high functional responsiveness to O_3 showed much greater functional decrements following 2 h of exposure to O_3 at 180 ppb with intermittent exercise in a chamber in the spring than they did in the following autumn or winter; moreover, their responses in the following spring were equivalent to those in the preceding spring. These findings suggest that some of the variability in acute response coefficients reported for earlier controlled human exposures to O_3 in chambers could have been caused by seasonal variations in responsiveness which, in turn, may be related to a long-term adaptation to chronic O_3 exposure.

Epidemiological studies of populations living in southern California suggest that chronic oxidant exposures do affect baseline respiratory function. Detels et al. (*55*) compared respiratory function at two points in time five years apart in Glendora (a high-oxidant community) and in Lancaster (a lower oxidant community, but not low by national standards). Baseline function was lower in Glendora, and there was a greater rate of lung function decline over five years.

Kilburn et al. (*56*) reported that nonsmoking and ex-smoking wives of Long Beach shipyard workers had significantly lower values of FEV_1, midexpiratory flow, terminal expiratory flow, and carbon monoxide diffusing capacity than those in a matched population from Michigan. The oxidant exposures in Long Beach and Michigan are not known precisely, but those in Long Beach are similar to those in Lancaster, whereas those in Michigan generally are much lower. Both of these epidemiological studies suggest premature aging of the lung in terms of lung function, which might be expected on the basis of the cumulative changes in lung structure seen in the animals that undergo chronic exposure protocols at concentrations that occur regularly in ambient air in southern California (*57–63*).

An autopsy study of 107 lungs from accident victims 14–25 years old in Los Angeles County by Sherwin and Richters (*64*) reported that 27% had what were judged to be severe degrees of structural abnormalities and bronchiolitis not expected for such young subjects, and another 48% of them had similar, but less severe abnormalities. In the absence of corresponding analyses of lungs of comparable subjects from communities having much lower levels of air pollution, the possible association of the observed abnormalities with chronic O_3 exposure remains speculative. Some of the abnormalities observed could have been caused by smoking or drug abuse, although the authors noted that published work on the association between smoking and small airway effects showed lower degrees of abnormality [Cosio et al. (*65*)].

Although the results of these studies strongly suggest serious health effects, they have been found wanting for standards setting by EPA staff (*66*). The basis for the skepticism about these findings lies in the uncertainty about the exposure characterization of the populations and the lack of control of possibly important confounding factors. Some of these limitations are inherent in large-scale epidemiological studies. Others can be addressed in more carefully focused study protocols.

Further evidence for chronic effects of O_3 recently were reported by Schwartz (*67*), based on an analysis of pulmonary function data from the second National Health and Nutrition Examination Survey (NHANES II, 1976–1980). Using ambient O_3 data from nearby monitoring sites, he reported a highly significant reduction in lung function, associated with exposure to O_3, for persons living in areas in which the annual average O_3 concentrations exceeded 40 ppb.

In summary, chronic exposures to ambient air appear to produce a functional adaptation which persists for at least a few months after the end of the O_3 season, but which dissipates by the spring. Several population-based studies of lung function indicate that accelerated aging of the lung may be associated with living in communities with persistently elevated ambient O_3, but the limited ability to assign exposure classifications of the various populations accurately in these studies makes a cautious assessment of these data prudent.

Discussion

Little progress has been made in controlling O_3 in ambient air, as indicated by the presence of record high ambient concentrations during the summer of 1988. This phenomenon was observed not only in the United States; it also occurred in Brazil, where O_3 levels in São Paulo state in 1988 were higher than in previous years. Furthermore, O_3 exposures in the heavily populated eastern United States take place as prolonged daily peaks that last 6–8 h or more, rather than sharp peaks that last a few hours. Because the various transient effects on lung function are more directly proportional to cumulative daily exposure than to peak hourly concentration, and because the current 1-h NAAQS of 120 ppb is based on the assumption of sharp daily peaks, the degree of protection provided by the current NAAQS is much lower than previously believed. The apparently reversible effects that have followed acute exposures lasting from 5 min to 6.6 h include changes in lung capacity, flow resistance, epithelial permeability, and reactivity to bronchoactive challenges. These effects may persist for many hours or days after the exposure

ceases. Repetitive daily exposures over several days or weeks can exacerbate and prolong these effects.

Most of the data we have on transient functional effects of O_3 have been obtained from controlled human exposure studies. Such studies can provide information on chronic effects of pollutants only to the extent that prior exposures affect the transient response to single exposure challenges. Furthermore, the interpretation of the results of such tests is limited by our generally inadequate ability to characterize the nature and magnitude of the prior chronic exposures. Most of the limited data we have on the effects of chronic O_3 exposures on humans come from epidemiological studies.

Epidemiological studies offer the prospect of establishing chronic health effects attributable to long-term O_3 exposure in relevant populations, and offer the possibility that the analyses can show the influence of other environmental factors on responses to O_3 exposure. On the other hand, the strengths of any of these associations may be difficult to establish because of the complications introduced by uncontrolled cofactors which may confound or obscure the underlying causal factors.

The plausibility of accelerated aging of the human lung caused by chronic O_3 exposure is greatly enhanced by the results of a series of recent chronic animal exposure studies in rats and monkeys (*57–63*). There is little reason to expect humans to be less sensitive than rats or monkeys. On the contrary, humans have a greater dosage delivered to the respiratory acinus than do rats for the same exposures. Another factor is that the rat and monkey exposures were to confined animals with little opportunity for heavy exercise. Thus humans who are active outdoors during the warmer months may sustain greater effective O_3 exposures than the test animals. Finally, humans are exposed to O_3 in ambient mixtures. The potentiation of the characteristic O_3 responses by other constituents of ambient air, seen in the short-term exposure studies in humans and animals, also may contribute to the accumulation of chronic lung damage from long-term exposures to ambient air containing O_3.

The lack of a more definitive data base on the chronic effects of human exposures to ambient O_3 is a serious failing which must be addressed with a long-term research program. The potential impacts of such exposures on public health deserve serious scrutiny and, if they turn out to be substantial, strong corrective action. Further controls on exposure to ambient O_3 will be extraordinarily expensive, and will need to be very well justified.

In summary, the control of ambient O_3 to levels within the current NAAQS presents an intractable problem; the current NAAQS contains little, if any, margin of safety against effects considered to be adverse; and about one-half of the U.S. population resides in communities in which the O_3 NAAQS is exceeded. It is therefore important that health scientists and control agency personnel understand the nature and extent of human exposures and the effects they produce to communicate health risks effectively to the public, and to help develop realistic priorities and feasible options for reducing human exposures.

Acknowledgments

This research was supported by Cooperative Agreement No. CR 811563 between the U.S. Environmental Protection Agency and NYU Medical Center, and is part of a Center program supported by Grant ES 00260 from the National Institute of Environmental Health Sciences.

Some of this material was previously published in *J. Air Pollut. Control Assoc.* (1989, *39*, 672–95). Additional material will appear in a chapter of *Environmental Toxicants*, published by Van Nostrand Reinhold. The author gratefully acknowledges permission to reproduce material from these publications.

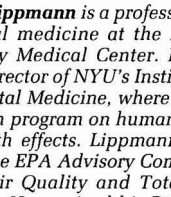

Morton Lippmann *is a professor of environmental medicine at the New York University Medical Center. He also is deputy director of NYU's Institute of Environmental Medicine, where he directs a research program on human exposure and health effects. Lippmann is chairman of the EPA Advisory Committee on Indoor Air Quality and Total Human Exposure. He received his B.Ch.E. from Cooper Union, his M.Ind.Hyg. from Harvard, and his Ph.D. in environmental health sciences from New York University. He won the Donald E. Cummings Award of the American Industrial Hygiene Association in May 1991.*

References

(1) Bates, D. V. *Environ. Res.* **1989**, *50*, 230–37.
(2) American Conference of Governmental Industrial Hygienists. *Threshold Limit Values and Biological Exposure Indices for 1989–1990;* ACGIH: Cincinnati, OH, 1989.
(3) Wayne, W. S.; Wehrle, P. F.; Carroll, R. E. *J. Am. Med. Assoc.* **1967**, *199*, 901–04.
(4) DeLucia, A. J.; Adams, W. C. *J. Appl. Physiol.* **1977**, *43*, 75–81.
(5) *Air Quality Criteria for Ozone and Other Photochemical Oxidants.* Environmental Criteria and Assessment Office, U.S. Environmental Protection Agency: Research Triangle Park, NC, 1986; EPA/600/8-84/0206F.
(6) *Review of the NAAQS for Ozone*; Clean Air Scientific Advisory Committee. U.S. Environmental Protection Agency: Washington, DC, 1989; EPA-SAB-CASAC-89-1092.
(7) Hayes, S. R. *J. Air Waste Manage. Assoc.* **1991**, *41*, 161–70.
(8) Gerrity, T. R. et al. *J. Appl. Physiol.* **1988**, *65*, 393–400.
(9) Miller, F. J.; Menzel, D. B.; Coffin, D. L. *Environ. Res.* **1978**, *17*, 84–101.
(10) Overton, J. H.; Miller, F.J. Presented at the 1987 Annual Meeting of the Air Pollution Control Association, New York, June 1987; Preprint 87–99.4.
(11) Hatch, G. E.; Koren, H.; Aissa, M. *Health Phys.* **1989**, *57*(S1), 37–40.
(12) Gerrity, T. R.; Wiester, M. J. Presented at the 1987 Annual Meeting of the Air Pollution Control Association, New York, June 1987; Preprint 87–99.3.
(13) Overton, J. H.; Graham, R. C. *Health Phys.* **1989**, *57*(S1), 29–36.
(14) Costa, D. L. et al. In *Atmospheric Ozone Research and Its Policy Implications;* Schneider, T. et al., Eds.; Elsevier: Nijmegen, The Netherlands, 1989; pp. 733–43.
(15) Fouke, J. M.; Delemos, R. A.; McFadden, E. R., Jr. *Am. Rev. Respir. Dis.* **1988**, *137*, 326–30.
(16) Folinsbee, L. J.; McDonnell, W. F.; Horstman, D. H. *J. Air Pollut. Control Assoc.* **1988**, *38*, 28–35.
(17) Horstman, D. H. et al. *Am. Rev. Respir. Dis.* **1990**, *142*, 1158–63.
(18) McDonnell, W. F. et al. *Arch. Environ. Health* **1991**, *46*, 145–50.
(19) Lippmann, M. *J. Air Pollut. Control Assoc.* ***1988***, *38*, 881–87.
(20) Hazucha, M. J. *J. Appl. Physiol.* **1987**, *62*, 1671–80.
(21) McDonnell, W. F. et al. *Am. Rev. Respir. Dis.* **1985**, *131*, 36–40.
(22) Kagawa, J. *Int. Arch. Occup. Environ. Health* **1984**, *53*, 345–58.
(23) Shephard, R. J. et al. *Environ. Res.* **1983**, *31*, 125–37.
(24) Drechsler-Parks, D. M.; Bedi, J. F.; Horvath, S. M. *Exp. Geront.* **1987**, *22*, 91–101.
(25) Reisenauer, C. S. et al. *J. Air Pollut. Control Assoc.* **1988**, *38*, 51–55.
(26) Koenig, J. Q. et al. *Am. Rev. Respir. Dis.* **1987**, *136*, 1152–57.
(27) Linn, W. S. et al. *Am. Rev. Respir. Dis.* **1978**, *117*, 835–43.
(28) Linn, W. S. et al. *Arch. Environ. Health* **1983**, *38*, 278–83.
(29) Solic, J. J.; Hazucha, M. J.; Bromberg,

P. A. *Am. Rev. Respir. Dis.* **1982**, *125*, 664–69.
(30) McDonnell, W. F. et al. *Toxicol. Indust. Health* **1987**, *3*, 507–17.
(31) Folinsbee, L. J.; Hazucha, M. J. In *Atmospheric Ozone Research and Its Policy Implications*; Schneider, T. et al., Eds.; Elsevier: Nijmegen, The Netherlands, 1989; pp. 483–92.
(32) Rombout, P.J.A.; Lioy, P. J.; Goldstein, B. D. *J. Air Pollut. Control Assoc.* **1986**, *36*, 913–17.
(33) Hayes, S. R. et al. Draft Final Report, Systems Applications, Inc.: San Rafael, CA, 1987.
(34) Koren, H. S. et al. *Am. Rev. Respir. Dis.* **1989**, *139*, 407–15.
(35) Devlin, R. B. et al. *Am. J. Respir. Cell Mol. Biol.* **1991**, *4*, 72–81.
(36) Foster, W. M.; Costa, D. L.; Langenback, E. G. *J. Appl. Physiol.* **1987**, *63*, 996–1002.
(37) Spektor, D. M. et al. *Am. Rev. Respir. Dis.* **1988**, *137*, 313–20.
(38) Spektor, D. M. et al. *Am. Rev. Respir. Dis.* **1988**, *138*, 821–28.
(39) Kinney, P. L.; Ware, J. H.; Spengler, J. D. *Arch. Environ. Health* **1988**, *43*, 168–73.
(40) Lippmann, M. et al. *Adv. Modern Environ. Toxicol.* **1983**, *5*, 423–46.
(41) Spengler, J. D. et al. *Environ. Health Perspect.* **1989**, *79*, 43–51.
(42) Linn, W. S. et al. *Toxicol. Indust. Health* **1988**, *4*, 505–20.
(43) Hammer, D. I. et al. *Arch. Environ. Health* **1974**, *28*, 255–60.
(44) Makino, K.; Mizoguchi, I. *NipponKoshu Eisei Zasshi* **1975**, *2*, 421–30.
(45) Altshuller, A. P. *J. Air Pollut. Control Assoc.* **1977**, *27*, 1125–26.
(46) National Research Council. In *Ozone and Other Photochemical Oxidants*; Committee on Medical and Biologic Effects of Environmental Pollutants, National Academy of Sciences: Washington, DC, 1977; pp. 323–87.
(47) Schoettlin, C. E.; Landau, E. *Publ. Health Rep.* **1961**, *76*, 545–48.
(48) Whittemore, A.; Korn, E. *Am. J. Public Health* **1980**, *70*, 687–96.
(49) Holguin, A. H. et al. *Trans. APCA* **1985**, 262–80; TR-4.
(50) Schwartz, J.; Zeger, S. *Am. Rev. Respir. Dis.* **1990**, *141*, 62–67.
(51) Ostro, B. D.; Rothschild, S. *Environ. Res.* **1989**, *50*, 238–47.
(52) Bates, D. V.; Sizto, R. *Environ. Health Perspect.* **1989**, *79*, 69–72.
(53) Ozkaynak, H.; Kinney, P. L.; Burbank, B. Presented at the 1990 Annual Meeting of Air and Waste Management Assoc.; AWMA, Pittsburgh, PA, 1990; Preprint 90-150.6.
(54) Kinney, P. L.; Ozkaynak, H. *Environ. Res.* **1991**, *54*, 99–120.
(55) Detels, R. et al. *Chest* **1987**, *92*, 594–603.
(56) Kilburn, K. H.; Warshaw, R.; Thornton, J. C. *Am. J. Med.* **1985**, *79*, 23–28.
(57) Huang, Y. et al. *Am. J. Aerosol Med.* **1988**, *1*, 180–83.
(58) Chang, L. et al. *Toxicol. Appl. Pharmacol.* **1991**, *109*, 219–34.
(59) Tepper, J. S. et al. *Fundam. Appl. Toxicol.* **1991**, *17*, 52–60.
(60) Grose, E. C. et al. In *Atmospheric Ozone Research and Its Policy Implications*; Schneider, T. et al., Eds.; Elsevier: Nijmegen, The Netherlands, 1989; pp. 535–44.
(61) Hyde, D. M. et al. In *Atmospheric Ozone Research and Its Policy Implications*; Schneider, T. et al., Eds.; Elsevier: Nijmegen, The Netherlands, 1989; pp. 525–32.
(62) Tyler, W. S. et al. *Toxicology* **1988**, *50*, 131–44.
(63) Raub, J. A.; Miller, F. J.; Graham, J. A. *Adv. Mod. Environ. Toxicol.* **1983**, *5*, 363–67.
(64) Sherwin, R. P.; Richters, V. In *Tropospheric Ozone and the Environment*; Berglund, R. L.; Lawson, D. R.; McKee, D. J., Eds.; Air & Waste Management Association: Pittsburgh, 1991; pp. 178–196; TR-19.
(65) Cosio, M. G.; Hole, K. A.; Niewohner, D. E. *Am. Rev. Respir. Dis.* **1980**, *122*, 265–71.
(66) "Review of the National Ambient Air Quality Standards for Ozone—Preliminary Assessment of Scientific and Technical Information"; OAQPS Draft Staff Paper, U.S. Environmental Protection Agency: Washington, DC, Nov. 1988.
(67) Schwartz, J. *Environ. Res.* **1989**, *50*, 309–21.
(68) McDonnell, W. F. et al. *J. Appl. Physiol.* **1983**, *54*, 1345–52.
(69) Linder, J. et al. *Schweiz. Ztschr. Sportmed.* **1988**, *36*, 5–10.
(70) Schelegle, E. S.; Adams, W. C. *Med. Sci. Sports Exerc.* **1986**, *18*, 408–14.
(71) Kehrl, H. R. et al. *Am. Rev. Respir. Dis.* **1987**, *135*, 1174–78.

NEW RELEASES
FROM THE ACS SYMPOSIUM SERIES

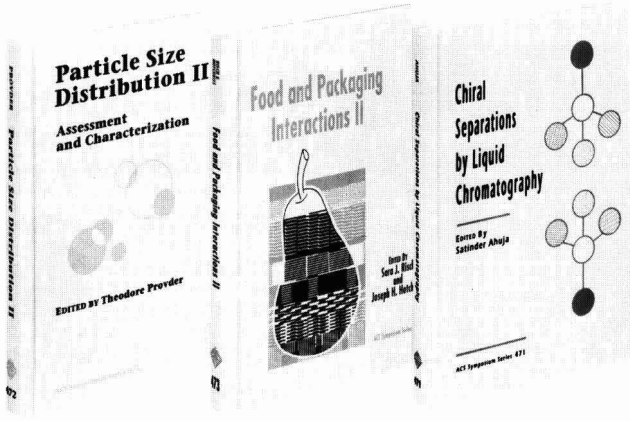

Particle Size Distribution II
Assessment and Characterization

This compendium of current work in the field features the latest technology now in use for particle size distribution assessment. Among the new techniques discussed are capillary hydrodynamic fractionation, field flow fractionation, disc centrifuge photosedimentometry, on-line measurements, fractals, electrophoretic characterization, image analysis, and electric sensing zone. A review chapter examines turbidimetry, an old technique that has been revitalized with new mathematical approaches.

Theodore Provder, Editor
ACS Symposium Series No. 472
400 pages (1991) Clothbound
ISBN 0-8412-2117-0
$89.95

Food and Packaging Interactions II

The most comprehensive and current information available on food packaging interactions, including presentations on migration, scalping, permeability, and microwave susceptor packaging products. A valuable resource for food product development scientists and engineers who need to understand what can happen to foods in different types of packages and regulatory agencies who must keep pace with new developments and maintain appropriate regulations. Includes information on regulations of packaging for the United States, United Kingdom, and European Community.

Sara J. Risch and Joseph H. Hotchkiss, Editors
ACS Symposium Series No. 473
270 pages (1991) Clothbound
ISBN 0-8412-2122-7
$59.95

Brassinosteroids
Chemistry, Bioactivity, and Applications

With contributions from all over the world, this volume presents an accurate and comprehensive picture of the present state of research and development in brassinosteroids. Provides a survey of the chemistry, synthesis, physiology, and practical applications of brassinosteroids, in experimental and agricultural references alike. Presents results of large-scale field trials in China, which strongly indicate the economic potential of these compounds as environmentally benign agricultural chemicals to significantly increase crop yields.

Horace G. Cutler, Takao Yokota, and Gunter Adam, Editors
ACS Symposium Series No. 474
358 pages (1991) Clothbound
ISBN 0-8412-2126-X
$84.95

Radiation Effects on Polymers

Reviews the fundamental chemistry and physics of polymer-radiation interaction and examines recent progress in most major areas of the field. Covers fundamentals of polymer radiation chemistry, technological applications of radiation to polymers (including radiation processing, radiation curing, sterilization, cross-linking, polymerization, grafting, x-ray resists, and others), and degradation and stabilization of irradiated polymers (including nuclear plants, scintillation detectors for particle physics, and others).

Roger L. Clough and Shalaby W. Shalaby, Editors
ACS Symposium Series No. 475
640 pages (1991) Clothbound
ISBN 0-8412-2165-0
$109.95

Emerging Technologies for Materials and Chemicals from Biomass

As nonrenewable chemical feedstocks are depleted, new sources of materials and chemicals must be developed to fill the need. This new volume examines the technologies now emerging for the use of biomass as an environmentally friendly and sustainable solution to the problem. Its 25 chapters are divided into three sections covering: lignocellulosic materials and composites; biopolymers (alloys, derivatives, and blends) and chemicals and fuels from biomass and wastes. Each section opens with review chapters summarizing potentials and opportunities.

Roger M. Rowell, Tor P. Schultz, and Ramani Narayan, Editors
ACS Symposium Series No. 476
480 pages (1992) Clothbound
ISBN 0-8412-2171-5
$99.95

Chiral Separations by Liquid Chromatography

Presenting state-of-the-art information, this volume covers all the major modes of separation and offers contributions from the leading researchers who developed these techniques. It provides a detailed review of the commonly used columns: brush type, cyclodextrin, polysaccharide carbonate, and protein. In addition, the volume provides significant discussion on the use of chiral discriminators or selectors.

Satinder Ahuja, Editor
ACS Symposium Series No. 471
240 pages (1991) Clothbound
ISBN 0-8412-2116-2
$59.95

Expression Systems and Processes for rDNA Products

This fascinating volume provides a wealth of information on developments in expression system technologies. Among the topics covered in its nine chapters are bacterial hosts (*E.coli*), yeast (*Saccharomyces cerevisiae*), and insect cells. In addition, the book examines process technologies, including high cell density bacterial fermentations, biocatalysis, and process issues with recombinant microorganisms.

Randolph T. Hatch, Charles Goochee, Antonio Moreira, and Yair Alroy, Editors
ACS Symposium Series No. 477
130 pages (1992) Clothbound
ISBN 0-8412-2172-3
$34.95

Order from:
American Chemical Society
Distribution Office, Dept. 23
1155 Sixteenth St., N.W.
Washington, DC 20036
or CALL TOLL FREE: 800-227-5558
or in Washington DC: 202-872-4363
and use your credit card!

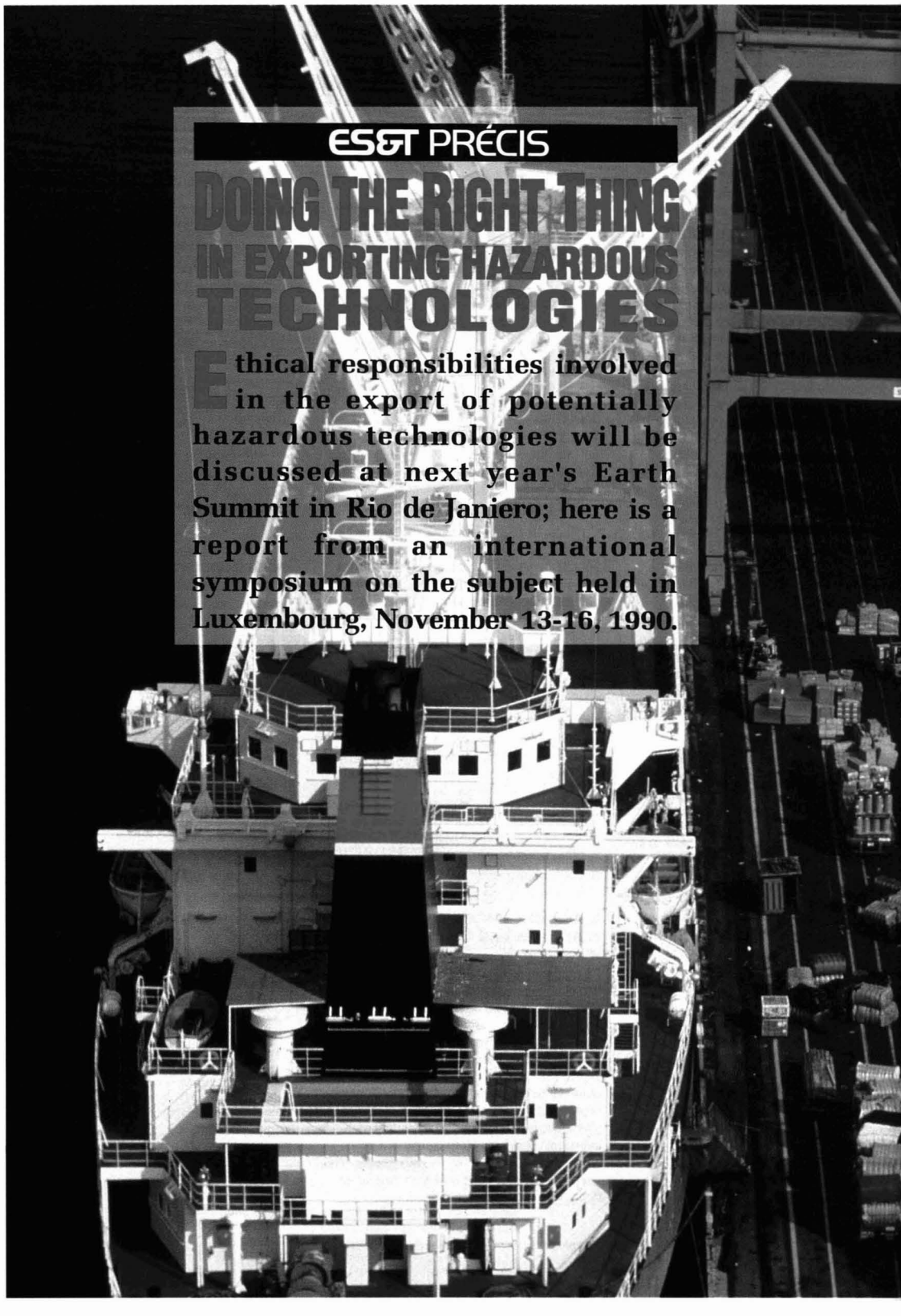

ES&T PRÉCIS

DOING THE RIGHT THING IN EXPORTING HAZARDOUS TECHNOLOGIES

Ethical responsibilities involved in the export of potentially hazardous technologies will be discussed at next year's Earth Summit in Rio de Janiero; here is a report from an international symposium on the subject held in Luxembourg, November 13-16, 1990.

0013-936X/91/0925-1964$02.50/0

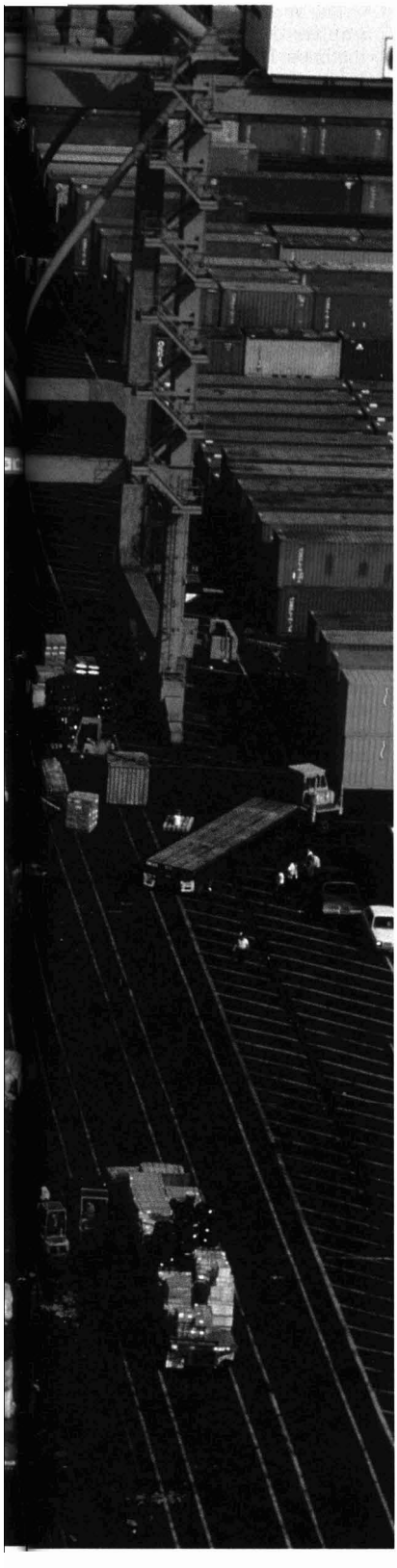

Ortwin Renn
Halina S. Brown
Clark University
Worcester, MA 01610-1477

Allen L. White
Tellus Institute
Boston, MA 02110-3509

To facilitate new ways of thinking about the technology transfer process—particularly as Western multinational corporations (MNCs) appear poised to export potentially hazardous technologies to Eastern Europe and the Soviet Union—Clark University, in conjunction with the Center for Population Studies in Luxembourg, the Gerling Consulting Group (Zürich, Switzerland, and Cologne, Germany), the Stockholm Environment Institute, and the Boston Institute for Responsible Management, organized a symposium in November 1990 in Luxembourg under the patronage of the Luxembourg government. The symposium brought together representatives of industry, government, insurance and consulting companies, academia, and international organizations to discuss experiences with and ethical issues surrounding hazardous technology export from Western nations to Third World Countries. The conference participants discussed, among other topics, the opportunities and risks of biotechnology transfer, the siting of chemical production facilities, and waste management issues.

Rather than report on each presentation, we focus on the key issues addressed during the symposium, and synthesize the many perspectives expressed in the individual papers, panel discussions, and plenary debates. The participants developed a set of ethical and pragmatic guidelines for technology transfer, which were later summarized by the conference organizers and endorsed by most participants. The resulting document has been forwarded to the Geneva-based Preparatory Committee for the 1992 United Nations Conference on Environment and Development in Brazil. (This document can be obtained from O. Renn, CENTED, Clark University, Worcester, MA 01610.) The following sections reflect the major arguments of this document.

Précis articles are reports of meetings of unusual significance, international or national developments of environmental importance, significant public policy developments, and related items.

Pragmatism and conciliation

The decade of the 1980s witnessed a significant shift in the nature of the debate over technology transfer by MNCs to Third World countries (*1, 2*). Until then, although the debate was a continuum rather than a dichotomy, it was dominated by two opposing camps. One, when taken to its extreme, advocated foreign investments of all types in order to accelerate economic development (*3*). The other viewed foreign investments as a strategy of global capitalism to exploit the human and environmental resources of Third World countries (*4–6*). [For a comprehensive review of different theoretical perspectives that underlie contrasting assessments of the impact of MNC technologies on Third World countries, see Chapter 4 of Jenkins (*6*).] Both camps were driven more by ideology than by analysis in expressing their respective viewpoints.

Today, formerly dichotomous viewpoints are shifting toward a new paradigm less constrained by ideological imperatives. This paradigm seeks to identify the elements of technology transfer that are mutually beneficial to the MNC and the host country, and to determine appropriate policies for risk reduction. Host country self-determination and the legacy of uncontrolled foreign investments are helping to shape this emerging paradigm.

The Union Carbide gas leak disaster in Bhopal, India, was a watershed in the evolution of this new vision of corporate responsibility in developing countries. Against the backdrop of immense personal tragedy, the Bhopal accident demonstrated vividly that cooperation between the MNC and the host country is essential to ensure adequate protection for workers, the community, and the environment. The simplistic view that foreign investment automatically benefits the host country, even when substantial hazards are involved, could no longer be sustained. At the same time, the exploitation perspective was equally unsatisfactory in explaining the disaster. Instead, a mix of management failures, poor training and supervision, gradual divestment, and technologies inappropriate to local conditions combined to create the preconditions for an acute breakdown of human and hardware systems (*7*).

With the collapse of the communist system, the ideological competition between capitalism and socialism has given further momentum to more pragmatic approaches to technology transfer and international cooperation.

At its core, the new paradigm views MNC and host country goals in managing imported technologies as non-zero-sum with significant benefits to both parties, yet requiring trade-offs and painful choices among desirable private and public goods. It impels the re-evaluation of investment strategies, corporate behavior, and national goals in light of these benefits and trade-offs. Successful cooperation among MNCs and host countries reveals that explicit mentioning of values and trade-offs in negotiations enhance performance and cooperation between host countries' regulatory institutions and foreign investors. Such a strategy calls for the consideration of ethical principles to guide MNCs, host countries, and parent countries in their technology transfer decisions.

Several existing codes of ethical conduct designed to guide extraterritorial corporate, and, in some cases, governmental behavior show close ties to early ideological interpretations of hazardous technology transfer. A perceived need to "control" inappropriate MNC activities is a major theme presented in several codes drafted during the 1970s (*8–12*). Emphasizing the pervasive role of MNCs in the world economy, these codes sought to control corporations with appropriate laws, policies, and regulations adopted by governments and international organizations.

Other codes of conduct affecting technology transfer have been drafted by organizations that cast the foreign activities of MNCs in a more favorable light (*13–16*). Rather than regulate MNCs, governments are encouraged to facilitate their positive contributions through the creation and development of effective capital markets and infrastructure. Insofar as regulations are necessary, it is suggested that they be framed in such a way that the rights of existing enterprises are respected, new investment is encouraged, and flexible application of codes and guidelines is practiced.

Our reading of these and other codes reveals their increasing detail and pragmatism in balancing MNC and host country interests. Notable among these is the Conseil Européen des Fédérations de l'Industrie Chimique's "Principles and Guidelines for the Safe Transfer of Technology" (*13*). In addition to prescribing the allocation of responsibilities between involved parties (technology suppliers and receivers, contractors, and host states), the guidelines explicitly cover seven detailed stages of technology transfer, from its procurement to implementation and routine operation. Taken as a whole, we have found existing codes and related ethical literature (*17*) to contain a wide range of prescriptive criteria useful for the structuring of corporate and national behavior in environment, health, and safety.

At the beginning of a new decade and with an eye toward the new millennium, it is timely to consolidate these guidelines, to integrate the often confusing "recipes" for ethical conduct into a consistent structure, and to evaluate the "real world" experiences (*18–22*) with respect to achieving the desired goals. Such review is all the more relevant as the world faces new challenges involving the export of hazardous technologies from the industrialized West to Eastern Europe and the Soviet Union. Former communist countries, eager to attract foreign investment, are positioned to set new standards. Governments and potential investors will benefit from integrated guidelines for all stages of the technology transfer process.

Principles of ethical conduct

Drawing from the major schools of ethics in philosophy, the export of technologies and materials from industrialized to developing or less developed countries may be analyzed within the following four ethical paradigms (*23*):

- Utilitarian. Whatever promises the most benefits for all parties involved, is also the most desirable arrangement for the proposed transaction or transfer.
- Deontological. Based on civil rights and generally accepted standards of decent behavior, arrangements are acceptable only if they meet these standards regardless of actual outcome.
- Fiduciary. One of the parties takes special responsibility for the arrangement of the transaction and acts as a patron for the other parties.
- Consensual. All arrangements are ethically acceptable if all the parties affected explicitly or implicitly give prior consent to them.

The application of each principle implies different procedures and methods. If a utilitarian perspective is accepted, options for arranging transfers or exports would be evaluated according to their cost/benefit ratio, and measures to increase safety or environmental quality according to their cost-effectiveness.

In contrast, the deontological principle would oblige the parties to meet special ethical criteria, for example to reduce the risk to some acceptable level or to implement the best available pollution control technology. The obligation to achieve "equivalent" safety and environmental protection levels (equal ends through possibly different means) in the host country and the exporting country is a typical and widely used criterion based on deontological reasoning.

According to the fiduciary approach, one party, for example the corporation, assumes responsibility for negative impacts of the transaction on other parties (even without legal obligation) and acts as an advocate to serve their interests. A typical example might be the corporate arrangements to ensure safe and environmentally beneficial use of their products after they have been sold to customers, commonly referred to as product "stewardship."

Finally, consensual principles focus on the procedures of reaching an agreement. All parties involved should be given the opportunity to review the present knowledge of potential impacts of the transaction and then to select implicitly or, even better, explicitly, an arrangement that they all regard as beneficial.

Each of these principles has obvious advantages and shortcomings. If applied correctly, the utilitarian approach guarantees the optimal allocation of given resources for obtaining a specific set of objectives, but may not be equitable or respect individual rights. The pursuit of deontological criteria prevents or at least mitigates unwanted consequences, but may waste valuable monetary or material resources. The fiduciary principle obliges the most appropriate party to base its actions on an integration of values and interests of all parties involved, but is likely to produce biased value sets if the values of the patron conflict with the values of another party. Informed consent ensures that all parties perceive a subjective benefit from the selected arrangement, but

this perception may be based on incomplete or biased information or may be wrongly inferred from indications of implicit approval, such as absence of organized opposition.

Given the imperfections of any one of the four principles, a combination is preferable in order to take advantage of the merits of each and compensate for the shortcomings. The following guidelines emerge:

(1) MNCs should accept a fiduciary responsibility for their facilities and products and act in the interest of the people who are affected by their economic activity. A rule of thumb here is: Don't do anything that you would object to in your own country under similar circumstances.

(2) It is essential to gain explicit prior consent insofar as this is technically and politically feasible. Prior consent can be accomplished through:

- accepting the host country's standards and regulations;
- negotiating acceptable arrangements with the legally responsible host country's agencies;
- providing full information about potential impacts to all constituencies;
- creating a vehicle to elicit public concerns and possible objections; and
- providing constituents with an opportunity to voice their consent or dissent.

(3) Fundamental civil rights should not be traded off against economic benefits or other objectives. In addition, the rule that health and safety standards should be equivalent (though not necessarily identical) to those of the exporting country seems wise to adopt. It should be waived only in exceptional circumstances, for example, to avoid a severe economic disruption.

(4) If an MNC abides by Guidelines 1, 2, and 3, all other choices left to the corporation or the host country should be made on the basis of utilitarian methods, i.e., cost-benefit, cost-effectiveness, and other utility optimization techniques.

Delineation of procedures

If these four guidelines are accepted as a basis for organizing the transfer of hazardous technologies or materials, the next step is to specify concrete objectives and appropriate procedures. Objectives are yardsticks to measure the success or failure of any given transaction with respect to the four guidelines. Procedures, in turn, define the steps necessary to implement these objectives. The participants of the Luxembourg symposium suggested many objectives and procedures that would meet the ethical guidelines. Among the most important are the following:

(1) In accordance with the fiduciary commitment, it is essential that the MNC, on its own initiative or through mandate by a host government, provide diverse options, all of which are capable of meeting the goals intended by the transaction. These options should include nontechnological solutions as well as solutions based on indigenous technologies or methods, assuming these are technically and economically feasible. It should not be automatically assumed that the technical options that are preferred in industrialized countries are always the most appropriate method of providing the same or a similar service in many developing countries or in Eastern European countries. At the same time, however, a well-meaning paternalistic offer of only so-called "appropriate technologies" is also inadequate insofar as the MNC unilaterally determines what is appropriate.

"The Luxembourg Symposium provided an opportunity for industrialists, consultants, administrators, and academics to discuss their perspectives. . ."

(2) Each of these options should be carefully analyzed for potential impacts, both positive and negative. This analysis serves two functions. It provides the basic material for the various constituencies to review the impacts and gain the knowledge necessary to approve or disapprove a planned transaction. It also helps to establish a data base to evaluate different options and later measures of safety and environmental protection according to cost-effectiveness. Uncertainty about future impacts will remain, but the impact analysis provides the best current knowledge available to make a prudent decision.

(3) A preliminary selection of options should occur on the basis of firm deontological principles. Any option that violates any basic individual right (as given in the UN Bill of Rights or other international code) or any host country law or regulation (unless explicitly overruled by the host country authority) does not qualify for further consideration. In addition, all options should be dropped that do not provide a level of safety and environmental protection equivalent to that of an identical facility or technology in the exporting country. In exceptional cases, one may waive this principle if the evidence shows clearly and unambiguously that a cancellation of the proposed transaction may lead to a less desirable environmental outcome than its implementation. It should be noted, however, that in almost every case a new option can be designed that meets the objective of equivalent safety *and* is economically and technically feasible. The burden of proof for justifying a waiver of the equivalence principle rests on the corporation.

(4) The principle of equivalent levels of safety and environmental protection does not necessitate the export of identical safety and environmental practices. The goal is to have functional equivalents available that achieve approximately equal performance using a variety of means. It is prudent to use the tools of utility optimization methods to select the measures that will ensure an equivalent degree of safety and environmental protection. Regulations or strict rules requiring the use of identical means may result in a waste of scarce resources. Flexible responses to different levels of workers' qualifications, the relative prices for labor and machines, infrastructural conditions, and other situational variables may be necessary to ensure economical

operation and competitive advantages.

(5) Notwithstanding the need to be flexible in selecting the means for ensuring equivalent levels of safety, it is helpful to set priorities for the selection of means, particularly if the potential benefits of each option are difficult to quantify. Proposers and host countries should develop priority lists which they can use in later negotiations. A priority list for safety technologies may appear as follows (ordered from first to last priority):

- inherently safe technologies (physical properties);
- forgiving technologies (able to withstand human error);
- passive safety devices (do not need human intervention to be activated);
- active safety devices (do need human intervention to function);
- accident mitigation technologies (protection of workers and residents in the case of accidents).

These technologies can and should be combined to enhance the overall safety level, but such a priority list helps to determine the feasibility of the higher order means before turning to a lower order solution. The same concept can be applied to pollution management. A priority list may appear as follows:

- avoidance of pollutants (through materials and process innovation);
- establishment of closed cycles (recycling or reuse of potential pollutants);
- volume reduction through recycling;
- application of the "as low as reasonably achievable" principle (to reduce emissions of pollutants);
- incorporation of best available control technologies to achieve levels below permissible limits; and
- meeting, but not achieving levels lower than, regulatory standards.

(6) Option selection and modification should be achieved by consent between the proposer and the host country agency. It seems advisable to focus first on the shared values and goal and then turn to controversial issues. These negotiations should be preceded by an agreement by the host country and the proposer to commit themselves to a specific option and its special modifications in terms of safety standards and environmental protection. This process should incorporate the impact analysis (providing the factual base for debating each option) and the preferences of both parties (providing the value base for aligning each other's interests) into the negotiations. It is not necessary to restrict the negotiations through special rules other than fairness, honesty, good will, consistency and, if mutually agreed to, a procedure for dispute resolution.

(7) After an agreement is reached, it is the obligation of the proposer to inform affected host country constituents insofar as is possible. Even if public involvement is not mandated in the host country, every effort should be made to provide information to the affected public and to establish a forum for feedback. Organizing such an involvement process proves difficult in many recipient countries, especially in those countries unaccustomed to public scrutiny of private and official decisions. A process will be successful when proposers are cognizant of these constraints while seeking to inform the public of potential side effects and to incorporate local conditions (often unknown by the regulator) into the technical design or institutional management of the technology or facility. (An additional benefit is that a public aware of side effects is less at risk than an uninformed public.)

(8) After the selected option is implemented, fiduciary responsibility should be the guiding principle for the operating phase. Regardless of the host country's ability to monitor or control safety and pollution, the operators should act as if they were entrusted by the host country to assume responsibility for the impacts of their actions on anything that the host country values, ranging from workers' safety, community health, and preservation of natural habitats to conservation of cultural artifacts. Many MNCs have developed sophisticated and effective protocols to ensure self-regulation even in the absence of external pressure or legal obligations. Because the corporate safety culture practices (i.e., the guiding principles and values that act as internalized motivators for all employees within a company with respect to safety and environmental health) differ considerably, it is not appropriate to standardize these protocols and to develop a boilerplate for all purposes. It is important, however, that each company create a system of internal checks and balances. This system should ensure and specify monitoring requirements, safety checks, emission controls, and impact assessments. The less a host country exercises supervision in environment, health, and safety, the more important becomes the internal corporate organization to ensure controls.

(9) Within reasonable limits, corporate responsibility extends to upstream processing of the product and downstream distribution, even in the absence of legal requirements. The latter, known as product stewardship, is particularly pertinent to developing countries where end-users are often ill informed and emergency medical response systems nonexistent or substandard. However, this responsibility can only be assumed within reasonable boundaries. Car manufacturers, for example, cannot be held responsible for an accident caused by a drunken driver. What constitutes a reasonable boundary cannot be defined in abstract, but depends on the nature of the technology and the sociocultural context in which it is placed. It appears, however, that warning about risks and training consumers to handle the product safely fall within the responsibility of the producer.

These nine specifications and four principle guidelines offer a foundation for MNCs to design their own guidelines or evaluate their existing rules. Principles and guidelines applicable to MNCs are equally valid for host countries and the international community. Safety and environmental protection equivalent to those of the exporting country, adherence to inviolate rights and values, enlargement of technology options to serve host country wants and needs, and assurance of corporate liability are also relevant host country objectives.

To realize these principles and guidelines requires the development of policies by host countries, the exporting countries, and the international community. Policy structure largely depends on the country's political system, its culture, and its regulatory style. However, policies can be classified in terms of compliance mechanisms (information, incentive, and coercion) and implementing agency (international, governmental, corporate).

In reviewing the policy instruments—self-regulation by the MNCs, provision of economic incentives for environmentally re-

sponsible behavior, or imposition of regulatory standards upon the MNCs—it seems advisable to reserve national standards for inviolable values (such as protection of life and health) and for other national objectives that are impossible or extremely difficult to link to the self-interest of the MNCs. Examples of the latter are equitable development (i.e., equal development opportunities for all regions of a country and for all social classes) or national self-sufficiency. Excessive standards may deter potential investors and, given that provision for adequate health and safety levels is in the self-interest of many MNCs, may turn out to be redundant or even counterproductive. However, most MNCs prefer to adjust to prescribed standards rather than to face high degrees of regulatory uncertainty.

International guidelines may help host countries to use internationally available expertise to articulate national standards and to build regulatory capacity. Another possibility, although difficult to accomplish, may be the establishment of an international body with authority to monitor facilities in all member countries. The major emphasis should be on linking economic incentives with self-regulation within the context of acceptable host country environmental targets and risks. If effectively implemented, an international organization is the most flexible, cost-effective, and nonbureaucratic path by which to meet the desired objectives.

In conclusion . . .

The Luxembourg Symposium on Values and Responsibilities in the Transfer of Hazardous Technologies provided an opportunity for industrialists, consultants, administrators, and academics to discuss their perspectives; to review their experience with existing codes of conduct and corporate performance; and to outline a list of principles, guidelines, and procedures for responsible and mutually beneficial pathways to sustainable development in the Third World and Eastern European countries.

The major conclusion of the symposium was that, despite many drawbacks and problems, cooperation between MNCs and host European countries can be arranged in a mutually beneficial manner. Principles of ethical conduct have helped to shape successful policies in the past; they will continue to be needed for meeting the challenges of the future.

A fiduciary approach to safety and environmental management that is sensitive to cultural values and lifestyles of the host country, coupled with good-faith attempts to gain approval by affected constituencies, is at the heart of the recommendations. In addition, constitutional rights, international law, and—to a lesser degree—the rule of equivalent safety and environmental quality should be regarded as inviolate values which should not be sacrificed for economic gain.

On the procedural side, governments are well advised to take advantage of the self-interest of MNCs and encourage self-regulation. Legal controls and regulations are necessary, but should be coupled with economic incentives to ensure cost-effectiveness and bureaucratic simplicity. Corporations should develop policies for internal monitoring and constant quality control within the organization. This is particularly essential in countries with weak regulations and inadequate enforcement.

Responsible export of hazardous technologies poses a major challenge in today's global economy. Corporate and host country environmental goals are invariably pursued concurrent with economic development, social justice, national identity, and political autonomy. Balancing these goals is a complex task for host countries and MNCs, particularly when hazardous technologies are involved. The participants of the Luxembourg symposium expressed hope and confidence that the outcome of their deliberations may help all parties to cope with this task.

Acknowledgment

The authors thank Jeffery J. Himmelberger for research assistance in preparing this article.

Ortwin Renn *is associate professor of environment, technology, and society at Clark University and senior investigator at the Clark Center for Technology, Environment, and Development, an interdisciplinary research institute devoted to the study of hazards and risk communication in contemporary societies. Renn received an M.A. in sociology and economics (European Diploma) and a doctorate degree in social psychology, both from the University of Cologne (School of Economics and Social Sciences). He has published five books and more than 50 articles, serves on several national and international advisory boards, and is a member of the panel on environmental standards of the West German Academy of Sciences and Technology in Berlin.*

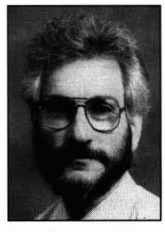

Halina S. Brown *is associate professor of environment, technology, and society at Clark University. She was the chief toxicologist for the Massachusetts Department of Environmental Protection, later receiving her Ph.D. in chemistry from New York University. Her current research interests include mechanisms of chemical carcinogenesis, environmental health risk assessment, and hazard management in international technology transfer.*

Allen L. White *is director of the Risk Analysis Group at the Tellus Institute in Boston and senior research associate at the Center for Technology, Environment, and Development at Clark University. He received an M.A. and Ph.D. in geography from Ohio State University. His principal research interests are international environmental policy, facility locational analysis, and corporate environmental management. He has advised the U.S. Agency for International Development, the United Nations Center for Transnational Corporations, EPA, and state and local governments.*

References

(1) Gladwin, T. In Pearson, C. S., Ed.; *Multinational Corporations, Environment, and the Third World: Business Matters*; Duke University Press: Durham, NC, 1987.

(2) Lele, S. M. *World Development* **1991,** *19*(6), 607–21.

(3) Balasubramanyam, V. N. *Multinational Enterprises and the Third World*; Trade Policy Research Centre: London, 1980; Thames Essay No. 26.

(4) Helleiner, G. K. *World Development* **1975,** *3*(4).

(5) Stewart, F. "International Technology Transfer: Issues and Policy Options"; World Bank: Washington, DC, 1979; Staff Working Paper 344.

(6) Jenkins, R. *Transnational Corporations and Uneven Development: The Internationalization of Capital and the Third World*; Methuen: London, 1987.
(7) Bowonder, B.; Kasperson, J. X.; Kasperson, R. E. *Environment* **1985,** *27,* 6–13, 31–37.
(8) *Tripartite Declaration of Principles Concerning Multinational Enterprises and Social Policy*; International Labour Office: Geneva, 1977.
(9) *Guidelines for Multinational Enterprises*; Organization for Economic Cooperation and Development: Paris, 1976.
(10) *Transnational Corporations: Issues Involved in the Formulation of a Code of Conduct*; United Nations Centre on Transnational Corporations: New York, 1976.
(11) *The United Nations Code of Conduct on Transnational Corporations*; United Nations Centre on Transnational Corporations: New York, 1986.
(12) Bavaria, J. *Issues in Science and Technology* **1989–90,** *Winter,* 28–31.
(13) *Principles and Guidelines for the Safe Transfer of Technology*; Conseil Européen des Fédérations de l'Industrie Chimique: Brussels, 1987.
(14) *Summary Description and Guiding Principles for Responsible Care: A Public Commitment*; Chemical Manufacturers' Association: Washington, DC, 1990.
(15) *Guidelines for International Investment*; International Chamber of Commerce: Paris, 1972; Brochure No. 272.
(16) United Nations Environment Programme. *APELL: Awareness and Preparedness for Emergencies at Local Level*; Industry and Environment Office: Paris, 1988.
(17) Shue, H. *Ethics* **1981,** *91,* 579–606.
(18) Economic and Social Commission for Asia and the Pacific/United Nations Centre on Transnational Corporations. *Environmental Aspects of Transnational Corporation Activities in Pollution-Intensive Activities in Selected Asian and Pacific Developing Countries*; United Nations: Bangkok, 1990.
(19) Flaherty, M.; Rappaport, A. *Multinational Corporations and the Environment: A Survey of Global Practices*; Center for Environmental Management, Tufts University: Medford, MA, 1991.
(20) Leonard, J. *Pollution and the Struggle for the World Product: Multinational Corporations, Environment, and International Comparative Advantage*; Cambridge University Press: Cambridge, 1988.
(21) Morrison, C. *Managing Environmental Affairs: Corporate Practices in the U.S., Canada and Europe*; The Conference Board: New York, 1991; Report Number 961.
(22) *Benchmark Corporate Environmental Survey: First Statistical Results, Management Systems and Methodology*; United Nations Centre on Transnational Corporations: New York, 1991.
(23) Frankena, W. K. In Goodpaster, K. E.; Sayre, K. M., Eds. *Ethics and Problems of the 21st Century*; University of Notre Dame Press: Notre Dame, 1979, pp. 3–20.

One chemist understands laboratory safety. The other doesn't.

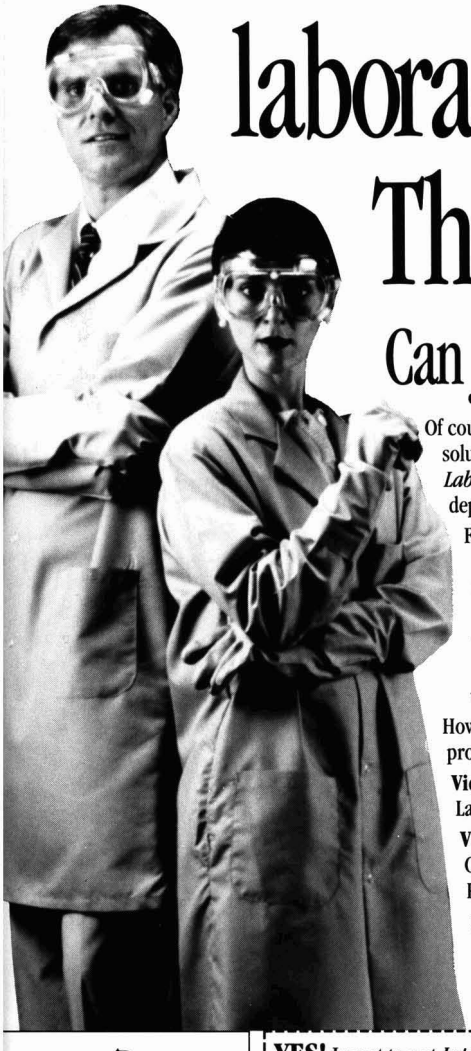

Can *you* tell the difference?

Of course not. That's why the American Chemical Society developed a ready-to-use solution to your safety training problems. Presenting *Introduction to Chemical Laboratory Safety*. It's a brand new video series designed to give chemists an in-depth overview of laboratory safety techniques.

From personal protective equipment to laboratory practices to specific techniques for handling hazardous chemicals... this video series covers safety from the working chemist's point of view. The emphasis is on proven, practical ways to incorporate safety techniques into your laboratory's daily routine.

Video One: Introduction to Laboratory Safety
Basics of chemical safety... how regulations define acceptable levels of risk

Video Two: Protection Against the Odds
How to eliminate hazards and use ventilation, containment, and personal protective equipment

Video Three: Safe Laboratory Procedures
Laboratory practices... handling chemical transfers... emergency procedures

Video Four: Chemical Safety and Environmental Regulations
OSHA regulations, the Hazard Communication Standard, Chemical Hygiene Plans, RCRA, waste disposal methods, and more!

Plus four Student Manuals! Easy-to-use student manuals serve as on-going references.

Make safety an everyday occurrence!

Produced by the American Chemical Society

For more than one hundred years, chemists have relied on the American Chemical Society for news, information, and legislative representation. Today, more than 140,000 chemists benefit from ACS services, which include scientific journals and periodicals, books, annual meetings, training programs, and much more.

YES! I want to put *Introduction to Chemical Laboratory Safety* to work for my laboratory.

Number of copies	Item	U.S. & Canada Price	Export Price
_____	Complete *Introduction to Chemical Laboratory Safety* course, including four videos and four Student Manuals *V4800*	$1,950	$2,340
_____	Video #1* *V4801*	$ 615	$ 738
_____	Video #2* *V4802*	$ 695	$ 834
_____	Video #3* *V4803*	$ 695	$ 834
_____	Video #4* *V4804*	$ 495	$ 594
_____	Additional copies of Student Manual* *V480S*	$ 28	$ 34
_____	Preview Tape	$ 25	$ 31

**One copy of the Student Manual accompanies each tape purchase.*

Total amount due $ _____

Please check method of payment:

❑ Check enclosed (payable to ACS)

❑ Bill me (with approved credit)

❑ Purchase order. Number _____

❑ Visa or MasterCard Expiration Date _____

Name of Cardholder _____

Card Number _____

Signature _____

Ship to: Name _____

Title _____

Organization _____

Address _____

City _____ State ____ Zip _____

Mail this coupon to: American Chemical Society
Distribution Office, Dept. 29
P.O. Box 57136, West End Station
Washington, DC 20037

ES&T

RESEARCH NEEDS

By Martin Alexander

The good news about bioremediation is that it can destroy toxic, hazardous, or other unwanted compounds at some sites in the field effectively and inexpensively. The bad news is, it is not currently applicable to other sites or compounds.

Nevertheless, because of the positive outcome of many bioremediation efforts, their lower costs as compared with other technologies, and the frequent absence of any undesirable products or consequences from such approaches, EPA's Bioremediation Action Committee convened a workshop in April in Washington, DC, to make recommendations to the agency. Specifically, participants were to recommend the most appropriate high-priority research needs to promote bioremediation and to devise means to overcome the constraints on the effectiveness of this technology at the more difficult sites or for the more refractory chemical mixtures. In effect, the workshop was asked

0013-936X/91/0925-1972$02.50/0

how to increase the good news and reduce the bad.

Four priority research areas

Participating in the workshop, which I chaired, were 45 specialists from the United States, Canada, and Australia, including engineers and scientists from private industry, academia, and governmental agencies. The participants' range of experience included practical work in the field, laboratory research, and government policy. They suggested four major areas for high-priority research:

- determining factors that govern the availability of pollutants for bioremediation and devising ways to increase their availability for microbial destruction;
- improving the design of processes for bioremediation;
- overcoming problems associated with scale-up from simple laboratory systems to field operations; and
- developing innovative bioremediation processes.

Microorganisms are amazingly versatile in destroying organic compounds. Probably every molecule of biosynthetic origin—and uncounted numbers of simple, complex, or novel molecules made by chemists in the laboratory or generated by industry—can be transformed by one or another bacterium, fungus, or mixture of microorganisms. The conversions may take place within or below the soil, in pristine or wastewaters, and at shallow or great depths. They occur in dilute or reasonably concentrated solutions, in aerated or anoxic environments, and at modestly low or high pH values.

Bioremediation currently is being used at highly dissimilar sites to decompose many types of pollutants. Possibly the largest such activity to date has been that in Prince William Sound to destroy oil released into the water from the *Exxon Valdez*. Hydrocarbons from leaking underground storage tanks are being destroyed, and the polluted groundwater is being freed of the unwanted compounds by enhancing microbial activity in the aquifers. Surface soils that have been tainted with a variety of materials are being cleaned by indigenous microorganisms whose activities have been promoted by various approaches used by bioremediation companies. Even sites containing some of the persistent chlorinated compounds are being remediated in these ways. Feasibility studies also are under way at many other locations and for additional compounds.

Biodegradability varies widely

The success of these bioremediation efforts, however, and the frequent ease of isolating microorganisms that degrade an array of compounds that are major environmental pollutants have resulted in the assumption by many nonspecialists that it would be simple to bioremediate nearly all sites contaminated with biodegradable molecules. Because bacteria and fungi can be readily obtained that, in the laboratory, not only metabolize these substrates but use them to support microbial proliferation, some nonspecialists believe that all that is required is to add the microorganisms to the contaminated environment and the problem is solved. Alternatively, because the indigenous biodegrading populations needed only O_2, N, or P to enhance growth on the compound or a supplemental carbon source to cometabolize it, the solution to the problem is presumed to be straightforward.

> . . .Compounds that would be destroyed by microorganisms are not easily degraded in polluted soils and aquifers.

However, the reality is quite the contrary. Many compounds that normally would be quickly destroyed by microorganisms apparently are not easily degraded in polluted soils, subsoils, and aquifers because they are not readily available. The chemicals may be sorbed, dissolved in nonaqueous-phase liquids, present in a physically inaccessible state, or bound in some way that prevents microorganisms with biodegradative enzymes from carrying out rapid transformations.

Research designed to explain and overcome the problem of poor availability to microorganisms of chemicals that are otherwise easily destroyed should make bioremediation more widely useful. Research on process design may follow many directions; the workshop recommended several different research needs for in situ bioremediation and above-ground bioreactors as well as for land treatment and composting. Scale-up from the laboratory to the field sometimes poses difficulties, and related issues were considered. In addition, because of difficulties in bioremediation of complex wastes—including those that contain substances toxic to the biodegrading microorganisms—and of compounds that are only biologically transformed by cometabolism, an exploratory program is needed to seek innovative processes for complex wastes and pollutants transformed only by cometabolism.

Although EPA convened the workshop, its recommendations are relevant to the missions of other governmental agencies' programs as well. The recommendations also should be of interest to scientists and engineers in industry and universities who are investigating means of eliminating unwanted chemicals from soils, aquifers, and surface waters. Undoubtedly, the outcome of the research will make the good news better and the bad news less frequent.

A detailed report on the workshop can be obtained from Tom Baugh, U.S. Environmental Protection Agency, RD-681, Washington, DC 20460.

Martin Alexander is Liberty Hyde Bailey Professor of Soil Science in the Department of Soil, Crop and Atmospheric Sciences at Cornell University. He is a member of the EPA Bioremediation Action Committee and the Army Science Board.

ES&T

THE GREENING OF ENVIRONMENTAL LABELING

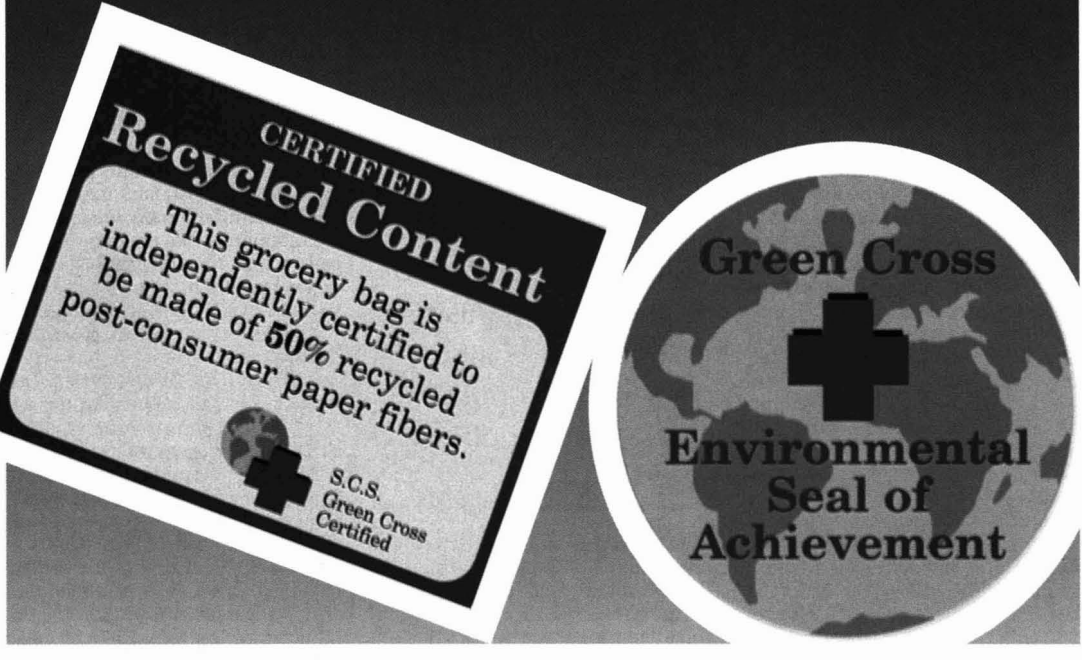

By Alan Newman

With surveys indicating that consumers are willing to pay more for "environmentally friendly" products, and manufacturers rushing to cash in on this new market, government and private agencies in many countries are developing criteria for what makes one product environmentally better than another. In a recently issued report, the Organization for Economic Cooperation and Development (OECD) has studied progress and trends towards environmental or "green" labeling within its member countries (*1*). The report, *Environmental Labelling in OECD Countries*, finds that many developed countries are well ahead of the United States in implementing national labeling programs.

Germany takes the lead

The former West Germany has taken the lead in these programs, issuing the world's first green label in 1978. Today, Germany's *umweltzeichen* (environmental label) identifies more than 3600 products in 64 product categories. A 1988 consumer poll found that nearly 80% of respondents recognized the label.

Labels are found on a wide range of goods, including retreaded tires, batteries low in hazardous substances, copiers with low emissions and that reduce waste, low-noise lawn mowers and construction machines, water-efficient plumbing materials, energy-efficient boilers and windows, and biodegradable lubricating oils.

Anyone can propose a product category. To determine a category's suitability and the appropriate criteria for awarding labels, a complex, four-step process is followed. Studies and hearings are conducted by the Federal Environmental Agency and the nonprofit Institute for Quality Assurance and Labeling (RAL).

0013-936X/91/0925-1974$02.50/0

Based on their reports, the independent, 11-member Environmental Label Jury (ELJ) decides whether to add the new category. Members of ELJ are drawn from scientific and environmental organizations, trade unions, industry, consumer groups, the German protestant church, federal states, and the news media.

Once a category is established, manufacturers submit products for labeling at their own discretion. ELJ also decides which products fit the criteria and awards labels. A legal contract signed by the manufacturer and administered by RAL finalizes the process. Because the government cannot coerce manufacturers into meeting criteria, consumer choices drive the program.

To cover costs, manufacturers pay RAL a one-time 300-DM ($190) application charge, an annual contract fee based on product sales, and contribute to a fund for advertising the label.

International view

A decade after Germany issued its first green label, Canada established its Environmental Choice labeling program following the German model. However, in running Environmental Choice the Canadian government plays a significant role.

The program is administered and legally indemnified by the Canadian Ministry of Environment. An independent, 16-member advisory board with broad-based representatives appointed by the environment minister serves as jury and final advisor on approving criteria and labels. Establishment of a product category in Canada adds an additional step to the German approach: a 60-day period for public comment before final approval.

Japan's EcoMark label program, begun in 1989, is establishing categories for products that meet specific goals such as minimization of environmental impact from product use and disposal, and significant potential for environmental improvement with product use. The program is administered within the government's environmental agency. A five-person, technically oriented committee with both governmental and nongovernmental representatives awards labels.

Other developed countries are establishing labeling programs, and OECD predicts that as many as 22 of its member countries will have some type of labeling by 1992. Of particular interest is the establishment of common standards for Norway, Sweden, and Finland under a joint Nordic Council Program, which could be a model for the European Community.

In the United States efforts to pass legislation in Congress for a national program have been defeated and, according to the OECD, are "unlikely to pass in the near future." EPA is developing voluntary guidelines for the terms "recycled" and "recyclable," and a few states have passed legislation dealing with product claims of recycling. California has gone farthest, legislating definitions for a host of terms such as "ozone-friendly" and "photodegradable."

With the U.S. government out of the picture, private organizations are implementing their own labeling programs. Green Cross Certification Company (Oakland, CA) has recently begun labeling products. According to Linda Brown, Green Cross "certifies to the consumer that the product's claims are valid and state-of-the-art." Thus the Green Cross label would accompany terms such as "recycled material" or "biodegradable." Brown says that certification is a two-way street because companies also learn the implications of environmental labels on products.

Green Cross operates as a self-funded program, charging fees for audits even if the product fails to win approval. In addition to certifying claims on labels, Green Cross will conduct life-cycle audits. In these cases, the label would certify a range of claims or "achievements" for the product.

The nonprofit Green Seal Program (Washington, DC) has yet to issue a label, but, according to spokesperson Susan Alexander, is close to finalizing standards for products such as facial tissues and re-refined motor oil using life-cycle criteria. Current funding for Green Seal comes from foundations and "concerned individuals."

A Pandora's box

Despite the potential benefits of green labeling, the implementation of these products opens a Pandora's box of decisions. For instance, OECD points out that spray deodorants without chlorofluorocarbons represent an environmental step forward, but roll-on deodorants expel no organics and could claim to be an even better environmental choice. Juries have tried to compare products that they believe compete with each other. Thus, roll-ons could be considered a different market segment than spray deodorants.

Beyond questions of criteria, the development of a category does not ensure that manufacturers will submit products for labeling. According to OECD, in Japan and Germany label applications have concentrated in only a few categories. Thus more than half of the German labels have been awarded in just four categories: paints and varnishes, gas burners, stripping agents for wastewater treatment, and recycled paper.

Labeling also raises questions about foreign trade. As part of their programs, German and Canadian representatives visit manufacturing plants to ensure compliance with labeling criteria. For products manufactured on foreign soil, the program overseers must rely on good-faith assurances from the company executives or complaints about violations from competitors. Ironically, in the late 1970s, when German paper manufacturers boycotted a label marking recycled products, it was the granting of a label to an American company that ended the opposition.

The U.S. Green Cross and Green Seal programs have found one way around the dilemma of foreign manufacturers. Green Seal has entered into an alliance with Underwriter's Laboratory (UL) which is already based in 74 countries. UL will inspect plants for Green Seal as well as provide technical support for standards. Similarly, Green Cross is employing the Canadian-based SNC Lavalin process engineering firm, which also has international branches, for plant inspections.

Nevertheless, labeling may produce some economic gains for domestic manufacturers. According to the report, at least in these early days of labeling, the main beneficiaries have been small and medium-sized companies trying to capitalize on environmental concerns. Ideally, labeling will also provide long-term benefits for the environment.

Reference

(1) "Environmental Labelling in OECD Countries"; OECD: Paris, 1991. [Available from OECD, 2 rue André-Pascal, 75775 Paris, Cédex 16, France; (33-1)45-24-82-00 or in the United States from OECD Publications and Information Center, 2001 L Street, N.W., Suite 700, Washington, DC 20036; (202) 785-0350.]

Alan Newman is an associate editor on the Washington editorial staff of ES&T.

0013-936X/91/0925-1976$02.50/0

A SEA OF CHANGE:

Monitoring the Oceans' Carbon Cycle

By David M. Karl and Christopher D. Winn

The Earth undergoes major processes of change that are reckoned in scales of decades to millennia (*1*). Most of these changes result from natural causes. During the past century, however, human activities have contributed directly to what is now considered an inevitable, detrimental change in the global environment (*2*). Although the proximate cause of this change appears to be the atmospheric accumulation of so-called "greenhouse" gases (CO_2, H_2O, NO_2, CH_4, chlorofluorocarbons) as a direct consequence of urbanization and industrialization, the ultimate cause clearly is overpopulation of our planet.

Because of their ability to store and transport large amounts of heat and to serve as a potential sink for anthropogenic CO_2, the world's oceans may play an important role in modulating global climate. Unfortunately, the rates of these fundamental processes are not well known (*3, 4*); consequently, predicting global environmental change currently is not possible. Long-term records of relevant biogeochemical parameters are essential for documenting ecosystem changes and for differentiating natural ecosystem variability from changes induced by human activities. However, long-term studies generally have been discouraged, especially in academic institutions, because of the relatively high costs involved and negative attitudes about "environmental monitoring." Consequently, time-series data are rare. Most of the time-series data currently available are based on retrospective studies such as ice core or sediment core analyses.

> "Long-term records of relevant biogeochemical parameters are essential for documenting ecosystem changes"

In 1986, the International Council of Scientific Unions (ICSU) established the International Geosphere–Biosphere Programme (IGBP): A Study of Global Change. As described by executive director and secretariat Thomas Rosswall, "IGBP will be a worldwide research effort, unprecedented in its comprehensive interdisciplinary scope, to address the functioning of the Earth system and to understand how this system is changing. The body of information generated by the IGBP will form the scientific underpinning for predictions relating to future causes and effects of global change" (*2*).

The major oceanic component of IGBP is the Joint Global Ocean Flux Study (JGOFS), established in 1987 as a core project of IGBP under the auspices of the Scientific Committee for Ocean Research (SCOR). JGOFS research will focus on the oceanic carbon cycle and its sensitivity to change, and on the regulation of the atmosphere–ocean CO_2 balance (*5, 6*). The U.S. component of JGOFS consists of five specific program elements:

- process studies designed to capture key regular events;
- time-series observations of long duration at strategic sites;
- a global survey of important oceanic properties;
- a vigorous modeling effort to assimilate results, create knowledge, and generate testable hypotheses; and
- development of an accessible, composite biogeochemical data base (*7*).

Of these program elements, the time-series studies will be crucial for assessing the baseline or mean state of oceanic ecosystems and the natural variability therein. The

Views are insightful commentaries on timely environmental topics, represent an author's opinion, and do not necessarily represent a position of the society or editors. Contrasting views are invited.

studies are prerequisites for the design of any program to measure human activity-induced global environmental change (*8, 9*).

In 1988, two U.S.–JGOFS time-series stations were established: one in the North Atlantic Ocean near Bermuda (*10*) and the other in the North Pacific Ocean near Hawaii. This article will focus on the Hawaii Ocean Time-series (HOT) program.

The oceanic carbon cycle

The ocean and atmosphere systems are closely coupled, and the flux of carbon across the air–sea interface is substantial on a global scale. It is generally believed that the oceans have removed a significant portion of anthropogenic CO_2 added to the atmosphere; however, the absolute partitioning between the ocean and terrestrial spheres is not well documented (*4*).

The cycling of carbon within the ocean is controlled by a set of reversible oxidation–reduction reactions that involve dissolved inorganic carbon (DIC) and organic matter, in which marine biota serve as the critical catalysts. Principal pathways for the production and decomposition of organic matter involve prokaryote and eukaryote oxygenic photoautotrophy and aerobic bacterial respiration, respectively (*11*). The determination of the rates and mechanisms of the removal of DIC from the ocean surface by biological processes, the export of biogenic carbon (as organic and carbonate particles) to the ocean's interior, and the sites of remineralization and burial of biogenic carbon all are important to the JGOFS program (*6*). The continuous downward flux of biogenic materials, termed the "biological pump" (*12*), is a central component of all contemporary studies of biogeochemical cycling in the ocean, and therefore, of all studies of global environmental change. Recent estimates indicate that the oceanic biological pump can remove ~ 7.4 gigatons (1 gigaton = 10^{15} g) of C per year from the oceans (*13*). This value is approximately 10–20% of global primary production, and is roughly equivalent to the annual input of CO_2 to the atmosphere by fossil fuel burning.

As the particles sink through the mesopelagic zone (200–2000 m depth), more than 90% of the exported organic matter is recycled to DIC through the combined activities of bacteria and metazoans. These intermediate-depth waters thus can be viewed a "biological filter," at least with respect to the transport of particulate organic matter. Consequently, less than 1% of the organic carbon initially produced near the ocean surface ever enters the deep sea, and only a small fraction of that amount is preserved permanently in abyssal sediments. Despite the importance of the biological pump and biological filter, we lack a detailed understanding of the structure, mechanisms, and rates of these processes. The HOT program is designed, in part, to provide a comprehensive and quantitative description of the organic carbon cycle in the upper kilometer of the North Pacific Ocean.

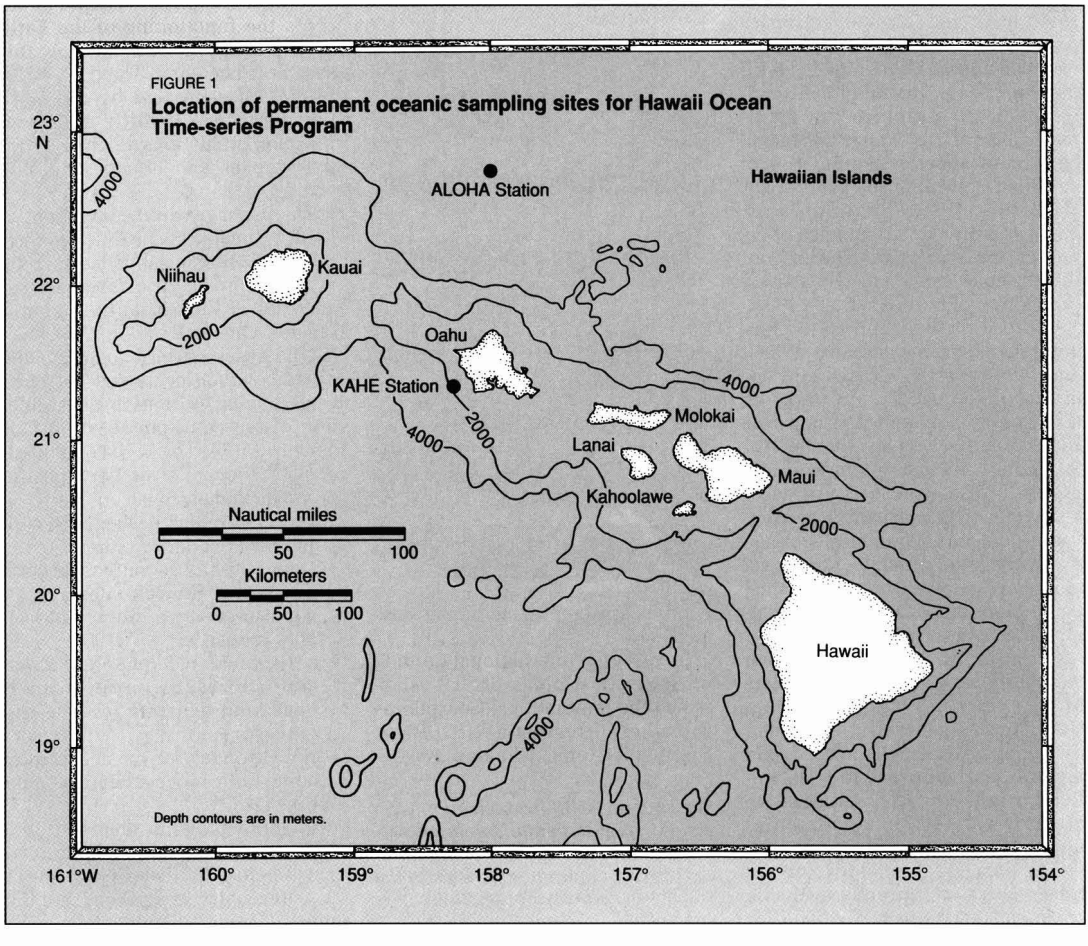

FIGURE 1
Location of permanent oceanic sampling sites for Hawaii Ocean Time-series Program

TABLE 1
Summary of Hawaii Ocean Time-series Program measurements

Parameter	Depth range (m)	Analytical procedure
Continuous profiles		
Depth (pressure)	0–4800	Pressure transducer on SeaBird CTD[a]-rosette package
Temperature	0–4800	Thermistor on SeaBird CTD-rosette package
Salinity (conductivity)	0–4800	Conductivity sensor on SeaBird CTD-rosette package
Dissolved oxygen	0–4800	Beckman polarographic sensor on SeaBird CTD-rosette package
Fluorescence	0–1000	Sea-Tech fluorometer on SeaBird CTD-rosette package
PAR[b] and natural fluorescence	0– 150	Biospherical Instruments, PNF-300
Discrete water bottle samples		
Dissolved oxygen	0–4800	Winkler titration
Dissolved inorganic carbon	0–4800	Coulometry
Dissolved nitrate and nitrite (low level)	0– 200	Chemiluminescence
Dissolved nitrate and nitrite (standard)	0–4800	Autoanalyzer
Dissolved phosphorus (low level)	0– 200	Magnesium-induced coprecipitation, spectrophotometry
Dissolved phosphorus (standard)	0–4800	Autoanalyzer
Dissolved silica	0–4800	Autoanalyzer
Dissolved organic carbon	0–1000	High-temperature oxidation, infrared detection
Dissolved organic nitrogen	0–1000	UV digestion, autoanalyzer
Dissolved organic phosphorus	0–1000	UV digestion, autoanalyzer
Particulate carbon and nitrogen	0–1000	High-temperature combustion, gas chromatography
Particulate phosphorus	0–1000	High-temperature ashing, spectrophotometer
Pigments, chlorophyll *a*	0– 200	High-pressure liquid chromatography and fluorometry
Primary production	0– 200	"Clean" ^{14}C in situ incubations
Adenosine triphosphate	0–1000	Boiling buffer extraction, firefly bioluminescence
Bacteria and cyanobacteria	0–1000	Epifluorescence microscopy
Lipopolysaccharide	0–1000	*Limulus* amoebocyte lysate assay
Sediment traps		
Total mass	150, 300, 500	Filtration and gravimetric analysis
Particulate carbon and nitrogen	150, 300, 500	High-temperature combustion, gas chromatography
Particulate phosphorus	150, 300, 500	High-temperature ashing, spectrophotometry
Identification	150, 300, 500	Brightfield[c] and epifluorescence microscopy
Calcium carbonate	150, 300, 500	Weight loss on acidification of total mass
Biogenic silica	150, 300, 500	Sample digestion, spectrophotometry

[a] Seabird is manufacturer; CTD = conductivity-temperature-depth.
[b] Photosynthetically available radiance.
[c] Visible or white light microscopy.
Note: The mention of any manufacturer or brand of any equipment or instrument does not constitute an endorsement by the authors, *ES&T*, or the American Chemical Society.

HOT site selection

The central portion of the North Pacific Ocean is the largest uniform body of water on our planet; delimited from 15° N to 35° N latitude and 135° E to 135° W longitude, it occupies approximately 20 × 10^6 km^2 of the Earth's surface. In October 1988, a permanent site, referred to as Station ALOHA (A Long-term Oligotrophic Habitat Assessment), was established about 100 km north of Oahu, HI, at 22° 45′ N, 158° 00′ W (Figure 1). Station ALOHA is in deep water (4750 m), 50 km upwind of the steep topography associated with the Hawaiian Ridge, and is relatively free of biogeochemical effects of the Hawaiian Islands. For these reasons, Station ALOHA is considered to be a valid benchmark for the study of oligotrophic oceanic processes. Station KAHE, a coastal site located off Kahe Point at the 1500-m isobath, also is routinely occupied as part of our field program.

The primary study area is characterized by warm (>24 °C) surface waters with low nitrate concentrations (<10 nM), shallow but seasonally variable mixed layers (40–100 m depth), low standing stocks of living organisms, and a persistent deep water maximum in chlorophyll concentration at approximately 100 m (*14*). As with most complex oceanic phenomena that have been investigated to date, we expect that time-series measurements of individual components of the carbon cycle will contain a substantial amount of random or "white" noise [i.e., constant variance per unit frequency (*15–17*)]. The separation of signal from noise obviously is fundamentally important to the HOT program. Variability in time and space will need to be assessed because it will be impossible to define ecosystem variability and variations rigorously without knowledge of local-scale (10–100 km) heterogeneity. Although the variability in the rates of key biogeochemical processes in the oligotrophic North Pacific Ocean on annual time scales was expected to be small relative to other marine ecosystems that are dominated by strong seasonal cycles, we already have observed considerable variability (factors of 3- to 7-fold) in key biogeochemical processes, such as rates of primary production and particle flux, during our first three years of investigation.

Core parameters

Ideally, the suite of time-series parameters should collectively provide the data base necessary for calibration and validation of existing biogeochemical models, including

local meteorology; upper ocean physics; and rates of organic particle production, export, and remineralization (Table 1). Because the magnitude of most long-enduring changes in oceanic properties is likely to be small relative to natural variability, it is essential that each measurement be made at the highest level of precision and accuracy. Therefore, well-structured quality control and assurance and interlaboratory comparison and calibration programs are crucial. Although it is straightforward to estimate analytical precision, accuracy is problematic because of a scarcity of certified reference materials for many of the desired analytes and rate processes. This becomes increasingly important as global data sets are established that comprise the collective contributions of many individual laboratories.

Our specific cruise objectives, sampling strategies, and analytical protocols are described in detail elsewhere (*14, 18*), and will be summarized here only briefly. Currently, data are collected at approximately monthly intervals during five-day research cruises; station time at ALOHA typically is 72 h. During this time, we deploy and recover a free-drifting, satellite-tracked sediment trap mooring with individual collectors positioned at depths of 150, 300, and 500 m. We also conduct a 12-h in situ primary productivity experiment using a separate radio-tracked buoy and collect discrete water samples to depths of 4700 m for specific chemical and biochemical determinations (Table 1).

During each HOT cruise, a "burst" of consecutive profiles of water temperature and conductivity from the surface to 1000 m also is made over a 36-h period to span the local inertial period (~ 31 h) and three semidiurnal tidal cycles. This sampling strategy is designed so that the high-frequency signals can be averaged to prevent these components from "aliasing" the lower frequency signals that are of greater interest to our program (*14*). During a given 36-h period, vertical displacements of isotherms and associated biogeochemical gradients in excess of 30 m typically are observed in the upper portion of the water column. This regular, periodic movement of isotherms may have important implications for primary production and particle flux by displacing light-limited, nutrient-saturated algae into the lighted portion of the water column; these effects are not routinely included in oceanic productivity models.

To understand oceanic variability more fully and to quantify secular changes, it will be necessary to collect data at each time-series station for at least a decade, and probably longer. For example, current models suggest that the magnitude of the oceanic sink for CO_2 is 2 gigatons $year^{-1}$ (*19*), a "predicted" increase of approximately 1 mmol C m^{-3} $year^{-1}$ for surface waters. This annual increase in DIC is equivalent to the current analytical precision (0.05–0.10%) in the measurement of DIC; this again emphasizes the importance of maintaining an accurate, high-precision time-series data base. Moreover, the natural annual variability in DIC concentrations at Station ALOHA exceeds this "predicted" annual increase by at least an order of magnitude. Similarly, it has been demonstrated that the seasonal variability in mixed-layer pCO_2 near Bermuda is greater than the secular pCO_2 increase measured for the 24-year period 1957–1981 (*20*). Clearly, the unambiguous demonstration of a long-term increase in surface ocean DIC or pCO_2 will require at least a decade of careful measurement.

Finally, JGOFS time-series sites also are expected to provide calibration data for remotely sensed observations (e.g., from satellites and moored instruments), deep-water laboratories for the development and testing of novel techniques and instruments, and sites for educational activities and intercomparison experiments. In the future, additional JGOFS time-series sites will be established to document regional ecosystem variability and variations in other representative oceanic provinces. For this purpose, high-latitude stations, especially in the Southern Hemisphere, will be essential for a complete understanding of the sensitivity of the oceanic carbon cycle to global environmental change.

Prospectus

Long-term, time-series studies are ideally suited to the study of slow or subtle processes, rare or irregularly spaced events, and complex phenomena (*21*), all of which are fundamental to our understanding of biogeochemical cycles in the world ocean. The HOT program already has begun to furnish a time-series data set on oligotrophic ecosystem variability, a rich source of testable hypotheses. During the initial stages of what we hope will become a long-term study, it is essential to reevaluate the experimental design to ensure that the data being collected are the most relevant to JGOFS objectives. Preliminary results from our measurements at Station ALOHA indicate variability in biogeochemical processes at frequencies ranging from hours to months. Consequently, a strategy that calls for denser sampling ultimately may be required to resolve adequately the stochastic changes that appear to control oligotrophic ecosystem dynamics.

In the near future, we will establish the capability of making continuous measurements of sea-surface meteorology, upper ocean physics, dissolved gas concentrations, ocean optics, and particle flux from bottom-moored platforms. We also anticipate enlisting the unique capabilities of an instrumented, autonomous underwater vehicle to help resolve spatial and temporal variability in physical and biogeochemical processes. Finally, the deployment of a semipermanent (3- to 6-month duration) staffed research platform at Station ALOHA, which could be serviced by helicopter or high-speed surface craft, would greatly improve our ability to document and interpret variability in biogeochemical rate processes that are not amenable to remote sensing.

A longer term goal of oceanic time-series studies will be to establish the capability of obtaining systematic global measurements of key biogeochemical parameters in a manner analogous to the World Weather Watch program for atmo-

David M. Karl is chairman of the Biological Oceanography Research Division and professor of oceanography, School of Ocean and Earth Science and Technology, at the University of Hawaii in Honolulu.

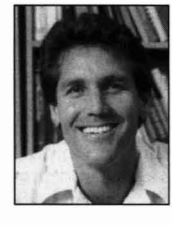

Christopher D. Winn is assistant research oceanographer, School of Ocean and Earth Science and Technology, University of Hawaii.

spheric processes (*22, 23*). The emergence of a coordinated and comprehensive global ocean observation network would provide numerous opportunities for ocean climate prediction and for basic research in oceanography.

References

(1) Committee on Earth Sciences. *Our Changing Planet: The FY 1990 Research Plan: A Report by the Committee on Earth Sciences.* The U.S. Global Change Research Program. Executive Office of the President: Washington, DC, 1989.
(2) Rosswall, T. *Environ. Sci. Technol.* **1991,** *25,* 567–73.
(3) Siegenthaler, T.; Wenk, T. *Nature* **1984,** *308,* 624–26.
(4) Tans, P. P.; Fung, I. Y.; Takahashi, T. *Science* **1990,** *247,* 1431–38.
(5) Brewer, P. G. et al. *EOS, Transactions of the American Geophysical Union* **1986,** *67,* 827–32.
(6) Scientific Committee on Ocean Research. *Joint Global Ocean Flux Study Science Plan, JGOFS Report #5;* SCOR Secretariat, Dalhousic University: Halifax, NS, Canada, 1990.
(7) U.S. Joint Global Flux Study. U.S. JGOFS Planning Report #11; JGOFS Planning Office: Woods Hole, MA, 1990.
(8) Wiebe, P. H. et al. *EOS, Transactions of the American Geophysical Union* **1987,** *68,* 1178–90.
(9) McGowan, J. A. *Trends in Ecology and Evolution* **1990,** *5,* 293–99.
(10) Knap, A. H.; Michaels, A. F. *U.S. JGOFS News* **1989,** *1,* 1–8.
(11) Karl, D. M. et al. *Nature* **1984,** *309,* 54–56.
(12) Moore, B.; Bolin, B. *Oceanus* **1987,** *29*(4), 9–15.
(13) Martin, J. H. et al. *Deep-Sea Research* **1987,** *34,* 267–85.
(14) Chiswell, S. E. et al. *Hawaii Ocean Time-series Program, Data Report #1.* University of Hawaii: Honolulu, 1990; SOEST Technical Report No. 1.
(15) Wunsch, C. *Deep-Sea Research* **1972,** *19,* 577–93.
(16) Steele, J. H. *Nature* **1985,** *313,* 355–58.
(17) Deuser, W. G. *Deep-Sea Research* **1986,** *33,* 225–46.
(18) Karl, D. M. et al. *Hawaii Ocean Time-series Program: Field and Laboratory Protocols;* University of Hawaii: Honolulu, 1990.
(19) Volk, T.; Liu, Z. *Global Geochemical Cycles* **1988,** *2,* 73–89.
(20) Todd, J. F. et al. "Atmosphere–Ocean Exchange of Carbon Dioxide: Implications for Climate and Global Change on Seasonal to Century Time-Scales"; Climate and Global Change Special Report #3; National Oceanic and Atmospheric Administration: Boulder, CO, 1990.
(21) Strayer, D. et al. *Long-Term Ecological Studies;* Occasional Publication of the Institute of Ecosystem Studies, #2; Institute of Ecosystem Studies: Millbrook, NY, 1986.
(22) Baker, D. J. *Oceanus* **1991,** *34,* 76–83.
(23) Lewis, J. K.; Passi, R. *EOS, Transactions of the American Geophysical Union* **1991,** *72,* 329–34.

ES&T

Risky Business

COMMUNICATING RISK

FOR THE GOVERNMENT

0013-936X/91/0925-1982$02.50/0

By E. Ann Cardinal

Often the government communicator hears the technical and scientific staff complain that "The public just doesn't understand the complexities of the problem." Just as often, the communicator hears from the public that "Your scientist treats me as if I'm stupid," or "You're not living this nightmare, *I* am!" As with many problems that affect the public and that need a governmental decision, scientists and the public both have legitimate claims. The problems are complex and the public does feel ill-equipped to understand the full complexity of the problem.

It would appear that there is little or no room for discussion and compromise between these two positions, but on closer scrutiny there are many areas where these two factions can agree and where the ultimate decision can benefit from the information of both sides.

Public's view of government's role

Many people see risk assessment and the management of risk, along with risk communication, as intrinsic roles of government agencies. However, the public has its own interpretation of how their government should assess, manage, and communicate risk.

The research literature on the subject indicates that the public and government scientists differ in the interpretation of "risk," especially environmental risk. A current example of this difference is how radon and asbestos are perceived.

EPA has determined that lifetime exposure to these two contaminants ranks among the highest potential environmental risks that have been identified to date and that the risks can be decreased by taking some action. The operative phrase here is "taking some action."

The Agency, working with school administrators and others, has set guidelines for managing asbestos-containing materials. The public has also taken a very active role in this process. Many schools have done tests and have determined that asbestos-containing materials exist in their buildings. After sharing this information with the teachers and parents (as they are required to do), local education officials find that only complete removal is satisfactory to the public, even though during remediation short-term exposure can actually increase. Parent organizations have demanded that schools be closed until the asbestos problem has been addressed. Where EPA has recommended just monitoring for asbestos that is neither friable nor a threat to children and workers, parents take children out of the building until the asbestos is removed.

Contrast this to the response to radon. EPA finds radon in most areas of the United States and has attempted to set safety limits in homes. In areas where very high levels of radon have been found, there are families who will not test for radon; others do test and find radon but do not remediate.

In areas with very high levels of radon in homes, EPA studies have found that some people are reluctant to test for fear they might uncover a problem requiring remediation. Still others offer explicit reasons their home will not have as severe a problem as their neighbor's, for example, the home has not been sealed as tightly as their neighbor's, or they have a basement "vent" such as an open window.

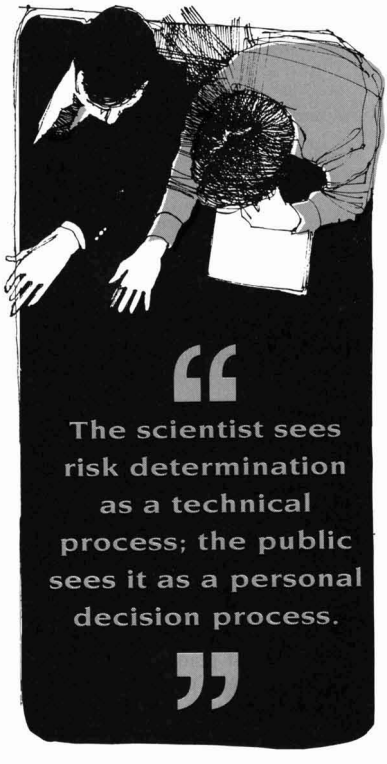

Public perception of risk

Why has the public reacted so intensely to asbestos and not to radon? As can be seen from Table 1, there are some differences in how the public perceives the problems. The most easily recognized differences are that asbestos can easily be seen, whereas radon cannot; radon is naturally occurring, whereas the asbestos material used in schools is considered nonnatural; homes are assumed to be safe—a parent would not knowingly subject his or her family to a hazard; and asbestos workers are known to get cancer, whereas there have been no "documented" cancers from radon.

People have made decisions about these two contaminants for some very common-sense reasons. Every day we make decisions about risky activities through a similar process. We first evaluate the risks involved in a particular activity, comparing this activity with past activities in which we have participated or with which we are familiar. We might talk with friends, neighbors, or a trusted expert. We then decide if the consequence of the activity is worth the risk.

If we find that an activity is very risky, our concern about it will be high and we may not do it or will take increased precautions. If we decide that the activity is low in risk, then our concern will also be low and we will probably participate in the activity without much precaution. It is important to keep in mind that this process can take seconds for a familiar activity or it can take several weeks or months for an unfamiliar activity.

To governmental technical and scientific staff, many of the public's reactions to government decisions seem out of line with the facts. Because it is based on education and access to information, the government's decision may be very different from the public's; this can cause havoc in the professional's life.

Government employees may be subjected to verbal and written abuse because of their own or an agency's position. The decision may be challenged by the press, by Congress, and even by superiors and peers. Professionals may find themselves at odds with friends, neighbors, and family. Even though their job descriptions may not say "communicator," most government employees—technical, scientific, legal, policy, press, or other—are likely to be asked to communicate some risk information to the public some time in their career.

The public believes that government has a basic responsibility to share all information on any action that it takes to protect the community. On the other hand, scientists and government agency officials con-

tend that information that has not been scientifically validated is not legitimate information.

If the government withholds information—no matter how preliminary—it is perceived by the public as not being truthful. If the government gives preliminary information that is later found to be erroneous, the public accuses the government of causing unnecessary alarm.

The scientist sees risk determination as a technical process; the public sees it as a personal decision process. The chart developed by Krimsky and Plough (Table 2) shows why public often reacts with anger and frustration to the government's comment that the risk is "negligible" or "acceptable." In their research, Krimsky and Plough found striking differences between how the public responds to scientific information and how the scientist views evidence. Technical rationales put everything in the third person. However, the cultural rationale personalizes all activities (e.g., the IRS always picks on the "little guy"). The technical rationale for controversy in science assumes that science will ultimately find a resolution and therefore the public need not worry. On the other hand, the public views scientific controversy as another reason for not trusting science to be able to answer public issues. The public perception of which expert to trust may have little or no relationship to the credentials of any of the "experts."

The scientist believes in and accepts structured scientific evidence as the basis for decisions, whereas the public tends to distrust scientific answers that cannot fully explain all their concerns. Consequently, the public will rely on familiar, personally known, and trusted friends with local knowledge to interpret the relevance of scientific information. As individuals we tend to rely on friends and local acquaintances to obtain information about some unfamiliar activity (e.g., in a new neighborhood, where to get your car fixed or hair cut). Local communities perceive that experts do not know the specific circumstances of their situation and therefore cannot judge what is best for their community (e.g., road designs, shopping centers, new home developments).

TABLE 1
Risk characteristics as perceived by the public for radon and asbestos

Radon	Asbestos
No perceptible cues	Visible
Naturally occurring	Nonnatural
No villain	Villain
Benign encounter	Benign encounter
Home/personal	School/public
Delayed effects	Delayed effects
Effects occur without drama	Worker lawsuits
Cannot prove cause of cancer	Known cause of cancer
Remediation cost to individual	Remediation cost to public

TABLE 2
Rationales used in assessing risk

Technical	Cultural
Trust in scientific methods, explanations, evidence	Trust in political culture and democratic process
Appeal to authority and expertise	Appeal to folk wisdom, peer groups, and traditions
Boundaries of analysis are narrow and reductionist	Boundaries of analysis are broad, include the use of analogy and historical precedent
Risks are depersonalized	Risks are personalized
Emphasis on statistical variation and probability	Emphasis on the impacts of risk on the family and community
Appeal to consistency and universality	Focus on particularity; less concerned about consistency of approach
Where there is controversy in science, the status quo is maintained	The public's response to scientific differences is, we will choose which one to believe
Those impacts that cannot be measured are less relevant	Unanticipated or unarticulated risks are relevant

Source: Krimsky and Plough.

Communicating risk to the public

Can the government ever predict how the public will react to information about a potential risk? Yes, if, early in the activity, communication planning is incorporated into the process according to a set of EPA guidelines published in April 1988 labeled the "Seven Cardinal Rules of Effective Risk Communication." Although they appear ineffective at first glance, use of these rules will help government staff communicate with the public:

- Accept and involve the public as a legitimate partner. Government must accept that the public has legitimate concerns, even when the community is angry. Do not become defensive; instead, encourage the public to discuss relevant facts. It may be necessary to meet with certain individuals to discuss personal problems.
- Plan carefully and evaluate your effort. Technical staff must work with the public affairs/outreach staff. Too often what appears to be a nonissue to a technical person becomes a headline story to the press officer. Government should speak with a single voice in order not to confuse and cause greater concern. Evaluate each planned activity so that the experiences will enable the agency to better prepare the next plan.
- Listen to the public's specific concerns. Technical and public/outreach staff must be quiet and listen not only to *what* is being said but *how*, the context of the discussion, the hidden meanings of the anger, and observe the body language. What appears to be an individual health issue may be a property issue to the larger community. Remember, no community is completely unified on a specific issue; however, the spokesperson for a particular group will attempt to convince the government that he or she speaks for the majority.
- Be honest and frank, but you do not have to tell all. Omit discussions that occurred prior to the final decision and every nuance of each issue that might affect the outcome. Nor should agency representatives always say, "I don't know," because you are obligating yourself and your agency to find-

ing the answer. Even though you wrote a highly technical report, the public really doesn't care; they only want to know the outcome.

- Coordinate and collaborate with other credible sources; otherwise it will be difficult to get these sources on board later. It is likely to appear to the public that you are attempting to justify your actions after the fact. Also, credible sources may find it hard to reconstruct all your decision steps.
- Meet media needs by having technical staff work with the press staff to ensure that accurate and timely information is given, and that the appropriate technical staff will be available for clarification. Early discussions with press staff can help in getting the word out to a large number of people at a specific time.
- Speak clearly and with compassion. Choose the appropriate staff to talk with the public and press. There should be "dry-run" presentations. The spokespersons must understand why there is concern or controversy and be well versed in the topic and comfortable with their role in the communication process. (If you do not agree with the decision, you probably should not be the one to communicate it.)

Risk communication is difficult because everyone will interpret every word using his or her individual definition. Because the concept of risk is difficult to understand, and because there are many different interpreters of the information, the government risk communicator must understand the concerns of the government and the public. Government staff must also understand that though it may appear that members of the public do not understand, they often do, and they have probably made their decision on the risk issue. They just choose not to agree with the government.

Additional reading

Communicating Radon Risk Effectively: A Mid-Course Evaluation; U.S. Environmental Protection Agency: Washington, DC, July 1987; EPA-230-07-89-029.

Evaluation and Effective Risk Com munications Workshop Proceedings; Interagency Task Force on Environmental Cancer and Heart and Lung Disease. U.S. Environmental Protection Agency: Washington, DC, January 1991; EPA/600/9-90/054.

Krimsky, S.; Plough, A. *Environmental Hazards: Communicating Risks as a Social Process*; Greenwood: Westport, CT, 1988.

Improving Risk Communication; National Research Council; National Academy Press: Washington, DC, 1989.

National Research Council. *Improving Risk Communication*; National Academy Press: Washington, DC, 1989.

Risk Communication About Chemicals in Your Community; U.S. Environmental Protection Agency: Washington, DC, December 1989; EPA-230/09-89-067.

Risk Communication Training Course Materials; U.S. Environmental Protection Agency: Washington, DC, 1989.

Summary Report of Radon Outreach Workshop; U.S. Environmental Protection Agency, Region III: Washington, DC, May 1990.

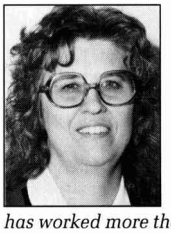

E. Ann Cardinal is program manager, Communications and Outreach, for Dynamac Corp., Rockville, MD. Formerly she was chief of Superfund community relations, EPA Region III. She has worked more than 20 years as a consultant, public interest group representative, and citizen activist.

ESET

REGULATING ENVIRONMENTAL CARCINOGENS:

Where do we draw the line?

0013-936X/91/0925-1986$02.50/0

By David C. Kocher and F. Owen Hoffman

We believe there is a fundamental problem with current regulatory policies for limiting routine exposures of the public to radionuclides and other carcinogens. Specifically, there is a clear inconsistency in the levels of acceptable health risk associated with (1) standards for radionuclides only developed under authority of the Atomic Energy Act and (2) standards developed under authority of other laws for all carcinogens, including radionuclides, or for chemical carcinogens only.

We first discuss the apparent inconsistencies in levels of acceptable risk associated with the two categories of standards described above. We then propose a set of principles, based on distinguishing unambiguously between unacceptable and trivial risks, which could provide more consistent regulation of carcinogenic risks to the public. Our proposed regulatory framework takes into account such important factors as costs of risk reduction in relation to benefits in risks averted, technical feasibility, and societal concerns (e.g., public perceptions of risk).

The Atomic Energy Act

The current framework for regulating radiation exposures of the public under authority of the Atomic Energy Act may be referred to as a "top-down" approach. This approach has two components (*1–4*). First, a limit on radiation dose to individuals from all sources of exposure except natural background, corresponding to an *upper bound* on acceptable risk, is established in radiation protection standards. Then, doses are *reduced* below the limit by requiring that exposures be kept "as low as reasonably achievable" (ALARA). In applying the ALARA principle to risk reduction, such factors as cost versus benefit, technical feasibility, and societal concerns are taken into account.

Dose limits in radiation protection standards for the public (*1–4*) correspond to a limit on acceptable lifetime risk from all nonnatural radionuclides of 5×10^{-3} (*2*). However, the development of many standards that specify lower dose limits for specific practices or sources (*5, 6*) and that represent an application of the ALARA principle virtually ensures that the lifetime risk from all nonnatural radionuclides will not exceed 10^{-3} (*1, 2*).

Regulations under other laws

The current framework for regulating exposures of the public to chemical carcinogens, and for regulating radiation exposures under laws other than the Atomic Energy Act, is the opposite of that described above and may be referred to as a "bottom-up" approach. In this approach, there is no standard that defines an upper bound on acceptable risk from all carcinogens and sources of exposure. Rather, for specific exposure situations only (*7, 8*), a *lower bound* on acceptable risk is established as a goal, and this goal then may be *increased* to reflect risks that reasonably can be justified. Examples are described below.

Zero risk was established as a goal by both the Delaney Clause of the Federal Food, Drug and Cosmetic Act Food Additives Amendment of 1958, which addresses carcinogenic food additives (e.g., pesticides), and by standards for radionuclides and chemical carcinogens in drinking water developed under the Safe Drinking Water Act (*9*). However, these goals have been relaxed, based on considerations of cost and technical feasibility, to permit lifetime risks of 10^{-6} for pesticides (*7*) and 10^{-4}–10^{-6} for carcinogens in drinking water (*6, 9, 10*). Acceptable risks of 10^{-4}–10^{-6} also have been embodied in standards developed under the Clean Air Act for airborne emissions of radionuclides and other carcinogens (*11, 12*) and in standards developed under the Comprehensive Environmental Response, Compensation, and Liability Act (CERCLA) for cleanup of hazardous substances (*13*).

Regulatory inconsistency

The "top-down" approach to regulating exposures to radionuclides under the Atomic Energy Act clearly is fundamentally different from the "bottom-up" approach to regulating exposures to radionuclides and other carcinogens under other laws. As a result, upper bounds on risks to the public regarded as "acceptable" in the two cases clearly are inconsistent—that is, lifetime risks of 10^{-3} or greater in the former, but 10^{-4}–10^{-6} in the latter.

This inconsistency is particularly apparent for disposal of low-level radioactive waste. For disposals permitted under the Atomic Energy Act (*14, 15*), limits on radiation dose to hypothetical inadvertent intruders onto disposal sites correspond to limits on lifetime risk in the range 5×10^{-3} to 2×10^{-2}. However, for past, unpermitted disposals subject to cleanup under CERCLA, current standards include a maximum lifetime risk to intruders of 10^{-4}–10^{-6} as a goal for remediation (*13*). This difference in acceptable risks for virtually identical practices seems quite illogical.

Proposal for consistent regulation

We believe that the fundamental inconsistency in current approaches to regulating exposures of the public to radionuclides and other carcinogens described above can be reconciled and that a reasonable basis for more consistent regulation of risks from all carcinogens can be developed. Our proposed regulatory framework, shown in Figure 1, contains three basic elements:

- A *de manifestis* lifetime risk in the range 10^{-1}–10^{-3}, which would define an upper bound on acceptable risk from all carcinogens and sources of exposure and above which regulatory action would be taken to reduce risks regardless of cost;
- A *de minimis* lifetime risk in the range 10^{-4}–10^{-6}, which would define risks from any carcinogen and source of exposure so trivial that regulatory action to reduce risks would be unwarranted; and
- For lifetime risks above *de minimis* levels, reduction of risks based on application of the ALARA principle.

Regarding the third element, we would emphasize that a *de minimis* risk is *not* the goal of ALARA (*1*).

The elements of this proposal are not new. A *de manifestis* risk and reduction of risks using the ALARA principle are fundamental tenets of radiation protection (*1–4*). For chemical carcinogens, all elements have been embodied in many decisions on whether or not to reduce risks by regulatory action, albeit only implicitly and on an ad hoc basis (*7*). However, in contrast to current regulatory policies for radionuclides or chemical carcinogens, we believe that all elements should be adopted as an explicit set of principles for regulating risks to the public from *all* exposures to *any* carcinogens.

The key to our proposal is to recognize that the lifetime risks of 10^{-4}–10^{-6} embodied in some standards are *de minimis* rather than *de manifestis* levels. This interpretation is clearly supported by an analysis that showed that regulatory authorities usually have not acted to reduce risks from chemical carcinogens

when the risk to a few individuals is below 10^{-4} and the average risk in large populations is below 10^{-6} (*7*). We believe that acceptance of lifetime risks of 10^{-4}–10^{-6} as *de minimis* is the only reasonable way to reconcile the "top-down" and "bottom-up" approaches currently used in regulating exposures of the public to radionuclides and other carcinogens.

The use of ranges for the *de manifestis* and *de minimis* risks would permit taking into account the size of an exposed population; that is, higher levels could be used when only a few individuals are at risk, but lower levels could be used for large populations (*7*). In addition, the proposed ranges for these risks permit considerable flexibility in accommodating the kinds of subjective societal judgments involved in applying the ALARA principle to particular exposure situations. Therefore, absolute uniformity of regulatory decisions for limiting carcinogenic risks to the public would not be required.

Discussion and conclusions

The proposed *de manifestis* and *de minimis* risks to the public are consistent with

- radiation protection standards for all nonnatural radionuclides (*1–4*),
- standards for exposure to naturally occurring radionuclides in uranium and thorium mill tailings (*16*), which correspond to a lifetime risk greater than 10^{-2} (*2, 6*),
- guidances on remedial action levels for exposure to natural background radiation, principally external radiation and radon decay products (*1, 17*), which correspond to risks of 10^{-2} or greater (*2, 17*),
- many regulatory decisions on whether or not to reduce risks from chemical carcinogens (*7*), and
- proposed exemption levels for radiation exposure (*1, 18, 19*), which correspond to risks of about 5×10^{-5}.

Our proposal also could be applied to accidental exposures to any carcinogens. Indeed, the *de manifestis* risks are consistent with guidelines for undertaking responses to radiation accidents (*20–22*), which correspond to risks of about $1–4 \times 10^{-3}$, and with the action level for PCBs in fish (*23*), which corresponds to a risk of about 10^{-3}.

Thus, our proposed regulatory framework is consistent with virtually all regulatory policies for limiting routine and accidental exposures of the public to radionuclides and other carcinogens. Again, however, this consistency is achieved only if the lifetime risks of 10^{-4}–10^{-6} embodied in some standards are interpreted as *de minimis*.

We believe that more consistent regulation of risks to the public from radionuclides and other carcinogens along the lines proposed here has two obvious benefits. First, it would encourage consideration of

FIGURE 1
Proposed framework for regulating exposure of the public to radionuclides and chemical carcinogens[a]

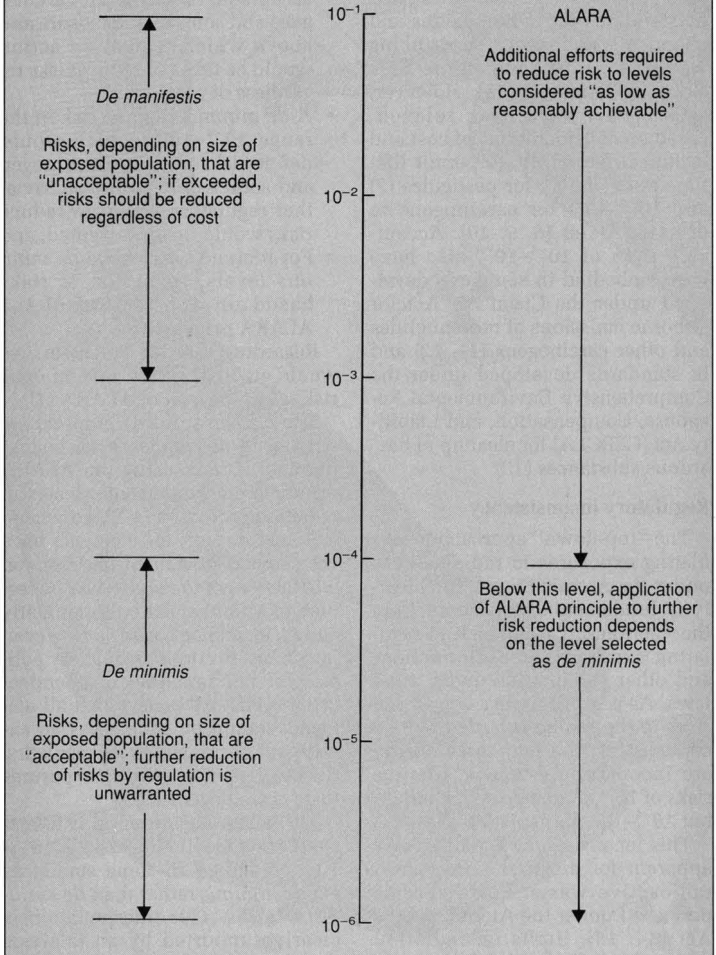

[a] The vertical scale denotes lifetime risk of stochastic health effects. Possible measures of risk include fatal cancers and hereditary effects, cancer incidence, or fatalities plus weighted nonfatal cancer incidence (*2*).

David C. Kocher is on the research staff in the Health and Safety Research Division at Oak Ridge National Laboratory. He has a Ph.D. in physics from the University of Wisconsin. He is currently working on environmental radiological assessments and the technical basis for radiation standards.

F. Owen Hoffman is on the research staff in the Environmental Sciences Division at ORNL. He has a Ph.D. in ecology from the University of Tennessee. His current research is on the validation and evaluation of methods for predicting transport and risk of radioactive and other potentially harmful substances in the environment.

risks from any carcinogen and source of exposure in the context of risks from all sources, as opposed to the rather piecemeal approach embodied in past regulatory decisions, particularly for chemical carcinogens (*7*).

Second, the proposed *de manifestis* risks are consistent with risks from naturally occurring carcinogens, which average about 10^{-2} for radionuclides (*2, 24*) and greater than 10^{-3} for other carcinogens (*25*). Therefore, the proposed *de minimis* levels would ensure that risks much lower than unavoidable background risks do not receive unwarranted attention.

References

(1) "Recommendations on Limits for Exposure to Ionizing Radiation"; National Council on Radiation Protection and Measurements; Report No. 91; NCRP: Bethesda, MD, 1987.

(2) International Commission on Radiological Protection Publication 60; *Ann. ICRP* **1991,** *21*(1-3), 1–201.

(3) "Radiation Protection of the Public and the Environment"; Department of Energy: Washington, DC, 1990; Order 5400.5.

(4) Nuclear Regulatory Commission. 10 CFR Part 20, *Fed. Regist.* **1991,** *56,* 23360–470.

(5) Mills, W. A. et al. "A Compendium of Major U.S. Radiation Protection Standards and Guides: Legal and Technical Facts"; Oak Ridge Associated Universities: Oak Ridge, TN, 1988; Report ORAU 88/F-111.

(6) Kocher, D. C. *Nuclear Safety* **1988,** *29,* 463–75 .

(7) Travis, C. C. et al. *Environ. Sci. Technol.* **1987,** *21,* 415–20.

(8) Travis, C. C.; Pack, S. R. Hattemer-Frey, H. A. *Health Phys.* **1989,** *56,* 527–31.

(9) U.S. Environmental Protection Agency; 40 CFR, Parts 140–49; U.S. Government Printing Office: Washington, DC, 1990; pp. 553–638.

(10) "Health Effects Assessment Summary Tables"; U.S. Environmental Protection Agency: Washington, DC; October 1989; Report OERR 9200.6-303-(89-4).

(11) U.S. Environmental Protection Agency. 40 CFR Part 61, *Fed. Regist.* **1989,** *54,* 38044–82.

(12) U.S. Environmental Protection Agency. 40 CFR Part 61, *Fed. Regist.* **1989,** *54,* 51654–715.

(13) U.S. Environmental Protection Agency. 40 CFR Part 300, *Fed. Regist.* **1990,** *55,* 8666–8865.

(14) Nuclear Regulatory Commission. 10 CFR Part 61, *Fed. Regist.* **1982,** *47,* 57446–82.

(15) "Management of Low-Level Waste"; Department of Energy: Washington, DC, 1988; Order 5820.2A, ch. III.

(16) U.S. Environmental Protection Agency. 40 CFR, Parts 190–259; U.S. Government Printing Office: Washington, DC, 1990; pp. 16–23.

(17) "A Citizen's Guide to Radon"; U.S. Environmental Protection Agency and Department of Health and Human Services. U.S. Government Printing Office: Washington, DC, 1986; Report OPA-86-004.

(18) "Principles for the Exemption of Radiation Sources and Practices from Regulatory Control"; International Atomic Energy Agency: Vienna, 1988; Safety Series Report No. 89.

(19) Nuclear Regulatory Commission. *Fed. Regist.* **1990,** *55,* 27522–37.

(20) Food and Drug Administration. *Fed. Regist.* **1982,** *47,* 47073–84.

(21) "Manual of Protective Action Guides and Protective Actions for Nuclear Incidents"; U.S. Environmental Protection Agency: Washington, DC, 1990; Report EPA/520/1-75-001.

(22) International Commission on Radiological Protection Publication 40; *Ann. ICRP* **1984,** *14*(2), 1–22.

(23) Food and Drug Administration *Fed. Regist.* **1983,** *49,* 21514–20.

(24) "Ionizing Radiation Exposure of the Population of the United States"; National Council on Radiation Protection and Measurements: Bethesda, MD 1987; Report No. 93.

(25) Travis, C. C.; Hester, S. T. *Risk Analysis* **1990,** *10,* 463–66.

Acknowledgments

Research sponsored by the U.S. Department of Energy under contract DE-AC05-84OR21400 with Martin Marietta Energy Systems, Inc.

Competitiveness and environmental quality

Alvin L. Alm

The competitive position of U.S. industry in the world market represents the most serious long-term problem afflicting the U.S. economy. Recessions will come and go, but as the world moves to a global economy, the U.S. competitive position will be critical to our economic well-being. Countries that have lost their competitive edge, such as Great Britain, will have a lower national income than other Western nations.

The ability of U.S. firms to compete will be based heavily on developing and maintaining strong positions in certain domestic markets, the quality of the U.S. labor force and educational system, the success of technological development, and the ability of our firms to upgrade quality. The determinants of a competitive edge are clearly set forth in a brilliant book, *The Competitive Advantage of Nations,* by Michael Porter of the Harvard Business School. Porter concludes that true success in global markets flows from innovation sparked by competitive domestic markets, availability of discriminating customers, and overcoming of short-term obstacles. Countries seeking true competitive advantage must aim for quality and service, not rely on low-cost labor or natural resource advantages. Porter does not believe higher environmental costs threaten the competitive position of the United States, but rather that they stimulate innovation.

Porter's view is not the conventional wisdom among economists and business people, some of whom argue that environmental expenditures add to the cost of U.S. goods, reducing their competitiveness in international markets. Proponents of this view conclude that the United States should impose less stringent standards or that other nations should be cajoled into establishing higher environmental standards.

Economic models

These views are buttressed by macroeconomic models that show poor economic performance caused by the imposition of environmental standards. But these models do not take into account the benefits of reducing the exposure of people and ecosystems to pollution. [See Regulatory Focus, Oct. issue, p. 1685.] For example, macroeconomic models portray production of cigarettes as a positive economic contribution, whereas measures to control unhealthy air pollutants are portrayed as a reduction to economic growth. This portrayal is particularly ironic because U.S. health costs are fast spiralling out of control, resulting in a significant reduction in productivity. The "productive" activity of producing cigarettes is not helping the matter, whereas reduction of air pollution is. I am not suggesting that cigarette production be banned, but we should account for its costs, just as we need to account for environmental benefits.

There is no way to correctly account for all the environmental benefits that flow from environmental requirements. We can only infer that the benefits must be close to or greater than costs, because the highest environmental expenditures, by far, are incurred in the countries with the healthiest economies.

On the margin, environmental costs may adversely affect trade for a few firms in a few industries, particularly in the extractive industries. The question is whether the worldwide concern over the environment will help or hurt the United States' competitive position in the long term.

According to Porter's thesis, tight environmental standards should help. Over the years, U.S. firms have developed technologies and services to characterize environmental problems and clean them up. Currently, the United States is far ahead of most other countries in providing environmental products and services. The U.S. environmental market has all the characteristics that should lead to global success, including discriminating customers, fierce domestic competition, and a well-trained work force.

What the government can do

What, if anything, should the government do to promote environmental markets in the future? First and foremost, the government should provide leadership in international environmental activities and aggressively support domestic environmental programs. As long as U.S. standards represent the "wave of the future," development of a domestic environmental control market should enhance export possibilities. Second, support for R&D and testing of domestic technology should help bring new products and technologies on line. Third, the government should positively promote exports to help get U.S. expertise in front of potential customers.

If the Michael Porter thesis is correct, the United States has a tremendous opportunity to develop a strong competitive position for environmental products and services. Considering the prize—a market estimated at $200 billion and growing—it is hard to ignore the allure of foreign environmental markets.

Alvin L. Alm is director and senior vice-president for energy and the environment for Science Applications International Corp., a supplier of high-technology products and services related to the environment, energy, health, and national security.

0013-936X/91/0925-1993$02.50/0

ES&T BOOKS

Policy Implications of Greenhouse Warming. National Academy of Sciences. National Academy Press, 2101 Constitution Avenue, N.W., Washington, DC 20418. 1991. xiii + 127 pages. $14.95 ($18, foreign), paper.

Policy Implications of Greenhouse Warming addresses a wide range of issues such as energy policy, deforestation, population growth, and the proper role of the United States in an international strategy. Research needs also are discussed, as are social and economic impediments to responses to the threat of global warming.

Biosynthesis and Biodegradation of Cellulose. Candace H. Haigler and Paul J. Weimer, Eds. Marcel Dekker, 270 Madison Ave., New York, NY 10016. 1991. xi + 684 pages. $175, cloth.

The enzymatic breakdown of cellulose could be a path toward the economical production of renewable fuels. *Biosynthesis and Biodegradation of Cellulose* explains the occurrence, functions, and production of cellulose in plants, and continues with discussions of the breakdown of cellulose by cellulase enzymes and by other means.

Acidic Deposition and Aquatic Ecosystems: Regional Case Studies. Donald F. Charles, Ed. Springer-Verlag, 175 Fifth Ave., New York, NY 10010. 1991. xii + 747 pages. $98, cloth.

Acidic Deposition and Aquatic Ecosystems explains acid deposition's path to waters and what its effects on waters and aquatic biosystems are. Case studies cover parts of the United States, including the Adirondack Mountains (NY), New England, Florida, and the Sierra Nevada and Cascade Mountains of the West. Long-term trends in water chemistry are discussed in one contributed paper.

Harnessing Science for Environmental Regulation. John D. Graham, Ed. Praeger Publishers, One Madison Ave., New York, NY 10010. 1991. viii + 242 pages. $39.95, cloth.

Harnessing Science for Environmental Regulation takes the position that advice from experts outside government "is critical to the competence and credibility of regulations designed to protect public health." The book examines three organizations formed to improve regulatory science: The Chemical Industry Institute of Toxicology, the Science Advisory Board of EPA, and the Health Effects Institute.

International Journal of Energy, Environment and Economics. T. Nejat Veziroglu, Ed. Nova Science Publishers, 283 Commack Rd., Suite 300, Commack, NY 11725-3401. 1991. Quarterly. $95 for individuals, $145 for libraries.

Among topics in the first issue are clean coal combustion, reduction of gaseous pollutant emissions, greenhouse effect, flywheel energy storage, trends in nonrenewable energy, and oceanic sinks for anthropogenic CO_2. The editor is director of the Clean Energy Research Institute of the University of Miami (FL).

Chemical Ecotoxicology. Jaakko Paasivirta. Lewis Publishers, 2000 Corporate Blvd., N.W., Boca Raton, FL 33431. 1991. 155 pages. $49.95; $60 outside United States, cloth.

Topics include cycles of chemicals in the environment, risk assessment and management, analysis of trace chemicals, organohalogens, mercury, oil residues in the environment, and forestry industry emissions. Author's work was described in *ES&T* [1988, *22*(9), 998].

Understanding Computer Use in Ground Water Science. National Water Well Association. NWWA Bookstore, P.O. Box 182039, Dept. 017, Columbus, OH 43218. 1991. $31.25 ($25 for NWWA members; add $3 for shipping and handling). Catalog No. K810.

This latest addition to the NWWA anthology series contains 24 papers on subjects such as aquifer analysis, pumping tests, chemistry, contaminant transport, regional hydrology, statistics, the unsaturated zone, and how computers are used to solve groundwater-related problems.

Environmental Biotechnology for Waste Treatment. Gary S. Sayler, Robert Fox, and James W. Blackburn, Eds. Plenum Publishing, 233 Spring St., New York, NY 10013-1578. 1991. 298 pages. $52.50 ($63 outside United States and Canada).

Environmental Biotechnology for Waste Treatment aims to integrate the latest engineering applications with the newest research advances. Topics include efficient agents for microbial degradation, bench-scale demonstrations of biodegradation of carcinogenic hydrocarbons, and microbiological aspects of bioremediation and biorestoration.

Microbial Production and Consumption of Greenhouse Gases: Methane, Nitrogen Oxides, and Halomethanes. John E. Rogers and William B. Whitman, Eds. American Society for Microbiology, 1325 Massachusetts Ave., N.W., Washington, DC 20005. 1991. 298 pages. $59.

Carbon dioxide is not the only gas that is suspected of causing global warming; gases such as methane, halomethanes, and NO_x also share the blame, according to many scientists. Papers in this book examine the microbial production and consumption of these gases and what role they and CO_2 will play in global warming.

Environmental Management in Developing Countries. Organization for Economic Cooperation and Development. OECD Publications and Information Center, 2001 L St., N.W., Suite 700, Washington, DC 20036-4910. 1991. $52.

This volume consists of papers from a Development Centre Seminar for practitioners and researchers from developing countries. It takes stock of the issues and practices of environmental management in a development context, as well as special difficulties faced by developing countries.

OSHA Technical Manual, second ed. Government Institutes, Inc., 4 Research Pl., Suite 200, Rockville, MD 20850. 1991. 265 pages. $63

0013-936X/91/0925-1994$02.50/0

($65 outside United States; prices include shipping), paper.

This updated edition provides technical guidance, especially for newly covered areas such as indoor air, hospitals, construction sites, and oil wells. Topics include sampling for surface contamination, shipping and handling of samples, personal sampling for air contamination, protective clothing, noise, and injuries.

The Dose Makes the Poison: A Plain-Language Guide to Toxicology, second ed. M. Alice Ottoboni. Van Nostrand Reinhold, 115 Fifth Ave., New York, NY 10003. 1991. $24.95.

Are chemicals in our air, food, and water harmful, and if so, to what degree? Effects of chemicals at home and at work are presented in layman's language. Topics include the way those chemicals that cause harm do so, what influences degrees of toxicity, paths of exposure, carcinogenesis, and teratogenesis. The author has been a staff toxicologist with the California State Department of Public Health.

Receptor Modeling for Air Quality Management. P. K. Hopke, Ed. Elsevier, P.O. Box 882, Madison Square Station, New York, NY 10159. 1991. x + 330 pages. $157.

This book examines the background and application of receptor models for source identification and quantitative mass apportionment of airborne pollutants. Ambient and source sampling are discussed, together with commonly used models, recent advances in this field of modeling, and the perspective of regulators on how models fit into the development of an air quality management plan. The book's aim is to furnish a guide to implementing receptor modeling as part of a management plan.

The Water Encyclopedia. Frits van der Leeden, Fred Louis Troise, and David Keith Todd, Eds. Water Information Center, 125 E. Bethpage Rd., Plainview, NY 11803. 1991. 800 pages. $135.

The aim of *The Water Encyclopedia* is to answer almost every statistical question that might be asked about water in one book, thereby eliminating the need to hunt through textbooks, journals, reports, and government publications.

ES&T MEETINGS

Jan. 8–10, 1992 Knoxville, TN
Molecular Biology for Environmental Scientists and Engineers
Center for Environmental Biotechnology

Workshop is designed for nonbiologists and will emphasize DNA structure and repair, mutagenesis, recombinant DNA, and related environmental issues. Attendance will be limited to 40 persons.

Fee is $135. Sue Markland Day, Center for Environmental Biotechnology, 10515 Research Dr., Suite 100, Knoxville, TN 37932; (615) 675-9450.

Jan. 14–16 Cambridge, MA
The World at Risk: Natural Hazards and Climate Change
Massachusetts Institute of Technology

Topics will highlight predicting hazards affected by climate change, outlining strategies for prevention or adaptation to such hazards, and engineering and governmental responses.

Fee is $50. Anne Slinn, Center for Global Change Science, MIT, Building 54-1312, Cambridge, MA 02139; (617) 253-4902; fax (617) 253-0354.

Jan. 15-17 Orlando, FL
International Conference on Hazard Identification and Risk Analysis, Human Factors, and Human Reliability in Process Safety
American Institute of Chemical Engineers

This conference will examine oil spills, occupational hazards, fires that involve toxic materials, human exposure, hazards caused by trace substances, and fault analysis.

Fee is $595. ETA, P.O. Box 2008, Westfield, NJ 07090; (908) 233-2300; Fax (908) 233-2015.

Jan. 22–24 Arlington, VA
EPCRA/SARA Title III Compliance Update; Form R Workshop; Data Management
Government Institutes, Inc.

These three seminars cover crucial aspects of the Emergency Planning and Community Right-to-Know Act (EPCRA), including compliance with EPCRA and managing Section 311, 312, and 313 data.

Tim Hohman, Government Institutes, Inc., 4 Research Pl., Suite 200, Rockville, MD 20850; (301) 921-2345.

Jan 27–31 Austin, TX
Advanced Water Pollution Control: Physical and Chemical Waste Treatment, Sludge Handling and Disposal
The University of Texas at Austin

This course teaches the fundamentals of physical and chemical methods for treatment and serves as a framework in the analysis, design, and operation of wastewater treatment facilities.

Fee is $760. Cathy Williams, Cockrell Hall 10.324, The University of Texas, Austin, TX 78712-1080; (512) 471-3396; fax (512) 471-0831.

Jan. 30–31 New Orleans, LA
Symposium on Superfund Risk Assessment in Soil Contamination Studies
American Society for Testing and Materials

Session topics will stress EPA-approved methodology and state-of-the-art modifications for handling site-specific and "real-life" problems in assessing risk at hazardous waste sites.

No symposium fee. Marsha Firman, ASTM, 1916 Race St., Philadelphia, PA 19103-1187; (215) 299-5400; fax (215) 977-9679.

Jan. 30–31 Houston, TX
Remedial Strategies and Decision Making
Geraghty & Miller, Inc.

"Remedial strategies" means groundwater remediation. Seminar topics will include soil remediation, bioremediation, waste minimization, site-specific risk assessment, and case histories.

Richard M. Miller, American Ecology Services, 127 E. 59th St., New York, NY 10022; (212) 371-1620.

Feb. 4–6 Cincinnati, OH
In Situ Treatment of Contaminated Soil and Water
Air & Waste Management Association

Topics will include in situ treatment technologies, delivery and recovery techniques, monitoring, regulatory issues, and case studies.

Janet M. Houthoofd, EPA, 5995 Center Hill Ave., Cincinnati, OH 45224; (513) 569-7524; fax (513) 569-7879.

Feb. 4–6 San Francisco, CA
National R&D Conference on the Control of Hazardous Materials
Hazardous Materials Control Research Institute

Topics will include innovative technologies, contaminated aquifer control, biotreatment, site safety, emergency response, toxics control, and state and federal programs.

R&D '92/HMCRI, 7237 Hanover Parkway, Greenbelt, MD 20770-3602; (301) 892-9500; fax (301) 220-3870.

Feb. 11–13 Dallas, TX
Solving Ground Water Problems with Models
The Association of Ground Water Scientists and Engineers

Conference topics will include mathematical techniques, geochemical and biochemical modeling, nonpoint pollution, wellhead protection, model calibration, and groundwater in wetlands.

Fee is $445 (NWWA members, $395; students, $100). Solving Ground Water Problems, National Water Well Association, P.O. Box 182039, Dept. #017, Columbus, OH 43218; (614) 761-1711; fax (614) 761-3446.

Feb. 23–27 Seattle, WA
1992 Annual Meeting
Society of Toxicology

0013-936X/91/0925-1996$02.50/0

Symposia will discuss genetic susceptibility to environmental agents, chemical allergy, risks to humans, controversies in cancer causation, and protein changes as indicators of toxicologic mechanisms.

Society of Toxicology, 1101 14th St., N.W., Suite 1100, Washington, DC 20005.

March. 1–6 Palm Coast, FL
Source Emission Monitoring and Analysis XVI
Engineering Foundation

This conference will focus on updates of EPA regulations and methods, air toxics, acid rain, area emissions, state experiences, and pollution prevention.

Engineering Foundation, 345 E. 47th St., New York, NY 10017; (212) 705-7835; fax (212) 705-7441.

March 2–6 Orlando, FL
Energy from Biomass and Wastes XVI
Institute of Gas Technology

Topics will include biomass production and component separation, municipal solid waste processing, alcohol fuels, genetic engineering, conversion of cellulosics, and environmental issues.

Susan Robertson, Institute of Gas Technology, 3424 S. State St., Chicago, IL 60616; (312) 567-3881; fax (312) 567-3857.

March 9–13 New Orleans, LA
PITCON '92; The 43rd Pittsburgh Conference on Analytical Chemistry and Applied Spectroscopy
Pittsburgh Conference

PITCON probably is the largest conference of its kind in the world. It will deal with subjects as diverse as supercritical extraction, EPA Methods for analyzing organics in water, analytical chemistry at the level of a single cell, and frontiers in chemometrics.

Pittsburgh Conference, Dept. CFP, 300 Penn Center Blvd., Suite 332, Pittsburgh, PA 15235-5503.

March 16–18 Budapest, Hungary
Stability and Change in Nature: Ecological and Cultural Dimensions
International Forum for Biophilosophy

Among questions studied will be: Is there a good reason to establish biodiversity as an objective of environmental policy? How can we act in the absence of scientific evidence? How seriously must we take hypothetical dangers?

Elly Janssens, International Forum for Biophilosophy, Craenendonck, 15, B-3000 Leuven, Belgium; phone 16 23 11 74; fax 16 20 53 08.

April 1–2 Arlington, VA
28th Annual Meeting
National Council on Radiation Protection and Measurements

The emphasis will be on radiation protection in medicine.

W. Roger Ney, NCRP, 7910 Woodmont Ave., Suite 800, Bethesda, MD 20814; (301) 657-2652; fax (301) 907-8768.

April 1–2 Montreal, Canada
Fifth Conference on Toxic Substances
Association for the Prevention of Atmospheric and Soil Contamination

Highlights will include polycyclic aromatic hydrocarbons, treatment technologies, disposal alternatives, and legal aspects.

Conrad Anctil, Ministère de l'Environnement du Québec, P.O. Box 11, Sainte-Foy, QC G1X 4E4, Canada; (418) 644-3420.

April 5–10 San Francisco, CA
203rd National Meeting of the American Chemical Society
American Chemical Society

This meeting will include numerous symposia on environmental chemistry and related subjects.

American Chemical Society, 1155 16th St. N.W., Washington, DC 20036-4800; (202) 872-4396; fax (202) 872-6128.

April 6–9 Washington, DC
2nd Annual Environmental Technology Exposition and Conference (ETEX '92)
The Interface Group

This conference is an international business forum for buyers and sellers of environmentally related products and services. It will cover the gamut of new technologies.

The Interface Group, 300 First Ave., Needham, MA 02194-2722; (617) 449-6600; fax (617) 449-6953.

April 6–10 Bangkok, Thailand
Pacific Basin Conference on Hazardous Waste
Pacific Basin Consortium for Hazardous Waste Research

Topics will include minimization, stabilization, risk assessment, data base development, and emergency planning.

Pacific Basin Consortium for Hazardous Waste Research, c/o East-West Center, 1777 East-West Rd., Honolulu, HI 96848; (808) 944-7555; fax (808) 944-7298.

April 20–23 Prague, Czechoslovakia
Energy and Environment: Transitions in Eastern Europe
University of North Dakota and Power Research Institute Prague

Topics will include coal cleaning, air and water quality, new clean coal use options, solid waste use and disposal, energy resources, and nonfuel uses of coal. One technical tour will visit the Northern Bohemia "Moonland," an area devastated by intense power and mining activity.

Mike Jones, Energy and Environmental Research Center, University of North Dakota, Box 8213, University Station, Grand Forks, ND 58202-8213; (701) 777-3120; fax (701) 777-5181.

April 22–29 Erice, Sicily, Italy
Innovative Technologies for Cleaning the Environment: Air, Water, and Soil
Department of Energy and others

Sessions will cover soil and groundwater contamination, surface water pollution, air pollution, pollution prevention, and cleanup in Eastern Europe, the Mediterranean, and the Persian Gulf.

Richard C. Ragaini, Environmental Protection Dept., Lawrence Livermore National Laboratory, P.O. Box 808, L-192, Livermore, CA 94550; (510) 423-8877; fax (510) 422-2528.

April 27–29 Tampa, FL
International Conference on Ground-Water Ecology
U.S. Environmental Protection Agency

Topics will highlight effects of pollutants on groundwater organisms, modeling of groundwater ecology, basic research needs, effects of atmospheric deposition, watershed planning, and case studies.

John Simons, Mail Code WH-550G, U.S. Environmental Protection Agency, 401 M St., S.W., Washington, DC 20460; (202) 260-7091.

AIR POLLUTION

Compressed air filtration. Filter removes particulates, water, *and* oil from compressed air with pressure drop not exceeding 3 psi. Ask for Bulletin 101. Deltech **99**

Breather for emergency response. Lightweight self-contained breathing apparatus gives at least 60 min protection in a hazardous environment, for example, during an emergency response. Biomarine **100**

Indoor air cleaning. UCAIR air cleaning system removes a wide range of indoor air pollutants, including volatile organic compounds. Union Carbide **101**

VOC destruction. RE-THERM system "has proven effective in controlling airborne volatile organic compounds and air toxics." System is a regenerative thermal oxidizer. REECO **102**

HAZARDOUS MATERIALS

Air stripping of VOCs. Pre-engineered air strippers remove more than 99% of volatile organic compounds by air stripping; other compounds also are removed, often with the same efficiency. Hydro Group **103**

Need more information about any items? *If so, just circle the appropriate numbers on one of the reader service cards bound into this issue and mail in the card. No stamp is necessary.*

CFC substitution. Company offers proprietary technology that will help industries and developing countries eliminate chlorofluorocarbons from their manufacturing processes, just as company has done. Northern Telecom **104**

FGD slurry recirculation. CB-SC pump recirculates wet slurries in flue gas desulfurization (FGD) plants. Pump is computer aided and has high hydraulic efficiency. Barrett, Haentjens **105**

Recycling commingled materials. System processes up to 300 tons per day of commingled steel, bi-metal, and aluminum cans; glass; plastics; newsprint; and corrugated paper. Mayfran International **106**

INSTRUMENTS

Fast toxicity test. Model 500 toxicity test system can furnish results in less than 30 min and screen 29 samples or process three complete serial dilution bioassays at a time. "Only a few mL " of sample are required for a full assay. Microtox **107**

Organic vapor sampling. Tenax™/CMS sampling tube provides a means to sample volatile nonpolar organic vapors such as aromatic and chlorinated hydrocarbons with detection possible at parts-per- billion level. MSA **108**

Monitoring water contaminants. Chemsensor is a portable device that measures chemicals in industrial water and groundwater in real-time and in situ. Package weighs less than 5 lb. Sippican **109**

H_2S calibrator. Model 727 portable H_2S calibrator is small enough to fit on belt and weighs 1.25 lb. It runs on a 1.5-V battery and can be used to calibrate any fixed or portable H_2S monitor. Texas Analytical Controls **110**

Companies interested in a listing *in this department should send their release directly to* Environmental Science and Technology, *Attn: Products, 1155 16th St., N.W., Washington, DC 20036.*

DO monitors. Series 9610 dissolved oxygen monitors can measure 0–20 ppm or 0–200% saturation. Probe mounting up to 1000 ft (305 m) from the receiver is available. Device uses microprocessor-based electronics. Capital Controls **111**

HPLC columns. OmniPac family of high-performance liquid chromatography columns combines advantages of ion chromatography and reversed-phase chromatography in a single solvent-compatible material. Packings are of highly crosslinked divinylbenzene polymer. Dionex **112**

Remote air sampling. SUMMA passivated 6-L canister will sample air at 2–500 cm^3/min without power or pump. It is based on EPA Method TO-14 for measuring volatile organic compounds and assures sample stability for gas chromatography. Andersen Instruments **113**

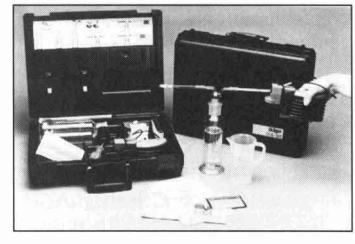

Water contamination testing. Portable DLE Kit provides on-site measurement of contaminants in water, including carbon tetrachloride, toluene, HCN, H_2S, benzene, gasoline, and trichloroethylene. National Draeger **114**

Submersible pH sensor. This pH sensor package is fully submersible and is "suitable for tough pH measurement" in applications such as oily wastewater, electroplating, wastewater treatment, and pulp and paper. George Fischer Signet **115**

H_2S in wastewater. Model 722R/500 offers continuous, unattended on-line analysis of H_2S in wastewater to ppm levels. Houston Atlas **116**

Stack gas measurement. Pathfinder long-path gas cell improves monitoring of stack gas from industrial

0013-936X/91/0925-1998$02.50/0

plants. Path length may vary from 0.4 to 12.4 m. Connecticut Instrument **117**

Portable gas detector. Triple Plus is a four-channel unit that can monitor the atmosphere continuously for flammable and toxic gases and oxygen levels. Up to four sensors can be fitted at any one time. Device weighs less than 2 lb. CEA Instruments **118**

Hydrocarbon monitoring in water. Aquascan can monitor volatile organic compounds such as benzene in water continuously in real time "at infinitesimal levels within minutes." It also sounds alarm when preset levels of VOCs are exceeded. Device is said to be the first of its kind. Sentex Sensing Technology **119**

Detection modules. Stand-alone detection modules use thermionic and flame ionization detectors to sniff out halogenated vapors from water and soil, electronegative vapors from various samples, and organic nitrogenated pollutants in water. Other applications are possible. DET **120**

Hazardous waste monitoring. CENTURY Organic Vapor Analyzer 128GC monitors volatile organics at hazardous waste sites to help meet Superfund requirements. Device is portable. Ask for laboratory application data sheet LAD 001–022. Foxboro **121**

NO_x monitoring. Model 7100 continuous emission monitoring system uses nonsampling electrochemical cell technology to provide EPA-certifiable NO_x monitoring of flue gases. Measuring ranges are selectable. Land Combustion **122**

SFE sample extraction. Supercritical fluid extraction of pesticides and polycyclic aromatic hydrocarbons from soil and certain other organic substances from other media can be quantitative. Ask for Applications Bulletin 71. Isco **123**

PUBLICATIONS

Clean Water Act issues. *ENSR NEWSLETTER* Number 3, 1991, contains an article on major issues of Clean Water Act reauthorization, by Windsor Sung, Ph.D., and on the new operating permit program of the Clean Air Act, by Robert Iwanchuk. ENSR **124**

Compliance calendars. Compliance Wall Planner for 1992 warns companies of EPA, DOT, and OSHA deadlines by which they must be in environmental or industrial hygiene compliance; the cost is $45 (three for $95) plus $3 for shipping and handling. Compliance Calendars **125**

Innovative PCB remediation. *ENVIRON Report* 1991, *5*(2), 2, describes innovative remediation technology options for polychlorinated biphenyls. Volume also contains an article on lead sources, exposures, and uptake. ENVIRON International **126**

Solar electricity. *Solar Electricity Today* is an introductory video (6 min, 20 s) that presents a summary of the status and prospects of solar electricity. Price varies with type of videotape. EPRI **127**

Questions about recycling. Recycling is no panacea for the nation's solid waste problem, according to the *Journal of Regulation and Social Costs* 1991, *1*(3). Article criticizes solid waste rules. National Chamber Foundation **128**

SERVICES

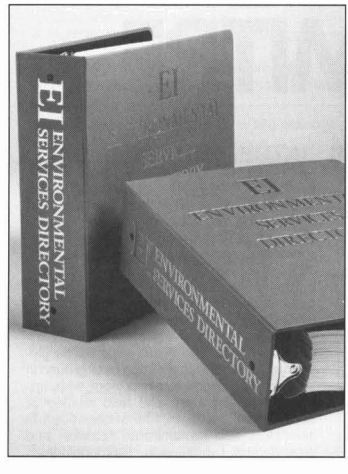

Environmental services. *EI Environmental Services Directory* is a 2000+ page reference that provides detailed information about 5300 environmental services in the United States. The reference is divided into states and then into categories of service. EI **129**

SOFTWARE

Recycling. Computer bulletin board provides users access to buyers and sellers of materials for recycling; emphasis is on Florida. Through a modem, dial 1-800-348-1239 for instructions on use. TREEO **130**

Environmental mapping. Global Positioning System is available for environmental mapping and resource management tasks as diverse as endangered species habitats, forest fires, and soil surveys. Trimble Navigation **131**

Regulatory compliance. RegScan Version 4.0 maintains data bases on EPA, OSHA, and Department of Transportation regulations with monthly updates. Searches are "speedy and complete." Regulation Scanning Technology **132**

Environmental modeling. Geoscience Modeling System portrays geological and environmental models in three dimensions. Site characterization and hydrogeological studies are among the significant features. Lynx Geosystems **133**

Hazardous substances. Environmental hazardous substances data base is especially applicable to real estate buyers and lenders to inform them about current and historical site activity with regard to hazardous substances. Data base emphasizes Illinois. Illinois State Museum **134**

Toxicity test information. Improved search and retrieval system for the AQUIRE data base is available; the data base now includes 105,300 toxicity studies that cover 5200 chemicals and 2400 species. AQUIRE is an EPA data base. Technical Database Services **135**

Chromatography management. PYRAMID Chromatography Manager provides graphics, "on-the-fly" editing, reconfiguration, and customization. Demonstration disk shows conversion of HPLC channel to GC specifications. Software works with Windows 3.0, but the demonstration does not require Windows. Axxiom Chromatography **136**

STANDARDS

Hazardous waste. EPA has certified 15 solid-waste reference samples; they are "the first commercially available reference materials made from 'real-world' hazardous wastes." Fisher Scientific **137**

CLASSIFIED SECTION

SUPERVISOR, BIOREMEDIATION RESEARCH

IGT, a leading energy and environmental R&D organization, has an immediate opening in our Biotechnology and Environmental Research area for a PhD in Environmental Engineering, Soil Microbiology, Agronomy, or Geotechnical Engineering, with a minimum 5-8 years experience in toxic and hazardous waste management R&D. Must have project management, proposal and report preparation, and field or large-scale test experience, along with the ability to assume technical- and management-related responsibilities.

Will be responsible for planning/designing soil and groundwater biotreatment experiments; analysis of data; report and proposal writing; and technical presentations for government- and industry-funded programs. Must have good oral and written communication skills, and the ability to work well with staff at all levels.

IGT offers a professional environment, excellent benefits, competitive salary, and 100% tuition assistance. For confidential consideration, please send resume with salary requirements to:

Personnel Dept. VS-3
Institute of Gas Technology
3424 S. State Street
Chicago, IL 60616

IGT

EOE/AA

HEAD, DEPARTMENT OF ENVIRONMENTAL SCIENCE AND ENGINEERING, OREGON GRADUATE INSTITUTE OF SCIENCE & TECHNOLOGY. Applications are invited from scientists and engineers who have (1) a distinguished record of scholarly productivity in environmental research, (2) a strongly funded research program, (3) extensive experience in teaching at the graduate level, and (4) strong evidence of leadership ability. The department operates a multidisciplinary research and education program covering the chemical, physical, biological, engineering, and computational aspects of the multimedia environment. Candidates should send a complete CV with the names and addresses of five references to **Dr. James J. Huntzicker, Provost, Oregon Graduate Institute, 19600 NW von Neumann Dr., Beaverton, OR 97006.** Closing date: 1/31/92. An equal opportunity/affirmative action employer.

POSITION AVAILABLE

Full-time, tenure-track position with developing and expanding undergraduate Environmental Sciences Program; to teach existing courses, develop an environmental sciences curriculum and research program; Ph.D. in environmental science or related discipline; research interests to complement existing science faculty. Send letter and names of three references to **Thomas J. Murphy, Depaul University, Environmental Sciences Program, 25 E. Jackson Blvd., Chicago, IL 60604** by 15 January 1992. Equal opportunity employer, M/F.

KUWAIT INSTITUTE FOR SCIENTIFIC RESEARCH

Kuwait Institute for Scientific Research (KISR) is a nonprofit organization actively engaged in applied research in the fields of environmental and earth sciences; food resources; engineering; petroleum, petrochemicals and materials and techno-economics.
KISR has vacancies in the following fields:

AIR POLLUTION

Major duties:
- Conducting research projects on the fate of air pollutants.
- Studying the effect of microscale & macroscale factors on the transportation & transformation of air pollutants.
- Correlating the air pollution studies to the environmental health program.
- Studying the composition & dynamic characteristics of air pollutants.
- Developing an air pollution index to be related to the human health program.

Qualifications:
Applicants should have a Ph.D. in Air Pollution Dynamics and Chemistry plus 5 years of related experience.

ANALYTICAL CHEMISTRY

Major duties:
- Conducting research projects on the environmental aspects and evaluating the analyses on environmental studies program.
- Participating and developing a software package to assist the research team.
- Reviewing analytical methodologies and supervising the analysis of samples.
- Traning the project team on sample preparation, analysis, experimentation and in preparation of reports.

Qualifications:
Applicants should have a Ph.D. in Analytical Chemistry plus 5 years related experience. Practical knowledge in using modern analytical techniques, eg., GC/MS, GC HPLC, SCFC, ICP and ASV.

ENVIRONMENTAL HEALTH
(Water Quality & Management)

Major duties:
- Conducting fish, bacterial and sediment assays.
- Participating in marine environmental studies related to the impacts of oil pollution on population dynamics and diversity of marine organisms.
- Conducting and supervising project activities related to marine and ecology studies and submitting reports.
- Training project team during the various stages of the project.

Qualifications:
Applicants should have a Ph.D. in Environmental Health–Water Quality and Management plus 5 years of related experience.

MICROBIOLOGY

Major duties:
- Conducting research projects on environmental pollution, such as: bioremediation technique for oil lakes and contaminated soil.
- Participating in the studies on biological engineering systems, and suggesting recommendations in solving problems.
- Involving in bioassay research program.
- Training the project team on various techniques of laboratory and finalizing reports.

Qualifications:
Applicants should have a Ph.D. in Microbiology plus 5 years of related experience.

ENVIRONMENTAL IMPACT ASSESSMENT

Major duties:
- Conducting research projects on EIA to define and evaluate health impact, environmental hazards, ecological effects and economical and social changes due to the existing urban activities, industrial expansion and other developmental changes.
- Initiating and following up research projects addressing to immediate and long term needs of the Government and industrial agencies.
- Supervising and training the project team throughout the various stages of project and final report preparation.

Qualifications:
Applicants should have a Ph.D. in EIA plus minimum of 5 years of experience on Environmental Impact Assessment of marine environment.

MARINE POLLUTION

Major duties:
- Conducting research projects on oil pollution assessment and fate of petroleum hydrocarbons in the marine environment.
- Reviewing and evaluating marine environmental studies program.
- Participating in multidisciplinary experimental investigations on the impacts of oil pollution on marine biota and ecology.
- Submitting, supervising and completing projects related to marine environmental studies.
- Training project team throughout the various stages of development of the project, field survey, sample analysis, experimentation and preparation of final reports.

Qualifications:
Applicants should have a Ph.D. in Chemistry (or related environmental and marine sciences) plus 5 years of experience.

KISR offers attractive tax free salaries commensurate with qualifications and experience and generous benefits that include: gratuity, free furnished air-conditioned accommendation, school tuition fees for children, six weeks annual paid vacation, air tickets, free medical care and life insurance.

Interested applicants are requested to send their Curriculum Vitae with supporting information not later than one month from the date of this publication, to:

Personnel Manager
Kuwait Institute for Scientific Research
P.O. Box 24885, 13109 Safat – KUWAIT.

CLASSIFIED SECTION

UTAH STATE UNIVERSITY

Graduate studies in Water and Environmental Engineering

If you are looking for an outstanding graduate program in water or Environmental Engineering consider the strengths of the Department of Civil and Environmental Engineering (CEE) and the Utah Water Research Laboratory (UWRL) at Utah State University:

- One of the largest and top-ranked university water research groups with a dedicated water and environmental engineering faculty of approximately thirty
- Large nationally- and internationally-recognized funded research programs
- Good working relationships with many other departments
- One of the largest and best equipped hydraulics laboratories with over 80,000 sq. ft. enclosed
- A well equipped environmental analysis laboratory with state-of-the-art chemical instrumentation and bioprocess facilities
- Excellent computer facilities including work station and supercomputer access for students
- Challenging, broad, and up-to-date coursework programs
- Graduate Research Assistantships which are awarded on a competitive basis
- A beautiful mountain valley location with year-round recreational opportunities

Programs lead to Masters (thesis and non-thesis) and Doctoral degrees, and a professional degree between the M.S. and Ph.D., specializing in Water Engineering:

- Fluid Mechanics and Hydraulics
- Groundwater
- Hydrology
- Water Resources

and Environmental Engineering:

- Hazardous and Toxic Waste Management
- Natural Systems Engineering

For more information on our graduate programs and current research programs send a letter describing your academic and research interests, with a resume, to: Professor D. S. Bowles, Head, Water Division (Telephone: 801/750-3157), or Professor R. C. Sims, Head, Environmental Division (Telephone: 801/750-2926) Utah State University, Logan, Utah 84322-8200. In keeping with AFFIRMATIVE ACTION/EQUAL OPPORTUNITY guidelines, minorities, the physically disadvantaged, and women are particularly encouraged to apply.

Graduate Fellowships in Water Sciences

Graduate stipends of $17,000 per annum will be awarded to Fellows appointed through the USDA National Needs in Water Sciences Training Program. The interdisciplinary nature of the program is designed for Fellows to initiate innovative research emphasizing systems science/computer modeling simulation as it relates to all aspects of water sciences. The program is directed by an interdepartmental committee of faculty and provides Fellows with broad and rigorous training in basic research and creative application of computer modeling and simulation. *Three Fellowships will be awarded to outstanding first year doctoral students in the 1992-93 academic year.* Minority students are encouraged to apply. Fellows must be U.S. Citizens or native residents of U.S. Protectorates. For information concerning the application procedure, please contact:

Dr. Frank M. D'Itri, Co-Director, 334 Natural Resources Bldg., MSU, East Lansing, MI 48824 (517) 353-3744

Dr. Boyd G. Ellis, Co-Director, 512 Plant and Soil Sciences, MSU, East Lansing, MI 48824 (517) 355-0217

Application Deadline: **December 31, 1991.**

MSU is an Affirmative Action/ Equal Opportunity Institution.

POSTDOCTORAL APPOINTEE

IGT, a leading energy and environmental R&D organization, has an immediate opening in our Biotechnology and Environmental Research area for a PhD in Microbiology, Biochemistry, Organic Chemistry or Agronomy. Actual research experience in microbiology, organic chemistry of oxidative reaction, bioremediation, and analytical chemistry of environmental samples required. Knowledge of EPA QA/QC protocols a plus.

Will be responsible for conducting task-related research for an ongoing EPA project, analyzing and reporting results, and suggesting future experiments. Must have excellent work habits, good oral and written communication skills, and be a self-starter who is able to work with minimal supervision.

IGT offers a professional environment, excellent benefits, and competitive salary. For confidential consideration, please send resume with salary requirements to:

Personnel Dept. BK-3
Institute of Gas Technology
3424 S. State Street
Chicago, IL 60616

IGT

EOE/AA.

DEPARTMENT OF GEOLOGY WASHINGTON STATE UNIVERSITY

A tenure-track Assistant/Associate Professor position will be available in low-temperature geochemistry in the Department of Geology. Washington State University, Tri-Cities campus with a research affiliation at Battelle-Pacific Northwest Laboratories beginning August, 1992 or later. Preference will be given to applicants with research interests in organic geochemistry or oxidation-reduction reactions at mineral/water interfaces. Experience in both experimental and modeling approaches to surface/aqueous geochemistry is desired. Candidates will be expected to divide their time equally between teaching and research, advise graduate students, seek extramural research funding and interact with the faculty on the Pullman campus.

The position requires a Ph.D. in the Geological Sciences with an emphasis in geochemistry and a strong interest in and demonstrated capacity for publishable research and successful teaching at the upper division undergraduate and graduate levels. A record of publication in refeered journals and extramural funding is desired. A letter of application, vitae and three letters of recommendation should be sent to: **Dr. P. E. Rosenberg, Search Committee, Department of Geology, Washington State University, Pullman, Washington 99164-2812; (509) 335-4368 FAX: (509) 335-7816.**

Screening of applications will begin on January 15, 1992 and will continue until a suitable candidate has been identified. Representatives of the geology faculty will interview selected candidates at the October, 1991 Meeting of the Geological Society of America in San Diego or in Pullman at a later date.

Washington State University is an EO/AA educator and employer. Protected group members are encouraged to apply.

GRADUATE STUDY in ENVIRONMENTAL ENGINEERING at Michigan Technological University. Motivated, bright individuals with a degree in engineering or the environmental sciences are sought for graduate study in the following areas: adsorption, photocatalytic oxidation, and biological treatment of hazardous pollutants; groundwater remediation; transport phenomena, waste minimization; and surface water quality modeling. Excellent facilities, enthusiastic faculty, and pristine living area. University fellowships, Department of Education fellowships, and research assistantships are available on a competitive basis. Contact: **Dr. C. Robert Baillod, Environmental Engineering Center, Michigan Technological University, Houghton, MI 49931 (906) 487-2530.** Michigan Tech is an Affirmative Action/Equal Opportunity Employer/educational institution.

GRADUATE STUDY in ENVIRONMENTAL SCIENCE AND ENGINEERING at the Oregon Graduate Institute. Highly qualified, strongly motivated students sought for exciting research programs in transport and fate of organic and inorganic contaminants, aquifer remediation, microbial ecology and physiology, biodegradation, biogeochemistry, analytical environmental chemistry, numerical modeling, estuarine and coastal studies, elemental cycling in terrestrial ecosystems, atmospheric chemistry and physics, and global climate change. Intensive research experience, state-of-the-art instrumentation, maximum faculty-student interaction. Twelve-month course Masters program. Research assistantships with tuition remission available to qualified Ph.D. applicants. Write: **Department of Environmental Science and Engineering, 19600 N.W. Von Neumann Dr., Beaverton, OR 97006, (503) 690-1196.** (Closing date 2/15/92 for Ph.D. applications. Applications for 12-Month M.S. program will be accepted after that date.) OGI is an Affirmative Action/Equal Opportunity Employer.

CLASSIFIED SECTION

Tulane University
Faculty Position in Environmental Restoration

The Department of Chemical Engineering at Tulane University is seeking to add a tenure-track faculty member with research interests in Environmental Restoration. We are particularly interested in individuals whose research specialization is in the area of Radioactive Waste Management and Disposal. The department seeks candidates who are capable of establishing an internationally recognized research program and who have a strong commitment to teaching at the graduate and undergraduate levels. The applicant should possess a Ph.D. in a technical field with at least one degree in Chemical Engineering. Appointments may be made at either the junior or senior level, depending on the qualifications and experience of the applicant. Review of applications will begin on January 15, 1992 and will continue until position is filled. Send letter of application, curriculum vitae, statement of research plans, and a list of three references to **Professor Peter N. Pintauro, Chair, Faculty Search Committee, Department of Chemical Engineering, Room 327 Boggs Center, Tulane University, New Orleans, LA 70118.** Tulane University is an Equal Opportunity Employer; applications from qualified women and minorities are encouraged.

The Illinois State Water Survey invites applications for an Assistant Professional Scientist in the Office of Atmospheric Chemistry. A major component of this job will be to develop and improve sample preparations and gas chromatography method for analysis of PCBs, pesticides, PAH's and other organic pollutants in air and precipitation samples. Assist in the laboratory operations and management of routine sample analysis for program involving large numbers of environmental samples. Ph.D. or M.S. in analytical chemistry or a related field with experience in the analysis of trace organic pollutants in environmental samples. Candidates must have experience with GC and GC/MF methods. Some laboratory management is desirable. Availability: January 1, 1992. Salary: Negotiable. Deadline: December 1, 1991. Position Number 3189. **Send resume to Joyce Changnon, Director of Human Resources, Illinois State Water Survey, 2204 Griffith Drive, Champaign, IL 61820. FAX: 217/333-6540.** The University of Illinois is an Affirmative Action Equal Opportunity employer.

ENVIRONMENTAL ENGINEER (Rank Open)—Research specialization open; preference for hazardous waste, combustion engineering, or atmospheric sciences. Post-doctoral research preferred. Tenure track position on the Bloomington Campus for the 1992–93 academic year. Requires appropriate terminal degree; more senior applicants must have credentials consistent with the proposed rank at a major research university. Must demonstrate a serious interest in applied research, professional service applications, and a commitment to high teaching standards. Graduate and undergraduate teaching will be expected. Ability to teach applied statistics to our undergraduate and professional masters students preferred. Interest in environmental and natural resources policy an important attribute for applicants.

Send application letter and vitae no later than January 10, 1992. Search will continue, however, until suitable candidate selected.

John L. Mikesell
Associate Dean for Academic Affairs
School of Public and Environmental Affairs
Indiana University
Bloomington, IN 47405

AN EQUAL OPPORTUNITY, AFFIRMATIVE ACTION EDUCATOR EMPLOYER AND CONTRACTOR, M/F

ENVIRONMENTAL ENGINEER. Use site assessment data to develop site Remedial Action Plan (RAP) consistent with SARA (Superfund Amendment and Reauthorization Act), RCRA (Resource Conservation and Recovery Act) and OSHA (Occupational Safety and Health Act) to reclaim the oil contaminated soil and groundwater and industrial wastewater. Use computer model to simulate and predict the subsurface contaminant transport and biodegradation and to prepare spreadsheets and presentations. 40 hrs/wk. Master's in Environmental Engineering. $29,038/yr. Apply at the Texas Employment Commission, Tyler, Texas or send resume to the Texas Employment Commission, TEC Building, Austin, Texas 78778. Job Order #6422214. Ad paid by An Equal Employment Opportunity Employer.

CLASSIFIED ADVERTISING RATES

Unit	1-T	3-T	6-T	12-T	24-T
1 Inch	$145	$140	$130	$125	$120

(Check Classified Advertising Department for rates if advertisement is larger than 10″.)
SHIPPING INSTRUCTIONS: Send all material to

Environmental Science & Technology
Classified Advertising Department
500 Post Road East
P.O. Box 231
Westport, CT 06881
(203) 226-7131/Fax (203) 454-9939

Gregory Chair in Civil Engineering

The College of Engineering at Texas A&M University invites applications and nominations for the Gregory Chair in Civil Engineering. Candidates for this chair should be engineers of national standing in the field of environmental engineering who can provide intellectual leadership for the Department as well as enrich the scholarly environment at Texas A&M University.

Applicants or nominees should have demonstrated the characteristics of originality, creativity and productivity in the areas of teaching and research. The holder of the Gregory Chair will be expected to maintain an active program of funded research, contribute to the teaching program and continue a leadership role in the environmental engineering profession at the national and international level.

Applications should include a detailed resume and be sent to: **Dr. Bill Batchelor, Chair, Gregory Chair Search Committee, Department of Civil Engineering, Texas A&M University, College Station. TX 77843-3136, 409/845-0311.** Review of applications will begin December 1, 1991. References will be requested of all finalists.

Texas A&M University is an equal opportunity/affirmative action employer with a strong commitment to the achievement of diversity among its faculty and staff.

ENVIRONMENTAL PROFESSIONALS

Join the team . . . Brown & Root, Inc., is gearing up for some of the most challenging projects in our history at our Houston, Texas Regional office. The following positions are currently available.

Environmental Specialist

Serves as technical lead for projects involving environmental assessments and impact studies.

Requirements of the position are:

- **MS degree in environmental discipline**
- **5 plus years experience in environmental impact analysis**
- **Experience with environmental regulations**

Responsibilities include:

- **Preparing environmental impact sections of permit applications**
- **Preparing environmental assessments and impact statements**
- **Acquisition of site data and use of models**
- **Interface with project staff and regulatory agencies**

Environmental Permitting Specialist

Serves as industrial environmental permitting specialist and technical liaison.

Requirements of the position are:

- **BS/MS environmental discipline**
- **5 plus years experience in environmental permitting**
- **Experience with environmental industrial permitting is essential**
- **Experience in private sector consulting desirable**

Responsibilities include:

- **Preparing permit applications for new or modified industrial facilities**
- **Analyzing regulatory requirements for industrial facilities**
- **Liaison with regulatory agency staff and negotiation of permits**
- **Interface with project engineering staff**

Brown & Root, Inc., offers competitive salaries, world class benefits and will soon feature a **New Employee Center** that will offer **Health and Child Care.** For consideration, send your resume with salary history to:

Brown & Root, Inc.
P.O. Box 3, RM 125
Dept. LS-8
Houston, TX 77001-0003

No phone calls, please
No agencies, please

Brown & Root, Inc.
An Equal Opportunity Employer
P.O. Box 3, Houston, TX 77001
A Halliburton Company

Brown & Root

professional consulting services directory

USE THE PROFESSIONAL CONSULTING SERVICES DIRECTORY

THE CONSULTANT'S DIRECTORY

UNIT	Six Issues	Twelve Issues
1″ × 1 col.	$70	$65
1″ × 2 col.	140	125
1″ × 3 col.	205	175
2″ × 1 col.	140	125
2″ × 2 col.	255	230
4″ × 1 col.	255	230

ENVIRONMENTAL SCIENCE
& TECHNOLOGY
500 Post Road East
P.O. Box 231
Westport, CT 06880
(203) 226-7131
FAX: (203) 454-9939

INDEX TO THE ADVERTISERS IN THIS ISSUE

Advertising Management for the American Chemical Society Publications

CENTCOM, LTD.

President
James A. Byrne

Executive Vice President
Benjamin W. Jones

Robert L. Voepel, *Vice President*
Joseph P. Stenza, *Production Director*

500 Post Road East
P.O. Box 231
Westport, Connecticut 06880
(Area Code 203) 226-7131
Telex No. 643310
Fax No. (203) 454-9939

ADVERTISING SALES MANAGER
Bruce E. Poorman

ADVERTISING PRODUCTION MANAGER
Jane F. Gatenby

SALES REPRESENTATIVES

Philadelphia, PA. . . . CENTCOM, LTD. GSB Building, Suite 405, 1 Belmont Ave., Bala Cynwyd, PA. 19004 (Area Code 215) 667-9666, FAX: (215) 667-9353

Westport, CT. . . . Edward M. Black, CENTCOM, LTD., 500 Post Road East, P.O. Box 231, Westport, CT 06880 (Area Code 203) 226-7131, FAX: (203) 454-9939

New York/New Jersey . . . Dean A. Baldwin, John F. Raftery, CENTCOM, LTD., Schoolhouse Plaza, 720 King Georges Post Road, Fords, NJ 08863 (Area Code 908) 738-8200, FAX (908) 738-6128

Cleveland, OH. . . . Bruce E. Poorman, CENTCOM, LTD., 325 Front St., Berea, OH 44017 (Area Code 216) 234-1333, FAX: (216) 234-3425

Chicago, IL. . . . Michael J. Pak, CENTCOM, LTD., 540 Frontage Rd., Northfield, Ill. 60093 (Area Code 708) 441-6383, FAX: (708) 441-6382

Houston, TX. . . . Michael J. Pak, CENTCOM, LTD., (Area Code 708) 441-6383

San Francisco, CA. . . . Paul M. Butts, CENTCOM, LTD., Suite 808, 2672 Bayshore Parkway, Mountainview, CA 94043 (Area Code 415) 969-4604, FAX: (415) 969-2104

Los Angeles, CA. . . . Paul M. Butts, CENTCOM, LTD., (Area Code 415) 969-4604

Boston, MA. . . . Edward M. Black, CENTCOM, LTD., (Area Code 203) 226-7131

Atlanta, GA. . . . CENTCOM, LTD., (Area Code 216) 234-1333

Denver, CO. . . . Paul M. Butts, CENTCOM, LTD., (Area Code 415) 969-4604

ES&T RESEARCH

Effect of Fuel Structure on Emissions from a Spark-Ignited Engine

Edward W. Kalser,* Walter O. Siegl, Yitshak I. Henig, Richard W. Anderson, and Frederick H. Trinker

Ford Motor Company, Scientific Research Laboratories, Mail Drop 3083, Dearborn, Michigan 48121-2053

■ Seven pure fuels (methane, ethane, propane, *n*-butane, isopentane, isooctane, and toluene) have been run in a single-cylinder production-type engine at four operating points. Measurements of the emitted engine-out hydrocarbons, NO_x, CO, and CO_2 have been made at each condition and show effects partially explainable by changes in flame temperature and H/C ratio of the fuel. The results show that both the total engine-out hydrocarbon emissions and the distribution of individual hydrocarbon species in the exhaust gas are sensitive to the fuel used. In the case of total hydrocarbon emissions, ethane produces the lowest and toluene the highest (4× ethane) under all operating conditions. The percentage contribution of unburned fuel to the hydrocarbon emissions varies from 95% for methane fuel to 50% or below for isooctane. These percentages are affected by engine operating parameters, particularly speed and spark timing. Olefins constitute the majority of the remaining emitted hydrocarbons for alkane fuels. Toluene also emits a large percentage of unburned fuel (80%) but little olefin (1%). Benzene (6%) and benzaldehyde (6%) are major nonfuel hydrocarbon emissions from toluene but are not observed to an appreciable extent from the alkane fuels (<0.3%).

Introduction

Tailpipe emissions are a critical consideration in the design process of automobiles because of government regulations based on environmental concerns. Current restrictions control the total mass of emitted non-methane hydrocarbons, CO, and oxides of nitrogen (*1*). Possible future requirements may regulate the photochemical reactivity of these emissions in the atmosphere, and such a change would require the control of specific hydrocarbon species in the exhaust in addition to the total mass.

In order to design power train systems that meet emissions standards, it is critical to understand the combined effects of engine design, catalyst design, and fuel composition on regulated emissions. A considerable effort has been expended in exploring the effects of variables related to engine design [e.g., crevice volumes (*2, 3*), oil films (*4–6*), and fuel/air equivalence ratio (*7–9*)] on hydrocarbon emissions. However, systematic studies of the effect of fuel composition on emissions have not been pursued as thoroughly. To better understand the effects of fuel structure on hydrocarbon, CO, and NO_x emissions, it is important to carry out experiments on single-component fuels to avoid the difficulties associated with the interpretation of emissions data from multicomponent mixtures. Measurement of emissions from a few pure hydrocarbon fuels has been carried out in the past (e.g., refs 7–9). However, no extensive experiments have been performed using a variety of fuel types in the same engine in order to carefully compare the effect of fuel structure on emissions under nearly identical engine operating conditions.

In our experiments, we compare the engine-out NO_x, CO, and, particularly, hydrocarbon (HC) emissions from four gaseous (methane, ethane, propane, and *n*-butane) and three liquid [isopentane, isooctane (2,2,4-trimethylpentane), and toluene] fuels using a single-cylinder engine. Both the total HC and individual HC species emissions were determined during these experiments. Finally, a mixture containing five liquid fuel components was also tested in the same engine to examine possible interactions between fuel components. The results of these experiments provide significant insight into the effect of fuel structure on HC emissions from spark-ignited engines.

Experiment

The engine used in these experiments is a single cylinder of 475-cm^3 displacement volume and a compression ratio of 9:1. It is based on a Waukesha CFR fuel testing engine. Modifications to the Waukesha include adapting a multicylinder head for single-cylinder operation and the fabrication of an aluminum block to support a cast-iron drop-in liner. The head incorporates a helical intake port and masked intake valve to generate a swirl ratio of 3, promoting rapid combustion and a high tolerance to dilution. The engine is equipped with a production-type piston-ring assembly package and is controlled by a dynamometer facility.

The base-line engine condition was a fuel/air equivalence ratio (Φ) of 0.9 (fuel lean), MBT (minimum advance before top dead center for best torque) spark timing, 1500 rpm, 90 °C coolant temperature, and a load of 3.8 bar IMEP. These steady-state conditions are typical of a midspeed, midload cruise. A slightly fuel lean mixture was chosen for most measurements to minimize the effect on hydrocarbon emissions of small errors in setting the fuel/air ratio. The gaseous fuels (methane, ethane, propane, and *n*-butane) were mixed with the inlet air upstream of the intake manifold while liquid fuels (isopentane, isooctane, toluene, and the multicomponent mixture) were introduced by a fuel injector located in the intake port. The multicomponent fuel (tracer fuel) consisted of 7.3 mol % (moles of species per total moles in mixture) *n*-pentane, 6.4% *n*-hexane, 5.7% *n*-heptane,

0013-936X/91/0925-2005$02.50/0

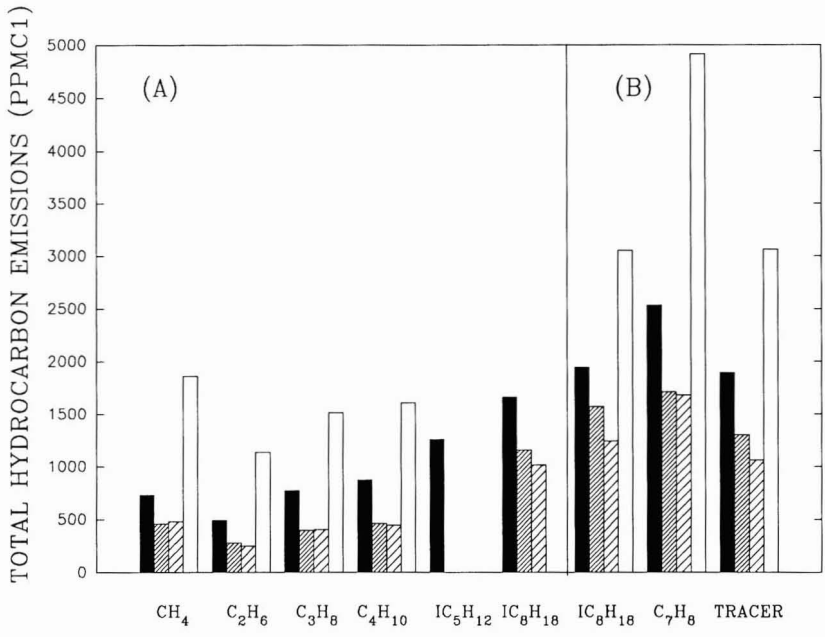

Figure 1. Total wet hydrocarbon emissions measured with the hot FID detector: solid bar, base line; fine crosshatched bar, MBT-12° spark timing; coarse crosshatch, 2500 rpm; unfilled bar, $\Phi = 1.15$. Section B data were obtained from the engine when the total HC emissions from isooctane and propane fuels were 20% larger than in (A) (see text).

36.2% toluene, and 44.4% isooctane. At base-line condition, MBT spark advances (crank angle degrees BTDC) were as follows: CH_4 (19), C_2H_6 (15), C_3H_8 (17), C_4H_{10} (18), C_5H_{12} (20), C_8H_{18} (23), C_7H_8 (19), tracer (22).

In addition to the base-line condition, experiments were carried out at either 2500 rpm, MBT-12° spark advance (retarded timing), or $\Phi = 1.15$ while the other conditions were kept the same as base line. Spark sweeps were carried out for each fuel to identify the MBT spark timing. Maintaining a consistent spark timing for all fuels is vital when comparing HC and NO_x emissions, because these emissions are strongly dependent on spark advance (7). In this engine, the crank angle of peak cylinder pressure at MBT spark timing for all seven fuels was earlier found to be 13° after top dead center. Consequently, for all of the current MBT data, the angle of peak pressure was maintained at 13 ± 1° for each fuel. The air flow required to maintain the specified load was similar at the same engine condition for all of the fuels (varying between 7.7 and 7.9 kg/h under base-line conditions).

An emissions console provided dried engine-out exhaust gas measurements of CO, CO_2, O_2, and NO by passing the exhaust gas through a cooled trap. Total hydrocarbon emissions were determined by using a heated flame ionization detector (FID) connected to the exhaust system by a heated sample line to minimize loss of low-volatility HC species in the sampling system and were, therefore, measured wet. In addition to the total HC measurements, individual HC species mole fractions were measured by withdrawing partially dried exhaust gas samples from the exhaust pipe for gas chromatographic (GC) analysis. These samples were stored at reduced pressure (120 Torr) in a darkened Pyrex flask to reduce residual water condensation and sample loss on the walls. All emissions data are engine-out measurements with no catalytic after-treatment.

Two gas chromatographs were used in the hydrocarbon species analyses. Undiluted exhaust emissions from the gaseous fuels were analyzed on a 6-ft Durapak column (*n*-octane/Porasil C) at 70 °C. This column separates hydrocarbons up to C_5 in 10 min, and after this period, the helium carrier gas flow is reversed to back-flush any remaining heavier hydrocarbons. Both the individual species and the lumped-together back-flushed hydrocarbons are detected by a flame ionization detector. The second GC, described in detail in ref 10, is capable of separating C_1–C_{10} hydrocarbons with no known overlap. This latter GC was used primarily to analyze diluted (9:1) exhaust samples from the liquid fuels. The GC analyses identified 90 ± 10% of the species contributing to the hot FID total HC measurement for all fuels except isooctane and toluene for which approximately 80 ± 10 and 70 ± 10%, respectively, were identified. Aldehyde emissions were not measured with the exception of benzaldehyde. The difference between the hot FID and GC total carbon values could arise either from loss of some heavier components during sampling or the presence of oxygenates that are not detected by our GC column.

Results

(a) Total HC Emissions. Figure 1 presents the total undiluted exhaust HC emissions [in ppm C_1 ($\sum$ppm(i) × carbon no.(i) for all HC species i where ppm(i) = $P(i)/P$-(total) × 10^6)] measured by the hot FID with no water removed for the seven pure fuels and the tracer fuel mixture. Data are available at the four engine conditions studied for all fuels except isopentane, for which data were obtained only at the base-line condition. The data presented in this figure are split into two groups: those that were obtained before and after the total HC emissions from the engine increased by approximately 20% as determined by measurements using propane or isooctane fuel. This difference was caused by running the engine between data sets A and B under different conditions, which may have changed the amount of deposits in the cylinder. Within each data set, the HC emissions remained constant upon repeat measurements. The first group (A of Figure 1)

includes the gaseous fuels, isopentane, and measurements with isooctane fuel that gave lower total HC emissions. The HC emissions of toluene and the tracer fuel were measured relative to the higher emission value of isooctane, as shown in section B of Figure 1. Within each group, the HC emissions were reproducible to 5% upon repeat measurements made with either propane or isooctane fuel.

As can be seen in Figure 1, the total hydrocarbon emissions mole fraction is strongly affected by the fuel used. These emissions vary by as much as a factor of 4 at the base-line condition, with toluene exhibiting the highest and ethane the lowest HC mole fraction in the exhaust for all conditions studied. Because the air flow through the engine is nearly identical for all fuels at the same operating condition, the engine-out hydrocarbon mass emissions per kilowatt-hour would be directly related to the total HC mole fractions (ppm C_1) presented in Figure 1. All four engine conditions studied show the same trend. Methane has approximately 50% larger HC emissions than ethane, which is followed in turn by monotonically increasing HC emissions as the carbon number of the alkane fuels increases. Toluene, although it has fewer carbon atoms than isooctane, always has the highest HC emissions. These results demonstrate the substantial sensitivity of total engine-out HC emissions to the structure of fuel molecules and illustrate the importance of chemistry in determining HC emissions.

During fuel-lean operation, two primary sources of HC emissions have been identified: storage of fuel in crevice volumes (*2, 3*) and dissolving of fuel in oil films (*4–6*), both of which shield fuel from the passage of the flame in the combustion chamber. In-cylinder sampling measurements have demonstrated that incomplete combustion in the bulk gas does not contribute to HC emissions at fuel-lean equivalence ratios except at high dilution levels (*11, 16*). Furthermore, for HC fuels having carbon numbers less than 6, the effect of an oil film is expected to be minimal since the solubility of these fuels in oils is small (*12*). Thus, for the C_1–C_5 fuels, storage in crevice volumes is the major source of HC emissions.

The fraction of the initial fuel charge stored in the crevices should be similar for all fuels, because to a first approximation the fuel affects neither the volume nor the filling pattern of the crevices. Much of the observed difference in total HC emissions for the C_1–C_5 fuels must result, therefore, from two critical differences caused by fuel structure: (1) different amounts of total carbon are present in the intake charge at the same Φ because of the different H/C ratios of the fuels; and (2) different degrees of burnup of fuel molecules occur upon exiting the crevice volumes because of their different reactivity, diffusion rate, and flame temperature. With respect to observation 1, a $\Phi = 0.9$ intake mixture of each of the fuels tested contains the following total HC carbon mole fractions (ppm C_1): CH_4 (86 000), C_2H_6 (102 000), C_3H_8 (109 000), C_4H_{10} (113 000), C_5H_{12} (115 000), C_8H_{18} (119 000), and C_7H_8 (144 000). Therefore, if all storage and burnup factors were identical, isopentane would emit a factor of 1.13 more carbon-containing species (HC and carbon oxides) than an ethane-fueled engine, far less than the observed difference, and ethane would have 20% more HC (and carbon oxide) emissions than methane fuel, opposite to the observed data.

The effect of H/C ratio on CO and CO_2 emissions is illustrated in Figure 2. The CO_2 mole fractions (moles of CO_2 per total moles in exhaust gas) are reproducible to better than ±3% upon repeat measurements, which were carried out with propane or isooctane fuel. The CO mole

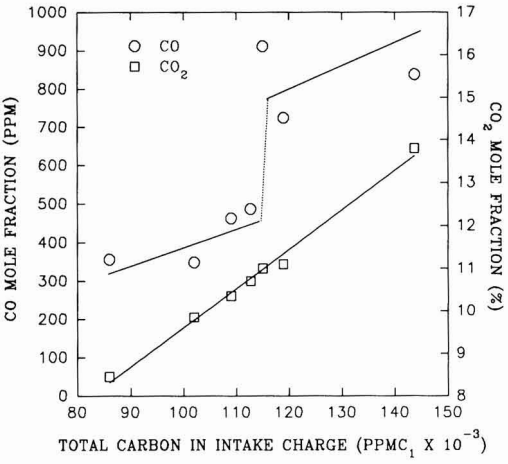

Figure 2. CO and CO_2 mole fractions plotted as a function of the initial carbon content of the intake mixture.

fractions had a larger error (±10%), possibly because of small differences in setting the fuel/air ratio. Note that the carbon dioxide does increase linearly, and the line through the data is that anticipated on the basis of the change in initial carbon content. The CO also increases, although there appears to be a break between the liquid and gaseous fuels, with the liquid fuels having somewhat higher CO emission. The two solid lines through the CO data are those predicted on the basis of the initial carbon content in the intake mixture with the left point of each line fixed at its average measured value. It is possible that this discontinuity might result from slightly poorer mixing of the fuel charge within the cylinder after injection and evaporation of the liquid fuels in the intake port. To provide better mixing in one test, isooctane was injected into the intake manifold upstream of the intake port and the inlet air was heated to approximately 373 K. Both the HC and CO emissions were identical with those obtained with the normal unheated port injection, suggesting that mixing may not be the cause of the slightly increased CO emission from the liquid fuels.

Unlike the CO_2 results, the HC data in Figure 1 are not directly related to the initial carbon content of the intake charge, and this suggests that burnup must play an important role in determining the HC emissions. It has been determined previously that 60–80% of the material stored in crevices burns up before exiting the exhaust pipe, with much of this burnup occurring within the engine cylinder (*13*). Partial burnup of hydrocarbons stored in crevices or oil films could impact HC emissions significantly because the seven fuels may have very different reactivity with respect to this burnup process. In order to estimate the effect of burnup on HC emissions, the free-radical species most responsible for consuming the fuel as it exits from storage areas into the hot burned gas must be identified. On the basis of equilibrium calculations carried out for $\Phi = 0.9$ mixtures in the temperature range 1500–2800 K, the hydroxyl radical is present at approximately 8 times the density of the next most abundant reactive species (H or O atoms). Therefore, it is reasonable to assume that the chemical consumption rate of stored fuel molecules is controlled by their OH reaction rate constants.

While rate constants for the reaction of OH with the fuel hydrocarbons are not available at flame temperatures, they have been measured near 1000 K for methane, ethane, propane, and toluene, yielding relative values of 1, 4.6, 6.6,

and 3, respectively (*14*), based on $k(CH_4) = 1.93 \times 10^{-12}$ cm^3/molecule·s). Extrapolating these non-Arrhenius rate expressions developed for temperatures below 1000 K, the relative rate constants at 1700 K are calculated to be 1, 3.2, 3.9, and 2.3 [using $k(CH_4) = 1.93 \times 10^{-12}$ cm^3/molecule·s]. Estimation of OH rate constants for alkanes based on structure can also be used to determine the relative rate constants for all of the alkane fuels (*17*). This results in rate constant ratios of 1:3.7:5.8:7.8:10.1:13.6 for methane, ethane, propane, *n*-butane, isopentane, and isooctane at 1000 K and 1:2.4:3.6:4.9:5.9:8.2 at 1700 K from the measured values cited above for CH_4. Although the calculated rates at 1700 K lie closer together, the trends remain the same, with methane being by far the least reactive fuel. The higher reactivity of ethane in comparison to methane could explain a reduction in total HC emissions when ethane fuel is used. However, propane, butane, isopentane, and isooctane all have larger rate constants for OH reaction than ethane, because they contain additional abstractable hydrogen atoms. On the basis of the above argument, the total emissions for these fuels might be expected to be less than that of ethane, opposite to the observed trend. Thus, features other than OH reactivity must contribute significantly to the burnup of stored hydrocarbons. The increased carbon content as the H/C ratio decreases is also insufficient to explain the magnitude of the observed trends as mentioned previously. The equilibrium OH density in the burned gas at a given temperature will increase with increasing H/C ratio of the fuel, and this could lead to additional burnup for the lighter alkane fuels. However, the equilibrium OH density for isooctane is only 8% less than that of ethane, and this effect seems too small to influence the HC emissions significantly.

Differences in adiabatic flame temperature of the fuels could affect burnup by changing the temperature of the burned gas. Calculations of adiabatic flame temperatures were carried out for each fuel by assuming that the initial temperature and pressure of the inlet charge were 350 K and 0.5 atm, respectively. The charge was adiabatically compressed by a factor of 9 by using the heat capacity appropriate for each fuel mixture, and the gas was then allowed to burn at constant volume. The adiabatic flame temperatures calculated in this manner are methane 2774 K, ethane 2800 K, propane 2804 K, butane 2805 K, isopentane 2804 K, isooctane 2800 K, and toluene 2863 K. The burned gas temperatures are nearly identical for all fuels except methane and toluene. The slightly lower flame temperature of methane could contribute to the observed higher exhaust HC mole fractions relative to ethane, although the difference is small. Thus, the effect of burned gas temperature alone does not seem sufficient to explain the observed trends in the HC emissions.

An additional aspect that might contribute significantly to the burnup of stored hydrocarbons later in the cycle is molecular diffusion. Gas stored in ring crevices will be laid down along the wall in a layer a few tenths of a millimeter thick as the piston descends. This wall layer is of the order of the thickness of the thermal boundary layer, which is characterized by a sharp decrease of the temperature and, consequently, equilibrium free-radical concentrations as the wall is approached. At sufficiently large distances from the wall, the temperature and the associated equilibrium OH density should be high enough to rapidly consume all hydrocarbons regardless of the fuel species. For example, at a typical average pressure of 5 atm during the expansion stroke and an equilibrated OH density at 1700 K (2×10^{14} molecules/cm^3), the half-life for a molecule having an OH rate constant of 3.7×10^{-11} cm^3/molecule·s [that observed for propane (*14*)] would be 0.1 ms (approximately 1 crank angle degree). This is a fast consumption rate on the engine time scale and is a temperature far below that reached in the combustion process. The time required for a fuel molecule in the layer deposited near the wall to reach this distance will, however, be inversely related to the molecular diffusion constant of the fuel species. On the basis of this assumption, higher molecular weight hydrocarbon species, which have slower diffusion rates, would exhibit less burnup, and have higher engine-out emissions, as is observed. This is a consequence of late-cycle burnup alone, assuming that sources of HC emissions are identical for all of the fuels.

(b) Hydrocarbon Species in the Exhaust. Table I presents the engine-out exhaust HC species concentrations at base-line condition for each of the fuels tested. Careful GC analyses of exhaust samples from propane fuel by both GC techniques revealed that species with a higher molecular weight than propane contribute <3% to the total HC emissions. Thus, for a properly operating engine, any contribution of burning engine oil to the total HC emissions seems negligible. For every fuel, the major HC species present in the exhaust is the fuel itself. However, the fractional contribution of unburned fuel to the total HC emissions varies substantially, as shown in Table I. For methane fuel, exhaust methane comprises 95% of the identified hydrocarbons. Higher molecular weight alkane fuels emit a smaller percentage of unburned fuel, falling to 50% for isooctane. Under lean conditions, the balance of the HC emissions from alkane fuels consists primarily of olefins formed by β-scission of alkyl radical C–C bonds (*15*) for the higher molecular weight fuels. To a lesser extent, disproportionation reactions of methyl radicals may generate C_2H_4 from highly branched alkanes such as isooctane. Products that can be formed by β-scission are italicized in Table I. H-atom elimination from alkyl radicals is also a probable source of olefins, particularly for the light hydrocarbon fuels (e.g., C_3H_6 from C_3H_8 and C_2H_4 from C_2H_6).

The HC emissions from toluene fuel are of a substantially different character. They consist primarily of unburned fuel (83%) and have very low olefin content (1%). The balance of the identified emissions are aromatic fragmentation (benzene) or partial oxidation (benzaldehyde) products. Although benzene currently is a nonregulated HC emission, it is a species of potential health concern and is generated in appreciable quantity (6%) only by the aromatic fuel. Of the alkane fuels, only isooctane produces any measurable benzene (0.3%).

The major exhaust HC species from tracer fuel are those expected from the two principal components present in the mixture. For this reason, to a first approximation, knowledge of the exhaust species formed by pure fuels provides useful information about emissions from fuel mixtures. These species analyses demonstrate that not only the total engine-out HC emissions but also the distribution of species are very sensitive to the fuel type.

Tables II–IV present exhaust HC species emissions for the three other engine conditions. For retarded spark and higher speed operation, the contribution of the unburned fuel to the total HC emissions becomes smaller although it remains a major component in the exhaust, as has been observed previously (*7*). During fuel-rich operation, methane and acetylene emissions contribute a larger fraction to the exhaust hydrocarbons than under lean conditions. This has been observed in more limited engine fuel tests (*7–9*, *11*) and results primarily from incomplete combustion in the chamber during flame passage (*11*).

corrected 8 Oct. 93/AP

Third line from the bottom of column 1, should read "...equilibrated OH density at 1500 K and $\Phi = 1$..."

corrected 8 Oct. 92 /AF

Table I. Measured Species Mole Fractions (ppm C_1)[a] in Exhaust at Base-Line Condition

	fuel							
exhaust species	CH_4	C_2H_6	C_3H_8	C_4H_{10}	C_5H_{12}	C_8H_{18}	C_7H_8	tracer
methane	700	3	11	10	33	28	14	22
acetylene	4	8	19	18	49	35	54	44
ethylene	22	170	*196*	*235*	*198*	59	14	109
ethane	12	374	6	5	13	17		8
allene					7	20		15
propyne				130		17		13
propylene			102	(90)	*166*	*141*		119
propane			423	3				
1,3-butadiene					13	4		10
trans-2-butene					*43*			
cis-2-butene					*27*			
isobutene					*97*	*351*		221
2-methylbut-1-ene					11	13		5
n-butane				555				
pentane								32
isopentane					596			
hexane								30
2-methylpent-1-ene						5		7
4,4-dimethylpent-1-ene						*8*		6
4,4-dimethyl-*trans*-pent-2-ene						*22*		18
2,4-dimethylpent-1-ene						*14*		9
2,4-dimethylpent-2-ene						*24*		15
heptane								36
isooctane					9	790		415
benzene						5	95	43
toluene							1283	460
ethylbenzene							12	10
benzaldehyde							80	34
unburned fuel,[b] %	95	67	56	61	48	51	83	56

[a] ppm C_1(species i) = ppm(i) × carbon no.(i). These data are undiluted and partially dried samples having less than 5% water remaining. [b] Contribution of unburned fuel to total HC emissions.

Table II. Measured Species Mole Fractions (ppm C_1)[a] in Exhaust at MBT-12°

	fuel						
exhaust species	CH_4	C_2H_6	C_3H_8	C_4H_{10}	C_8H_{18}	C_7H_8	tracer
methane	493	2	7	7	35	15	26
acetylene	3	8	14	19	50	89	63
ethylene	14	134	140	176	88	25	117
ethane	8	156	4	4	22		9
allene					26		13
propyne					17		13
propylene			64	85	166		100
propane			159				
1,3-butadiene					9	7	11
trans-2-butene							
cis-2-butene							
isobutene					376		162
2-methylbut-1-ene				195	15		5
n-butane				(555)			
pentane							14
isopentane							
hexane							12
2-methylpent-1-ene					6		
4,4-dimethylpent-1-ene					8		
4,4-dimethyl-*trans*-pent-2-ene					22		11
2,4-dimethylpent-1-ene					13		5
2,4-dimethylpent-2-ene					23		8
heptane							14
isooctane					528		183
benzene					7	126	46
toluene						922	277
ethylbenzene						12	9
benzaldehyde						97	30
unburned fuel,[b] %	95	52	41	40	37	71	44

[a] ppm C_1(species i) = ppm(i) × carbon no.(i). These data are undiluted and partially dried samples having less than 5% water remaining. [b] Contribution of unburned fuel to total HC emissions.

(c) NO_x Emissions. The emitted mole fractions of NO_x for dried exhaust gas samples are presented in Figure 3 for each engine condition. The instrument used for these measurements has a scale maximum of 3000 ppm, and for

Table III. Measured Species Mole Fractions (ppm C_1)[a] in Exhaust at Φ = 1.15

	fuel						
exhaust species	CH_4	C_2H_6	C_3H_8	C_4H_{10}	C_8H_{18}	C_7H_8	tracer
methane	1814	108	166	167	300	148	252
acetylene	28	101	161	180	248	362	268
ethylene	114	286	252	289	165	32	198
ethane	38	724	28	19	37		30
allene					21		17
propyne					25		17
propylene			85	106	168		141
propane			837				
1,3-butadiene					8	6	9
trans-2-butene							
cis-2-butene							
isobutene					328		210
2-methylbut-1-ene					11		6
n-butane				952			
pentane							63
isopentane							
hexane							66
2-methylpent-1-ene							
4,4-dimethylpent-1-ene					4		
4,4-dimethyl-*trans*-pent-2-ene					14		16
2,4-dimethylpent-1-ene					7		
2,4-dimethylpent-2-ene					14		8
heptane							86
isooctane					1412		825
benzene					9	410	141
toluene						3756	827
ethylbenzene						19	20
benzaldehyde						31	12
unburned fuel,[b] %	91	60	55	56	51	79	58

[a] ppm C_1(species *i*) = ppm(*i*) × carbon no.(*i*). These data are undiluted and partially dried samples having less than 5% water remaining.
[b] Contribution of unburned fuel to total HC emissions.

Table IV. Measured Species Mole Fractions (ppm C_1)[a] in Exhaust at 2500 rpm

	fuel						
exhaust species	CH_4	C_2H_6	C_3H_8	C_4H_{10}	C_8H_{18}	C_7H_8	tracer
methane	474	3	8	9	43	17	31
acetylene	4	4	22	28	61	105	73
ethylene	22	152	156	194	110	39	127
ethane	7	100	4	3	20		9
allene					27		13
propyne					27		16
propylene			65	90	162		94
propane			126				
1,3-butadiene							6
trans-2-butene							
cis-2-butene							
isobutene				2[illegible]	302		136
2-methylbut-1-ene					12		8
n-butane				160			
pentane							9
isopentane							
hexane							8
2-methylpent-1-ene							
4,4-dimethylpent-1-ene					6		
4,4-dimethyl-*trans*-pent-2-ene					15		8
2,4-dimethylpent-1-ene					9		5
2,4-dimethylpent-2-ene					13		6
heptane							8
isooctane					281		113
benzene					9	144	47
toluene						834	209
ethylbenzene						13	7
benzaldehyde						96	30
unburned fuel,[b] %	94	39	33	33	26	67	36

[a] ppm C_1(species *i*) = ppm(*i*) × carbon no.(*i*). These data are undiluted and partially dried samples having less than 5% water remaining.
[b] Contribution of unburned fuel to total HC emissions.

any case in which 3000 ppm is reached, the value represents a lower limit to the actual NO_x mole fraction. Methane has the lowest NO_x level of any of the gaseous fuels, reflecting the smaller N_2 fraction in the mixture and

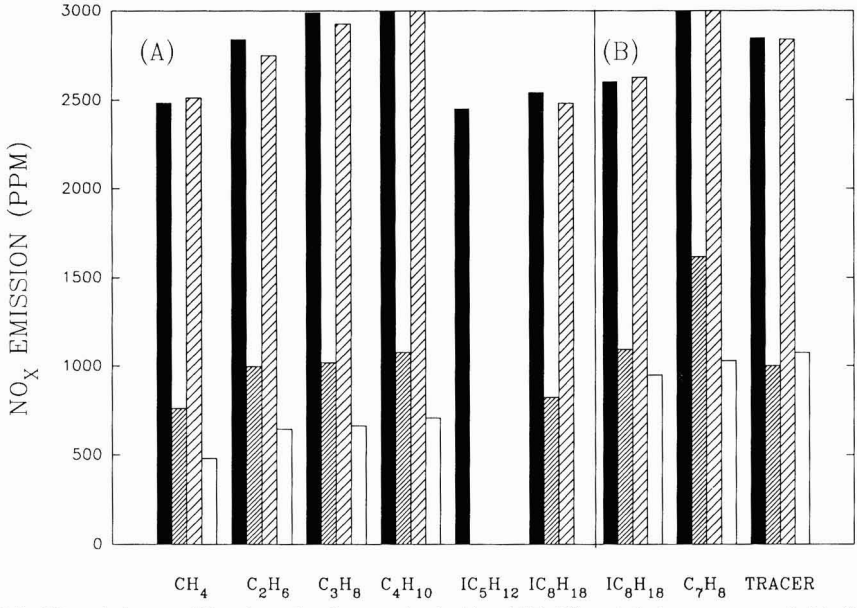

Figure 3. Total dry NO_x emissions: solid bar, base line; fine crosshatched bar, MBT-12° spark timing; coarse crosshatch, 2500 rpm; unfilled bar, $\Phi = 1.15$. The maximum detector response is 3000 ppm; values that reach 3000 ppm are lower limits. Section B data were obtained from the engine when the total HC emissions from isooctane and propane fuels were 20% larger than in (A) (see text).

a lower adiabatic flame temperature. The remaining gaseous fuels show a small increase in NO_x as the number of carbon atoms in the molecule increases, although the change is not very great, consistent with the similar flame temperatures of these fuels presented earlier. Isopentane and isooctane emit 15% less NO_x than any of the gaseous fuels other than methane. This might result in part from evaporative cooling of the intake charge by the liquid fuels during fuel injection.

Conclusions

These engine experiments have determined both the total engine-out exhaust hydrocarbon emissions and the individual hydrocarbon species from a single-cylinder engine operated on seven pure hydrocarbon fuels [four gaseous (methane, ethane, propane, and *n*-butane) and three liquid (isopentane, isooctane, and toluene)] and one fuel mixture. The results prove that the total emissions and individual species concentrations are influenced significantly by the chemical structure of the fuel. Total HC emissions span a factor of 4 under the same operating conditions, with ethane producing the lowest and toluene the highest total HC emissions. In all cases, unburned fuel constitutes a large fraction of the emitted hydrocarbons although the percentage contribution varies from 95% for methane to 50% for isooctane at the base-line engine condition. High speed or retarded spark operation reduces the unburned fuel contribution by up to a factor of 2 for some fuels. Olefins formed by C–C bond scission of alkyl radicals makeup the bulk of the remainder of the HC emissions from the alkane fuels. For the aromatic fuel, toluene, olefins are not observed in appreciable quantity, but benzene and benzaldehyde are present. It is probable that both the total HC emissions and individual species mole fractions in the exhaust are controlled by the post-combustion burnup of fuel stored in crevices and oil films under fuel-lean conditions. During fuel-rich operation, methane and acetylene, formed by incomplete combustion in the bulk gas, contribute a greater amount to the HC emissions for all fuels.

The mole fraction of CO_2 increases with decreasing H/C ratio of the fuel as expected, with toluene producing approximately 60% more CO_2 than methane for the same output power. NO_x emissions show a much smaller, but still significant (20%), variation with fuel structure. This latter observation can be explained in part by differences in adiabatic flame temperature and, in the case of the liquid fuels, evaporative cooling of the intake charge during fuel injection.

Registry No. CH_4, 74-82-8; C_2H_6, 74-84-0; C_3H_8, 74-98-6; C_4H_{10}, 106-97-8; IC_5H_{12}, 78-78-4; IC_8H_{18}, 540-84-1; CH_3Ph, 108-88-3; C_6H_6, 71-43-2; CHOPh, 100-52-7; CO, 630-08-0; NO_x, 11104-93-1; CO_2, 124-38-9; C_2H_2, 74-86-2; C_2H_4, 74-85-1; C_3H_6, 115-07-1; allene, 463-49-0; propyne, 74-99-7; 1,3-butadiene, 106-99-0; *trans*-2-butene, 624-64-6; *cis*-2-butene, 590-18-1; isobutene, 115-11-7; 2-methylbutene, 563-46-2; pentane, 109-66-0; hexane, 110-54-3; 2-methyl-1-pentene, 763-29-1; 4,4-dimethyl-1-pentene, 762-62-9; 4,4-dimethyl-*trans*-2-pentene, 690-08-4; 2,4-dimethyl-1-pentene, 2213-32-3; 2,4-dimethyl-2-pentene, 625-65-0; heptane, 142-82-5; ethylbenzene, 100-41-4.

Literature Cited

(1) United States Clean Air Act 1990. For summary, see: Lee, B. *J. Air Waste Manage. Assoc.* **1991**, *41*, 16.
(2) Adamczyk, A. A.; Kaiser, E. W.; Lavoie, G. A. *Combust. Sci. Technol.* **1983**, *33*, 261.
(3) Furuham, S.; Takeishi, Y. *JSAE Trans.* **1972**, *No. 4*.
(4) Ishizawa, S.; Takagi, Y. *JSME Int. J.* **1987**, *30*, 260.
(5) Kaiser, E. W.; LoRusso, J. A.; Lavoie, G. A.; Adamczyk, A. A. *Combust. Sci. Technol.* **1983**, *28*, 69.
(6) Schramm, J.; Sorenson, C. *SAE Tech. Pap. Ser.* **1989**, *No. 890622*.
(7) Kaiser, E. W.; Rothschild, W. G.; Lavoie, G. A. *Combust. Sci. Technol.* **1983**, *32*, 245.
(8) Ninomiya, J.; Golovoy, A. *SAE Tech. Pap. Ser.* **1969**, *No. 690504*.
(9) Dempster, N. M.; Shore, P. R. *SAE Tech. Pap. Ser.* **1990**, *No. 900354*.

(10) Kaiser, E. W.; Andino, J. M.; Siegl, W. O.; Hammerle, R. H.; Butler, J. W. *J. Air Waste Manage. Assoc.* **1991**, *41*, 195.
(11) LoRusso, J. A.; Kaiser, E. W.; Lavoie, G. A. *Combust. Sci. Technol.* **1983**, *33*, 75.
(12) Adamczyk, A. A.; Kach, R. A. *Combust. Sci. Technol.* **1986**, *47*, 193.
(13) Namazian, M.; Heywood, J. B. *SAE Tech. Pap. Ser.* **1982**, *No. 820088*.
(14) Atkinson, R. *Chem. Rev.* **1986**, *86*, 69.
(15) Dryer, F. L.; Glassman, I. *Prog. Astronaut. Aeronaut.* **1979**, *62*, 255.
(16) Lavoie, G. A.; Adamczyk, A. A.; Kaiser, E. W.; Cooper, J. W.; Rothschild, W. G. *Combust. Sci. Technol.* **1986**, *49*, 99.
(17) Atkinson, R. *Int. J. Chem. Kinet.* **1986**, *18*, 555.

Received for review March 12, 1991. Revised manuscript received June 13, 1991. Accepted June 24, 1991.

Dynamic Partitioning of Semivolatile Organics in Gas/Particle/Rain Phases during Rain Scavenging

Wangteng Tsai[†] and Yoram Cohen*

Department of Chemical Engineering, University of California, Los Angeles, California 90024

Hiroshi Sakugawa and Isaac R. Kaplan

Institute of Geophysics and Planetary Physics, University of California, Los Angeles, California 90024

■ A simple model for studying the below-cloud rain scavenging of semivolatile organics (RSSVO) is presented. The dynamic partitioning of semivolatile organics in gas/particle/rain phases during a rain event is discussed in relation to field data for rain scavenging of semivolatile organics. The RSSVO model considers the gas and particle scavenging, dry deposition, source emissions, atmospheric degradation of organics, and meteorological conditions such as height of cloud base, rain rate, wind direction, and temperature. Case studies for pyrene and fluoranthene rain scavenging are illustrated for the 11/9–10/82 and 3/11/82 Los Angeles rain events. It is shown, based on the above case studies, that (1) wet scavenging of semivolatile organics is affected by the variation of particle size distribution during rain events and (2) the chemical gaseous and particle-bound atmospheric concentrations vary significantly during rain events, and thus, the use of a time-invariant scavenging coefficient in multimedia mass balance calculations should be reexamined.

Introduction

Precipitation scavenging is an important intermedia transport process responsible for the removal of particle-bound air pollutants from the atmospheric via in-cloud and below-cloud scavenging. Numerous field studies and modeling studies of precipitation scavenging have been conducted since the early 1970s. Research activities on rain scavenging in the 1970s included studies on the collection efficiency of particles by raindrops with the goal of gaining basic understanding of scavenging mechanisms (*1–8*). In the 1980s, a greater emphasis was placed on integrated modeling and field studies in order to understand acid deposition. For example, numerous comprehensive models that include in-cloud and below-cloud scavenging mechanisms and cloud microphysics and chemistry have been developed and applied to identify and to quantify the major scavenging mechanisms responsible for the scavenging of acidic compounds (*9–19*). The interested reader is referred to excellent reviews of the complexity of precipitation scavenging published by Hales (*10, 20*) and to a comprehensive proceedings on the subject by Pruppacher et al. (*21*).

[†]Present address: Systech Engineering, Inc., 3744 Mt. Diablo Blvd., Ste 101, Lafayette, CA 94549.

In addition to the important link between precipitation scavenging and acidic deposition, rain scavenging has also been identified as an important pathway for chemical exchange between the atmosphere and natural water surfaces. For example, semivolatile organics such as polycyclic aromatic hydrocarbons (PAHs) and polychlorinated biphenyls (PCBs) are removed from the atmosphere and enter water surfaces by dry deposition and by precipitation scavenging of gases and particles (*22*). The relative importance of gas and particle wet scavenging processes depends on the particle size distribution, the partitioning of organic compounds in the gas and particle phases, and the Henry's law constant (*23*). Given the complexity of rain scavenging, it has been common practice in most mass balance studies to apply empirical approaches that make use of an overall rain scavenging ratio ($W_{overall}$) for the calculation of wet deposition fluxes (*22–30*), as defined below:

$$W_{overall} = W_g(1 - \phi) + W_p\phi \quad (1)$$

in which

$$W_g = C_w^{(d)}/C_a^{(g)} \quad (2)$$

$$W_p = C_w^{(p)}/C_a^{(p)} \quad (3)$$

where W_g and W_p are the gas and particle scavenging ratios, respectively, and ϕ is the fraction of organic compound adsorbed on the atmospheric particle phase. $C_w^{(d)}$ is the dissolved pollutant concentration in rainwater at ground level, $C_w^{(p)}$ is the pollutant concentration, in the particle-bound form, in rainwater, and $C_a^{(g)}$ and $C_a^{(p)}$ are the atmospheric concentrations of the chemical in the gaseous and particle phases, respectively. It is important to note that often W_g and W_p have been taken as time-invariant parameters independent of the particle size distribution and the rate of rainfall.

In this paper, we explore the process of below-cloud rain scavenging for semivolatile organics through the use of a simple rain scavenging model that accounts for the dynamic partitioning of semivolatile organics in the gas/particle/rain phases, as well as the dynamic variation of particle size distribution during the rain event. Finally, a discussion is presented regarding the uncertainty in estimating the scavenging ratio in relation to the interpretation of field data for rain scavenging of semivolatile organics.

 0013-936X/91/0925-2012$02.50/0

Rain Scavenging of Semivolatile Organics (RSSVO): Model Description

The formulation of the present model for the rain scavenging of semivolatile organics (RSSVO) is based on a chemical mass balance that includes the gas, particle, and rain phases in the below-cloud region. We approximate the complex below-cloud rain scavenging process by taking the atmospheric air phase (below-cloud) to be uniform and where convective winds are neglected. Another major assumption, consistent with other studies (*31*, *32*), is that the particle-bound pollutant is adsorbed onto the particle surface with an equal tendency to adsorb on various particle surfaces (e.g., coarse or fine particles). Clearly, these are oversimplifications of the physical phenomena; nonetheless, the current approach is sufficient for the purpose of demonstrating the macrodynamics of below-cloud rain scavenging processes. Accordingly, the overall chemical mass balance on the below-cloud air phase (including the gas and particle phases) can be expressed by

$$(1 - q)\frac{d(V_a C_a)}{dt} = -C_a^{(g)} H_{wa} J_{rain} A \Lambda_g^* - C_a^{(p)} J_{rain} A \Lambda_p - k V_a C_a + S_a \quad (4)$$

where

$$C_a = C_a^{(g)} + C_a^{(p)} \quad (5)$$

$$C_a^{(p)} = C_a \phi \quad (6)$$

$$C_a^{(g)} = C_a(1 - \phi) \quad (7)$$

$$\Lambda_g^* = W_g / H_{wa} \quad (8)$$

$$\Lambda_p = \overline{C_{wf}^{(p)}} / C_a^{(p)} \quad (9)$$

in which $C_a^{(g)}$ and $C_a^{(p)}$ are the concentrations of the gaseous and particle-bound chemical in the atmospheric phase (ng/m^3 of air), respectively, and C_a is the total chemical concentration in the atmosphere (ng/m^3 of air). $\overline{C_{wf}^{(p)}}$ is the chemical concentration, in the particle-bound form, in rainwater (averaged over raindrop size) at ground level (ng/m^3 of water). The fraction of the organic compound adsorbed onto the atmospheric particle phase is denoted by ϕ, and q is the volume fraction of the atmosphere occupied by raindrops, which is taken to be time invariant during a rain event of a given intensity. The volume of the atmosphere is denoted by V_a (m^3), H_{wa} is the dimensionless water to gas partition coefficient (i.e., it is also equivalent to the gas scavenging ratio at the equilibrium condition) for the given chemical, J_{rain} is the precipitation rate (m/s), and A is the interfacial area (m^2) between the atmosphere and the land (or water) surface below, in the region under consideration. It is noted that the left-hand side of eq 4 represents the rate of accumulation of the chemical in the air phase. The first term on the right-hand side of eq 4 accounts for the rate of chemical mass scavenged by raindrops via gas absorption, where Λ_g^* is the normalized gas scavenging ratio (eq 8), which varies between 0 and 1. The second term represents the rate of removal of the particle-bound chemical through particle scavenging by raindrops where Λ_p is the particle scavenging ratio (eq 9). The third term represents the degradation by chemical reaction, which for simplicity we approximate by a first-order reaction where the reaction rate constant is given by k (s^{-1}). Finally, the last term, S_a, is the net input of the chemical into the atmosphere from source emissions (ng/s).

In order to determine the variation in the total atmospheric concentration of the chemical, C_a, during rain (using eq 4) one must first realize that the particle rain scavenging ratio Λ_p is a function of the particle size distribution. The particle size distribution, however, changes during the course of a rain event since the rain scavenging removal efficiency is a function of particle size. Also, the fraction of adsorbed chemical (eq 6) is a function of the particle surface area. As the particle size distribution changes, during rain, the available particle surface area for adsorption will change and thus ϕ will also vary during the course of a rain event. Therefore, the change in the adsorbed fraction ϕ is also reflected in a variation in the vapor-phase concentration of the chemical during rain. In the following section, the various model parameters in eq 4 and the solution algorithm are described.

1. Gas Scavenging Ratio. The normalized gas scavenging ratio (Λ_g^*) for chemicals that are nonreactive in the aqueous phase can be derived theoretically from a chemical mass balance on a raindrop as it falls from cloud base to ground level

$$\frac{d(C_w^{(d)}(4/3)\pi R_d^3)}{d\tau} = K_{OL}(C_a^{(g)} H_{wa} - C_w^{(d)})\pi R_d^2 + \sum_{j=1}^{m} K_{wpj}(C_j^{(p)} H_{wp} - C_w^{(d)}) S_{wj} \quad (10)$$

in which R_d is the radius of raindrop (m), $C_w^{(d)}$ is the chemical concentration (ng/m^3), in the dissolved form, within a given size raindrop, and $C_j^{(p)}$ is the chemical concentration (ng/m^3 of particle) in a particle in size interval j (with a total of m size intervals) within a given size raindrop. The total particle surface area (m^2) contributed by the particles with diameter of a within a given size raindrop is denoted by S_w. τ is the time of travel (below-cloud) for a raindrop (s), where $\tau = 0$ designates the starting time at the cloud base. The water to particle equilibrium partition coefficient is denoted by H_{wp} and K_{OL} and K_{wp} are the overall liquid-phase mass-transfer coefficient (m/s) for the mass transfer of chemicals from air to water (or water to air) and from the solid phase of the scavenged particles to water, respectively. It is acknowledged that, although the drop size may change during its journey from the cloud base to the ground, in the current simple model we neglect such variations in the drop size. Such effects can in principle be incorporated into the model calculations (*18*).

The left-hand side of eq 10 represents the rate of accumulation of chemical mass in the dissolved phase of a raindrop. The first term on the right-hand side of eq 10 accounts for the rain scavenging of pollutant via gas absorption. The second term in eq 10 represents the possible rate of increase in the dissolved chemical mass due to dissolution of the particle-bound chemical (scavenged by rain). The recent studies on the kinetics of hydrophobic organic compound adsorption to natural sediments and soils (*32*) and studies on regeneration kinetics of adsorbents (*33*) suggest that, for "semivolatile" chemicals with low solubility, the rate of dissolution from the particle phase is slow. In fact, an order of magnitude analysis suggests that, during the short residence time of the falling raindrops in the atmosphere, the rate of dissolution will be smaller than the rate of gas absorption by 2 orders of magnitude. Thus, the dissolution from the particle phase is neglected in the current work. The above simplification is consistent with other recent studies on rain scavenging of particle-bound organics (*34*). The effect of the above approximation is that the dissolved concentration in the raindrop will be somewhat underestimated and thus the driving force for gas absorption (and hence the rate of gas

absorption) will be accordingly overestimated.

Given the above simplifications, the average concentration of the dissolved chemical (in rainwater) at ground level, $\overline{C_w^{(d)}}$, is obtained by integrating eq 10 (for a single raindrop of size R_d) between the limits $\tau = 0$ to $\tau = L_c/v_t$ [L_c is the height of cloud base (m) and v_t is the terminal velocity of a given size raindrop (m/s)] and subsequently averaging the chemical concentration over the spectrum of raindrop sizes (*35*, *36*). Accordingly

$$\frac{\overline{C_w^{(d)}}/C_a^{(g)}}{H_{wa}} = \Lambda_g^* = \frac{1}{V_r}\int_0^\infty \left[1 - \left(1 - \frac{C_{wo}^{(d)}H_{aw}}{C_a^{(g)}}\right)\exp\left(\frac{-3K_{OL}L_c}{v_t R_d}\right)\right]\frac{4\pi R_d^3}{3}N_{R_d}\,dR_d \quad (11)$$

in which $C_{wo}^{(d)}$ is the dissolved pollutant concentration in a raindrop of radius R_d at the cloud base, and H_{aw} is the gas to water partition coefficient for the given chemical. The size distribution of raindrops N_{R_d} is defined such that $N_{R_d}\,dR_d$ is the number of falling raindrops in the size range R_d to $R_d + dR_d$ in a unit volume of air, and V_r is the volume of rain per unit volume of air ($m^3\ m^{-3}$) given by

$$V_r = \int_0^\infty \frac{4\pi}{3}R_d^3 N_{R_d}\,dR_d \quad (12)$$

Note that V_r is related to q, the volume fraction of the atmosphere occupied by rain drops [i.e., $q = V_r/(1 + V_r)$].

In order to calculate Λ_g^*, it is necessary to specify K_{OL}, v_t, and N_{R_d}. The overall mass-transfer coefficient (K_{OL}) can be estimated by use of the two-film resistance theory (*37*), i.e.

$$\frac{1}{K_{OL}} = \frac{1}{k_l} + \frac{H_{wa}}{k_g} \quad (13)$$

where k_l and k_g are the liquid-side and gas-side mass-transfer coefficients, respectively. The gas-side mass-transfer coefficient (k_g) can be calculated from (*38*)

$$k_g = (D_g/2R_d)(2 + 0.6Sc^{1/3}Re^{1/2}) \quad (14)$$

in which D_g is the chemical diffusivity in the gas phase estimated by the Chapman–Enskog method (*39*). Sc is the gas-phase Schmidt number [$Sc = \nu_{air}/D_g$, in which ν_{air} is the air kinematic viscosity (m^2/s)] and Re is the raindrop's Reynolds number ($Re = R_d v_t/\nu_{air}$). The liquid-side mass-transfer coefficient (k_l) was estimated from a parameterization of the numerical model of Walcek et al. (*40–42*) for mass transfer of trace gases into raindrops. Accordingly

$$k_l R_d/D_l = 14.5 \quad (15)$$

in which

$$\begin{aligned} D_l/D_o &= 1 && R_d < 5 \times 10^{-4}\ m \\ &= 21.34(R_d/R_{do}) - 20.34 && 5 \times 10^{-4}\ m < R_d < 9 \times 10^{-4}\ m \\ &= 18.07 && R_d > 9 \times 10^{-4}\ m \end{aligned} \quad (16)$$

where D_o and D_L are the molecular and effective diffusivities (m^2/s) in the water phase, respectively, R_d is the raindrop radius (m), and R_{do} is the limiting reference radius of 5×10^{-4} m. The molecular mass diffusivity in the aqueous phase, D_o, can be calculated by using the Wilke–Chang correlation (*39*).

The raindrop terminal velocity, v_t (m/s), is calculated by using the empirical correlation of Easter and Hales (*9*)

$$\begin{aligned} v_t &= 81.1R_d && R_d \le 5 \times 10^{-4}\ m \\ &= 130(2R_d)^{1/2} && R_d > 5 \times 10^{-4}\ m \end{aligned} \quad (17)$$

The raindrop size distribution can be conveniently approximated by the Marshall–Palmer distribution (*43*):

$$N_{R_d} = N_o \exp(-cR_d) \quad (18)$$

where N_o is a constant with the value of $8 \times 10^6\ m^{-4}$, R_d is the drop radius (m), and c is a parameter that varies with the rate of rainfall J_{rain} (m/s)

$$c = 8.2 \times 10^3(3.6 \times 10^6 J_{rain})^{-0.21} \quad (19)$$

With the correlations for K_{OL}, k_g, k_l, v_t, and N_{R_d}, the gas scavenging ratio, Λ_g^*, can be obtained from eq 11 for selected chemicals, as a function of the height of cloud base, the rate of rainfall, and the dissolved pollutant concentration in the raindrop at cloud base relative to the equilibrium concentration.

2. Particle Scavenging Ratio. The average concentration of the particle-bound chemical in rainwater at ground level, $\overline{C_{wf}^{(p)}}$, can be determined from a mass balance on the particle-bound chemical in a raindrop of radius R_d (*36*, *44*) averaged over the spectrum of raindrop sizes. The change in the concentration of the particle-bound chemical in a single raindrop during its path to the ground is given by

$$\frac{d(C_w^{(p)}(4/3)\pi R_d^3)}{d\tau} = \int_0^\infty E(a,R_d)\left(\frac{\pi R_d^2 L_c}{L_c/v_t}\right)C_a^{(p)}F(a)\,da \quad (20)$$

where $C_w^{(p)}$ is the chemical concentration (ng/m^3 of water), in the particle-bound form, within a given size raindrop and $C_a^{(p)}$ is the chemical concentration in the particle phase of the atmosphere. The time of travel (below-cloud) for a raindrop is given by τ, where $\tau = 0$ designates the starting time at the cloud base. The collection efficiency of particle with diameter a by a raindrop of radius R_d is denoted by $E(a,R_d)$. The rate of particle collection is proportional to the volume of air swept by the raindrop, $\pi R_d^2 L_c$, divided by the time required for the raindrop to travel from the cloud base to the ground at a terminal velocity, v_t (i.e., L_c/v_t). Finally, $F(a)$ is the mass fraction distribution of the chemical in the particle phase (m^{-1}) such that $F(a)\,da$ is the mass of the chemical (ng) within the size fraction a to $a + da$. It is important to note that although eq 20 can be theoretically applied to calculate $C_w^{(p)}$, only limited data exist from which $F(a)$ can be determined (*45*, *46*); thus, the direct application of eq 20 is limited. Therefore, in the present model $F(a)$ is obtained theoretically, on the basis of the assumption that the particle-bound pollutant is adsorbed onto the particle surface with equal tendency to adsorb on various particle surfaces (e.g., coarse or fine particles) (*31*, *32*). Therefore, the mass fraction distribution $F(a)$ can be related to the particle size distribution

$$F(a)\,da = [C_s^{(p)}/C_a^{(p)}]f(a)\pi a^2 n(a)\,da \quad (21)$$

where $n(a)$ is the number distribution function of particles in the atmosphere (m^{-3}/m) and $C_s^{(p)}$ is the mass of particle-bound chemical adsorbed per unit surface area of particle (ng of chemical/m^2 of particle), which is related to the concentration $C_a^{(p)}$ by

$$C_s^{(p)} = C_a^{(p)}/S_T = C_a^{(p)}/\int_0^\infty \pi a^2 n(a)\,da \quad (22)$$

in which S_T is the total particle surface area per unit volume of air (m^2/m^3) and πa^2 is the external surface area for a particle (m^2) of diameter of a. Finally, $f(a)$ is a

correction factor that can be introduced to account for the intraparticle surface area that may participate in the adsorption of the organic chemical under consideration. Due to the lack of sufficient quantitative information on the morphology of atmospheric particles and the actual internal surface area that may be involved in the gas/particle partitioning process, $f(a)$ is taken to be unity in the subsequent model calculations. Furthermore, as indicated in the works by Whitby (*47*) and Seigneur et al. (*48*), the trimodal log-normal distribution can adequately characterize the atmospheric particle size distribution. Consequently, the trimodal log-normal distribution is utilized as the initial particle size distribution in this model.

The mass concentration of the particle-bound chemical, $C_{wf}^{(p)}$, in a raindrop of radius R_d (assuming constant radius during the journey to the ground), as it reaches ground level is obtained by integrating eq 20 (using eq 21) from $\tau = 0$ to $\tau = L_c/v_t$ (i.e., the time for the raindrop to reach ground level)

$$C_{wf}^{(p)} = C_{wo}^{(p)} + \frac{3C_s^{(p)}L_c}{4R_d}\int_0^\infty E(a,R_d)\pi a^2 n(a)\,da \qquad (23)$$

in which $C_{wo}^{(p)}$ is the initial concentration at the cloud base (i.e., as a result of in-cloud scavenging) of the particle-bound chemical in a given size raindrop. Subsequently, the average concentration of the particle-bound chemical in the rain at ground level, $\overline{C_{wf}^{(p)}}$, is derived by averaging eq 23 over the entire spectrum of drop sizes

$$\overline{C_{wf}^{(p)}} = \frac{1}{V_r}\int_0^\infty \left(C_{wo}^{(p)} + \frac{3C_s^{(p)}L_c}{4R_d}\int_0^\infty E(a,R_d)\pi a^2 n(a)\,da \right)\frac{4\pi}{3}R_d^3 N_{R_d}\,dR_d \qquad (24)$$

The concentration $\overline{C_{wf}^{(p)}}$ is expected to vary during rainfall as the concentration of the particle-bound chemical in the air phase, and the particle size distribution will vary due to primarily rain scavenging. Thus, in order to determine $\overline{C_{wf}^{(p)}}$ from eq 24, one has to first determine the temporal variation in the particle number distribution, $n(a)$. The particle size distribution $n(a)$ is affected by various transport processes such as rain scavenging, dry deposition, and source emissions. Therefore, a balance equation for the particle phase can be applied in order to determine the temporal variation in the number concentration of the various particle size ranges and hence particle surface area available for partitioning of the given chemical onto the particle phase. The particle balance equation, for an arbitrary particle size interval, is given by

$$(1-q)\frac{d(V_a N_j)}{dt} = -J_{rain}A\,\overline{N_{wfj}} - v_{dj}AN_j + G_{pj} \qquad \text{for } j = 1, 2, ..., m \qquad (25)$$

in which V_a is the volume of the atmospheric compartment and q is the volume fraction of the atmosphere occupied by raindrops. The particle number concentrations in the size interval $a_j - a_{j+1}$ in a unit volume of air and rain at ground level are denoted by N_j [e.g., $N_j = n_j(a)\,da$] and $\overline{N_{wfj}}$, respectively, m is the total number of particle size intervals, and v_{dj} is the dry deposition velocity of particles in size interval j. The term on the left-hand side of eq 25 represents the rate of change of particle number concentration in the atmosphere during a rain event. The first term on the right-hand side of eq 25 accounts for the rate of particle removal by rain scavenging, and the second term represents the removal of particles by dry deposition. Finally, the last term, G_{pj} is the rate of input of particles into the atmosphere from source emissions.

It is noted that $\overline{N_{wfj}}$ in eq 25 can be obtained by applying the equivalent of eq 24 for each particle size interval to obtain the concentration $\overline{C_{wfj}^{(p)}}$, and dividing the resulting equation by $\pi a_j^2 C_s^{(p)}$, the mass of particle-bound chemical adsorbed on the surface of each range of particle diameters a_j, i.e.

$$\overline{N_{wfj}} = \frac{\overline{C_{wfj}^{(p)}}}{\pi a_j^2 C_s^{(p)}} = \frac{1}{V_r \pi a_j^2 C_s^{(p)}}\int_0^\infty \left(C_{woj}^{(p)} + \frac{3C_s^{(p)}L_c}{4R_d}\int_{a_j}^{a_{j+1}} E_j(a,R_d)\pi a^2 n_j(a)\,da \right)\frac{4\pi}{3}R_d^3 N_{R_d}\,dR_d \quad \text{for } j = 1, 2, ..., m \qquad (26)$$

in which $C_{woj}^{(p)}$ is the initial concentration of the particle-bound chemical (at the cloud base) within a particle size range $a_j - a_{j+1}$, in a given size raindrop. $E_j(a,R_d)$ is the collection efficiency of particles by a raindrop of size R_d for the particle size interval j and $n_j(a)$ is the particle number distribution function for the particle size interval j.

The final expression for particle scavenging ratio (Λ_p) is obtained from eq 9, i.e., $\Lambda_p = \overline{C_{wf}^{(p)}}/C_a^{(p)}$, where $\overline{C_{wf}^{(p)}} = \sum_{j=1}^m \overline{C_{wfj}^{(p)}}$. Thus, Λ_p is given by

$$\Lambda_p = \frac{1}{\phi C_a V_r}\sum_{j=1}^m \int_0^\infty \left(C_{woj}^{(p)} + \frac{3C_s^{(p)}L_c}{4R_d}\int_{a_j}^{a_{j+1}} E_j(a,R_d)\pi a^2 n_j(a)\,da \right)\frac{4\pi}{3}R_d^3 N_{R_d}\,dR_d \qquad (27)$$

In order to calculate the particle scavenging ratio from eq 27, the fraction of the chemical adsorbed onto the particle phase ϕ, the collection efficiency $E(a,R_d)$, and the raindrop size distribution N_{R_d} need to be specified. The fraction of chemical adsorbed on the particle phase is approximated by using the Junge correlation (*49*)

$$\phi = bS_T/(P^\circ + bS_T) \qquad (28)$$

in which P° is the solute saturation vapor pressure (atm), S_T is the total surface area of airborne particulate matter per unit volume of air (m^2/m^3), and b is a parameter dependent on the sorbate molecular weight, the heat of desorption from the particle surface, and the heat of desorption of the liquid phase sorbate. According to the study of Junge (*49*), $b = 1.7 \times 10^{-6}$ atm-m, which is in good agreement with the calculated values for b by Pankow (*50*) (e.g., 1.3×10^{-6} and 1.7×10^{-6} atm-m for PAHs and organochlorines, respectively) based on laboratory data of Bidleman and Foreman (*51*) and field data of Bidleman et al. (*52*) and Yamasaki et al. (*53*). It is noted that eq 28 quantifies the partitioning of the exchangeable fraction of semivolatile organics between the particulate and the gaseous phases. Although the effect of nonexchangeable material on the gas–particle partitioning process can be significant for some organics (*54*), Bidleman (*28*) argued that until there is a better understanding of the differences in adsorptive properties of different atmospheric particles as reported from various collection sites, and of the magnitude of volatilization artifacts during air sampling, it may be preferable to use eq 28 to estimate gas–particle partitioning.

The evaluation of the particle scavenging ratio Λ_p (eq 27) requires a determination of the collection efficiency $E(a,R_d)$. There are a number of models that have been proposed for the collection efficiency. In this study we

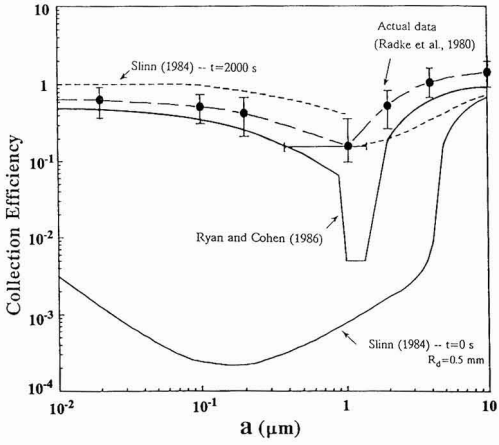

Figure 1. Actual and calculated collection efficiencies (E) as a function of particle diameter (a).

utilize the semiempirical model of Slinn (*55*) and the empirical correlation of Ryan and Cohen (*36*), which is based on the extensive field data of Radke et al. (*8*), as shown in Figure 1. Ryan and Cohen (*36*) expressed the collection efficiency as a function of particle size only noting that the available field data did not reveal a discernable dependence on the rate of rainfall. It is worth noting that the semiempirical collection efficiency model of Slinn (*55*) accounts for various collection mechanisms such as Brownian diffusion, interception, and inertial impaction, as well as the particle growth processes such as due to water vapor condensation (for $a > 1$ μm) and attachment to host particles (for $a < 1$ μm). The dependence of collection efficiency on the particle size and raindrop size is also treated in the Slinn model (*19*, *20*, *55*). Specifically, in Figure 1, the collection efficiency labeled $t = 0$ was obtained for dry particles and 0.5 mm radius raindrops. A higher collection efficiency is expected when the effect of water vapor is considered. For example, the collection efficiency labeled $t = 2000$ s, at $a < 1$ μm, was obtained following the approximate relation proposed by Slinn (*55*), $E = [1 - \exp(-\alpha t) + E(0) \exp(-\alpha t)]$, where α is the attachment rate for Brownian coagulation with droplets, t is the time scale for particle growth processes, and $E(0)$ is the collection efficiency for dry aerosols. The collection efficiency labeled $t = 2000$ s, at $a > 1$ μm, was obtained following Slinn (*55*) by assuming that during rainfall the particles grew by water vapor condensation to the size (and correspondingly increased collection efficiency) given by $a(t) = [a_o^2 + t/100]^{1/2}$, in which a_o is the diameter of dry aerosols. From Figure 1, it is seen that the effective collection efficiency of Slinn increases by about 3–4 order of magnitudes (for $a < 4$ μm) as the time scale for particle growth processes increases from 0 to 2000 s. This implies that the particle growth processes may significantly influence the collection efficiency. The comparison of the performance of the models of Slinn (*55*) and Ryan and Cohen (*36*) on the prediction of pollutant rain concentration is discussed under Case Studies.

Given the gas and particle scavenging ratios, the instantaneous total pollutant concentration in rainwater (i.e., dissolved plus particle bound), C_w (ng/L), at ground level, is given by

$$C_w = C_a^{(g)} H_{wa} \Lambda_g^* + C_a^{(p)} \Lambda_p \tag{29}$$

When model results are compared with field data it is important to note that pollutant rain concentrations reported in most field studies are the average pollutant rain concentrations in each sequential sample of rainwater collected during a rain event (*56–58*). The average pollutant rain concentration in each sequential sample, $\overline{C_w}$, can be easily obtained by performing a simple chemical mass balance on the pollutant in a rain sampler, i.e.

$$d(\overline{C_w} V_s)/dt = C_w J_{rain} A_s \tag{30}$$

in which V_s is the accumulated volume of rainwater in the sampler and A_s is the cross-sectional area of the sampler. The term on the left-hand side of eq 30 represents the rate of accumulation of chemical mass in the sampler, and the term on the right-hand side of eq 30 accounts for the rate of input of chemical mass into the sampler. The concentration $\overline{C_w}$ in the sampler is given from the solution of eq 30

$$\overline{C_w} = \frac{A_s}{V_s} \int_{t_0}^{t} C_w J_{rain} \, dt \tag{31}$$

where t_0 represents the beginning of the sampling period (i.e., $V_s = 0$), C_w is the instantaneous rainwater concentration obtained from eq 29, and the variables on the right-hand side of eq 29 are obtained from the solution of the RSSVO model (eqs 4–29), consistent with the measured rain concentration $\overline{C_w}$.

It is convenient to quantify the degree of rain scavenging by using the following overall rain scavenging ratios

$$W = C_w/C_a \tag{32}$$

and

$$\overline{W} = \overline{C_w}/\overline{C_a} \tag{33}$$

where W and $\overline{W}$ are the instantaneous and average overall scavenging ratios, respectively, and $\overline{C_a}$ is the average air-phase concentration of the chemical (during each sampling period of rain event) defined by

$$\overline{C_a} = \frac{1}{(t - t_0)} \int_{t_0}^{t} C_a \, dt \tag{34}$$

Equations 4–34, subject to the appropriate initial conditions, constitute the governing equations of the RSSVO model. In the present work the RSSVO model equations were solved simultaneously by the predictor and corrector method (*9*). The algorithm of the RSSVO model is shown schematically in Figure 2. The basic model results include the instantaneous concentrations of the dissolved and particle-bound chemical in rainwater (at ground level), the instantaneous gaseous and particle-bound concentrations in the atmospheric phase, and the variations in particle size distribution during rainfall. By use of these results, the various averaged concentrations can be determined as described above.

Case Studies

The RSSVO model was applied in a number of test studies to rain scavenging of pyrene and fluoranthene in Los Angeles. Sequential sampling data of rain rates and PAH concentrations in rainwater were previously reported by Kawamura and Kaplan (*56*) for rain events on 11/9–10/82 and 3/11/82 monitored in Los Angeles. In particular, the most complete field data sets for pyrene and fluoranthene in those two events were selected for this case study. The various model parameters for the two case studies are described below.

Model Input Parameters. The meteorological data required for the rain scavenging model include rain rate, height of cloud base, wind direction, and temperature.

Table I. Meterological Data Applied in the Simulation of the 3/11/82 and 11/9-10/82 (Los Angeles) Rain Events

samples	duration	precip rate,[a] mm/h	cloud base,[b] m	temp,[b] °C	wind directn[b]
		3/11/82			
A	11:00–13:35	1.8	3000	16.7	SW–W
B	13:35–15:05	2.4	3000	15.0	W–N
C	15:05–16:25	1.5	3000	15.0	NE
D	16:25–19:00	1.4	670	15.6	E–SE
E	19:00–20:00	2.2	850	15.0	SE
		11/9–10/82			
A	1:30–4:30	1.3	1830	13.3	SE–NE
break	4:30–9:30		2134	11.1	NE–E
B	9:30–12:45	2.0	400	13.3	E–SE–SW
C	12:45–16:00	1.1	850	14.4	SW–W
break	16:00–19:45		1520	11.7	W–NW
D	19:45–23:25	0.75	1220	11.1	N–NE
E	23:25–9:40	1.4	1160	10.6	SW–NE–E

[a] From Kawamura and Kaplan (*56*). [b] From the observations (on a 3-h interval) at Los Angeles International Airport, 10 km south to UCLA (*59*).

These meteorological data shown in Table I were obtained from the monitoring data of Kawamura and Kaplan (*56*) and observations at Los Angeles International Airport, 10 km south to UCLA (*59*). The compartmental data, emission rates of particles and PAHs, and physicochemical properties of PAHs are summarized in the Table II. Specifically, the surface area of Los Angeles County was determined to be approximately 1.04×10^{10} m^2 (*60*). The emission rate of particles from Los Angeles County was estimated to be 415 tons/day based on the emission inventory for the South Coast Air Basin of California (*61*). The mass concentration of total suspended particles in Los Angeles was estimated to be 80 μg/m^3 based on the monitoring study of Gray et al. (*62*). The emission rates of PAHs (S_a, ng/h) in Los Angeles were estimated from mobile source emission (E_{PAH}, μg/vehicle-km) and information on vehicle miles traveled in Los Angeles (VMT, miles/day). Accordingly, the emission rate for PAH was calculated from

$$S_a = (\text{VMT})(E_{PAH}) \qquad (35)$$

The daily average vehicle miles traveled for the Los Angeles County was reported to be 1.54×10^8 miles/day by the California Department of Transportation (*63*), which is the total VMT by various types of vehicles such as trucks and passenger cars. Although emission data for PAHs in Los Angeles are lacking, estimates can be made from the mobile source emission data recently reported by Benner et al. (*64*) for the Baltimore Harbor Tunnel and by Handa et al. (*65*) for two roadway tunnels in Japan. The average emission rates reported by Handa et al. (*65*) for pyrene (i.e., Nihonzaka Tunnel—15 and 32 μg/vehicle-km estimated for diesel-fueled and gasoline-fueled vehicles, respectively; Tsuburano Tunnel—47 and 91 μg/vehicle-km estimated for diesel-fueled and gasoline-fueled vehicles, respectively) are significantly higher than the pyrene emission values reported by Benner et al. (*64*) (i.e., 8 ± 3 μg of pyrene/vehicle-km). Therefore, the emission rates reported by Benner et al. and Handa et al. can be considered as the lower and upper limits, respectively. In the current work, average pyrene emission of 30 μg/vehicle-km, which is within the reported limits, was found to be a reasonable choice. It is important to note that, while Handa et al. (*65*) did not provide fluoranthene emission data, Benner et al. (*64*) reported fluoranthene emission to be nearly identical with pyrene emission. Thus, an average emission value of 30 μg/vehicle-km was also taken to be a reasonable approximation for the emission of fluoranthene. Subsequently, by use of the daily average vehicle miles traveled for Los Angeles County and eq 35, the daily average emission rates of pyrene and fluoranthene were estimated to be 3.1×10^{11} ng/h (Table II).

Since the actual diurnal variations in emission rates were not available, the potential effect of such emission variations, between morning and afternoon rush hours, were studied by estimating the likely range of these variations based on the diurnal change of traffic volume (*66*). Accordingly, the emission rates of particles and PAHs during the morning and afternoon rush hours were assumed to be a factor of 2.25 and 3.0, respectively, higher than the daily average emission rates. An additional simulation was carried out where the emission rates for the morning and afternoon rush hour periods were taken to be 50% lower than the above base values. Moreover, the emissions of

Table II. Compartmental Data for the Los Angeles County and Physicochemical Properties of Pyrene and Fluoranthene

(A) Compartmental Data

parameter	value	ref
land and water surface areas, m^2	1.04×10^{10}	California Almanac (*60*)
daily av emissn rate of particle matter, tons/day	415[a]	SCAQMD (*61*)
daily av emissn rates of pyrene and fluoranthene, ng/h	3.1×10^{11} [a]	eq 35 of this work
initial ambient air concn, ng/m^3		
pyrene	0.7[c] (0.7)[d]	Gordon and Bryan (*67*), Grosjean (*68*)[b]
fluoranthene	1.9 (1.2)	
Initial mass concn of total suspended particles, μg/m^3	80	Gray et al. (*62*)

(B) Physicochemical Properties

parameter	pyrene	fluoranthene	ref
mol wt	202	202	EPA (*69*)
degradatn rate const in atmosphere, h^{-1}	0.29	0.19	Dragoescu and Friedlander (*46*)
saturation vapor pressure, mmHg	2.5×10^{-6}	5.0×10^{-6}	EPA (*69*)
Henry's law const, Pa m^3 mol^{-1}	0.125	0.134	Baker and Eisenreich (*22*)
molal vol, cm^3/mol	213.8	217.3	Reid et al. (*39*)
bp, °C	388	377	Pearlman et al. (*70*)

[a] The diurnal variations of the emission rates of both particles and PAHs were taken into account in the model based on the diurnal change of traffic volume reported by the 1976 SCAG Urban/Rural Travel Survey (*66*). [b] The 1-year average (1971–1972) ambient air concentrations of pyrene and fluoranthene in Los Angeles reported by Gordon and Bryan (*67*) are 1.9 and 2.0 ng/m^3, respectively. The mean concentrations of pyrene and fluoranthene (for summer and winter 1981) in Los Angeles reported by Grosjean (*68*) are 1.62 (range 0.48–3.64) and 0.94 (range 0.24–1.98) ng/m^3, respectively. [c] 3/11/82 rain event. [d] 11/9–10/82 rain event.

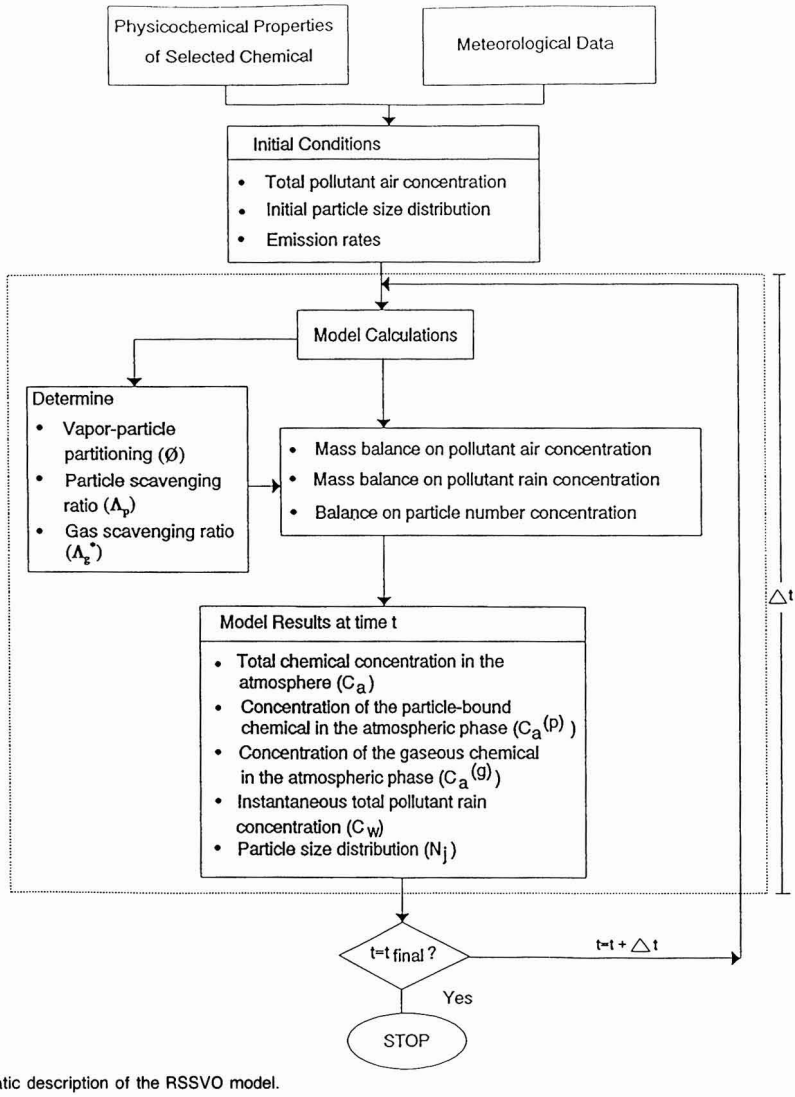

Figure 2. Schematic description of the RSSVO model.

particles and PAHs during the period of 11 p.m.–5 a.m. were assumed to be negligible.

The initial ambient air concentrations of PAHs for the simulations of rain events on 3/11/82 and 11/9–10/82 in Los Angeles were estimated from reported ambient air concentrations of PAHs in Los Agenels (*67*, *68*). Monitoring data were not available to establish the concentration of PAHs in the dissolved and particulate phases at the cloud base ($C_{woj}^{(p)}$ and $C_{wo}^{(d)}$). Thus, in the simulations described below, both $C_{woj}^{(p)}$ and $C_{wo}^{(d)}$ were taken to be zero. This assumption results in a lower limit estimate of the concentration of scavenged particles in rainwater at ground level. Finally, the pertinent physicochemical properties (e.g., degradation rate constant in atmosphere, solute saturation vapor pressure, Henry's law constant, molal volume, and boiling temperature) for pyrene and fluoranthene are given in Table II.

Simulation Results. Simulations of rain scavenging of pyrene and fluoranthene during the 3/11/82 and 11/9–10/82 rain events in Los Angeles were performed, given the above compartmental data, meteorological conditions, emission rates, and the physicochemical properties of the selected pollutants.

Figures 3 and 4 illustrate the comparison of actual and predicted pyrene and fluoranthene rain concentrations ($\overline{C_w}$) for each of the sequential samples taken during the 3/11/82 and 11/9–10/82 rain events. From Figures 3 and 4, it is seen that the predicted pyrene and fluoranthene rain concentrations, based on the collection efficiencies of Slinn (*55*) with t = 2000 s and of Ryan and Cohen (*36*), are in good agreement with the available field data. Although the time scale in the Slinn model could be optimized as an empirical parameter to provide better fit with the data, this was not attempted. Within the scope of this work it suffices to conclude that the Slinn model for the collection efficiency appears to be adequate in describing the data.

It is noted that both the field data and model prediction illustrate that pyrene and fluoranthene rain concentrations for the fourth and fifth samples of the 3/11/82 rain event increased drastically relative to the first three samples.

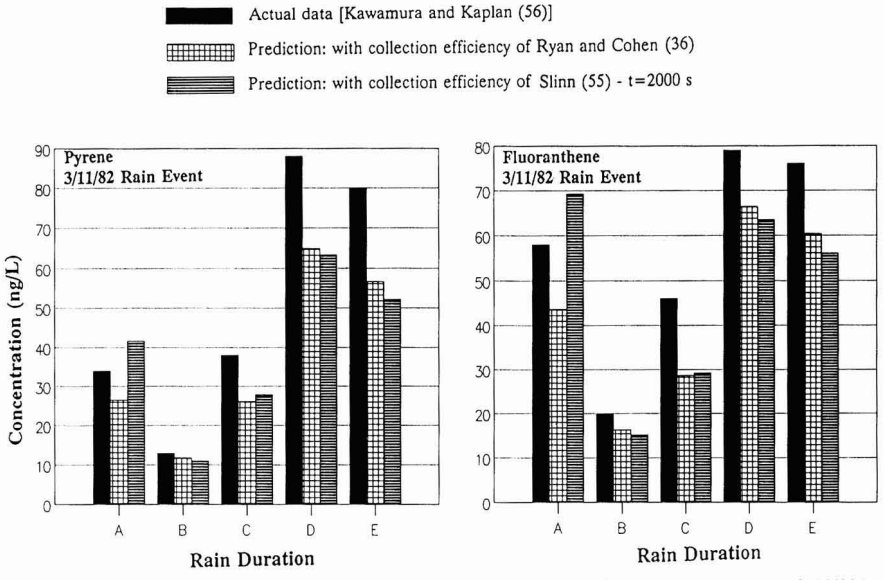

Figure 3. Predicted and measured pyrene and fluoranthene sampler rain concentrations ($-C_w$) at ground level for the 3/11/82 Los Angeles rain event. Time duration for each sequential rain sample: A, 11:00–13:35; B, 13:35–15:05; C, 15:05–16:25; D, 16:25–19:00; E, 19:00–20:00.

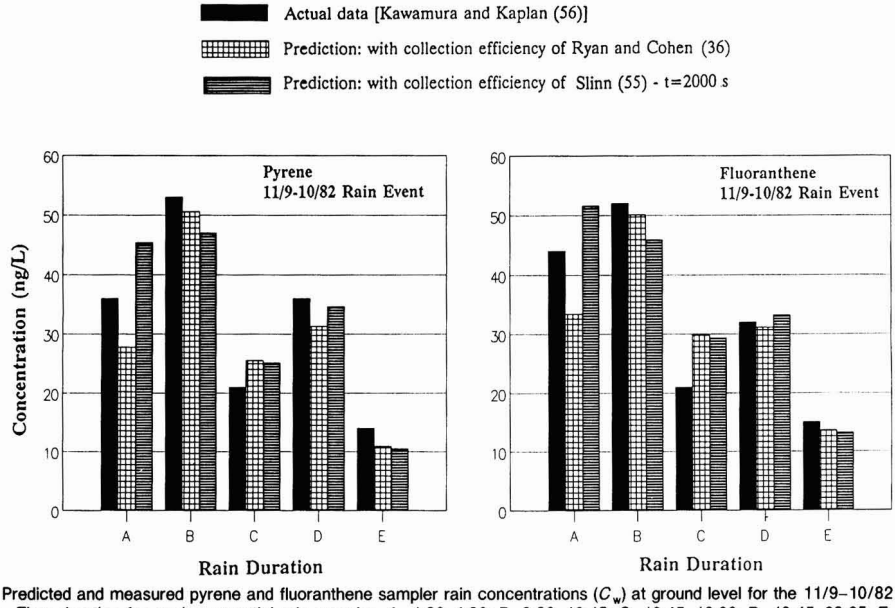

Figure 4. Predicted and measured pyrene and fluoranthene sampler rain concentrations (C_w) at ground level for the 11/9–10/82 Los Angeles rain event. Time duration for each sequential rain sample: A, 1:30–4:30; B, 9:30–12:45; C, 12:45–16:00; D, 19:45–23:25; E, 23:25–9:40.

The above trend is consistent with increased emissions during later afternoon rush hour traffic, the decrease in cloud base height, and easterly wind direction (e.g., wind blowing from downtown Los Angeles toward the UCLA sampling site), which transported the highly polluted air from downtown Los Angeles to the sampling site at UCLA (see Table I). It is also noted that, for the 11/9–10/82 rain event, the highest pyrene and fluoranthene rain concentrations were obtained for the second sample, which is consistent with the morning rush hour traffic, the low cloud base, and easterly wind direction (Tables I and II). Although the rush hour traffic in the late afternoon (e.g., during the break between the fourth and fifth sampling periods) could have allowed the atmospheric concentration of the pollutants to increase (Figure 6), the westerly wind (Table I) that carried the clean air from the coastal areas to the sampling site, as well as the higher cloud base relative to that in the period of the second sample, led to a lower pollutant rate concentrations for the fourth sample relative to the second sample. Clearly, the wind direction and height of cloud base are significant in determining the levels of pollutants in the collected rainwater. Specifically, the influence of the 50% decrease of rush hour emissions of particles and PAHs on the predicted pyrene rain concentrations for the 3/11/82 and 11/9–10/82 events is shown in Figure 5 [using the collection efficiency of Ryan and Cohen (*36*)]. From Figure 5, it is seen that the decrease of rush hour emissions significantly influences the agreement between the predicted and measured pyrene rain concentrations (e.g., samples D and E of the 3/11/82

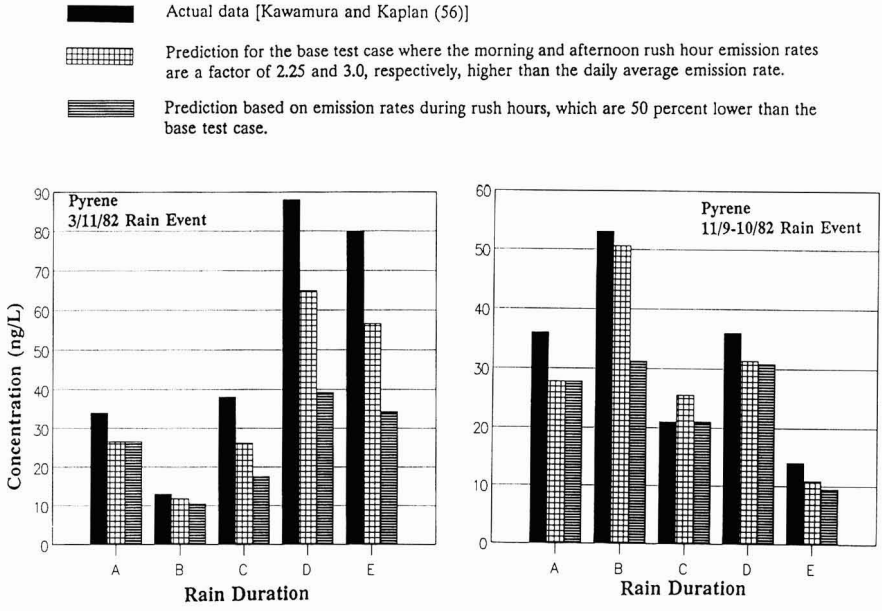

Figure 5. Influence of rush hour emissions on predicted ground-level pyrene rain concentrations (C_w) for the 3/11/82 and 11/9–10/82 Los Angeles rain events.

event and sample B of the 11/9–10/82 event). Although one could attribute part of the deviation of the predicted concentrations from the reported data to the neglect of the effect of convective winds in the simulations, it is difficult at present to evaluate the precise effect of convective winds since data on PAH emissions in the Los Angeles area are lacking. The availabilty of such data will undoubtedly improve the ability to better quantify the wet scavenging of PAHs.

It is important to note that in most field studies the reported rain scavenging ratio (eq 1) is determined on the basis of a constant atmospheric concentration (C_a). Due to sampling difficulties, reported field measurements of the rain scavenging ratio are generally values averaged over different sampling periods. In reality, pollutant concentrations in both air and rainwater are time dependent during rain events. Thus, the rain scavenging ratio is expected to vary with time during a given rain event. In the present model, the temporal variations in the atmospheric and rainwater concentrations are determined and thus one can evaluate the corresponding change in the rain scavenging ratio (eqs 32 and 33) during rain events. As an illustration, the predicted instantaneous total pyrene concentrations in rainwater (C_w) and in the air phase (C_a) and the instantaneous concentrations of the particle-bound pyrene in the atmosphere ($C_a^{(p)}$) and rainwater ($\overline{C_{wf}^{(p)}}$) at ground level for the 11/9–10/82 event (using the collection efficiency of Ryan and Cohen) are given in Figures 6 and 7, respectively. As Figure 7 illustrates, although less than 30% of the atmospheric pyrene exists in the particle-bound form (i.e., $C_a^{(p)}/C_a \leq 0.3$), particle scavenging accounts for more than ~50% of the resulting total pyrene rainwater concentration when $C_a^{(p)}/C_a \geq 0.05$. It is important to recognize that the concentration of pyrene in rainwater decreases drastically as the rainfall continues, especially during the initial periods of rainfall or at the initial period after the rainfall restarts following a break period (Figure 6). The pyrene air concentration during rainfall is sensitive to the variations of cloud base height and source emissions.

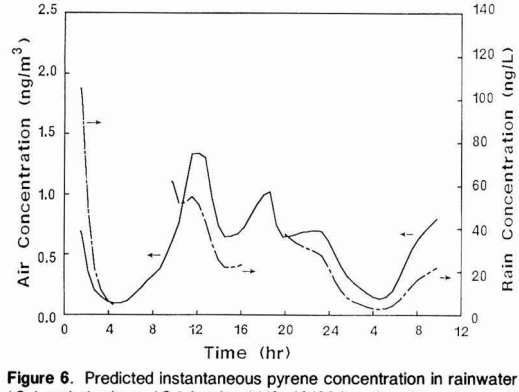

Figure 6. Predicted instantaneous pyrene concentration in rainwater (C_w) and air phase (C_a) for the 11/9–10/82 Los Angeles rain event.

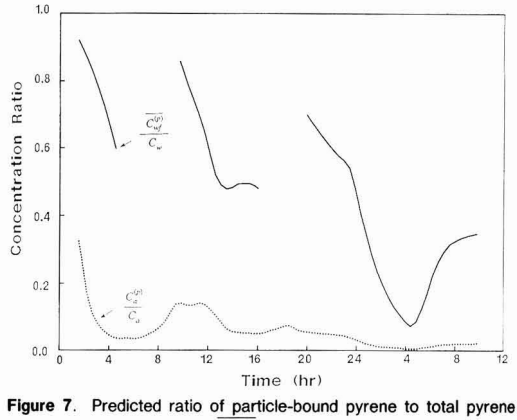

Figure 7. Predicted ratio of particle-bound pyrene to total pyrene concentrations in rainwater ($\overline{C_{wf}^{(p)}}/C_w$) and the ratio of particle-bound pyrene to total pyrene concentrations in the atmospheric phase ($C_a^{(p)}/C_a$) for the 11/9–10/82 Los Angeles rain event.

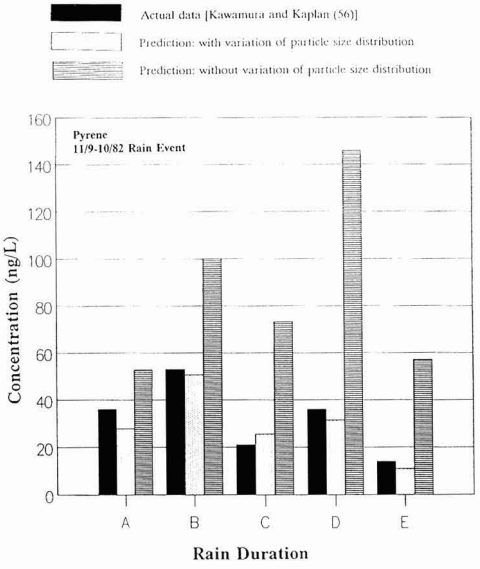

Figure 8. Comparison of predicted and measured pyrene sampler rain concentrations ($\overline{C_w}$) illustrating the effect of the variation of particle size distribution [based on the 11/9–10/82 rain event and using the collection efficiency of Ryan and Cohen (*36*)]. Time duration for each sequential rain sample: A, 1:30–4:30; B, 9:30–12:45; C, 12:45–16:00; D, 19:45–23:25; E, 23:25–9:40.

For example, the decrease in cloud base from 2134 to 400 m at the end of morning rush hour (Table I) led to an increase of pyrene air concentration in the initial period of the second sampling interval (i.e., 9:30–11:00 a.m.) for the 11/9–10/82 rain event. It is worth noting that during the breaks in the rain event (Table I), which cover the morning and afternoon rush hours, the atmospheric pyrene concentration increases due to automobile emissions. Consequently, a high pyrene rain concentration results at the initial period after the rainfall restarts following a break period.

The influence of the variation in the particle size distribution during rainfall on the concentration of the scavenged pollutant in rain is demonstrated for pyrene in Figure 8. From Figure 8, it can be seen that the neglect of the variation of particle size distribution (i.e., when a constant particle size distribution is assumed) results in the overprediction of pyrene rain concentration for the 11/9–10/82 event. The use of a constant particle size distribution will lead to an overestimate of the amount of particles remaining in the atmosphere, during the rainfall, and thus a significant overprediction of the pollutant rain concentration will result. An illustration of the change in the particle size distribution [distribution of particle number concentration, i.e., $dN/d\ (\log a)$] during rainfall is depicted in Figure 9 for the first sampling period of the 11/9–10/82 event (sample A in Figure 4). The above behavior is expected since particle rain scavenging, as can be concluded from the dependence of the collection efficiency on particle size (Figure 1), is sensitive to particle size. Specifically, the coarse particles ($a > 2\ \mu m$) and fine particles in the size range of $a < 0.4\ \mu m$ are removed efficiently by raindrops, whereas the wet removal of particles in the size range of $a = 0.4$–$2\ \mu m$ is less significant.

Given the chemical concentration in rainwater and in the atmospheric phase, it is possible to determine the temporal variations of the overall instantaneous and average scavenging ratios (defined by eqs 32 and 33, re-

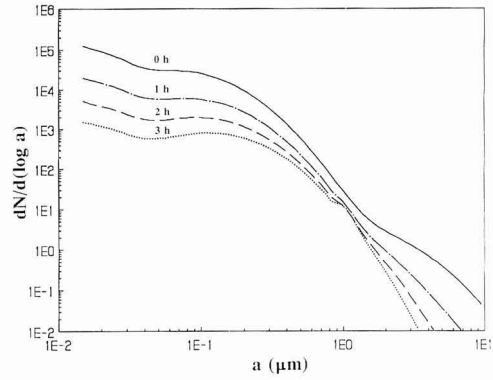

Figure 9. Change in the distribution of particle number concentration [$dN/d\ (\log a)$] during the first sampling period of the 11/9–10/82 rain event (sample A in Figure 4).

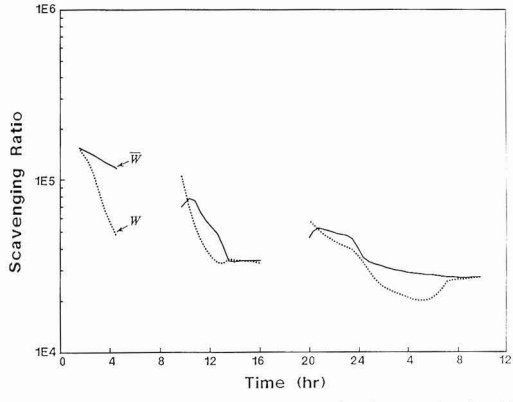

Figure 10. Predicted overall scavenging ratio of pyrene for the 11/9–10/82 rain event [using the collection efficiency of Ryan and Cohen (*36*)].

spectively) as illustrated in Figure 10 for the rain scavenging of pyrene during the 11/9–10/82 rain event (using the collection efficiency of Ryan and Cohen). The predicted overall scavenging ratios, W and $\overline{W}$, vary in the range of 2.03×10^4–1.53×10^5 and 2.72×10^4–1.53×10^5, respectively. The nearly order of magnitude variation in the scavenging ratios during rainfall suggests that the application of average experimental values of rain scavenging ratios for mass balance calculations is questionable. It is also important to note that the reporting basis for field-measured scavenging ratios is not uniform. Some studies report the scavenging ratios, as calculated from eq 1, based on atmospheric concentration measured before, during, or even after the specific rain event (see Table III). Yet, in some studies the reported scavenging ratios are values representing time periods that may be as long as several months in duration. The inconsistency in the reporting basis for rain scavenging ratios ultimately results in an uncertainty as to the extrapolation of reported values to other regions, different rain conditions, or atmospheric concentrations. Despite the uncertainty regarding the calculation basis (i.e., the pollutant air concentration) for field-measured scavenging ratios, the present model calculations for Los Angeles are compared with those reported by Ligocki et al. (*24*, *25*), Farmer and Wade (*71*), and McVeety and Hites (*72*), as shown in Table III.

The present study suggests that the rain scavenging ratio is not a universal constant that is characteristic of solely

Table III. Rain Scavenging Ratio of Pyrene and Fluoranthene

W ($\times 10^{-3}$)				
pyrene	fluoranthene	rain rate, mm/h	duration, h	basis of chem air concn
		1. Predicted in This Work[a]		
(i) 11/9–10/82				
20.3–153.0[b]	18.2–98.7[b]	1.4–2.4	9.0	instantaneous
12.1–153.0[c]	9.8–98.7[c]			initial
27.2–153.0[c]	21.5–98.7[c]			cumulative av during each sampling period
(ii) 3/11/82				
16.3–264.0[b]	14.9–174.0[b]	0.8–2.0	22.2	instantaneous
16.0–145.0[c]	8.6–93.5[c]			initial
35.4–145.0[c]	26.0–93.5[c]			cumulative av during each sampling period
		2. Reported from Other Field Studies		
7.8[d]	8.9[d]	not reported	5.8–41.5	not clearly specified
9.1[e]	10.4[e]	1.1	not clearly specified	av during rain event
3.3[f]	4.8[f]	not reported	not reported	summer arithmetic av

[a] Collection efficiency of Ryan and Cohen (*36*) is used. [b] Using the instantaneous pyrene or fluoranthene rain concentration. [c] Using the cumulative average pyrene or fluoranthene rain concentration. [d] Mean scavenging ratio reported by Farmer and Wade (*71*) for seven rain events (1982–1983) at an urban site in Norfolk, VA. [e] Calculate on the basis of data of Ligocki et al. (*24*, *25*) on 3/16–20/84 Portland, OR, rain event. Note that rain duration was not specifically reported; however, the sample date (e.g., 3/16–20/84) and total rainfall amount (2.1 cm) were reported (*24*, *25*). [f] Mean scavenging ratio reported by McVeety and Hites (*72*) for measurements of air and rain concentrations of PAHs at Siskiwit Lake. Note that the rain samples were collected on a weekly basis and thus the results are averages for the total number of discrete rain events.

the chemical being scavenged by rain. The rain scavenging ratio is a function of numerous variables including the chemical type, rate and duration of rainfall, height of cloud base, source emissions during rainfall, particle size distribution, and temperature. Consequently, in order to properly interpret rain scavenging data, field studies should at the minimum report the above information. Also, since the rain scavenging ratio can vary significantly during rainfall, it is important that a consistent basis is used for reporting the concentrations in the atmospheric and rainwater phases. Simultaneous measurements of the atmospheric and rainwater concentrations would best serve to validate and improve existing rain scavenging models. Admittedly, such studies are difficult and represent an experimental challenge. Finally, it should be recognized that pollutant concentrations in the atmospheric phase can vary with vertical distance above ground level; in such cases the concept of a rain scavenging ratio is inappropriate and more definitive detailed models should be used.

Summary and Conclusion

Below-cloud rain scavenging of semivoltaile organis was investigated by a mass balance model that accounts for the dynamic partitioning of atmospheric organics in gas/particle/rain phases during a rain event. Results of case studies for pyrene and fluoranthene illustrated that (1) the variation of particle size distribuition during rainfall affects the prediction of rain scavenging of particle-bound organics and (2) the clarification of the basis of ambient air concentration of the selected chemical that is utilized in the calculation of scavenging ratio is essential for reducing the uncertainty associated with the use of scavenging ratios reported from field studies.

The current model was rewritten in a flexible modular form. Thus, the code (written in Fortran and executable on the IBM PC/XT/AT-type computers) can be easily modified to accommodate different collection efficiencies, initial partial size distributions, raindrop size distribution, chemical sorption model, etc. Since the model is a dynamic box-type model, it is especially suited for dynamic multimedia mass balance studies of particle-bound organics. It is noted that, if spatial resolution of concentrations in the atmosphere (e.g., vertical concentration profiles) is of interest, then the present approach will have to be modified to account for vertical concentration profiles as well as the effect of convective winds. Work is currently underway to include the detailed mechanisms of rain scavenging of semivolatile organics into a comprehensive precipitation scavenging model.

Copies of the RSSVO model software can be obtained upon request by writing to Professor Yoram Cohen at the National Center for Intermedia Transport Research.

Acknowledgments

We thank J. M. Hales for his helpful comments.

Registry No. Pyrene, 129-00-0; fluoranthene, 206-44-0.

Literature Cited

(1) Grover, S. N. *Pageoph* **1976**, *114*, 509–520.
(2) Grover, S. N.; Pruppacher, H. R.; Hamielec, A. E. *J. Atmos. Sci.* **1977**, *34*, 1655–1663.
(3) Wang, P. K.; Pruppacher, H. R. *J. Atmos. Sci.* **1977**, *34*, 1664–1669.
(4) Beard, K. V. In *Precipitation Scavenging (1974)*; ERDA Symposium Series; (Champaign, IL, Oct 14–18, 1974, Semonin, R. G.; Beadle, R. W., Coordinators) CONF-741003, NTIS; 1977; pp 183–194.
(5) Slinn, W. G. N. *Water, Air, Soil Pollut.* **1977**, *7*, 513–543.
(6) Williams, A. L. In *Precipitation Scavenging (1974)*; ERDA Symposium Series; (Champaign, IL, Oct 14–18, 1974, Semonin, R. G.; Beadle, R. W., Coordinators) CONF-741003, NTIS; 1977; pp 258–275.
(7) Davenport, H. M.; Peters, L. K. *Atmos. Environ.* **1978**, *12*, 997–1008.
(8) Radke, L. F.; Hobbs, P. V.; Eltgroth, M. W. *J. Appl. Meteorol.* **1980**, *19*, 715–722.
(9) Easter, R. C.; Hales, J. M. PLUVIUS: A Generalized One-Dimensional Model of Reactive Pollutant Behavior, Including Dry Deposition, Precipitation Formation, and Wet Removal. Report PNL-4046 ED2; Batelle Pacific Northwest Laboratories: Richland, WA, 1984.
(10) Hales, J. M. *Atmos. Environ.* **1989**, *23*, 2017–2031.
(11) Lee, I.-Y.; Shannon, J. D. *Atmos. Environ.* **1985**, *19*, 143–149.
(12) Carmichael, G. R.; Peters, L. K.; Kitada, T. *Atmos. Environ.* **1986**, *20*, 173–188.
(13) Hong, M.-S. Carmichael, G. R. *Atmos. Environ.* **1986**, *20*, 1989–1986.
(14) Rutledge, S. A.; Hegg, D. A.; Hobbs, P. V. *J. Geophys. Res.* **1986**, *91D*, 385–402.
(15) Hegg, D. A.; Rutledge, S. A.; Hobbs, P. V. *J. Geophys. Res.* **1986**, *91D*, 403–416.

(16) Seigneur, C.; Saxena, P. *Atmos. Environ.* **1984**, *18*, 2109–2124.
(17) Seigneur, C.; Saxena, P. *Atmos. Environ.* **1988**, *22*, 101–115.
(18) Tsai, W.; Altwicker, E. R. *Atmos. Environ.* **1990**, *24A*, 2473–2483.
(19) Tsai, W.; Altwicker, E. R.; Asman, W. A. H. *Atmos. Environ.* **1990**, *24A*, 2485–2498.
(20) Hales, J. M. In *Air Pollutants and Their Effects on the Terrestrial Ecosystem*: Legge, A. H., Krupa, S. V., Eds.; Advances in Environmental Science and Technology; J. Wiley & Sons: New York, 1986; Vol. 18, Part 4, pp 211–251.
(21) Pruppacher, H. R., Semonin, R. G., Slinn, W. G. N., Eds. *Precipitation Scavenging, Dry Deposition, and Resuspension*; Proceedings of the Fourth International Conference, Santa Monica, CA, 29 November–3 December, 1982; Elsevier: New York, 1983.
(22) Baker, J. E.; Eisenreich, S. J. *Environ. Sci. Technol.* **1990**, *24*, 342–352.
(23) Eisenreich, S. J. In *Sources and Fates of Aquatic Pollutants*; Hites, R. A., Eisenreich, S. J., Eds.; Advances in Chemistry 216; American Chemical Society: Washington, DC, 1987; pp 393–469.
(24) Ligocki, M. P.; Leuenberger, C.; Pankow, J. F. *Atmos. Environ.* **1985**, *19*, 1609–1617.
(25) Ligocki, M. P.; Leuenberger, C.; Pankow, J. F. *Atmos. Environ.* **1985**, *19*, 1619–1626.
(26) Schroeder, W. H.; Lane, D. A. *Environ. Sci. Technol.* **1988**, *22*, 240–246.
(27) Eisenreich, S. J.; Willford, W. A.; Strachan, W. M. J. In *Intermedia Pollutant Transport: Modeling and Field Measurements*; Allen, D. T., Cohen, Y., Kaplan, I. R., Eds.; Plenum: New York, 1989; pp 19–40.
(28) Bidleman, T. F. *Environ. Sci. Technol.* **1988**, *22*, 361–367.
(29) Czuczwa, J.; Leuenberger, C.; Giger, W. *Atmos. Environ.* **1988**, *22*, 907–916.
(30) Leuenberger, C.; Czuczwa, J.; Heyerdahl, E.; Giger, W. *Atmos. Environ.* **1988**, *22*, 695–705.
(31) Rounds, S. A.; Pankow, J. F. *Environ. Sci. Technol.* **1990**, *24*, 1378–1386.
(32) Wu, S. C.; Gschwend, P. M. *Environ. Sci. Technol.* **1986**, *20*, 717–725.
(33) Costa, C.; Rodrigues, A. *Chem. Eng. Sci.* **1985**, *40*, 707–713.
(34) Mackay, D. M.; Paterson, S.; Schroeder, W. H. *Environ. Sci. Technol.* **1986**, *20*, 810–816.
(35) Cohen, Y. In *Pollutants in a Multimedia Environment*; Cohen, Y., Ed.; Plenum: New York, 1986; pp 117–131.
(36) Ryan, P. A.; Cohen, Y. *Chemosphere* **1986**, *15*, 21–47.
(37) Lewis, W. K.; Whitman, W. G. *Ind. Eng. Chem.* **1924**, *16*, 1215.
(38) Bird, R. B.; Stewart, M. E.; Lightfoot, E. M. *Transport Phenomena*; Wiley: New York, 1960; p 363.
(39) Reid, R.; Prausnitz, J.; Sherwood, T. *The Properties of Gases and Liquids*, 3rd ed.; McGraw Hill: New York, 1979; pp 57–58.
(40) Walcek, C. J.; Pruppacher, H. R. *J. Atmos. Chem.* **1984**, *1*, 269–289.
(41) Walcek, C. J.; Pruppacher, H. R.; Topalian, J. H.; Mitra, S. K. *J. Atmos. Chem.* **1984**, *1*, 291–306.
(42) Walcek, C. J.; Pruppacher, H. R. *J. Atmos. Chem.* **1984**, *1*, 307–324.
(43) Marshall, J. S.; Palmer, W. M. *J. Meteorol.* **1848**, *5*, 165–166.
(44) Scott, B. C. *Atmos. Environ.* **1982**, *16*, 1753–1762.
(45) Miguel, A. H.; Friedlander, S. K. *Atmos. Environ.* **1978**, *12*, 2407–2413.
(46) Dragoescu, C.; Friedlander, S. *Aerosol Sci. Technol.* **1989**, *10*, 249–257.
(47) Whitby, K. T. *Atmos. Environ.* **1978**, *12*, 135–159.
(48) Seigneur, C.; Hudischewskyj, A. B.; Seinfeld, J. H.; Whitby, K. T.; Whitby, E. R.; Brock, J. R.; Barnes, H. M. *Aerosol Sci. Technol.* **1986**, *5*, 205–222.
(49) Junge, C. E. In *Fate of Pollutants in the Air and Water Environments*; Suffett, I. H., Eds.; Advances in Environmental Science and Technology; J. Wiley & Sons: New York, 1977; pp 7–25.
(50) Pankow, J. F. *Atmos. Environ.* **1987**, *21*, 2275–2283.
(51) Bidleman, T. F.; Foreman, W. T. *Environ. Sci. Technol.* **1987**, *21*, 869–875.
(52) Bidleman, T. F.; Billing, W. N.; Foreman, W. T. *Environ. Sci. Technol.* **1986**, *20*, 1038–1043.
(53) Yamasaki, H.; Kuwata, K.; Miyamoto, H. *Environ. Sci. Technol.* **1982**, *16*, 189–194.
(54) Pankow, J. F. *Atmos. Environ.* **1988**, *22*, 1405–1409.
(55) Slinn, W. G. N. In *Atmospheric Science and Power Production*; DOE/TIC-27601; NTIS DE 84005177; U. S. Department of Energy: Springfield, VA, 1984; pp 466–532.
(56) Kawamura, K.; Kaplan, I. R. *Atmos. Environ.* **1986**, *20*, 527–535.
(57) Dawson, G. A. *Atmos. Environ.* **1978**, *12*, 1991–1999.
(58) Van Noort, P. C. M.; Wondergem, E. *Environ. Sci. Technol.* **1985**, *19*, 1044–1048.
(59) National Climatic Data Center, Climatological Data (California), 1982.
(60) *California Almanac*, 1984–1985 Edition; Fay, J. S., Lipow, A. G., Fay, S. W., Eds.; Presidio Press and Pacific Data Resources: California, 1984; Section 7.
(61) Air Quality Management Plan: 1988 revision; South Coast Air Quality Management District, 1988; Chapter 2.
(62) Gray, H. A.; Cass, G. R.; Huntzicker, J. J.; Heyerdahl, E. K.; Rau, J. A. *Environ. Sci. Technol.* **1986**, *20*, 580–589.
(63) Draft SCAG Projections Burden 87B; California Department of Transport, Southern California Association of Governments, 1987.
(64) Benner, B. A., Jr.; Gordon, G. E.; Wise, S. A. *Environ. Sci. Technol.* **1989**, *23*, 1269–1278.
(65) Handa, T.; Yamauchi, T.; Sawai, K.; Yamamura, T.; Koseki, Y.; Ishii, T. *Environ. Sci. Technol.* **1984**, *18*, 895–902.
(66) 1976 Urban and Rural Travel Survey; California Department of Transport, Southern California Association of Governments, 1976; Vol. 4, Chapter 7, pp 109–119.
(67) Gordon, R. J.; Bryan, R. J. *Environ. Sci. Technol.* **1973**, *7*, 1050–1053.
(68) Grosjean, D. *Atmos. Environ.* **1983**, *17*, 2565–2573.
(69) *USEPA, Superfund Public Health Evaluation Manual*; U.S. EPA, 1986.
(70) Pearlman, R. S.; Yalkowsky, S. H.; Banerjee, S. *J. Phys. Chem. Ref. Data* **1984**, *13*, 555–562.
(71) Farmer, C. T.; Wade, T. L. *Water, Air, Soil Pollut.* **1986**, *29*, 439–452.
(72) McVeety, B. D.; Hites, R. A. *Atmos. Environ.* **1988**, *22*, 511–536.

Received for review February 14, 1991. Revised manuscript received May 21, 1991. Accepted June 18, 1991. This work was funded in part by the United States Environmental Protection Agency Grant CR-812271-03 to the National Center for Intermedia Transport Research at UCLA and the University of California Toxic Substances Research and Training Program.

Environ. Sci. Technol. 1991, 25, 2024–2030

Chemistry of a Near-Shore Lake Region during Spring Snowmelt

Chad P. Gubala* and Charles T. Driscoll

Department of Civil and Environmental Engineering, 220 Hinds Hall, Syracuse University, Syracuse New York 13244-1190

Robert M. Newton

Department of Geology, Smith College, Northampton, Massachusetts 01603

Carl L. Schofield

Department of Natural Resources, Fernow Hall, Cornell University, Ithaca, New York 14853

■ The thermal and chemical characteristics of a spawning area within a base-neutralized lake were monitored through the spring snowmelt of 1989. While the greater part of the lake remained relatively neutral, severe pH (<5.0) and acid neutralizing capacity (ANC; <0 μequiv L^{-1}) depressions were observed in the upper (1–1.5 m) portion of the water column. Thermal stratification of the near-shore area and a combination of groundwater and surface runoff events controlled the hydrologic response and the changes in water chemistry that occurred during the acid pulse. Dilution of basic cations (SBC) combined with NO_3^- eluted from the snowpack and/or soils resulted in low ANC, low pH runoff affecting the near-shore area. Increases in monomeric Al and H^+ were coincident with the ANC depression, creating a harmful environment for fish fry emerging from the spawning zone.

Introduction

The end of the winter (late March to early April) in the Adirondack region of New York State often coincides with snowmelt and marked declines in lake water and streamwater acid neutralizing capacity (ANC) (*1*, *2*). The degree of ANC depression and associated biotic effects depends largely upon the surficial geology and morphometry of lake/watershed systems (*2–4*). Most lakes in the Adirondacks are ice-covered and exhibit thermal stratification during peak spring discharge resulting in noticeable pH and ANC depression during snowmelt (*2*).

Episodic acidification and the degree of ANC depression of surface waters during spring are controlled in part by hydrologic flow paths (*4*). In many parts of the Adirondack region of New York State surficial deposits are shallow and neutralization of acidic snowmelt is incomplete during transport through the terrestrial environment. Small, high-elevation Adirondack lakes with relatively large watersheds (watershed to lake surface area ratio of >6) may be particularly sensitive to episodic acidification since they tend to have larger snowpacks, shallower deposits of glacial till, and faster flushing rates (*4*, *5*). As the hydrology returns to "low-flow" conditions following snowmelt, acidic precipitation may be neutralized more completely as the hydrologic residence time within the watershed increases and runoff contacts deeper, base-rich geologic material.

The biological consequences of springtime ANC and pH depressions in Adirondack lakes are profound (*6*). In particular, the thermal and chemical environments of lake spawning areas are critical to the survival of early life stages of fish. The declines in pH, ANC, and Ca^{2+} and increases in monomeric Al that coincide with spring snowmelt are potentially lethal to young fish inhabiting the near-shore zone. Several laboratory and field studies (*7–9*) have noted the potential significance of episodic acidification in near-shore areas for survival of early life history stages of brook trout (*Salvelinus fontinalis*) and lake trout (*Salvelinus namaycush*). However, the actual consequences of these events on egg and fry survival rates of naturally reproducing populations have not yet been firmly established.

Table I. Lake and Watershed Characteristics of Woods Lake

basin area, km^2	2.07
lake surface area, km^2	0.23
watershed area, km^2	1.84
maximum basin relief, m	122.0
forest cover, %	98.1
av thickness of surficial deposits, m	1.9
lake volume, 10^5 m^3	8.14
maximum lake depth, m	11.6
mean lake depth, m	3.5
lake surface altitude, m	606
lake area/watershed area	0.13
av lake water residence time, days	174

Logistical constraints have limited the intensive collection of samples from near-shore regions of Adirondack lakes during snowmelt episodes. Observations from lake inlets, water columns, and outlets have been made (*1*), but these may not be indicative of the chemical conditions of important spawning areas that are affected by a combination of hydrologic sources (e.g., groundwater, streamwater, snowmelt water). In response to this problem, a device was constructed and employed to explicitly monitor the chemical and thermal conditions of a near-shore spawning area within an experimental lake in the Adirondacks (*10*). The water quality data collected with this near-shore sampling device are examined in this study and compared to inlet, outlet, and in-lake observations to assess the relative contribution of various hydrologic inputs (i.e., groundwater/porewater, surface runoff) in controlling the chemical conditions of the near-shore area. Moreover, because temporal patterns in pelagic and/or outlet waters are often used to assess the magnitude of episodic acidification, the results from this study are also used to illustrate the limitations of interpreting results from these sampling areas in the absence of in-lake data.

Site Description

Woods Lake (42°52′ N, 71°58′ W), located in the west-central region of the Adirondack Park of New York State, is typical of chronically acidic lake/watershed systems in that area (refs 3, 4, and 11; Figure 1a–c, Table I). The lake is small and shallow with a short lake water residence time (ref 12; 174 days). It is surrounded by a watershed characterized by shallow deposits of glacial till and acidic soils (*13*). The 110–140 cm of acidic precipitation that enters the Woods Lake watershed each year (*14*) is only partially neutralized before entering the lake (refs 4, 15, and 16; Table I). Acidification of inlet and lake

*Present address: ManTech Environmental Technology, Inc., 200 SW 35th St., Corvallis, OR 97333.

 0013-936X/91/0925-2024$02.50/0

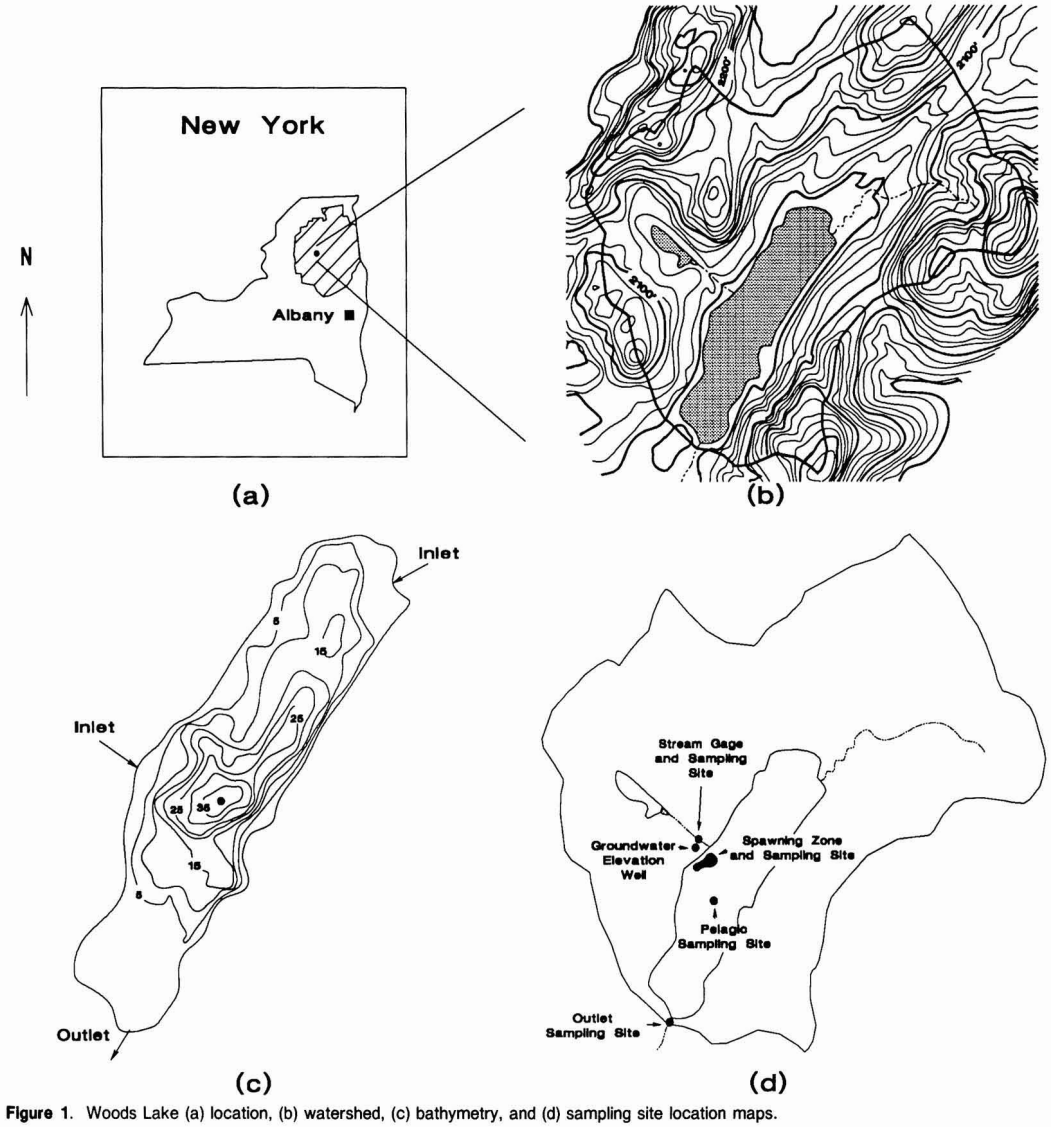

Figure 1. Woods Lake (a) location, (b) watershed, (c) bathymetry, and (d) sampling site location maps.

waters is particularly severe during spring snowmelt (March–April), when approximately 25% of the annual hydrologic input enters the lake. During this period, hydrologic flow paths are altered by the routing of water through upper acidic soil horizons resulting in limited neutralization of drainage water (*4*, *17*, *18*).

Methods

Woods Lake was treated by addition of $CaCO_3$ in 1985 and again in 1987 to mitigate acidic conditions (*19*). Since 1985, the lake generally had a positive ANC, with the exception of the upper few meters of the water column during the periods of spring snowmelt (*20*). A description of these manipulations and subsequent results are detailed elsewhere (*12*, *19–29*). While the ANC of Woods Lake had been artificially increased by $CaCO_3$ addition, the findings of this paper may be directly relevant to Adirondack lakes with naturally low mean summertime ANC values (25–100 μequiv L^{-1}) that are particularly susceptible to episodic acidification during spring snowmelt (*2*).

The data used in this analysis were derived primarily from the Lake Acidification Mitigation Program (LAMP) and the Experimental Watershed Liming Study (EWLS). Inlet, deep-water column, outlet, and near-shore lake water sampling was conducted as part of the EWLS pretreatment program at various intervals through a period from June of 1988 to May of 1989 (Figure 1d). Near-shore sampling was accomplished by means of an episodic event sampler (EES) (*10*). A set of protocols has been used for the chemical analysis of all aqueous samples and is detailed elsewhere (*27*).

One parameter of particular interest in this study is Al. Inorganic species of aqueous Al are thought to be toxic to fish (*30*). Samples collected were analyzed for inorganic monomeric Al and organic monomeric Al by the fractionation procedure developed by Driscoll (*31*). In acidic waters of Woods Lake, inorganic monomeric Al comprises most of the solution Al (*27*, *28*). Therefore, the Al monitoring data are generally reported as monomeric Al. However, to determine the equivalence of Al (Al^{n+}) in

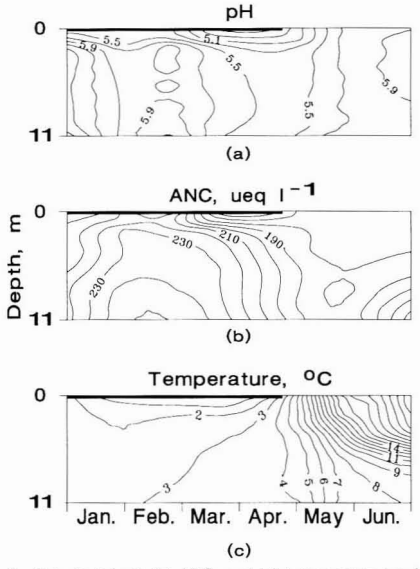

Figure 2. Pelagic (a) pH, (b) ANC, and (c) temperature isopleths at Woods Lake during spring 1989.

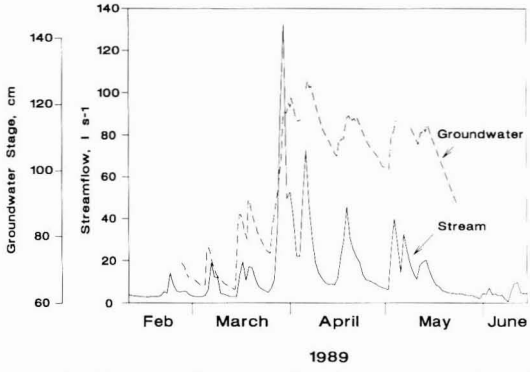

Figure 3. Inlet stream discharge and relative groundwater stage at Woods Lake during spring 1989.

solution, values of inorganic monomeric Al, pH, F^-, SO_4^{2-}, and temperature were used as input to a chemical equilibrium model to calibrate the speciation of Al (*32*).

Results

Prior to the application of $CaCO_3$, marked declines in pH or ANC were not evident at a water column (pelagic) sampling station in Woods Lake (12-m total depth), as the lake was already acidic (*20*). However after base treatment, pH and ANC depressions were evident to a depth of 1–2 m in the lake during snowmelt periods (ref 20; Figure 2a,b). Snowmelt acidification was restricted to the surface of the lake because acidic meltwater enters under ice cover at a temperature of less the 1 °C and has a lower density than that of the lower waters (3 °C; Figure 2c). As a result, this water migrates along the ice/water interface before exiting by the lake outlet. After ice-out and spring turnover, the acidity of the upper waters was lessened through mixing with the remainder of the lake.

Finely resolved sampling of 2- and 3-m-depth near-shore regions during the snowmelt period of 1989 yielded a more detailed depiction of episodic acidification in a biotically important region of the lake. Several interconnected phenomena are apparent in these data.

A knowledge of the hydrologic patterns during snowmelt is necessary to understand the temporal trends of the chemistry of the near-shore area. Groundwater stage began to increase in pulses in mid-March, a few days prior to the peak streamflow (Figure 3). This pattern is common for snowmelt hydrology within the Adirondacks, as relatively shallow deposits of glacial till (<3 m) become saturated with meltwater and poise the system for rapid flow during spring snowmelt (*33*). This increase in groundwater stage increases in-seepage of water into the littoral region of the lake (*34*). After snowmelt, both groundwater and streamflow return to base conditions and have diminishing influence upon the near-shore area.

As noted at the pelagic station, a subtle, but distinct temperature gradient existed at both the 2- and 3-m stations (Figure 4a). As low-temperature meltwater (1 °C) initially entered under the ice, it apparently remained isolated between the ice and the higher temperature, higher density water below. Once the ice began to melt, exposing the water to solar radiation and wind, the near-shore region rapidly became isothermal.

pH and ANC depressions were apparent at both the 2- and 3-m sampling stations during snowmelt and peak stream discharge (Figures 3 and 4b,c). However, the region where ANC became negative and pH decreased to 4.8 was limited to a depth of approximately 1–1.5 m. After the peak melt period, both ANC and pH slowly increased as the near-shore waters mixed with the bulk of the lake water.

The combination of uniformly high SO_4^{2-} (*1*, *3*), basic cation (SBC) dilution, and NO_3^- release resulted in dilute, negative ANC meltwater (Figures 4d, 6, and 7a). Declines in ANC were correlated with both decreasing SBC (ANC = $-88 + 0.58$SBC; $r^2 = 0.84$, $p < 0.001$) and increasing NO_3^- (ANC = $65 - 0.86NO_3^-$; $r^2 = 0.33$, $p < 0.01$; Figure 5a,b), although a stronger relationship was evident between ANC and SBC. The fact that the ranges of SBC dilution (~200 μequiv L^{-1}) and NO_3^- increase (~80 μequiv L^{-1}) were of similar magnitude and slopes of regression analyses with ANC are somewhat less than 1 suggest that both processes significantly contributed to ANC loss. The less than stoichiometric relationships between ANC, SBC, and/or NO_3^- can also be attributed to exponential increases in Al^{n+} that occurred with decreasing pH, particularly at ANC values below 0 μequiv L^{-1} (Figure 5c).

Aluminum dissolution in acidic waters is a strong pH buffer and diminishes the extent of ANC depression (*2*, *16*, *35*). The highest NO_3^- concentrations were evident at the lowest ANC values (Figure 5b). Indeed, variations in NO_3^- show a near-stoichiometric relationship with the sum of H^+ and Al^{n+} [$(H^+ + Al^{n+}) = -20 + 0.83NO_3^-$; $r^2 = 0.74$, $p < 0.0001$; Figure 5d]. Increases in monomeric Al were coincident with depressions in pH and ANC and showed pronounced spatial and temporal gradients. Monomeric Al decreased with depth and increased with peak discharge at both the 2- and 3-m sampling stations (Figure 7b). This Al^{n+} is likely released from dissolution/exchange reactions with mineral soil (*36*) or sediment (*37*).

Constituents that are indicative of groundwater inputs to the lake, such as H_4SiO_4, displayed systematic temporal and spatial variability through the melt period (Figure 7c). The timing of the pulsed increases in groundwater stage roughly correlates with enrichment of SBC, ANC, pH, and H_4SiO_4 near the sediment/water interface of the 2-m station and to a lesser extent, the 3-m station.

Discussion

The disparities between the timing and magnitude of surface runoff and groundwater inputs into Woods Lake

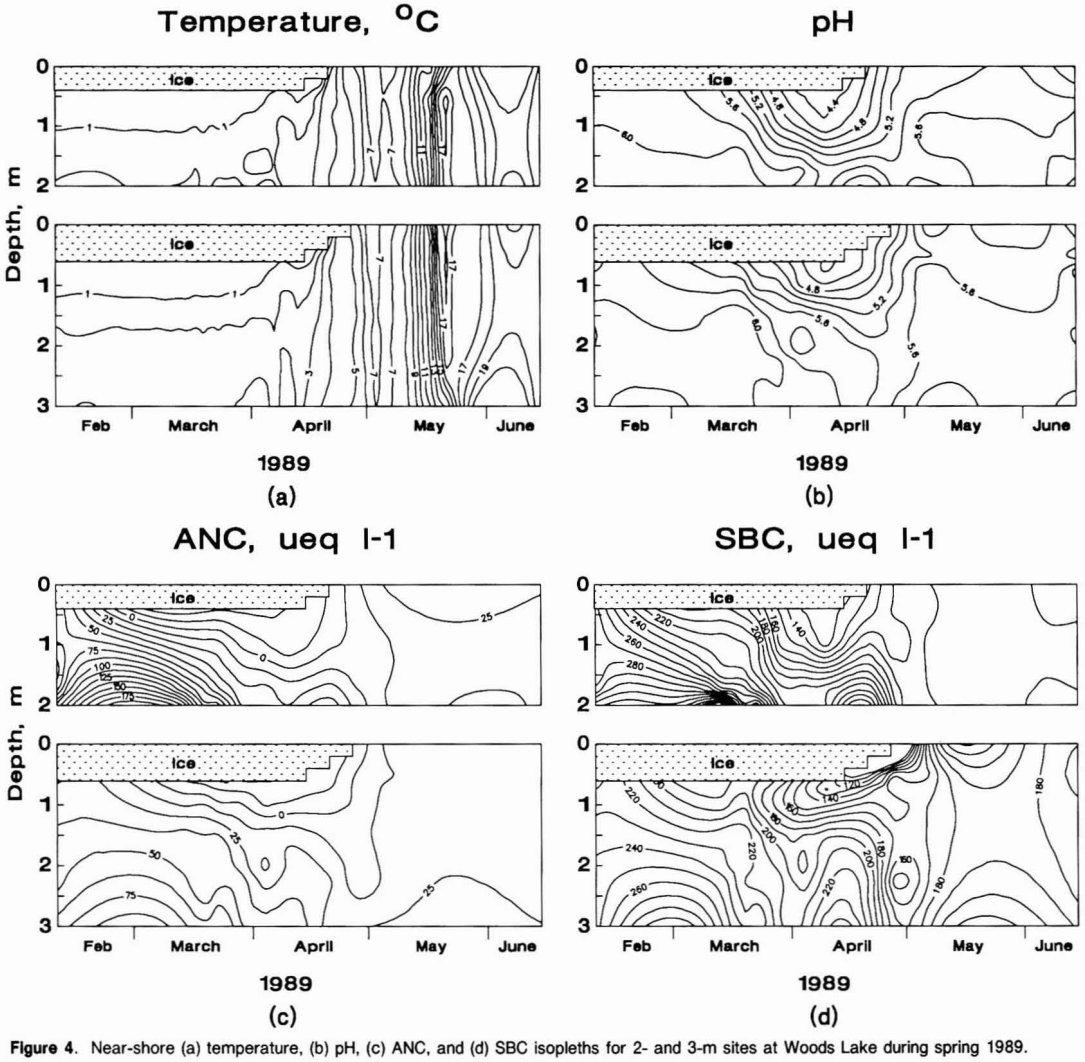

Figure 4. Near-shore (a) temperature, (b) pH, (c) ANC, and (d) SBC isopleths for 2- and 3-m sites at Woods Lake during spring 1989.

during spring snowmelt largely explain the spatial and temporal variation in chemistry of its littoral region. The advection of ANC-rich groundwater and porewater into the near-shore region, promoted by the increase in groundwater stage during the initial period of spring snowmelt, was quickly overwhelmed by the subsequent surface runoff. While the seepage rate into the near-shore area was not directly measured during this study, previous estimates have shown this rate to be approximately 55×10^3 m^3 $month^{-1}$ during March, April, and May (*12*). Based upon visual inspection of the near-shore area in Woods Lake, the hydrologically active region of the lake shore is approximately 40×10^3 m^2. Therefore, the groundwater seepage rate of 21 L s^{-1} during this period over the 40×10^3 m^2 region equates to approximately 53×10^{-4} L s^{-1} m^{-2}. Compared to the maximum surface runoff from the inlet stream affecting the study area (130 L s^{-1}), the rate of groundwater in-seepage is negligible. Rapid surface runoff dominates the hydrologic input during most of the melt period and largely controls the chemistry of the near-shore region.

Groundwater in-seepage in nearby Dart's Lake has been shown to diminish exponentially with the distance from shore (*35*). Therefore, the disparate effects of an increasing groundwater table upon the 2- and 3-m stations are consistent with current hydrogeologic findings and were to be expected. While relative lake stage was not recorded during the 1989 melt period, observations from other snowmelt periods indicate that groundwater may increase to as much as 0.5 m above the lake, promoting advective transport of groundwater constituents into the littoral regions prior to peak discharge. However, with increases in discharge and lake stage, the hydraulic head between groundwater and lake levels diminishes, greatly reducing rates of in-seepage (*35*). Prior to spring turnover of the near-shore area, thermal gradients between the sediment porewater and the water column may also promote advective transport of chemical constituents via conduction and/or convection.

Thermal stratification of the near-shore region, affected by ice cover and possibly temperature density differences across the sediment/water interface, limits the extent of mixing of waters to a depth of 1–2 m. Water entering the near-shore region from surface runoff remains isolated from lower waters affected by groundwater/porewater inputs due to the weak density differences affected by

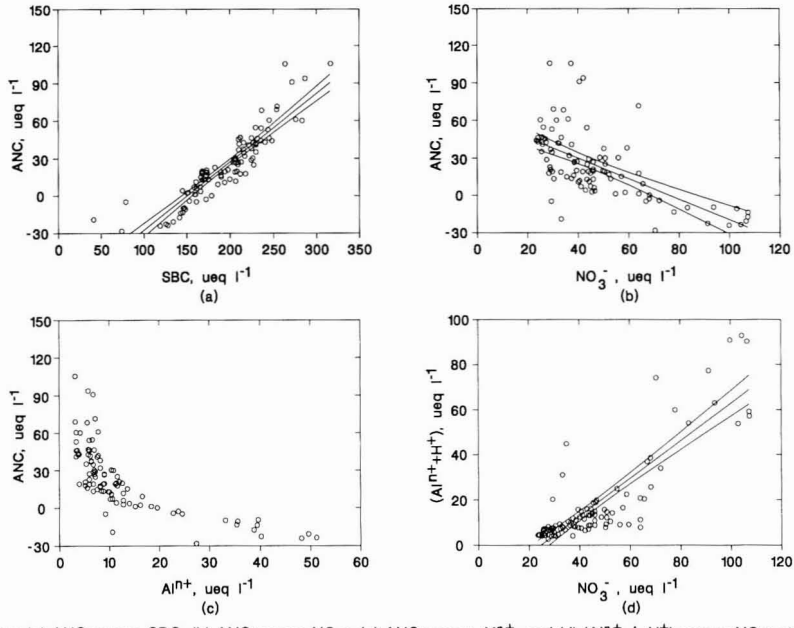

Figure 5. Near-shore (a) ANC versus SBC, (b) ANC versus NO_3^-, (c) ANC versus Al^{n+}, and (d) (Al^{n+} + H^+) versus NO_3^- at Woods Lake during spring 1989.

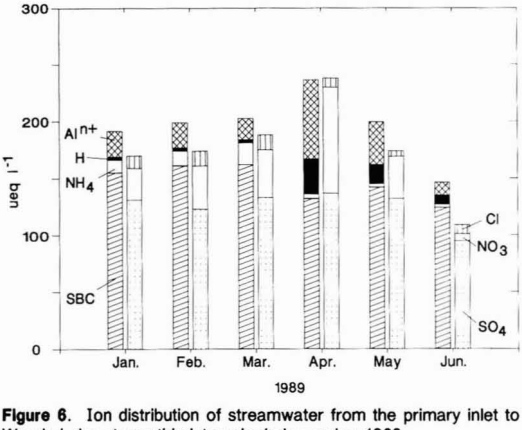

Figure 6. Ion distribution of streamwater from the primary inlet to Woods Lake at monthly intervals during spring 1989.

thermal variations. Thermal stratification and the resulting mixing pattern persist only until ice-out, when wind and solar radiation act to break apart the density strata. Soon after ice-out and turnover, most of the chemical constituents in the near-shore region become completely mixed and their concentrations more closely approximate whole-lake conditions.

The magnitude and distribution of certain key chemical parameters in the near-shore area during the melt period likely have a profound effect upon the biotic resources of the lake. Fish eggs may remain well protected within a chemically favorable environment near the sediment/water interface during their development. Groundwater/porewater inputs, relatively high in SBC and ANC, and low in inorganic monomeric Al, a potential toxicant, provide a chemically stable environment for egg development. However, emerging brook trout fry, seeking to reach the water's surface to fill swim blatters with air soon after ice-out, must move through the harsh chemical environment of the upper waters, low in pH and ANC and high in monomeric Al. This pattern may lead to acute or chronic mortality via exposure to high concentrations of monomeric Al (*38*). Indeed, the chemical phenomena reported in this paper have been used to explain the poor recruitment of brook trout stocked in Woods Lake following the whole-lake application of $CaCO_3$ (*22*). Even though the volume-weighted, whole-lake ANC has remained positive since base treatment in 1985 and the adult brook trout population has been observed to actively spawn, a naturally reproducing population has not developed. Episodic acidification of near-shore spawning areas may limit brook trout natural reproduction by direct fry mortality.

Previous studies of the episodic acidification of Adirondack lakes have been limited to the interpretations of outlet stream chemistry and/or depth profiles from pelagic stations (*1*, *2*). Our investigation provides a good opportunity to compare traditional outlet/pelagic sampling results with detailed monitoring of the more biologically relevant near-shore region during snowmelt. Examination of chemical parameters monitored at the near-shore region, upper pelagic station, and lake outlet showed similar concentrations during the period of maximum discharge (Figures 2, 7, and 8). This suggests that the chemical characteristics of outlet and upper pelagic waters during peak episodic acidification may be roughly indicative of the near-shore area. However, an understanding of the hydrodynamics of the lake is critical to an accurate assessment of the biological effects of an acidic snowmelt event. For example, inspection of the outlet chemistry may lead to the conclusion that Woods Lake is entirely acidic when, in reality, the portion of the water column below approximately 2 m remained amenable for aquatic biota. However, even taking the pelagic data in concert with the outlet chemistry may lead to faulty hypotheses regarding the actual biological effects of episodic acidification within the lake. Assuming, from the pelagic data, that the most harmful waters penetrate to a depth of 2 m throughout the

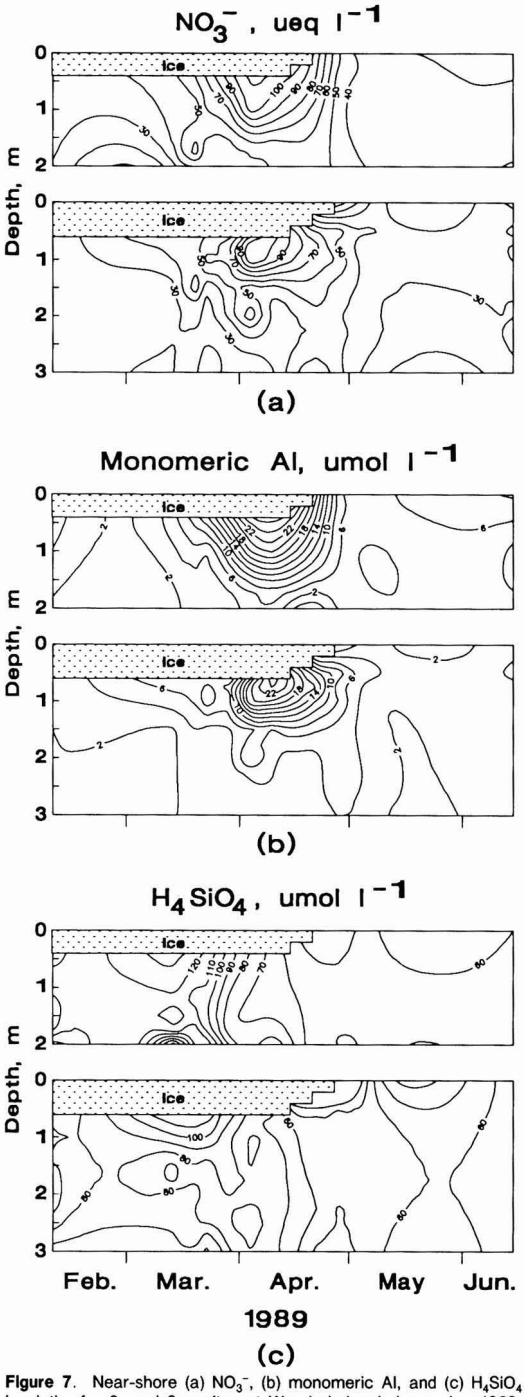

Figure 7. Near-shore (a) NO_3^-, (b) monomeric Al, and (c) H_4SiO_4 isopleths for 2- and 3-m sites at Woods Lake during spring 1989.

lake, one might hypothesize that the benthos of the near-shore spawning areas were similarly affected. As was shown in this study, a modicum of groundwater in-seepage coupled with thermal stratification kept the littoral waters near the sediment/water interface from becoming acidic. Therefore, while the maximum effects of in-lake episodic acidification were in close agreement with the lake outlet trends, the actual depth of penetration of the acidic waters

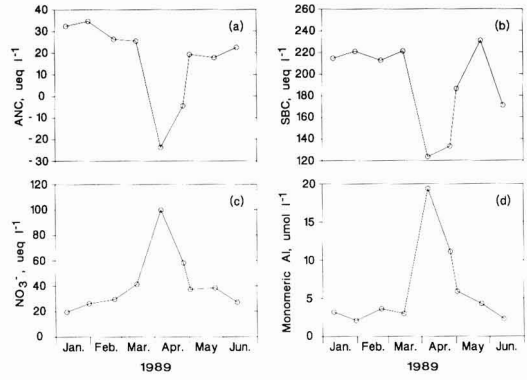

Figure 8. Concentrations of (a) ANC, (b) SBC, (c) NO_3^-, and (d) monomeric Al at the Woods Lake outlet during spring 1989.

during a snowmelt event varied spatially throughout the lake. This variation is significant in understanding fisheries' development and mechanisms of mortality.

Summary

The chemical characteristics of a near-shore area of Woods Lake varied in response to changes in hydrologic inputs and flow paths. During the winter, slow advective and diffusive transport of groundwater and porewater constituents affected the near-shore area. Groundwater stage increased just prior to the increase in the inlet hydrograph, promoting advective transport of chemical constituents across the sediment/water interface. Surface runoff during snowmelt then supplanted groundwater inputs as the primary water source. During this period, the water quality of a critical near-shore spawning area degraded as acidic snowmelt, low in SBC, was quickly transported into the lake. Weak conditions of thermal stratification that developed under the ice were sufficient to isolate the acidic meltwaters within the top 1–1.5 m of the water column while water near the sediment/water interface remained relatively circumneutral. The chemical environment for benthic biota remained acceptable. However, fish fry that must migrate from the benthos to the water's surface following ice-out may be greatly affected by the high concentrations of monomeric Al associated with the acidic meltwater.

Episodic acidification of the near-shore area of Woods Lake was promoted by the dilution of SBC and release of NO_3^- from the watershed. Concentrations of NO_3^- were strongly related to changes in pH and monomeric Al. Therefore, decreasing atmospheric SO_4^{2-} loadings alone may not completely mitigate the biological consequences of acidic deposition. Episodic acidification of low-ANC lakes during spring snowmelt may persist after the atmospheric deposition of SO_4^{2-} is reduced.

The additional information provided by this study may be used to temper the interpretations of episodic event studies based solely upon the temporal trends in water quality of lake outlets. Even though the peak discharge concentrations of ANC, SBC, NO_3^-, and monomeric Al were similar for the near-shore area, deep-water station, and lake outlet during the acidic snowmelt event, the biological consequences of episodic acidification may be misjudged without an adequate understanding of lake hydrodynamics.

Acknowledgments

We acknowledge the help of J. Boljonis, C. Keleher, and V. Bleete.

Registry No. Al, 7429-90-5.

Literature Cited

(1) Galloway, J. N.; Hendry, G. R.; Schofield, C. L.; Peters, N. E.; Johannes, A. J. *Can. J. Fish. Aquat. Sci.* **1987**, *44*, 1595–1602.
(2) Schaefer, D. A.; Driscoll, C. T.; van Dreason, R.; Yatsko, C. P. *Water Resour. Res.* **1990**, *26*, 1639–1647.
(3) Galloway, J. N.; Schofield, C. L.; Peters, N. E.; Hendry, G. R.; Altwicker, E. R. *Can. J. Fish. Aquat. Sci.* **1983**, *40*, 799–806.
(4) Driscoll, C. T.; Newton, R. M.; Gubala, C. P.; Baker, J. P.; Christensen, S. W. Adirondack Mountains: Regional Analysis of Surface Water Acidification. In *Acidic Precipitation and Surface Water Acidification: Regional Case Studies*; Charles, D. F., Ed.; Springer-Verlag: New York, 1990.
(5) Kretser, W.; Gallagher, J.; Nicolette, J. Adirondack Lakes Study, 1984–1987. Adirondack Lake Survey Corp., Ray Brook, NY, 1989.
(6) Baker, J. P.; Christensen, S. W.; Creager, C. S.; Warren-Hicks, W.; Godbout, L. Identification of critical values for effects on fish populations. Final Project Report submitted to the U.S. Environmental Protection Agency, Washington, DC, 1988.
(7) Johnson, D. W.; Webster, D. A. *J. Fish Res. Board Can.* **1977**, *34*, 2215–2218.
(8) Gunn, J. M.; Noakes, D. L. G. *Water, Air, Soil Pollut.* **1986**, *30*, 497–503.
(9) Gunn, J. M.; Keller, W. *Water, Air, Soil Pollut.* **1986**, *30*, 545–552.
(10) Gubala, C. P.; Driscoll, C. T.; Newton, R. M.; Schofield, C. submitted for publication in *Water Resour. Res.*
(11) Driscoll, C. T.; Newton, R. M. *Environ. Sci. Technol.* **1985**, *19*, 1018–1024.
(12) Staubitz, W. W.; Zarriello, P. J. *Can. J. Fish. Aquat. Sci.* **1989**, *46*, 268–276.
(13) April, R. A.; Newton, R. M. *Water, Air, Soil Pollut.* **1985**, *26*, 373–386.
(14) Johannes, A. H.; Altwicker, E. R.; Clesceri, N. L. *Water, Air, Soil Pollut.* **1985**, *26*, 339–353.
(15) Goldtstein, R. A.; Chen, C. W.; Gherini, S. A. *Water, Air, Soil Pollut.* **1985**, *26*, 327–337.
(16) Schofield, C. L.; Galloway, J. N.; Hendry, G. R. *Water, Air, Soil Pollut.* **1985**, *26*, 403–423.
(17) Chen, C. W.; Gherini, S. A.; Goldstein, R. A. Modeling the lake acidification process. In *Ecological Effects of Acid Precipitation*; Wood, M. J., Ed.; EA-79-6-LD; Electric Power Research Institute: Palo Alto, CA, 1984; pp 5:1–5:43.
(18) Peters, N. E.; Murdoch, P. S. *Water, Air, Soil Pollut.* **1985**, *26*, 387–402.
(19) Porcella, D. B. *Can. J. Fish. Aquat. Sci.* **1989**, *46*, 246–248.
(20) Gubala, C. P.; Driscoll, C. T. *Water, Air, Soil Pollut.*, in press.
(21) Bukaveckas, P. A. *Can. J. Fish. Aquat. Sci.* **1989**, *46*, 352–359.
(22) Gloss, S. P.; Schofield, C. L.; Spateholts, R. L.; Plonski, B. A. *Can. J. Fish. Aquat. Sci.* **1989**, *46*, 277–286.
(23) Roberts, D. A.; Boylen, C. W. *Can. J. Fish. Aquat. Sci.* **1989**, *46*, 287–294.
(24) Schaffner, W. R. *Can. J. Fish. Aquat. Sci.* **1989**, *46*, 295–305.
(25) Schofield, C. L.; Gloss, S. P.; Plonski, B.; Spateholts, R. *Can. J. Fish. Aquat. Sci.* **1989**, *46*, 333–341.
(26) Evans, R. A. *Can. J. Fish. Aquat. Sci.* **1989**, *46*, 342–351.
(27) Driscoll, C. T.; Ayling, W. A.; Fordham, G. F.; Oliver, L. M. *Can. J. Fish. Aquat. Sci.* **1989**, *46*, 258–267.
(28) Driscoll, C. T.; Fordham, G. F.; Ayling, W. A.; Oliver, L. M. *Can. J. Fish. Aquat. Sci.* **1989**, *46*, 249–257.
(29) Fordham, G. F.; Driscoll, C. T. *Can. J. Fish. Aquat. Sci.* **1989**, *46*, 306–314.
(30) Driscoll, C. T.; Baker, J. P.; Bisogni, J. J.; Schofield, C. L. *Nature* **1980**, *284*, 161–164.
(31) Driscoll, C. T. *Int. J. Environ. Anal. Chem.* **1984**, *16*, 267–283.
(32) Schecher, W. D.; Driscoll, C. T. *Water Resour. Res.* **1987**, *23*, 525–534.
(33) Newton, R. M.; Driscoll, C. T. *Water Resour. Res.*, submitted.
(34) Schafran, G. C.; Driscoll, C. T. *Water Resour. Res.*, submitted.
(35) Bisogni, J. J., Jr.; Driscoll, C. T. Characterization of the pH buffering systems in dilute Adirondack surface waters. A-073-NY; Office of Water Research and Technology Project, Albany, NY, 1979.
(36) Dahlgren, R. A.; McAvoy, D. C.; Driscoll, C. T. *Environ. Sci. Technol.* **1990**, *24*, 531–537.
(37) Hedin, L. O.; Likens, G. E.; Postek, K. M.; Driscoll, C. T. *Nature*, in press.
(38) Schofield, C. L.; Trojnar, J. R. Aluminum toxicity to brook trout (*Salvelinus fontinalis*) in acidified waters. In *Polluted Rain*; Toribara, T. Y., Miller, M. W., Eds.; Plenum Press: New York, 1980; pp 341–362.

Received for review September 14, 1990. Revised manuscript received June 14, 1991. Accepted June 26, 1991. This study was funded as part of the Experimental Watershed Liming Study (EWLS) by the Electric Power Research Institute, the Empire State Electric Energy Research Corp., and Living Lakes, Inc.

Environ. Sci. Technol. 1991, 25, 2031–2038

Fractal Dimensions of Aggregates Determined from Steady-State Size Distributions

Qing Jiang and Bruce E. Logan*

Environmental Engineering Program, Department of Civil Engineering, University of Arizona, Tucson, Arizona 85721

■ Aggregates formed by Brownian motion, shear coagulation, and differential sedimentation have fractal geometries. In order to model coagulation of fractal aggregates, we have derived a set of collision functions containing a fractal dimension for use in a general coagulation equation. These collision functions predict greater collision frequencies than models based on aggregates with Euclidean properties. Assuming only one mechanism of aggregate formation is dominant for a range of particle sizes, we also incorporated a fractal dimension in a dimensional analysis of steady-state particle-size distributions. Using particle-size distributions observed in marine systems, we calculated that aggregates formed by shear coagulation had fractal dimensions greater than 2.4, whereas aggregates formed from differential sedimentation had lower fractal dimensions in the range of 1.6–2.3. Reported fractal dimensions for many biological aggregates from bioreactors and marine systems are in the range expected for differential sedimentation. Fractal dimensions of inorganic colloidal aggregates are in the range expected for aggregation by Brownian motion and shear coagulation.

Introduction

Recent studies indicate coagulation can be an important mechanism of particle removal in lakes (*1*, *2*) and oceans (*3*). In freshwater systems, collision efficiencies are low (≃0.001–0.1), and coagulation is strongly influenced by surface chemistry of the particles (*4*). In marine systems, large aggregates have been shown to have high sticking efficiencies (*5*). In the deep ocean, McCave (*6*, *7*) predicted that low particle concentrations would result in slow coagulation rates except under specific conditions where particle concentrations are much higher, such as benthic boundary layers and near ocean outfalls (*8*, *9*). Algal blooms have also been observed to rapidly flocculate forming large amorphous aggregates up to 20 mm in size (*10*). A coagulation model developed by Jackson (*3*) was used to show that diatom aggregates can be formed by shear and differential sedimentation, but he hypothesized that these types of aggregates are only formed in the absence of grazing. Aggregates can also be produced in the ocean from feeding webs and other material produced by small animals, such as fecal pellets (*10*).

Coagulation has been modeled through two approaches: by solving a general dynamic equation describing coagulation or by developing solutions for coagulation based on a dimensional analysis. A simplified equation for coagulation by the first approach (*11*) is

$$\frac{\partial n(v)}{\partial t} = \frac{1}{2}\int_0^v \beta(\bar{v},v-\bar{v})n(\bar{v})n(v-\bar{v})\,d\bar{v} - \int_0^\infty \beta(v,\bar{v})n(v)n(\bar{v})\,d\bar{v} \quad (1)$$

where $n(v)\,dv$ is the number concentration of flocs in the volume interval v to $v + dv$. The first term on the right-hand side of the equation describes coagulation of similar flocs to form flocs of size v, and the second term represents the loss of flocs of volume v through collision with other flocs. Numerical solutions have been provided by several researchers for hydrosol dynamics (*12*, *13*), but none of these solutions have been verified with experimental data.

A second approach to describe particle sizes during coagulation was used by Hunt (*8*, *14*) and McCave (*6*, *7*). This approach is based on a dimensional analysis of particle-size distributions and requires four assumptions: (1) floc-size distributions are in a steady state, with a constant source of particles, which coagulate through the size distribution to form aggregates that are removed through sedimentation; (2) only one coagulation mechanism (Brownian, fluid shear, differential settling) is dominant at a given particle size; (3) particle sticking efficiency is constant and independent of particle size; (4) each mechanism can be characterized by a single parameter. Theoretical predictions were verified by analyzing particle-size distributions of clay particles (<2 μm) undergoing Brownian and shear coagulation in seawater (*8*) and compared with marine particle-size distributions (*14*).

The premise of both coagulation models is that aggregates formed during coagulation are composed of particles evenly spaced and uniformly distributed in spherical aggregates. However, it is now known that aggregates formed by Brownian motion have fractal structures (*15–18*). Therefore, the density of fractal aggregates is not constant, and the properties of fractal aggregates, such as mass and encased volume, do not dimensionally scale according to the mathematics of Euclidean geometry. For example, the number of particles, N, in an aggregate of uniformly distributed spherical monomers (*19*) is

$$\dot{N} = (\dot{\zeta}\dot{\xi}/\dot{\xi}_o)(d/d_o)^3 \quad (2)$$

where the superscript • is used to denote variables based on Euclidean geometry, $\dot{\zeta}$ is a packing factor, d is the aggregate diameter, d_o is the diameter of primary particles composing the aggregate, and $\dot{\xi}$ and $\dot{\xi}_o$ are shape factors of the aggregate and primary particles. An analogous expression for the number of particles in an aggregate for fractal aggregates cannot be directly developed, since for a fractal aggregate

$$N \neq \zeta(v/v_o) \quad (3)$$

For a fractal aggregate, we choose packing and shape factors that will be reduced to their Euclidean counterparts, and obtain

$$N = \psi^{D/3}(l/l_o)^D \quad (4)$$

where $\psi = \zeta\xi/\xi_o$, l is the characteristic length of a fractal aggregate, here defined as the longest aggregate length, l_o is the length of primary particles in the aggregate, and D is the fractal dimension. Comparison of eqs 2 and 4 shows that $D = 3$ for Euclidean objects. However, aggregates formed from metal colloids, soot, aerosols, silica, and polystyrene (*18*, *20*) have fractal, or noninteger, dimensions significantly less than 3.

Since aggregates are fractal and have nonuniform properties, both of the above coagulation theories need to be revised to include the fractal geometry of the aggregates. In this paper we derive a set of collision frequency func-

0013-936X/91/0925-2031$02.50/0

tions that incorporate fractal dimensions of aggregates and show that collision rates for fractal aggregates are greater than rates for Euclidean aggregates. We also demonstrate that fractal dimensions affect steady-state size distributions in marine systems.

Methods

Characteristics of Fractal Aggregates. In order to describe coagulation by use of fractal geometry, the properties of the fractal aggregates must be cast in terms of fractal dimensions. These properties, such as mass, volume, density, porosity, and settling velocity affect particle collisions and, therefore, coagulation rate. Below, we derive equations for fractal aggregates based on relationships used for Euclidean objects.

(a) Aggregate Mass. If we assume that aggregates are composed of spherical particles with diameter d_o and density $\dot{\rho}_o$, the mass of each primary particle, $\dot{m}_o$, is

$$\dot{m}_o = \dot{\rho}_o \dot{\xi}_o d_o^3 \tag{5}$$

The mass of an aggregate, $\dot{m}$, is the product of the number and mass of primary particles or, for a Euclidean aggregate, is

$$\dot{m} = \dot{m}_o \dot{N} = \dot{\rho}_o \dot{\xi} \dot{\xi} d^3 \tag{6}$$

For a fractal aggregate, we define the mass of the primary particle as

$$m_o = \rho_o \xi_o l_o^3 \tag{7}$$

Combining eqs 4 and 7, we obtain for fractal aggregates

$$m = \rho_o \psi^{D/3} \xi_o l_o^{3-D} l^D \tag{8}$$

(b) Aggregate Volume. The volume of an aggregate can be defined in two ways: as an encased volume or as an occupied or solid volume. According to the first definition, the volume of an aggregate is calculated as the spherical volume that encases the aggregate, or $\dot{v}_e = \dot{\xi} d^3$. For a fractal aggregate, we can similarly calculate this volume substituting l for d, or

$$v_e = \xi l^3 \tag{9}$$

The solid volume of the aggregate, v, is calculated as the total volume occupied by all primary particles in the aggregate. The difference between the encased volume, v_e, and the solid volume, v, is that the former includes both the volume of particles and the volume of the pores. The solid volume for a fractal aggregate is related to its mass by $m = v\rho_o$, or by using eq 8

$$v = \psi^{D/3} \xi_o l_o^{3-D} l^D \tag{10}$$

As eq 10 shows, v does not scale to an integer power of 3, as assumed in previous models (*8*, *14*). These changes affect the relationships between aggregate characteristics such as density, porosity, and settling velocity.

(c) Aggregate Density. The density of an aggregate is defined as the total mass of primary particles in the aggregate per encased volume, or $\dot{\rho} = \dot{m}/\dot{v}_e$ for Euclidean aggregates, and $\rho = m/v_e$ for fractal aggregates. Using this definition and eq 8, the fractal density, ρ, is

$$\rho = \rho_o \psi^{D/3} (\xi_o/\xi)(l/l_o)^{D-3} \tag{11}$$

Since density is a function of aggregate size, and usually decreases with the size of the aggregate, the collision of two aggregates produces an aggregate of a larger encased volume than the sum of two original aggregate volumes.

(d) Aggregate Porosity. The porosity of a fractal aggregate, ϵ, can be expressed in terms of the encased and solid volume as

$$\epsilon = 1 - v/v_e \tag{12}$$

From the definition of v and v_e, eq 12 becomes

$$\epsilon = 1 - \psi^{D/3} (\xi_o/\xi)(l/l_o)^{D-3} \tag{13}$$

(e) Settling Velocity. Relationships to describe the settling velocity of impermeable spheres are based on a force balance on a settling aggregate (*21*), or

$$v_e(\dot{\rho}_a - \rho_w)g = \tfrac{1}{2}\dot{A}\ \rho_w \dot{C}_D \dot{U}^2 \tag{14}$$

where $\dot{\rho}_a$ is the bulk aggregate density, which includes the mass of both primary particles and liquid in the encased aggregate volume, ρ_w is the fluid density, g is the gravitational constant, $\dot{A}$ is the projected surface area of the aggregate perpendicular to the direction of settling, $\dot{C}_D$ is a drag coefficient, and $\dot{U}$ is the aggregate settling velocity. The bulk aggregate density can be obtained from the identity

$$(\rho_a - \rho_w) = (1 - \epsilon)(\rho_o - \rho_w) \tag{15}$$

which is valid for either fractal or Euclidean objects. In order to specify a similar relationship for the settling velocity of fractal aggregates, three assumptions are necessary. First, on the basis of the analysis contained in Logan and Hunt (*22*), it is assumed that the advective flow through the highly porous aggregate does not significantly affect settling velocity. Second, the projected surface area is assumed to be a function of an additional fractal dimension defined as

$$A = \xi_2 l_o^{2-D_2} l^{D_2} \tag{16}$$

where ξ_2 is the shape factor and D_2 is the fractal dimension that relate aggregate size to projected area in two dimensions. The area defined by the two-dimensional fractal dimension, D_2, is not equal to an encased area, A_e, for the same reasons that the fractal volume is not equal to the encased volume. Third, the empirical expression for the drag coefficient for spheres (*23*)

$$C_D = (24/\dot{\mathrm{Re}}) + [6/(1 + \sqrt{\dot{\mathrm{Re}}})] + 0.4 \tag{17}$$

where the Reynolds number, $\dot{\mathrm{Re}} = \dot{U}\,\mathrm{d}/\nu$, is assumed valid for fractal aggregates, and ν is the fluid kinematic viscosity. An analysis by Alldredge and Gotschalk (*10*) on marine snow aggregates, which are known to be fractal (*24*), suggests that the above empirical drag coefficient does not accurately predict settling velocities at larger Reynolds numbers ($\dot{\mathrm{Re}} > 1$). However, Alldredge and Gotschalk were unable to derive a more accurate expression. In order to use this expression in the current scaling relationships, we approximate the drag coefficient in eq 17 as a power law function in terms of a Reynolds number ($\mathrm{Re} = Ul/\nu$) for a fractal aggregate as

$$C_D = a\mathrm{Re}^{-b} \tag{18}$$

where a and b are determined for different ranges of Reynolds numbers from eq 17. For $\mathrm{Re} \leq 0.1$, $a = 24.0$ and $b = 1.0$; for $0.1 < \mathrm{Re} < 10$, $a = 29.03$ and $b = 0.871$; and for $10 < \mathrm{Re} < 100$, $a = 14.15$ and $b = 0.547$. As shown in Figure 1, the power law function is within 10% of values calculated from eq 17.

Substituting eqs 10, 16, and 18 into an analogous expression of eq 14, we obtain for fractal aggregates

$$U = \left[\frac{2g\xi_o}{a\rho_w\xi_2}(\rho_o - \rho_w)\psi^{D/3} l_o^{1+D_2-D_\nu-b} l^{D+b-D_2}\right]^{1/(2-b)} \tag{19}$$

If the aggregate is Euclidean, i.e., a sphere with $D = 3$, and $\mathrm{Re} \ll 1$, eq 19 reduces to Stokes law. For fractal aggregates, D_2 must be less than or equal to 2. As discussed by

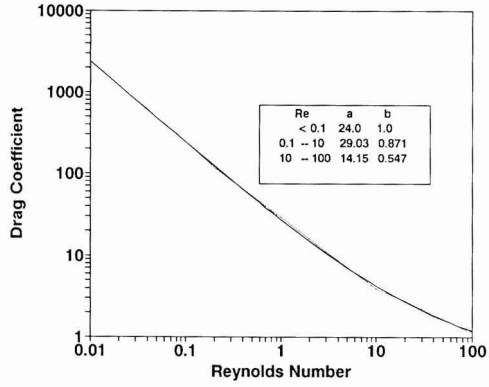

Figure 1. Drag coefficients as a function of Reynolds number for an empirical equation (—) versus the power-law equation (•••) assumed here of the form $C_D = a\mathrm{Re}^b$. Note that the two lines are nearly coincident.

Meakin (*17*), if D is less than 2, then D_2 = D; when D is greater than 2, $D_2 = 2$.

Collision Frequency Functions. Coagulation of particles occurs by three coagulation mechanisms: Brownian motion, shear and differential sedimentation. Collision frequency functions for fractal aggregates can be derived for each coagulation mechanism by using size–volume relationships. In this analysis, we assume that collision frequency functions, expressed as a function of the size of the aggregate, are valid for fractal aggregates of size l or Euclidean aggregates of size d. Therefore, the collision frequency functions for fractal aggregates can be written by replacing aggregate diameter, d, with the aggregate length, l.

The collision frequency function for Brownian motion, β_B, based on Smoluchowski's equation and Einstein's relationship, is

$$\beta_B(l_i,l_j) = (2kT/3\mu)[(l_i + l_j)^2/(l_i l_j)] \qquad (20)$$

where k is the Boltzmann constant, T is absolute temperature, and μ is the fluid viscosity.

The collision frequency for shear coagulation (*11*) is

$$\beta_{sh}(l_i,l_j) = (G/6)(l_i + l_j)^3 \qquad (21)$$

where G is the fluid shear rate.

The third coagulation mechanism, differential sedimentation, occurs when a faster settling floc overtakes and collides with a slower settling floc. The collision frequency for differential sedimentation is the collision cross section times the difference in the floc settling velocities, assuming a constant floc density

$$\dot{\beta}_{ds}(d_i,d_j) = \frac{\pi}{4}(d_i + d_j)^2|\dot{U}_i - \dot{U}_j| \qquad (22)$$

For fractal aggregates, we use the settling velocity in eq 19 and replace the aggregate diameter with the aggregate length, l, to obtain

$$\beta_{ds} = \frac{\pi}{4}\left[\frac{2g\xi_o}{a\rho_w\xi_2}(\rho_o - \rho_w)\psi^{D/3}\nu^{-b}l_o^{1+D_2-D}\right]^{1/(2-b)}(l_i + l_j)^2 \times |l_i^{(D+b-D_2)/(2-b)} - l_j^{(D+b-D_2)/(2-b)}| \qquad (23)$$

The collision frequency equations for fractal aggregates can be expressed in terms of solid volume. These collision functions are

$$\beta_B(v_i,v_j) = \frac{2kT}{3\mu}[v_i^{-(1/D)} + v_j^{-(1/D)}](v_i^{1/D} + v_j^{1/D}) \qquad (24)$$

$$\beta_{sh}(v_i,v_j) = \frac{G}{6\psi\xi_o}v_o^{1-(3/D)}(v_i^{1/D} + v_j^{1/D})^3 \qquad (25)$$

$$\beta_{ds}(v_i,v_j) = \frac{\pi}{4}\left[\frac{2g}{a\rho_w\xi_2}(\rho_o - \rho_w)\nu^{-b}\right]^{1/(2-b)} \times \xi_o^{-(1/3)}\psi^{-(1/3)[(b-D_2)/(2-b)+2]}v_o^{-(1/3)-(1/D)[(b-D_2)/(2-b)+2]} \times |(v_i^{(1/D)[(D+b-D_2)/(2-b)]} - v_j^{(1/D)[(D+b-D_2)/(2-b)]})| \times (v_i^{1/D} + v_j^{1/D})^2 \qquad (26)$$

where v_o is the volume of primary particles in the aggregate. These equations do not include correction factors suggested by others (*7*, *13*) to reduce collisions between dissimilar-sized particles.

Dimensional Analysis. The assumption of a dynamic steady state used in a dimensional analysis implies that there is a continuous source of primary particles that coagulate through the size distribution to form aggregates that are removed through sedimentation (*11*, *25*, *26*). Thus, larger aggregates undergoing coagulation by shear or differential sedimentation would primarily be produced by aggregates formed by Brownian coagulation of the smallest (submicron) particles. In marine systems, however, particles can be produced de novo that are on the same order in size as aggregates produced from Brownian coagulation. A dimensional analysis also requires the four assumptions made by Hunt (*14*), as described in the Introduction. These assumptions and limitations may not be critical factors in the current calculations since previous research by Hunt (*14*) has shown that a dimensional analysis does result in steady-state size distributions in agreement with observations. In the current analysis, we modify relationships used in a dimensional analysis to include size–mass relationships based on fractal geometry.

In our analysis we define $n(v)$ as a continuous function describing the number of aggregates per volume of fluid per solid volume interval, in units of $L^{-3}\ l^{-3}$, where L is a fluid-length unit and l is the aggregate-length unit. For a steady-state size distribution, Hunt (*14*) defined $\dot{E}$ ($l^3\ L^{-3}\ t^{-1}$) as the steady-state particle volume flux through the size distribution. In our analysis, we define a fractal solid volume flux, denoted by E, which has the same dimensions as $\dot{E}$.

The characteristic parameters for each coagulation mechanism, based on fractal geometry, are

$$K_B = kT/\mu \qquad [L^3\ t^{-1}]$$
$$K_{sh} = Gv_o^{1-(3/D)} \qquad [L^3\ l^{-9/D}\ t^{-1}] \qquad (27)$$
$$K_{ds} = \left[\frac{g\nu^{-b}(\rho_o - \rho_w)}{\rho_w}\right]^{1/(2-b)} v_o^{(1/3)-(1/D)([(b-D_2)/(2-b)]+2)} [l^{-(3/D)[(4+D-b-D_2)/(2-b)]}L^3\ t^{-1}]$$

where K_B, K_{sh}, and K_{ds} are the characteristic parameters for Brownian, shear motion, and differential sedimentation, respectively, which are obtained from the collision frequency functions (eqs 24–26), except the independent variables are not included.

The size distribution has the functional form of

$$n(v) = n(v,E,K_B,K_{sh},K_{ds}) \qquad (28)$$

By selecting a size interval where only one coagulation mechanism is dominant, eq 28 becomes an expression of four variables and three units (l, L, and t). Using the Buckingham π theorem, we can obtain a size-distribution function for each coagulation mechanism as

$$n(v) = A_B\left(\frac{E}{K_B}\right)^{1/2} v^{-(3/2)} \qquad (29)$$

$$n(v) = A_{sh}\left(\frac{E}{K_{sh}}\right)^{1/2} v^{-(3/2)[1+(1/D)]} \quad (30)$$

$$n(v) = A_{ds}\left(\frac{E}{K_{ds}}\right)^{1/2} v^{[-(3/2)-(1/2D)[1+[(2+D-D_2)/(2-b)]]]} \quad (31)$$

where A_B, A_{sh}, and A_{ds} are dimensionless constants that must be experimentally determined.

The size distribution function, $n(l)$ is a continuous function describing the number of aggregates per volume fluid per floc length interval. The relationship between $n(v)$ and $n(l)$ is

$$n(l) = n(v)\, dv/dl \quad (32)$$

and by taking the derivative of eq 10, we determine

$$dv/dl = \psi^{D/3}\xi_o l_o^{3-D} D l^{D-1} \quad (33)$$

Combining eqs 32 and 33, we obtain

$$n(l) = \psi^{D/3}\xi_o l_o^{3-D} D l^{D-1} n(v) \quad (34)$$

Using eq 34 in eqs 29–31, the size-distribution functions based on $n(l)$ are

Brownian

$$n(l) = A'_B (E/K_B)^{1/2} l^{-[1+(D/2)]} \quad (35)$$

Shear

$$n(l) = A'_{sh} (E/K_{sh})^{1/2} l^{-(1/2)(D+5)} \quad (36)$$

Differential Sedimentation

$$n(l) = A'_{ds} (E/K_{ds})^{1/2} l^{-(1/2)[3+D+[(2+D-D_2)/(2-b)]]} \quad (37)$$

where A'_B, A'_{sh}, and A_{ds} are functions of l_o and D. The size distribution functions $n(l)$ and $n(v)$ are summarized in Table I.

Results

Effect of Fractal Structures on Collision Rates. When fractal dimensions are included in expressions for collision frequency functions and when packing and shape factors for Euclidean and fractal objects are equal, particles are predicted to collide more frequently than when $D = 3$. This occurs because the size of the fractal aggregate increases faster during coagulation than aggregates with constant size–mass relationships. In Figure 2 we plot collision frequencies for coagulation via Brownian, shear, and differential sedimentation (for Re $\ll$ 1) as a function of aggregate size for different fractal dimensions. Collision frequencies are calculated as a ratio of collision frequencies at fractal dimensions of 1.5, 2, and 2.5 versus collision frequencies at $D = 3$. As the fractal dimension decreases, the collision frequency of fractal aggregates is larger than for Euclidean aggregates. For example, during shear coagulation, aggregates with a fractal dimension of 1.5 could collide 774 times as frequently as aggregates with a fractal dimension of 3. For flocs with the same solid volume, collision frequencies could be up to 8.4 and 91 times as large as predicted from conventional models for coagulation by Brownian and differential sedimentation. A constant porosity could be chosen to make coagulation rates equal to Euclidean and fractal aggregates, but the magnitude of the porosity would be variable for different fractal dimensions.

Fractal Dimensions from Size Distribution Functions. The equations derived for the fractal size distributions, $n(v)$, based on coagulation by Brownian motion, shear, and differential sedimentation (Table I) are identical

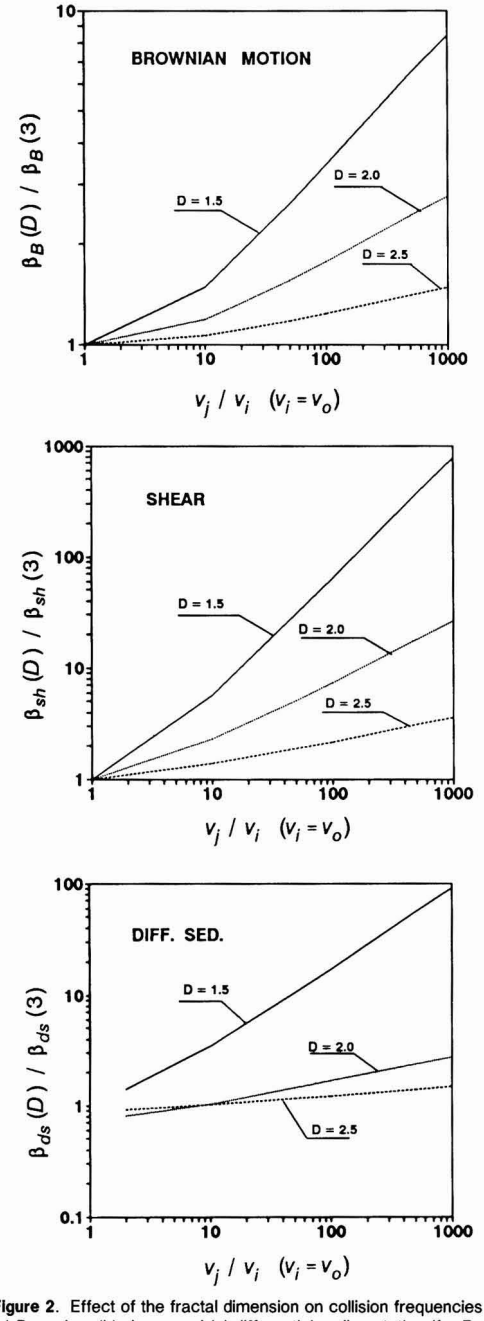

Figure 2. Effect of the fractal dimension on collision frequencies for (a) Brownian, (b) shear, and (c) differential sedimentation (for Re $\ll$ 1), where $\beta(D)$ is the collision frequency for a fractal aggregate at the indicated value of D, and $\beta(3)$ is the collision frequency for a Euclidean object. (v_j is the volume of the aggregate colliding with a particle volume v_o.)

with those previously presented (*8*, *14*) if the fractal dimension in each size-distribution equation is set equal to a Euclidean value of 3 and Re $\ll$ 1.

Hunt (*14*) compared steady-state size distributions from marine systems with his predicted relationships based on a dimensional analysis. In this study, we can make an analogous comparison of size distributions with our dimensional analysis based on fractal aggregates. The fractal

Table I. Size Distribution Functions for Fractal Aggregates

coagulation mechanism	$n(v)$	A'	$n(l)$
Brownian	$A_B\left(\frac{E}{K_B}\right)^{1/2} v^{-3/2}$	$A_B D(\xi_o l_o^{3-D}\psi^{D/3})^{-1/2}$	$A'_B\left(\frac{E}{K_B}\right)^{1/2} l^{-[1+(D/2)]}$
shear	$A_{sh}\left(\frac{E}{K_{sh}}\right)^{1/2} v^{-(3/2)[1+(1/D)]}$	$A_{sh} D(\xi_o l_o^{3-D}\psi^{D/3})^{-(1/2)[1+(3/D)]}$	$A'_{sh}\left(\frac{E}{K_{sh}}\right)^{1/2} l^{-(1/2)(D+5)}$
differential sedimentation	$Ads\left(\frac{E}{K_{ds}}\right)^{1/2} v^{[-(3/2)-(1/2D)[1+[(2+D-D_2)/(2-b)]]]}$	$A_{ds} D(\xi_o l_o^{3-D} \times \psi^{D/3})^{-(1/2)[1+(1/D)[1+[(2+D-D_2)/(2-b)]]]}$	$A'_{ds}\left(\frac{E}{K_{ds}}\right)^{1/2} \times l^{-(1/2)[3+D+[(2+D-D_2)/(2-b)]]}$

Table II. Fractal Dimensions and Slopes Determined from Dimensional Analysis of Steady-State Size Distributions in Marine Systems

	Brownian	shear	differential sedimentation
size range, μm	<2	2–40	>40
slope [log $n(l)$ vs log l]			
predicted in this work	$-\left(1+\frac{D}{2}\right)$	$-\frac{(D+5)}{2}$	$-\frac{1}{2}\left[3+D+\frac{2+D-D_2}{2-b}\right]$
predicted by Hunt (*14*)	$\frac{-5}{2}$	−4	$\frac{-9}{2}$
observed	−2.65	−3.7 to −4.4	−4.65, −5.2, −5.3
slope [log $n(v)$ vs log v]			
predicted in this work	$-\frac{3}{2}$	$-\frac{3}{2}\left(1+\frac{1}{D}\right)$	$-\frac{3}{2}-\frac{1}{2D}\left(1+\frac{2+D-D_2}{2-b}\right)$
predicted from Hunt (*14*)	$-\frac{3}{2}$	−2	$-\frac{13}{6}$
observed		−1.9 to −2.13	−2.22, −2.40, −2.43
fractal dimension		2.4–3.75	1.61–2.31

dimension in eqs 30 and 31 can be obtained from the slope in a plot of log $n(v)$ versus log v. Hunt used data available in the literature to calculate several such slopes. These size distributions were originally obtained by using particle counters for marine particles larger than 2 μm, and from direct microscopic observation for smaller sized particles. Although size distributions are reported in terms of aggregate diameter, d_p, particle counters (resistance type) measure the volume occupied by primary particles comprising the aggregate (i.e., v not v_e); d_p is the equivalent spherical diameter based on instrument calibration with solid spheres. As a result of this calibration procedure, aggregate size, l, is underestimated. However, aggregate size data [$n(l)$] reported in ref 14 can be converted back into solid volume [$n(v)$] with the equation

$$s_v = (s_l - 2)/3 \tag{38}$$

where s_v is the slope based on the particle–volume log–log plots, and s_l is a slope based on the particle-length log–log plots. This equation can be verified by either comparing equations presented in ref 8 with ref 14, or for fractal aggregates, comparing eqs 29–31 with 35–37.

The observed and predicted slopes of log–log plots of size distributions as reported by Hunt (*14*) and calculated here are shown in Table II. The size range over which each coagulation mechanism operates is assumed to be the same as determined by Hunt (*14*). From the range of reported slopes for particles assumed to be produced by shear coagulation, we calculate fractal dimensions of 2.4–3.75 for aggregates developed from shear coagulation; however, it is unlikely that D is greater than 3. Several factors may help explain the magnitude of this fractal dimension. First, the size range calculated for aggregates formed by shear coagulation (2–40 μm) is typical of nonaggregated particles in the water column, such as phytoplankton. Since particle counters do not distinguish between amorphous aggregates and solid particles, it may be that some particles analyzed in the shear coagulation size range are not aggregates, but microorganisms such as single-celled phytoplankton with Euclidean, and not fractal, structures. A second source of error is the sensitivity of the magnitude of the fractal dimension to the slope. For example, fractal dimensions in a wide range of $1 < D < 3$ produce slopes in the narrow range of 2.17–2.5. Third, many marine aggregates contain actively growing microorganisms (*27*), resulting in aggregates formed by growth of cells already in the aggregate, and not by coagulation of unattached particles.

For particles assumed to be produced by differential sedimentation, slopes of −2.22 to −2.53 were calculated for fractal size distributions by using slopes of −4.65 and −5.2 reported by Hunt (Table II). A third set of data also reported by Hunt (*14*) indicated a slope of −5.6, but our examination of the data reported by Faist (*28*) provided a slope of −5.3. Using slopes of −4.65, −5.2, and −5.3, we obtained fractal dimensions in the range of 2.31, 1.67, and 1.61. All Reynolds numbers were less than 0.1 independent of our assumed value of D_2, resulting in $b = 1$. The assumption that $D_2 = D$ when D is less than 2 increased the calculated fractal dimension. If we assumed that $D_2 = 2$, we would calculate fractal dimensions of 1.25 and 1.15, for slopes of −5.2 and −5.3, respectively.

Only a single slope of −2.65 was reported by Hunt (*14*) for small aggregates (<2 μm) assumed to form by Brownian

coagulation. However, a fractal dimension cannot be calculated from a dimensional analysis for aggregates formed from Brownian motion since D does not appear in the final expression for the slope calculated by using eq 29 (Table II) based on aggregate volume.

Discussion

There is now substantial evidence that aggregates formed from coagulation processes possess fractal structures (*15–18, 29*). As a result, existing coagulation models based on Euclidean scaling relationships must be modified to account for the scaling properties of fractal aggregates. Collision functions based on fractal geometry (Table I) indicate more frequent collisions between fractal aggregates ($D < 3$) than Euclidean objects ($D = 3$). Fractal aggregates have a larger size, and therefore a greater collision probability, than aggregates assumed to have a constant porosity.

Using a dimensional analysis based on a fractal scaling relationships, we calculated fractal dimensions of aggregates formed in marine systems. For aggregates formed from differential sedimentation and shear coagulation, we determined $1.61 \leq D \leq 2.31$ and $2.4 \leq D \leq 3.75$, respectively. Fractal dimensions could not be calculated for aggregates formed by Brownian motion by use of the dimensional analysis since D did not appear in the final dimensional analysis based on aggregate volume (eq 29). However, computer simulations describing colloidal aggregation have shown that aggregates formed through the collision of clusters (cluster–cluster) have fractal dimensions of either 1.8 or 2.2 (*18*). These simulations have been experimentally verified by measurement of the fractal dimensions of a variety of colloidal aggregates formed by Brownian motion (*18*). The two different values of the fractal dimension occur as a function of different particle stickiness. Particles that stick immediately upon contact with other particles cannot penetrate the aggregate since they collide with particles on the aggregate exterior and stick. Aggregates formed from these particles are classified as "diffusion limited" and have fractal dimensions of $D = 1.8$. As the collision probability approaches zero, however, particles may collide many times before sticking; these cells can penetrate the aggregate, increasing the aggregate density. These aggregates are referred to as "reaction limited", with $D = 2.2$ (*18*). Since different types of aggregates have different values of D, fractal classification of aggregates formed by Brownian motion identifies both the aggregate formation mechanism as well as the collision efficiency of cells composing the aggregate.

The different ranges of the fractal dimensions presented in Table III indicate that different values of the fractal dimension occur as a result of different coagulation mechanisms. Conversely, this suggests that the magnitude of the fractal dimension for a collection of aggregates could be a useful reference for identifying a coagulation mechanism. Although the fractal dimensions determined for coagulation by Brownian motion ($1.8 \leq D \leq 2.2$) and differential sedimentation ($1.61 \leq D \leq 2.31$) overlap, it is unlikely that we would need to distinguish between aggregates formed by these two different coagulation mechanisms. Aggregate formation by Brownian motion is likely to be dominant only for small particles, on the order of 1 μm or less (*7*). Therefore, these two coagulation mechanisms are easily distinguished by the absolute aggregate size. The fractal dimensions of aggregates formed by shear coagulation ($D \geq 2.4$) are larger than those determined for the other two coagulation mechanisms, suggesting that shear coagulation produces denser aggregates than other coagulation mechanisms. However, it is not clear that all particles measured in the 2–40-μm size distribution were aggregates produced by coagulation since this size range includes solid particles such as single-celled phytoplankton. Thus, it may be that most particles analyzed in this size range in marine systems are not aggregates, but other objects with Euclidean, and not fractal, structures. Additional information, which could be obtained through direct observation via photographs, is necessary to clarify the types of particles present in the 2–40-μm size distributions.

Table III. Fractal Dimensions of Various Types of Aggregates

	fractal dimension	ref
Computer Models		
Brownian motion		
diffusion limited	1.8	18
reaction limited	2.2	18
Dimensional Analysis		
shear	2.4–3.75	*a*
differential sedimentation	1.61–2.31	*a*
Zoogloea ramigera		
rotating tubes	1.8±0.03	29
benchtop bioreactor	3.0±0.04	29
Marine Snow		
general	1.26±0.06	24
general	1.39±0.15	24
diatom aggregates	1.52±0.19	24
Activated Sludge		
	1.0	24
	1.4	31
	1.44–1.49	31
	1.55–2.0	31
	1.70–2.07	31
Inorganic Aggregates		
alum	1.59–1.97	31
alum	2.30–2.32	31
clay–iron	1.92	31
clay–magnesium	1.91	31
ferric	2.61–2.81	31

[a] This study.

The fractal dimensions determined by Lin et al. (*18*) for coagulation by Brownian motion and the fractal dimensions for coagulation by shear and differential sedimentation are compared to reported fractal dimensions of a variety of types of organic and inorganic aggregates in Table III. On the basis of eq 4, Logan and Wilkinson (*29*) determined the fractal dimension of 3.0 ± 0.4 for macroscopic aggregates (0.4–1.4 mm) of *Zoogolea ramigera* grown in a laboratory benchtop fermentor. This fractal dimension is within the range of values calculated from marine distributions for aggregates formed by shear coagulation. However, when bacterial aggregates were developed in rotating test tubes, *Z. ramigera* aggregates had a fractal dimension of 1.8 ± 0.3. The fractal dimension obtained for the rotating tube aggregates is smaller than the range of fractal dimensions indicated for shear coagulation. The results of the dimensional analysis imply that aggregates formed in the rotating tubes were not formed by shear coagulation, but by differential sedimentation. Since these aggregates settled to the bottom of the rotating tubes during culture growth and coagulation, this conclusion is reasonable.

To our knowledge, there are no reports of fractal dimensions of aggregates formed by differential sedimentation that have been generated either through computer simulations or through experiments. However, Logan and

Wilkinson (*24*) estimated fractal dimensions of marine snow aggregates assumed to be formed by differential sedimentation using in situ data reported by others (*10*, *30*). They obtained fractal dimensions of 1.39 ± 0.15 from size–porosity data and 1.26 ± 0.26 from settling velocity data, for marine snow aggregates 0.4–20 mm in length. They also calculated a fractal dimension of 1.52 ± 0.19 for diatom aggregates using data on the number of diatoms per aggregate, for aggregates 7–20 mm in length. The magnitude of these fractal dimensions obtained from in situ studies is within the range predicted by the fractal size distribution analysis for aggregates formed from differential sedimentation.

Li and Ganczarczyk (*31*) determined fractal dimensions for a variety of aggregates formed in water and wastewater treatment processes. Inorganic flocs have higher fractal dimensions in the range of 1.59–2.85. The primary particles forming these inorganic aggregates are colloidal (<1 μm), so we would expect these aggregates to be formed by either Brownian motion or shear coagulation. The clay flocs have fractal dimensions in the Brownian motion range of 1.8–2.2, but the fractal dimensions for alum flocs span the range of values for shear and Brownian motion. The ferric aggregates are in the range indicated for shear coagulation. Activated sludge flocs had fractal dimensions ranging from 1.4 to 2.07 (Table III). Since these flocs are very large, this suggests formation by differential sedimentation. Activated sludge flocs containing a large number of filamentous microorganisms have a lower fractal dimension of 1.0 (*24*).

In general, the fractal dimensions of biological aggregates obtained from natural and engineered environments (1.0–1.5) are smaller than other fractal dimensions determined for inorganic colloidal aggregates. Part of the reason for fractal dimensions below values of 1.61–2.31 determined here may be due to different scaling relationships used to relate settling velocity to aggregate size. Li and Ganczarczyk (*31*) assumed that $v \sim l^{D-1}$. Although Logan and Wilkinson used $v \sim l^{D+1-D_2}$, they assumed $D_2 = 2$, which reduced their expression to the same as that of Li and Ganczarczyk. In the present study, we have used $v \sim l^{(D+b-D_2)/(2-b)}$. If $D < 2$ and we can assume $D_2 = D$, then settling velocity is only a function of the power law relationship and is not a function of the fractal dimension. Therefore, at Re > 1, aggregate settling velocities are most sensitive to values of b. For example, marine snow aggregates analyzed by Logan and Wilkinson (*24*) had a fractal dimension of $D = 1.39 \pm 0.15$ determined from size–porosity data, and Reynolds numbers in the range of 0.1–10 (*10*). In this range, $b = 0.871$, and we would expect that $v \sim l^{0.87}$, but it was observed that $v \sim l^{0.26}$. These differences could either be due to different values of D_2 than assumed here or errors introduced by using drag coefficients developed for spheres for nonspherical fractal aggregates. From size-projected area data (*32*), $D_2 = 1.46 \pm 0.16$. Within a standard error, $D = D_2$ since $D = 1.39 \pm 0.15$. Therefore, the differences in observed and calculated relationships between size and settling velocity are probably a result of our assumption of the drag coefficient for these aggregates.

The collision functions derived by using fractal relationships are only a first step in modifying coagulation theory to incorporate fractal geometry. Existing collision models predict a very low probability of collisions between dissimilar-sized spheres in marine systems (*7*). However, collisions between dissimilar-sized aggregates are probably more likely for fractal aggregates than spheres. The larger cross-sectional area and branches of a fractal aggretate not only allow for increased collisions between colliding particles, but the open-branched structure of a fractal will permit advective flow through the aggregate (*33*, *34*) resulting in collisions between aggregates that would not occur if the aggregates were constrained to follow streamlines that did not cross the aggregate surface. The effect of fractal geometry on flow-through porous objects is a emerging field with important implications for coagulation theory.

Conclusions

Coagulation equations and a self-similar size-distribution analysis used to describe coagulation can be modified to incorporate the fractal geometry of aggregates. We have proposed a set of collision functions containing a fractal dimension that can be used in the general coagulation equation. Through the use of a fractal size distribution analysis, we have calculated that aggregates formed by shear coagulation should have fractal dimensions greater than 2.4, whereas aggregates formed from differential sedimentation would have lower fractal dimensions in the range of 1.6–2.3. Most biological aggregates from engineered bioreactors and marine systems have fractal dimensions in the range expected for differential sedimentation. Fractal dimensions of inorganic and colloidal aggregates were in the range expected for aggregation by Brownian motion and shear coagulation.

Acknowledgments

We thank James R. Hunt, Charles R. O'Melia, William Becker, and Kwok-Keung Au for many helpful comments made during their review of an earlier manuscript.

Literature Cited

(1) O'Melia, C. R. In *Chemical Processes in Lakes*; Stumm, W., Ed.; Wiley: New York, 1985; Chapter 10.
(2) Weilenmann, U.; O'Melia, C. R.; Stumm, W. *Limnol. Oceanogr.* **1989**, *34*, 1–18.
(3) Jackson, G. A. *Deep Sea Res.* **1990**, *37*, 1197–1211.
(4) Ali, W.; O'Melia, C. R.; Edzwald, J. K. *Water Sci. Technol.* **1984**, *17*, 701–712.
(5) Alldredge, A. L.; McGillivary, P. M. *Deep Sea Res.* **1991**, *38*, 431–443.
(6) McCave, I. N. *Deep Sea Res.* **1975**, *22*, 491–502.
(7) McCave, I. N. *Deep Sea Res.* **1984**, *31*, 329–352.
(8) Hunt, J. R. *J. Fluid Mech.* **1982**, *122*, 303–309.
(9) Farley, K. J. *J. Environ. Eng.* **1990**, *116*, 144–165.
(10) Alldredge, A. L.; Gottschalk, C. *Limnol. Oceanogr.* **1988**, *33*, 339–351.
(11) Friedlander, S. K. *Smoke, Dust and Haze*; Wiley: New York, 1977; pp 177–208.
(12) Lawler, D. F.; O'Melia, C. R.; Tobiason, J. E. *Adv. Chem. Ser.* **1980**, *No. 189*, 353–388.
(13) Valiolis, I. A.; List, E. J. *Environ. Sci. Technol.* **1984**, *18*, 242–247.
(14) Hunt, J. R. *Adv. Chem. Ser.* **1980**, *No. 189*, 243–257.
(15) Weitz, D. A.; Huang, J. S.; Lin, M. Y.; Sung, J. *Phys. Rev. Lett.* **1985**, *47*, 1400–1403.
(16) Witten, T. A.; Cates, M. E. *Science* **1986**, *232*, 1607–1612.
(17) Meakin, P. *Adv. Colloid Interface Sci.* **1988**, *28*, 249–331.
(18) Lin, M. Y.; Lindsay, H. M.; Weitz, D. A.; Ball, R. C.; Klein, R.; Meakin, P. *Nature* **1989**, *339*, 360–362.
(19) Feder, J. *Fractals*; Plenum Press: New York, 1988; pp 31–38.
(20) Weitz, D. A.; Olivera, M. *Phys. Rev. Lett.* **1984**, *52*, 1433–1436.
(21) Bird, R. B.; Stewart, W. E.; Lightfoot, E. N. *Transport Phenomena*; Wiley: New York, 1960; p 59.
(22) Logan, B. E.; Hunt, J. R. *Limnol. Oceanogr.* **1987**, *32*, 1034–1048.
(23) White, F. M. *Viscous Fluid Flow*; McGraw Hill: New York, 1974; p 209.

(24) Logan, B. E.; Wilkinson, D. B. *Limnol. Oceanogr.* **1990**, *35*, 130–136.
(25) Friedlander, S. K. *J. Meterol.* **1960**, *17*, 373–374.
(26) Friedlander, S. K. *J. Meterol.* **1960**, *17*, 479–483.
(27) Alldredge, A. L.; Cole, J. J.; Caron, D. A. *Limnol. Oceanogr.* **1986**, *31*, 68–78.
(28) Faist, W. K. *Adv. Chem. Ser.* **1980**, *No. 189*, 259–282.
(29) Logan, B. E.; Wilkinson, D. B. *Biotechnol. Bioeng.* **1991**, *38*, 389–396.
(30) Logan, B. E.; Alldredge, A. L. *Mar. Biol.* **1989**, *101*, 443–450.
(31) Li, D.-h.; Ganczarczyk, J. J. *Environ. Sci. Technol.* **1989**, *23*, 1385–1389.
(32) Alldredge, A. L. University of California, Santa Barbara, unpublished.
(33) Adler, P. M. *J. Colloid Interface Sci.* **1981**, *81*, 531–535.
(34) Adler, P. M. In *The Fractal Approach to Heterogeneous Chemistry*; Avnir, D., Ed.; Wiley: New York, 1989; Chapter 4.2.

Received for review March 4, 1991. Revised manuscript received June 17, 1991. Accepted June 26, 1991. Funding for this research was provided through ONR Contracts N000014-88-K0387 and 423G004-01.

Interactions of Acidic Metal-Rich Coal Pile Runoff with a Subsoil

Michael A. Anderson,*,† Paul M. Bertsch,‡ Steven B. Feldman,§ and Lucian W. Zelazny§

Department of Soil and Environmental Sciences, University of California, Riverside, California 92521, Division of Biogeochemistry, University of Georgia, Savannah River Ecology Laboratory, Drawer E, Aiken, South Carolina 29801, and Department of Crop and Soil Environmental Sciences, Virginia Polytechnic Institute and State University, Blacksburg, Virginia 24061

■ Highly acidic and metal-rich runoff from coal storage facilities can have a dramatic impact on local surface water and groundwater quality. In order to identify important reactions governing metal transport within subsurface environments subject to infiltration of coal pile runoff (CPR), samples of uncontaminated subsoil adjacent to a coal stockpile runoff containment basin at the U.S. Department of Energy's Savannah River Site were collected and subjected to leaching with acidic, metalliferous CPR. Effluent was collected and multicomponent transport through the subsoil evaluated. Mass balance calculations, a sequential dissolution scheme in which column leaching was terminated and elements were partitioned to water, 1 M NH_4Cl, and ammonium oxalate in the dark-extractable phases, and mineralogical and surface chemical analyses were used to identify important chemical processes and mineralogical alterations occurring during leaching.

Introduction

Analogous to mining operations, the storage of coal can also generate highly acidic, metal-rich leachate resulting from the oxidation of sulfidic ores present in coal as impurities (*1*, *2*). Additional water quality concerns with regard to coal storage include that coal stockpiles are relatively abundant, not restricted to areas associated with mining operations, and often uncontrolled.

The interaction of these metalliferous acid leachates with more alkaline surface waters results in neutralization or dilution of acidity, precipitation of iron and aluminum hydroxides, oxyhydroxides, and/or basic sulfates (*3–6*), and sorption or coprecipitation of heavy metals to the freshly precipitated materials (*7–11*). Wangen and Jones (*12*) evaluated the capacity of different soils to neutralize coal mineral waste leachate and found that carbonate content governed acidity and also the metal concentrations of soil column effluent. A naturally acidic soil, with no free carbonates present, afforded little attenuation (*12*).

Inasmuch as a significant portion of the U.S. coal reserves and coal stockpiles resides within moderately to highly weathered geologic regions with limited carbonate alkalinity, an evaluation of the subsurface mobility of contaminants from coal pile runoff within a weathered, naturally acidic subsoil was undertaken.

Experimental Section

Study Site. Soil samples were collected from a site immediately adjacent to the D-area coal pile runoff (CPR) containment basin at the U.S. Department of Energy's Savannah River Site near Aiken, SC (Figure 1). The coal stockpile is 3.6 ha in areal extent, containing approximately 131 000 metric tons of low-S (1–2%) coal. The basin is 5.1 ha with a volume capacity near 3.8×10^{10} L. Monitoring well data (*13*) indicate significant degradation of groundwater downgradient of the coal pile and basin.

Soil Sampling and General Characterization. The basin was created by excavation and removal of the surficial 1–2 m of Fuquay soil (loamy, siliceous, thermic arenic Plinthic Paleudults). Subsoil was sampled 0.25–0.75 m below the basin surface, or approximately 2.25–2.75 m below the natural soil surface, by augering in uncontaminated soils adjacent to the basin. Bulk densities were determined on samples extruded from cores of known volume (*14*). The samples were weighed prior and subsequent to oven drying at 105 °C. Bulk densities were taken as the oven dry weight divided by core volume. Porosities were calculated from the bulk densities assuming a particle density of 2.65 g cm^{-3} (*15*). Particle-size distributions were determined via a modified pipet method (*16*).

Bulk soil samples were air-dried and passed through a 2-mm sieve. Soil pH was determined on 1:1 soil–water equilibrations (*17*). Noncrystalline and free oxide contents of triplicate 1-g (oven dry weight basis) subsamples were estimated via the 4-h ammonium oxalate in the dark (Ox) and dithionite–citrate–bicarbonate (DCB) procedures, respectively (*18*). Soil organic matter contents were determined with the Walkley–Black method (*19*). Cation-exchange capacities of the whole soils were determined by summation of native cations exchanged from triplicate 5-g (oven dry weight basis) subsamples with three 30-min extractions of 1 M NH_4Cl.

Column Leaching Experiments. Air-dried, <2-mm-diameter soils were packed into duplicate 25 cm × 2.54 cm columns to a uniform bulk density of 1.50 g cm^{-3}. Columns were then wet from the bottom with deionized water supplied at a constant flow equivalent to a Darcy velocity

† University of California.
‡ University of Georgia.
§ Virginia Polytechnic Institute and State University.

 0013-936X/91/0925-2038$02.50/0

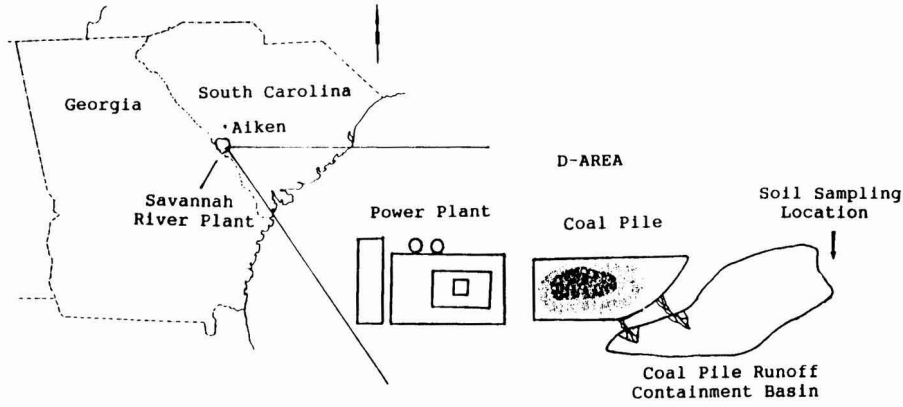

Figure 1. Study site.

(q) of 1.3 cm h^{-1} via a Dionex APM pump module (Dionex Corp., Sunnyvale, CA). Once steady saturated flow was attained, the columns were allowed to equilibrate overnight. Coal pile runoff collected from the basin was then supplied and the columns were leached under steady saturated flow (q = 1.3 cm h^{-1}). Effluent was collected via an LKB linear fraction collector. Column dispersivities were determined after leaching was completed via pulse injections equivalent to ~1 pore volume of 5 mM LiBr followed by additional runoff. Breakthrough data were then analyzed via the parameter estimation method of Parker and van Genucthen (*20*).

Results from the transport studies are presented using reduced values for time or, equivalently, as the number of pore volumes supplied to the columns (V/V_0), where V is the total volume supplied to the column and V_0 the total pore volume within the columns, and concentration (C/C_0), where C is the effluent concentration and C_0 the concentration of the influent.

Duplicated columns were also leached with 0–8, 12, and 60 pore volumes of CPR after which the leaching was stopped, and the soils were extruded and homogenized. The influence of increasing cumulative CPR influent flux on a number of chemical and mineralogical properties was then evaluated.

Element Partitioning. The partitioning of elements between operationally defined phases via sequential extraction techniques can be useful in assessing the bioavailability (*21*) and persistence (*22*) of metals within contaminated soils. For this investigation, elements were partitioned into three phases as a function of cumulative influent flux, water-soluble, 1 M NH_4Cl extractable, and ammonium oxalate extractable (Ox) fractions, corresponding roughly to water-soluble, exchangeable, and poorly crystalline phases (*18*), respectively. Water-soluble contents were determined from breakthrough curves. Dry weight samples (1.5-g equiv) were extracted twice with 7.5 mL of 1 M NH_4Cl and the supernatants combined, followed by a 10-mL deionized water wash, which was discarded. The previously extracted soils were then equilibrated with 30 mL of Ox reagent for 4 h in the dark (*18*).

Mineralogy. Silt (2–50 μm) and clay-sized (<2 μm) materials were separated from whole soils after Fe removal by DCB (*18*) via wet sieving and centrifugation (*23*). A tile mounting technique was used to prepare oriented clay mounts with Mg and K saturations (*24*). A clean, flat ceramic tile was placed in a suction apparatus and a clay suspension containing approximately 250 mg of sample was pipeted onto the tile. After free water had been drawn through the tile, 5 mL of 1 M KCl was added. This process was repeated a total of five times, followed by washing in a similar fashion with deionized water (five times). Analogously, Mg-saturated tiles were also prepared with 0.5 M $MgCl_2$, followed by one wash with 5 mL of 20% glycerol solution after the fifth water wash (Mg–gly).

The mounts were X-rayed with a Diano X-ray spectrometer (Diano Corp., Woburn, MA) from 2 to 32° 2θ at a step speed of 0.019° 2θ s^{-1} using a Cu source (wavelength 1.542 Å). The Mg–gly tile mounts were X-rayed at room temperature and after heating to 110 °C; the K-saturated tile mounts were X-rayed at room temperature and after heating to 110, 300, and 550 °C. Semioriented powder mounts of silt (2–50 μm) fractions (Na-saturated) were prepared by depositing oven-dried samples into a recessed holder and smoothing with a spatula. Clay (5 mg, <2 μm) subsamples from the K-saturated tile mounts were removed for analysis by differential scanning calorimetry (DSC). Samples were placed into gold pans and heated in an N_2 atmosphere to 625 °C at a rate of 20 °C min^{-1} with a Du Pont 1090 thermal analyzer (E. I. du Pont De Nemours and Co., Wilmington, DE).

Oxide mineralogy of the silt + clay (<50 μm) fractions were determined on nondeferrated samples by using X-ray diffraction (XRD). For these determinations, samples were scanned at a step speed of 0.00125° 2θ s^{-1}. A background diffractogram of a DCB-treated silt + clay sample (<50 μm) was subtracted from the oxide patterns.

Infrared Analysis. Fourier transform infrared analyses of silt + clay (<50 μm) fractions of soils leached with runoff were performed with a Digilab FTS-45 spectrophotometer (Bio-Rad, Digilab Division, Cambridge, MA) using diffuse reflectance (DRIFT). Sixty-four scans, sampled at 4-cm^{-1} resolution, were coadded to generate each spectrum.

Electrophoretic Mobility. Samples (~10 g) from soils leached with 0, 4, 8, 12, and 60 pore volumes of runoff from above were equilibrated with 30 mL of 1 M $NaClO_4$ and centrifuged; the supernatant was discarded. The process was repeated an additional four times, followed by two washes with 0.01 M $NaClO_4$. Samples were resuspended in 0.01 M $NaClO_4$ and wet sieved to remove >53-μm particles. The silt + clay (<50 μm) suspensions that passed the sieve were collected and 0.25-mL samples of these suspensions were then pipeted into 30-mL polycarbonate Oak Ridge tubes. Twenty-milliliter aliquots of 0.01 M $NaClO_4$ adjusted to pH 3, 4, 5, 7, and 9 with 0.1 M $HClO_4$ or NaOH were added; the resultant mixtures were equilibrated for 15 min and centrifuged and the supernatants

Table I. Composition of the Coal Pile Runoff Used in the Column Experiments

component	concn,[a] mg L^{-1}	component	concn,[a] mg L^{-1}
pH	2.13	K^+	1.668
		Li^+	0.232
Al^{3+}	101.0	Mg^{2+}	62.17
Be^{2+}	0.055	Mn^{2+}	7.302
Ca^{2+}	83.62	Na^+	11.52
Co^{2+}	0.461	Ni^{2+}	0.878
Cr^{3+}	0.010	H_4SiO_4	69.4
Cu^{2+}	0.262	SO_4^{2-}	2024
Fe^{2+}	4.70	Sr^{2+}	0.791
Fe^{3+}	119.5	Zn^{2+}	2.392

[a] Except pH.

discarded. Two additional treatments followed. The pH of an aliquot of the final wash was recorded before the sedimented material was resuspended (final suspension concentration was approximately 0.5 mg mL^{-1}).

The above treated suspensions were then analyzed for electrophoretic mobilities with a Zetasizer 3 (Malvern Instruments, Malvern, England). Cell chambers were filled with a solution equivalent in salt concentration and pH to that of the sample suspensions. Triplicate mobility determinations were made, with a 30-s count time and applied voltage and current of 80 mV and 3 mA, respectively.

Analytical. Hydrogen ion activities of the soil–water extracts and column effluent fractions were determined with a Radiometer GK2401C combined glass–calomel electrode and a Radiometer PHM 84 pH meter (Radiometer of America, Westlake, OH). Bromide concentrations were determined with a Fisher 13-620-520 Br^- ion specific electrode (Fisher Scientific, Fairlawn, NJ) and a Radiometer K401 reference electrode (Radiometer of America). Effluent fractions and extracts were analyzed for total dissolved major and trace element concentrations via inductively coupled plasma emission spectroscopy (ICPES). Sulfate analysis was performed using a Dionex System 2010i ion chromatograph (IC) (Dionex Corp.). Ferrous iron concentrations were determined via the *o*-phenanthroline method (*25*).

Speciation. Analytical speciation of elements was limited to S and Fe. Excellent agreement was obtained between total S via ICPES and S concentrations as SO_4^{2-} via IC (<1% deviation); as a result, all S was considered as SO_4^{2-} (Table I). Concentrations of Fe^{3+} were calculated from the difference between ICPES total Fe and *o*-phenanthroline-determined Fe^{2+}.

The CPR and column effluent samples were numerically speciated by use of MINTEQA2 (*26*) and saturation indexes (SI), defined as

$$SI = \log (IAP/K_{sp}) \quad (1)$$

where IAP is the ion activity product of a solution and K_{sp} is the solubility product for a given mineral phase, calculated. The reader is referred to ref 26 for a compilation of thermodynamic data used in these calculations.

Mass Balance. To properly account for components retained by the soil columns at any time, t, a mass balance about the column was calculated (Figure 2). The total volume of the column, V_T (L^3), was determined (127 cm^3). A total reactive mass of a component i, $M_{i,T}$ (M) was defined as

$$M_{i,T} = M_{i,aq} + M_{i,ex} + M_{i,ox} \quad (2)$$

where $M_{i,aq}$ is the total mass of component i in the aqueous phase, $M_{i,ex}$ is the total mass of component i on the exchange phase, and $M_{i,ox}$ is the total mass of component i that is extractable via the 4-h Ox procedure. Runoff of concentration $C_{i,in}$ ($M\ L^{-3}$) for each component (Table I) was supplied at constant volumetric flow Q, (for this investigation, 6.8 $cm^3\ h^{-1}$). Column effluent of concentration $C_{i,out}$ ($M\ L^{-3}$) was collected as a function of time. The change in total component mass within the column over time was, since V_T is constant, expressed by the equation

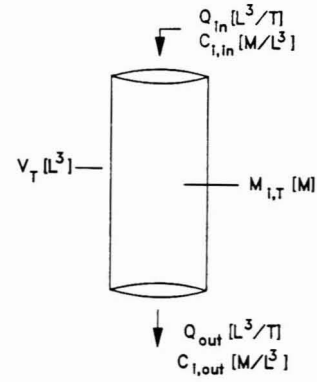

Figure 2. Mass balance about column.

$$\Delta M_{i,T}/\Delta t = Q(C_{i,in} - C_{i,out}) \quad (3)$$

Solutions to eq 3 for the components evaluated were compared to that component mass which was recovered by the sequential extraction procedure.

Results and Discussion

Coal Pile Runoff. The CPR was highly acidic, with considerable dissolved SO_4^{2-}, Fe^{3+}, and Al concentrations (Table I). The runoff also had elevated concentrations of alkaline earth and transition metals (Table I). A redox potential of 0.77 V (pe = 13.05) was calculated for the CPR based upon Fe^{2+} and Fe^{3+} concentrations by use of MINTEQA2.

Results from MINTEQA2 speciations also indicated that the influent CPR was undersaturated with respect to a number of Al-bearing minerals, including jurbanite ($AlOHSO_4$) (SI = −0.51), gibbsite ($Al(OH)_3$) (SI = −5.95), and alunite ($KAl_3(SO_4)_2(OH)_6$) (SI = −5.65). The CPR was supersaturated with respect to Na–jarosite ($NaFe_3(SO_4)_2(OH)_6$), K–jarosite ($KFe_3(SO_4)_2(OH)_6$), H–jarosite ($HFe_3(SO_4)(OH)_6$, and goethite (α-FeOOH), however (SI = 2.56, 5.08, 4.72, and 1.42, respectively). The CPR was also supersaturated with respect to quartz (α-SiO_2) (SI = 0.87), though slightly undersaturated with respect to amorphous SiO_2 (SI = −0.43).

Jurbanite has been previously suggested as controlling Al solubility within acid mine drainage and acid sulfate soils (*27*, *28*), though Nordstrom and Ball (*29*) and Filipek et al. (*30*) found that surface waters with pH <4.6 tended to transport Al conservatively and concluded that the semblance of dissolved Al to that predicted by jurbanite solubility is likely coincidental. Jarosite has been suggested as controlling Fe solubility within acid sulfate systems (*6*), though significant supersaturation of acid mine drainage with respect to jarosite, as observed here, has also been reported (*7*, *30*).

Soil. The subsoil is characteristic of soils within the highly weathered southeastern Upper Coastal Plain region, having naturally low pH (4.96), a modest cation-exchange capacity (6.82 $cmol_c\ kg^{-1}$), a predominance of exchangeable Al (83.9%), and a coarse texture (sandy clay loam). The

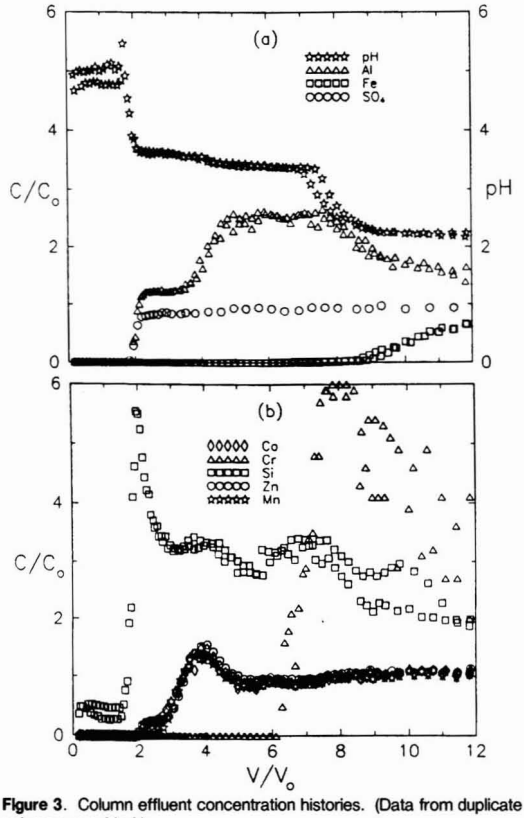

Figure 3. Column effluent concentration histories. (Data from duplicate columns provided.)

soil also had a low organic matter content (<0.15%). The bulk density for the first sampling depth (0–0.25 m beneath basin surface, or 2–2.25 m below natural soil surface) was 1.53 g cm^{-3}. A saturated hydraulic conductivity of approximately 1 cm h^{-1} was estimated from particle size and bulk density data (*31*). The subsoil possessed significant quantities of DCB- and Ox-extractable Fe (0.83 and 0.05% on a weight basis, respectively).

Quartz comprised the major mineral component within the subsoil (80%), accounting for all sand and silt-sized material. Kaolinite, a common 1:1 weathering product of 2:1 phyllosilicate minerals and a dominant mineral within the highly weathered Piedmont and Coastal Plain provinces, was the next most abundant mineral (13%). A number of 2:1 phyllosilicate minerals were also present (3% smectite, 1% mica, 2% randomly interstratified mica–vermiculite, and 1% hydroxy-interlayered vermiculite).

Element Mobility. Reproducibility of columns and column effluent concentration histories was very good. The duplicate columns yielded fitted dispersion coefficients of 2.00 and 2.02 cm^2 h^{-1}, as well as very similar column effluent concentration histories (Figure 3).

A range in relative mobilities of components within the CPR was observed (Figure 3). Transport of conservative, nonreactive solutes through homogeneous porous media should result in column effluent concentration histories in which $C/C_0 = 0.5$ at $V/V_0 = 1$; observed breakthrough behavior deviated significantly from this general trend. The classical, one-region, convection–dispersion equation (CDE) was found to accurately describe the breakthrough of Br^- (as LiBr), however ($R^2 = 0.98$).

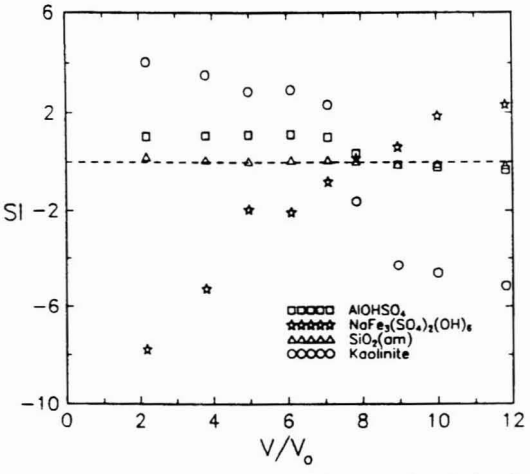

Figure 4. MINTEQA2-calculated saturation indexes for selected minerals from column effluent concentration data.

Hydrogen ion activity as a function of pore volume exhibited a two-step response. The pH remained essentially constant as the initial volumes of equilibrated deionized water were displaced with the CPR solution. After ~2 pore volumes, a slight rise in pH was observed, followed immediately by a rapid decrease to near pH 3.5 (Figure 3a). Apparent buffering reactions maintained effluent pH near 3.5 for an additional 5 pore volumes (despite supply of pH 2.1 influent solution) before descending toward the influent pH level (Figure 3a).

Appearance of both Al and SO_4^{2-} in the column effluent at a V/V_0 near 2 was also noted and coincided with the initial reduction in effluent pH (Figure 3a). Iron(III) was found within the column effluent when the effluent pH dropped below 3 (Figure 3a), where increased Fe solubility would be expected (*32*). Silicon slightly preceded sulfate and Al breakthrough (Figure 3b). Co, Mn, and Zn exhibited remarkably similar breakthrough behavior, appearing in the column effluent with sulfate, but reaching peak effluent concentrations closer to V/V_0 of 4 (Figure 3b). Chromium appeared in column effluent only after 6 pore volumes had passed the columns and pH descended below 3, and reached a peak effluent concentration at 8 pore volumes, the magnitude of which implies a net efflux from the soil.

Speciation of the column effluent yielded SIs for minerals that varied widely as a function of V/V_0 (Figure 4). The column effluent was slightly supersaturated with respect to jurbanite until approximately 8 pore volumes (Figure 4), which coincides with the decrease in effluent pH from 3.5 toward that of the influent (Figure 3a). Saturation indexes as a function of pore volume for H–, Na–, and K–jarosite all followed similar trends, with significant undersaturation at low V/V_0 and increasing SI with increasing V/V_0 (Figure 4). As with the CPR, under low-pH (high V/V_0) conditions, the column effluent was supersaturated with respect to the jarosites. The activity of Si in solution followed fairly closely that predicted from equilibrium with respect to an amorphous SiO_2 phase (Figure 4). While a number of solid phases have been proposed to control trace-metal solubilities in soils (*33*), no evidence for precipitation–dissolution reactions controlling metal mobility was found. The column effluent was also supersaturated with respect to kaolinite and other phyllosilicates at low V/V_0, whereas SI decreased below 0 at V/V_0 greater than 8 (Figure 4), which coincided with

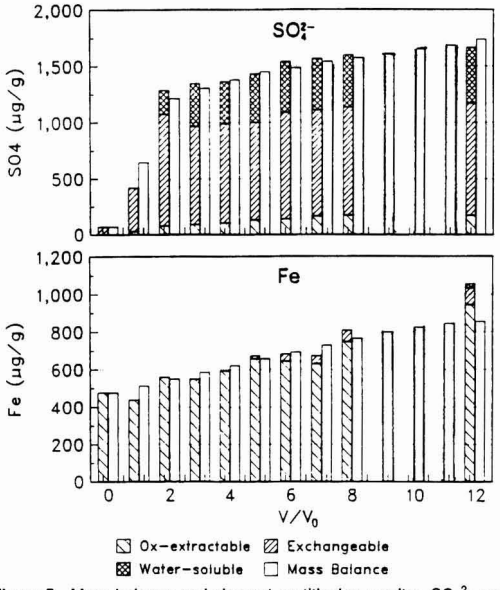

Figure 5. Mass balance and element partitioning results: SO_4^{2-} and Fe. (Element partitioning not determined on samples subjected to 9, 10, or 11 pore volumes of coal pile runoff.)

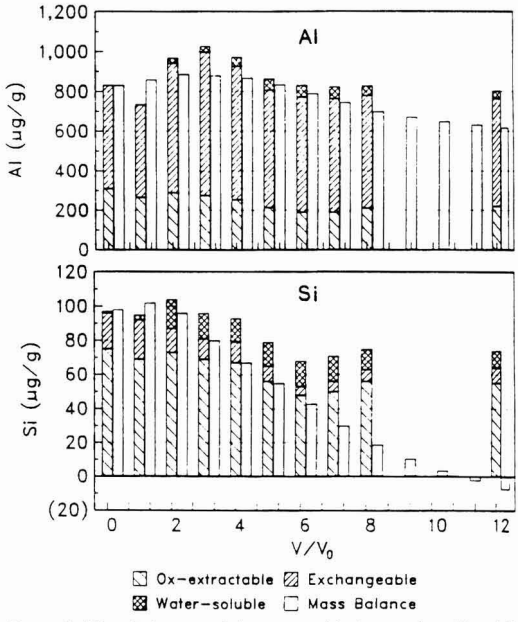

Figure 6. Mass balance and element partitioning results: Al and Si. (Element partitioning not determined on samples subjected to 9, 10, or 11 pore volumes of coal pile runoff.)

reduction in pH below 3.5 (Figure 3a). Thus, kaolinite and other minerals present in the soil matrix would be expected to dissolve and contribute structural elements to the solution (*30*, *34*).

Based upon observed effluent concentration histories and numerical speciation results, some reactions governing component mobility may be proposed. Given previous observations of sulfate sorption to soil and soil constituents (*35*, *36*) and precipitation of basic iron and aluminum sulfates (*6*, *28*), that sulfate is the predominant anion in the system, and the necessary condition of electroneutrality in solution, it appears that sulfate mobility governed initial appearance of certain cationic components in the column effluent. Sorption of sulfate via displacement of surface hydroxyls tends to increase pH (*35*) and accounts for the slight rise in pH noted (Figure 3a). Iron(III) flux through the soil exhibited a pronounced pH dependence, qualitatively following simple solubility–pH relations. Ion exchange apparently governed the mobility of Co, Mn, and Zn within the soil.

A feature common to all components except H^+, Fe^{3+}, and SO_4^{2-} is that of peak effluent concentrations exceeding influent or source concentrations (Table I). That is, the flux of CPR through soil generates so-called "concentration waves" via exchange, displacement of native soil cations, and precipitation–dissolution reactions. Such a phenomenon implies that even if runoff meets applicable water quality standards, groundwater downgradient may exceed concentration limits as the wave advances with the groundwater flow.

Element Partitioning. The distribution of elements between the water-soluble, 1 M NH_4Cl exchangeable, and Ox-extractable fractions varied for different components and as a function of CPR volume leached. Reproducibility of extractions was fair, with relative standard deviations (RSD) for triplicated extractions ranging from 2.9 to 12.2%, with an average RSD of 8.9%.

There was a modest amount of SO_4^{2-} initially present in the soil, which was recovered in the NH_4Cl extraction (Figure 5, SO_4^{2-}). Infiltration and movement of runoff through the soil column resulted in increasing total SO_4^{2-}, in good agreement with mass balance calculations (Figure 5, SO_4^{2-}). Extraction results indicated the SO_4^{2-} partitioned principally to the NH_4Cl-extractable fraction, with some residing within the aqueous and also the Ox-extractable phases (Figure 5, SO_4^{2-}). Total sorbed SO_4^{2-} (as sum of extractable SO_4^{2-}) measured near 1000 $\mu g\ g^{-1}$ of soil with nearly 80% recoverable in the NH_4Cl. Singh (*35*) reported a similar magnitude of SO_4^{2-} sorption (approximately 1000 $\mu g\ g^{-1}$) and noted increased sorption with decreasing pH; however, he found only 20% was desorbed with 0.01 M $Ca(NO_3)_2$. The difference in desorption efficiencies between the neutral salt extractants likely resulted from the significantly higher salt concentration used in this study. A monotonic increase in Ox-extractable sulfate with increasing V/V_0 was also noted in this investigation.

Iron was found to reside almost entirely within the Ox-extractable fraction prior to addition of CPR, with Ox-extractable Fe increasing steadily with increasing pore volumes (Figure 5, Fe). Partitioning of limited quantities of Fe first to the exchange phase, at pH 3.5, and subsequently to a water-soluble phase as the pH dropped near 2 (12 pore volumes) was also observed. The increase in Ox-extractable Fe between 0 and 8 pore volumes can be directly related to the retention of Fe within the soil column (i.e., the lack of Fe within the column effluent (Figure 3a)), in good agreement with mass retained via mass balance calculations (Figure 5, Fe). Mass balance calculations did, however, underestimate the extractable total reactive Fe for the sample subjected to 12 pore volumes (Figure 5, Fe). It appears that as the soil buffer capacity was exhausted and the pH dropped to near 2, additional native crystalline Fe phases were destabilized and thus became extractable in the Ox treatment.

Aluminum was distributed between the exchangeable and Ox-extractable pools prior to addition of leachate, as illustrated (Figure 6, Al). A maximum in exchangeable Al was noted after approximately 3 pore volumes of CPR were

supplied, preceding the wave of increased Al in fractions collected at subsequent pore volumes from the leaching experiments (Figure 3a), with some water-soluble Al also detectable after 2 pore volumes (corresponding to the reduction in effluent pH to 3.5) (Figure 6, Al). A gradual reduction in Ox-extractable Al with increasing pore volumes was also noted, implying dissolution of native poorly crystalline Al phases.

Silicon resided chiefly within the Ox and, to a lesser extent, exchangeable pools, though some Si was in solution prior to leaching (Figure 6, Si). Maximum water-soluble Si occurred at 2 pore volumes (Figure 6, Si). Leaching of the sample resulted in a gradual diminution in Ox-extractable Si to a minimum at 6 pore volumes, which was followed by increasing Ox-extractable Si. Mass balance calculations indicated a net export of Si out of the system, which completely exhausted the total initial reactive mass specified (Figure 6, Si). Deviation between observed and predicted total reactive Si indicates that an additional phase not initially accounted for is capable of transforming to these more labile phases represented by the NH_4Cl and Ox fractions. Desilication and formation of oxidic components is well-documented within soils subjected to naturally acidic conditions (e.g., spodic horizons formed under coniferous vegetation) as well as clays and sediments subjected to acid mine water (*30*, *34*).

No detectable Co or Zn was identified in the three pools prior to leaching with the CPR (Figure 7, Co and Zn). Exchangeable forms were noted after 1 pore volume, with additional exchangeable and also soluble metal contents occurring upon extraction after 2 pore volumes. Exchangeable Zn tended to decrease somewhat between 2 and 3 pore volumes (coincident with maximal exchangeable Al) before ascending again (Figure 7, Zn). Such behavior implies that Zn and Al are competing for available exchange sites within the soil. Cobalt exhibited somewhat different behavior in that exchangeable Co tended to increase generally with increasing leaching volumes (Figure 7, Co). In neither case was there evidence for sorption or precipitation of these metals. Manganese was found in minor quantities prior to leaching within an Ox-extractable phase (Figure 7, Mn). A maximum in exchange-phase Mn occurred at 2 pore volumes (Figure 7, Mn), with a minimum again coincident with peak effluent Mn concentration from the breakthrough experiments (Figure 3b) and maximum exchange-phase Al (Figure 6, Al). No evidence for accumulation in or mobilization from the Ox phase was apparent. Thus, under the conditions evaluated here, specific interactions with hydrous oxides and coprecipitation with solid phases were of secondary importance in regulating Co, Mn, and Zn mobility. Rather, simple partitioning between aqueous and exchange phases constituted the principal reactions governing transport within acid runoff percolating through the subsoil.

Chromium was found associated with the Ox-extractable phase for all treatments, including the native condition (Figure 7, Cr). Chromium partitioning was limited to this phase until the seventh pore volume, whereas Cr was found in both the exchange and water-soluble phases (Figure 7, Cr), which coincides with the onset of significant elution of Cr from the soil column (Figure 3b). This partitioning behavior contrasts with that for the previous transition metals and implies that a sorption or coprecipitation reaction controlled Cr mobility. The low concentrations of Cr in the runoff (10 $\mu g\ L^{-1}$) resulted in negligible loading to the soil.

Clay Mineralogy. The potential for alterations in phyllosilicate mineralogy upon leaching with the runoff

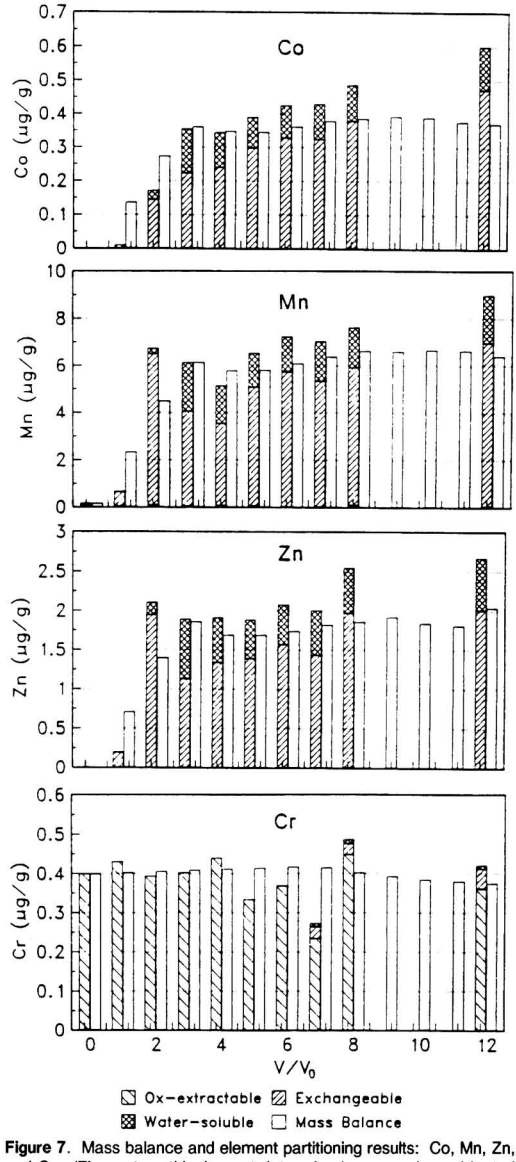

Figure 7. Mass balance and element partitioning results: Co, Mn, Zn, and Cr. (Element partitioning not determined on samples subjected to 9, 10, or 11 pore volumes of coal pile runoff.)

was evaluated through XRD and DSC analysis. Clay fractions from samples leached with 0, 4, 8, 12, and 60 pore volumes were X-rayed after Fe removal. Despite relatively high inputs of acidity, only subtle alterations were noted. For example, diffractograms of KCl, 25 °C treated clays showed no discernible differences in the dominant 7.2-(001) and 3.6-Å (002) reflections of kaolinite, suggesting that no substantial changes in the crystallinity of this mineral occurred after leaching (Figure 8). Some slight reduction in the broad low-angle reflection between 14 and 20 Å and a concomitant increase in the 10-Å reflection was noted, however (Figure 8), implying possible degradation of the weakly ordered interstratified mica–vermiculite mineral or dissolution of hydroxy–Al interlayers within hydroxy-interlayer vermiculite to yield a better defined 10-Å vermiculitic component upon prolonged leaching.

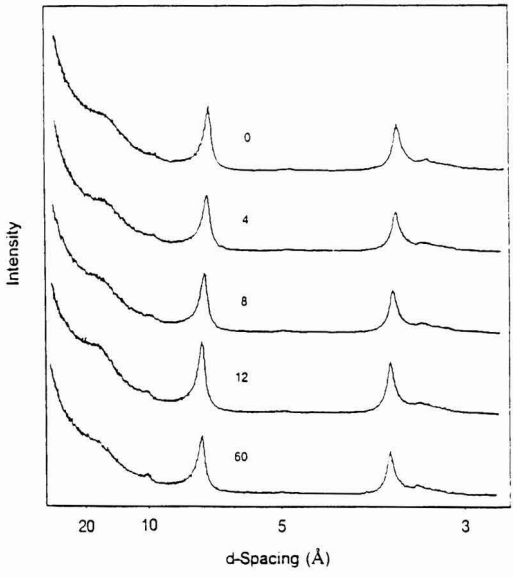

Figure 8. X-ray diffractograms of clay (<2 μm) fraction of subsoil after leaching with 0, 4, 8, 12, and 60 pore volumes of runoff (K-saturated, 25 °C).

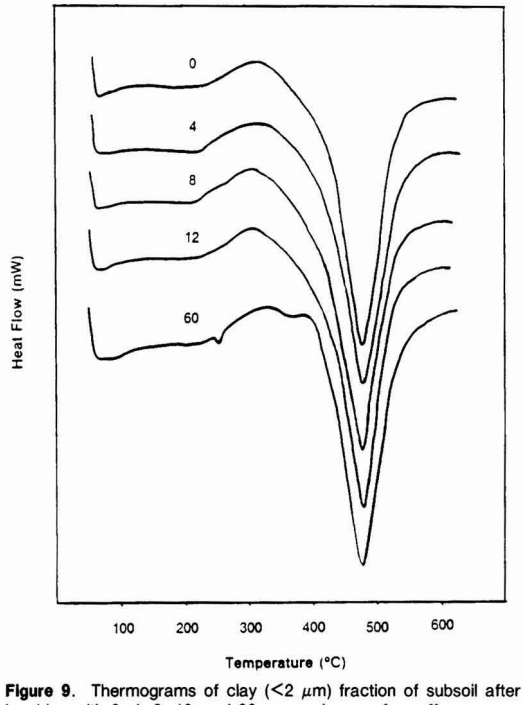

Figure 9. Thermograms of clay (<2 μm) fraction of subsoil after leaching with 0, 4, 8, 12, and 60 pore volumes of runoff.

Changes in DSC scans provided evidence for the dissolution of kaolinite and precipitation of gibbsite. There was a slight reduction in the area of the 480 °C kaolinite endotherm and the appearance of a subtle endotherm near 280 °C, characteristic for gibbsite, after leaching with 60 pore volumes of CPR (Figure 9). Gibbsite is a common weathering product resulting from desilication of phyllosilicates subjected to acidic conditions. The reduction in the low-temperature skewness of the kaolinite endotherm with increasing pore volumes and emergence of a more symmetrical endotherm at 60 pore volumes suggests gradual dissolution of hydroxy-interlayer Al as inferred from XRD analyses.

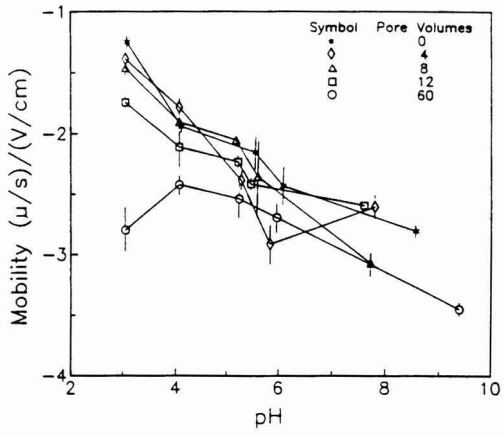

Figure 10. Electrophoretic mobility of silt + clay (<50 μm) fraction of subsoil after leaching with 0, 4, 8, 12, and 60 pore volumes of runoff.

The mineralogy of the oxidic phases was evaluated via differential XRD (i.e., subtraction of patterns of DCB-treated samples from that of untreated samples). Evidence for goethite (4.188-, 2.566-, 2.502-, 1.818-, and 1.515-Å reflections) and hematite (1.688- and 1.476-Å reflections) was found for the samples. No changes in the diffractograms with increasing pore volumes, and a general lack of characteristic peaks, including the strong jarosite reflection at 3.03 Å, suggest an absence of basic aluminum and iron sulfate phases forming during the leaching process, though analytical limitations on detection of small amounts of these phases preclude firm support for or against their existence.

Infrared Analysis. Infrared analysis of the samples yielded very similar spectra as well. Well-defined peaks at 3700, 3625, 1100, 1010, and 910 cm^{-1}, diagnostic for kaolinite (*37*), dominated the spectra. Broad absorbance bands centered near 3300 cm^{-1} and near 1640 cm^{-1} were also noted and correspond to water likely retained by swelling 2:1 minerals within the samples. Characteristic jarosite and sulfate absorbances at 1175, 1110, and 1020 cm^{-1} (*38*) were absent.

Electrophoretic Mobilities. Electrophoretic mobility of samples increased with increased leaching for any given suspension pH and increased with increasing suspension pH (Figure 10). The high mobilities even at low pH support the mineralogical data indicating appreciable constant-charge mineral content (*39*). The contribution of variable-charge minerals (e.g., kaolinite and oxyhydroxides) is also significant, as can be seen by the steep increase in mobility upon increasing suspension pH (Figure 10) (*40*). A somewhat flatter pH response with increasing pore volumes was observed (Figure 10). Additional charge was apparently generated via specific adsorption of sulfate to oxidic phases (*41*, *42*) and by dissolution of native constant charge-blocking oxidic phases.

Summary and Conclusions

Results of element partitioning via an operationally defined selective dissolution procedure were generally in good agreement with mass balance calculations and corroborate inferences made about element mobility from

breakthrough data. Iron was observed to accumulate within the soil column and was associated chiefly with the Ox-extractable phase. Aluminum was partitioned between the water, NH_4Cl-exchangeable, and Ox-extractable phases, with the water phase increasing and the Ox phase decreasing with increasing leaching. Silicon tended to follow Al to some extent, with Ox-extractable Si decreasing with increasing leaching. Cobalt and Zn were associated with the exchange phase early in the leaching process and then partitioned fairly consistently between the water and exchange phases, supporting the notion that ion exchange was the dominant mechanism governing mobility for these elements. Manganese followed the other divalent metal ions with the exception that a limited quantity was found associated with the Ox-extractable phase. Chromium departed significantly from the other first-row transition metals in that its mobility appeared to be governed by specific adsorption–desorption reactions.

Sustained leaching had little discernible effect on gross phyllosilicate mineralogy, though formation of gibbsite and limited degradation of hydroxy–Al interlayers within hydroxy-interlayered vermiculite was demonstrated after 60 pore volumes of CPR had been supplied to the column. Oxide mineralogy was fairly uniform, with goethite and hematite both present in the soils. Evidence for distinct basic aluminum or iron sulfate phases formed during leaching was generally lacking. Electrophoretic mobility increased (became more negative) with increased leaching, due in part to specific adsorption of sulfate and consequent generation of additional negative charge within the soil, and by dissolution of native charge-blocking oxidic phases.

These observations have a number of implications for soil and groundwater systems subject to infiltrating runoff from coal stockpiles and more generally from acid mine drainage. First of all, naturally acidic, noncarbonatic soils offer little resistance to subsurface migration of acidic, metal-rich runoff. As a result, coal stockpiles situated on such materials pose a serious threat to underlying groundwater systems. Facilities located on the Atlantic Coastal Plain, which possesses generally naturally acidic and often coarse-textured soils and relatively shallow aquifer systems, in particular are prone to degrade local water quality. The occurrence of both high industrial activity and urban populations over much of this physiographic province implies potentially severe local environmental problems.

The development of concentration waves attendant with infiltration and migration of runoff within subsurface materials further exacerbates potential water quality problems. That is, chromatographic and precipitation–dissolution reactions result in the development and movement of metals in waves of concentrations potentially greatly exceeding initial source concentrations. Discharge of effluent meeting appropriate water quality criteria may thus produce downgradient concentrations exceeding standards and source concentrations. This phenomenon poses difficult legal ramifications and also emphasizes the need for continued research evaluating multicomponent transport processes.

Acknowledgments

We thank Dr. Carl Strojan and Bruce Herbert for their thoughtful comments on an early draft of this manuscript.

Registry No. Al, 7429-90-5; Be, 7440-41-7; Ca, 7440-70-2; Co, 7440-48-4; Cr, 7440-47-3; Cu, 7440-50-8; Fe, 7439-89-6; K, 7440-09-7; Li, 7439-93-2; Mg, 7439-95-4; Mn, 7439-96-5; Na, 7440-23-5; Ni, 7440-02-0; Sr, 7440-24-6; Zn, 7440-66-6.

Literature Cited

(1) Davis, E. C.; Boegly, W. J. *J. Environ. Qual.* **1981**, *10*, 127–133.
(2) Swift, M. C. *Water Resour. Bull.* **1985**, *21*, 449–457.
(3) Theobald, P. K.; Lakin, H. W.; Hawkins, D. B. *Geochim. Cosmochim. Acta* **1963**, *27*, 121–132.
(4) Brady, K. S.; Bigham, J. M.; Jaynes, W. F.; Logan, T. J. *Clays Clay Miner.* **1986**, *34*, 266–274.
(5) Nordstrom, D. K.; Jenne, E. A.; Ball, J. W. In *Chemical Modeling of Aqueous Systems: Speciation, Sorption, Solubility, and Kinetics*; Jenne, E. A., Ed.; ACS Symposium Series 93; American Chemical Society: Washington, DC, 1979; pp 51–79.
(6) Nordstrom, D. K. In *Acid Sulfate Weathering*; Kittrick, J. A., Fanning, D. S., Hossner, L. R., Eds.; Soil Science Society of America Special Publication 10; Soil Science Society of America: Madison, WI, 1982; pp 37–56.
(7) Chapman, B. M.; Jones, D. R.; Jung, R. F. *Geochim. Cosmochim. Acta* **1983**, *47*, 1957–1973.
(8) Wangen, L. E.; Williams, J. M. *J.—Water Pollut. Control Fed.* **1982**, *54*, 1302–1310.
(9) Jones, K. C. *Environ. Pollut., Ser. B* **1986**, *12*, 249–263.
(10) Foster, P.; Hunt, D. T. E.; Morris, A. W. *Sci. Total Environ.* **1978**, *9*, 75–86.
(11) Robinson, G. D. *Chem. Geol.* **1981**, *33*, 65–79.
(12) Wangen, L. E.; Jones, M. M. *Environ. Geol. Water Sci.* **1984**, *6*, 161–170.
(13) *The Savannah River Plant's Groundwater Monitoring Program*; HP-88-098; Health Protection Department, Environmental Monitoring, Savannah River Plant, 1988.
(14) Blake, G. R.; Hartge, K. H. In *Methods of Soil Analysis, Part 1*; Klute, A., Ed.; Agronomy 9; American Society of Agronomy: Madison, WI, 1986; pp 363–382.
(15) Danielson, R. E.; Sutherland, P. L. In *Methods of Soil Analysis, Part 1*; Klute, A., Ed.; Agronomy 9; American Society of Agronomy: Madison, WI, 1986; pp 443–461.
(16) Miller, W. P.; Miller, D. M. *Commun. Soil Sci. Plant Anal.* **1987**, *18*, 1–15.
(17) McLean, E. O. In *Methods of Soil Analysis, Part 2*, Page, A. L., Miller, R. H., Keeney, D. R., Eds.; Agronomy 9; American Society of Agronomy: Madison, WI, 1982; pp 199–224.
(18) Jackson, M. L.; Lim, C. H.; Zelazny, L. W. In *Methods of Soil Analysis, Part 1*; Klute, A., Ed.; Agronomy 9; American Society of Agronomy: Madison, WI, 1986; pp 101–142.
(19) Allison, L. E. In *Methods of Soil Analysis, Part 2*; Black, C. A., Ed.; Agronomy 9; American Society of Agronomy: Madison, WI, 1965; pp 1367–1378.
(20) Parker, J. C.; van Genucthen, M. Th. Determining Transport Parameters from Laboratory and Field Tracer Experiments. *Va. Agric. Exp. Stn. Bull.* **1984**, *No. 84-3*.
(21) Jenne, E. A.; Luoma, S. N. In *Biological Implications of Metals in the Environment*; Proceedings, Hanford Life Science Symposium; Technical Information Center, Energy Research and Development Administration, Washington, DC, 1977; pp 110–143.
(22) Tessier, A.; Campbell, P. G. C.; Bisson, M. *Anal. Chem.* **1979**, *51*, 844–851.
(23) Whittig, L. D.; Allardice, W. R. In *Methods of Soil Analysis, Part 1*; Klute, A., Ed.; Agronomy 9; American Society of Agronomy: Madison, WI, 1986; pp 331–362.
(24) Rich, C. I.; Barnhisel, R. I. In *Minerals in Soil Environments*; Dixon, J. B., Weed, S. B., Eds.; Soil Science Society of America: Madison, WI, 1977; pp 797–808.
(25) *Standard Methods for the Examination of Water and Wastewater*, 17th ed.; American Public Health Association: Washington, DC, 1989; pp 3-102–3-106.
(26) Brown, D. S.; Allison, J. D. *MINTEQA2, an Equilibrium Metal Speciation Model*; EPA/600/3-87/012; U.S. EPA; Washington, DC, 1987.
(27) Van Breeman, N. *Soil Sci. Soc. Am. J.* **1973**, *37*, 694–697.
(28) Nordstrom, D. K. *Geochim. Cosmochim. Acta* **1982**, *46*, 681–692.
(29) Nordstrom, D. K.; Ball, J. W. *Science* **1986**, *232*, 54–56.

(30) Filipek, L. H.; Nordstrom, D. K.; Ficklin, W. H. *Environ. Sci. Technol.* **1987**, *21*, 388-396.
(31) Mishra, S.; Parker, J. C. *SOILPROP: A Program for Estimating Soil Hydraulic Properties and Their Uncertainty from Particle Size Data*; Center for Environmental and Hazardous Material Studies, Virginia Polytechnic Institute and State University, 1988; No. R8801.
(32) Baes, C. R., Jr.; Mesmer, R. E. *The Hydrolysis of Cations*; John Wiley and Sons: New York, 1976; pp 226-237.
(33) Lindsay, W. L. *Chemical Equilibria in Soils*; John Wiley and Sons: New York, 1979.
(34) Barnhisel, R. I.; Rotromel, A. L. *Soil Sci.* **1974**, *118*, 22-27.
(35) Singh, B. R. *Soil Sci.* **1984**, *138*, 346-353.
(36) Sigg, L.; Stumm, W. *Colloids Surf.* **1980**, *2*, 101-117.
(37) Farmer, V. C.; Palmieri, F. In *Soil Components. Inorganic Components*; Gieseking, J. E., Ed.; Springer-Verlag: New York, 1975; Vol. 2, pp 573-670.
(38) Omori, K.; Kerr, P. F. *Geol. Soc. Am. Bull.* **1963**, *74*, 709-734.
(39) Harsh, J. B.; Doner, H. E.; Fuerstenau, D. W. *Soil Sci. Soc. Am. J.* **1988**, *52*, 1589-1592.
(40) Williams, D. J. A.; Williams, K. P. *J. Colloid Interface Sci.* **1978**, *65*, 79-87.
(41) Rajan, S. S. S. *Soil Sci. Soc. Am. J.* **1978**, *42*, 39-44.
(42) Hansmann, D. D.; Anderson, M. A. *Environ. Sci. Technol.* **1985**, *19*, 544-551.

Received for review December 17, 1990. Revised manuscript received June 10, 1991. Accepted June 26, 1991. This research was partially supported by Contract DE-AC09-76SR00819 between the University of Georgia and the U.S. Department of Energy.

Parameterizing the Equilibrium Distribution of Chemicals between the Dissolved, Solid Particulate Matter, and Colloidal Matter Compartments in Aqueous Systems

James F. Pankow*,† and Stuart W. McKenzie‡

Department of Environmental Science and Engineering, Oregon Graduate Institute, 19600 N. W. Von Neumann Drive, Beaverton, Oregon 97006 and United States Geological Survey, Water Resources Division, 10615 S.E. Cherry Blossom Drive, Portland, Oregon 97216

■ The manner in which a chemical material partitions among the dissolved (D), particulate (P), and colloidal (C) phases affects both its chemical and physical behavior in the aquatic environment. The fractions of the chemical that are present in each of these three phases will be determined by the values of two simple parameters, K_pS_p/α_w and K_cS_c/α_w. The variables K_p and K_c are the particle/water and colloid/water partition constants (mL/g), respectively, S_p and S_c are the volume concentrations of particulate and colloidal material (mg/L), respectively, and α_w is the fractional volume of the system that is aqueous. This parameterization allows a rapid overview of how partitioning (1) changes as a function of chemical partitioning properties and water type, (2) affects *apparent* partition constants (i.e., K_p^{app} values) computed between the particulate phase and the remainder of the system, and (3) causes K_p^{app} values to become *independent* of chemical properties at high values of K_cS_c/α_w.

Introduction

The behavior and fate of an inorganic or organic species in an environmental system is closely tied to the manner in which that species is distributed between the various compartments present in that system. A priori, there is no limit on the number n_c of these compartments. For surface waters, it has currently become useful to take $n_c = 3$, with the three compartments corresponding to a dissolved, a suspended particulate solid, and a suspended colloidal matter phase (*1-6*). In groundwater and sediment/water systems, $n_c = 3$ is also often used, with the compartments considered including a dissolved, a stationary particulate solid, and a mobile colloidal matter phase.

In this paper, we will consider cases of the above type where $n_c = 3$. Thus, the term "dissolved (D) phase" will be used here when discussing the portion of some chemical that is dissolved and is surrounded only by the aqueous medium. "Particulate solid (P) phase" will be used when referring to the portion that is associated with particles that are sufficiently large that one can physically separate them from the remainder of the system. In the case of a sample of surface water, this separation might be carried out by filtration and/or centrifugation. "Colloidal (C) phase" will be used when referring to the portion that is associated with (1) very small particles that are difficult to remove by filtration or centrifugation *and/or* (2) dissolved humic molecules.

Unlike the D phase, under most circumstances neither the P phase nor the C phase will be a distinct thermodynamic phase. For example, the P phase will usually be composed of a variety of particle types, including various mineral phases as well as detrital organic matter. Nevertheless, since both D/P and D/C partitioning can be described by mean sorption constants (see below), then under conditions of constant pH, ionic strength, etc., both the particulate solid material and the colloidal material can be modeled as single phases.

The *distinction* between P-phase and C-phase material is always likely to be somewhat operational in nature. Indeed, the exact nature of this distinction will depend upon (1) the filtration process used to separate as many particles as possible from the D phase and (2) the degree of particulate loading on the filter and the manner in which that loading affects the particle-size-dependent efficiency of the filtration process.

The concentration of a species in the D phase is of interest because it affects the extent to which the species will be subject to transport by advection and molecular diffusion. In addition, the D-phase concentration is intimately related to the species' D-phase thermodynamic activity. This activity in turn reflects the positions of all chemical equilibria involving the species, including phase-partitioning equilibria. The amounts of the species that are associated with the P and C phases are of interest because those phases provide reservoirs for the release and storage of the species to and from the D phase, respectively. For

† Oregon Graduate Institute.
‡ United States Geological Survey.

 0013-936X/91/0925-2046$02.50/0

surface waters, where both the P and C phases are suspended in the water column, these two phases provide compartments by means of which significant advective transport and/or coagulation and sedimentation removal can occur. In the case of a deep lake, the time scale required for significant removal by sedimentation can be long, but it will also be relatively permanent. In a river subject to large, seasonal changes in flow, the time scale for removal can be short, but it will also be temporary.

Considerable progress has recently been made in understanding how partitioning occurs among the D, P, and C phases (*1–6*). That understanding has been obtained primarily by examining the individual effects of four variables, namely: (1) K_p, the P/D partition coefficient; (2) K_c, the C/D partition coefficient; (3) S_p, the mass/volume concentration of solid particulate phase; and (4) S_c, the mass/volume concentration of colloidal matter phase. However, with at least four separate variables (a fifth variable α_w will be introduced below), it is difficult to obtain a rapid overview of how the distribution among the D, P, and C phases changes from system to system, and from chemical to chemical within a given system.

Fortunately, at equilibrium, D/P/C partitioning can be parameterized in terms of two combined variables, K_pS_p/α_w and K_cS_c/α_w, where α_w is the volume fraction of the system occupied by the D phase. This approach allows the behavior of all types of D/P/C systems to be understood with a few simple plots. Four different types of surface water systems will be considered as examples. Considering that some type of distinction between P- and C-phase material is likely to remain useful in studying aqueous systems (e.g., due to the differing physical properties of P- and C-phase material), the formalism of the analysis presented here should remain useful even if methods for the facile filtration of very small particles can be developed.

Theory

Review of Governing Equations. Let C_d, C_p, and C_c represent the dissolved, particulate matter associated, and colloidal matter associated concentrations. The sum of these concentrations equals the total concentration, C_T. Expressed with an upper case C, these concentrations have dimensions of grams of a given substance per milliliter of *total system* (water + particulate matter + colloidal matter). Concentrations with a lower case c as introduced below will have dimensions of grams of a given substance per unit of an actual phase.

At equilibrium, the fractions ($0 \leq \alpha \leq 1$) of substance present in the dissolved, particulate, and colloidal phases are given by

$$\alpha_d = \frac{C_d}{C_d + C_p + C_c} = \frac{C_d}{C_T} \quad (1)$$

$$\alpha_p = \frac{C_p}{C_p + C_d + C_c} = \frac{C_p}{C_T} \quad (2)$$

$$\alpha_c = \frac{C_c}{C_c + C_d + C_p} = \frac{C_c}{C_T} \quad (3)$$

By definition, $\alpha_d + \alpha_p + \alpha_c = 1$.

In the D phase, we will deal with the case when the material of interest is present as a single chemical species. Chemicals that behave in this manner include organic compounds such as individual polychlorinated biphenyl (PCB) congeners, polycyclic aromatic hydrocarbons, pesticides, etc. Some inorganic species (e.g., the heavy metals) can also behave this way, though for inorganics the extent to which a single species dominates the D-phase chemistry will more often be dependent on the pH.

When there is only one form of the chemical of interest that is partitioning among the various phases (as with a hydrophobic organic compound like one of the PCB congeners), then the meanings of the above equations are clear. In addition, under constant solution-phase conditions (e.g., constant pH, etc.), the equations presented here will apply equally well to cases in which there is more than one D-phase species possible (as with a dissolved metal). Indeed, the single dissolved concentration in the above equations can be thought of as referring to the total D-phase concentration. The partitioning between the D phase and the P phase and between the D phase and the C phase is then handled in a manner that is analogous to how the partitioning between dissolved H_2CO_3* and gaseous CO_2 is dealt with in the case of carbon dioxide (note that the concentration $[H_2CO_3^*]$ equals $[H_2CO_3] + [CO_2]$ (*7*)).

Following Gschwend and Wu (*3*), let the concentration of solid particulate matter S_p be expressed in units of milligrams (dry weight) per liter of total system. The concentration of colloidal matter S_c has the same units. If c_p is the concentration of the material of interest in/on the P phase in units of grams per gram, and c_c is the concentration in/on the C phase in units of grams per gram, then

$$c_p = 10^6 C_p / S_p \quad (4)$$

$$c_c = 10^6 C_c / S_c \quad (5)$$

The factor of 10^6 provides the conversions between milliliters and liters and between milligrams and grams.

Let c_d be the dissolved concentration in units of grams per milliliter of D phase. The relationship between c_d and C_d is

$$c_d = C_d / \alpha_w \quad (6)$$

As noted above, α_w (dimensionless) is the volume fraction of the total system that is D phase: α_w = (volume of D phase (i.e., aqueous phase))/(total system volume). For surface water systems, 1 mL of total system will essentially contain very nearly 1 mL of D phase, and α_w will be very close to 1.0. Under these circumstances, $c_d \simeq C_d$. The value of α_w will decrease as the volume contributions of large and/or small particles increase. In river bottom waters that are transporting large quantities of bed sediments, S_p together with the solid portion of S_c can be sufficiently large that α_w might be as low as 0.9, or even smaller. In bed sediments and groundwater systems, α_w will be given by the porosity, which can extend from 0.9 for recently deposited fine-grained sediments, to 0.34 for a sandy aquifer, down to 0.2 and less for poorly sorted sedimentary deposits.

The thermodynamic partition coefficient K_p between the P and D phases is given by c_p/c_d (mL/g). The partition coefficient between the C and D phases, K_c, is given by c_c/c_d (mL/g). By eqs 4–6, we then have

$$K_p = 10^6 C_p \alpha_w / S_p C_d \quad (7)$$

and

$$K_c = 10^6 C_c \alpha_w / S_c C_d \quad (8)$$

Combining eqs 7 and 8 with eqs 1–3, we obtain

$$\alpha_d = [1 + K_pS_p/10^6\alpha_w + K_cS_c/10^6\alpha_w]^{-1} \quad (9)$$

$$\alpha_p = [1 + 10^6\alpha_w/K_pS_p + K_cS_c/K_pS_p]^{-1} \quad (10)$$

$$\alpha_c = [1 + 10^6\alpha_w/K_cS_c + K_pS_p/K_cS_c]^{-1} \quad (11)$$

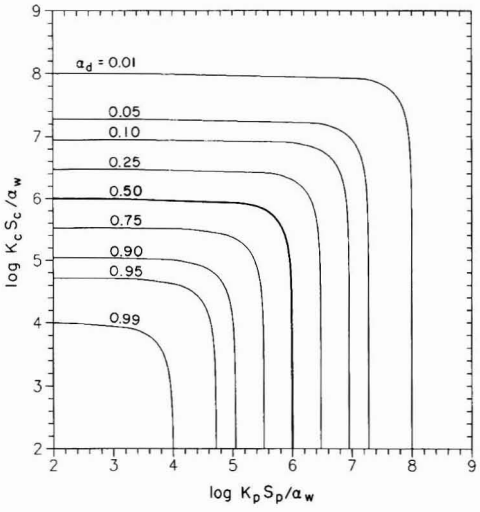

Figure 1. Lines of constant α_d value (isopleths) in the range 0.01–0.99 as functions of log K_pS_p/α_w and log K_cS_c/α_w.

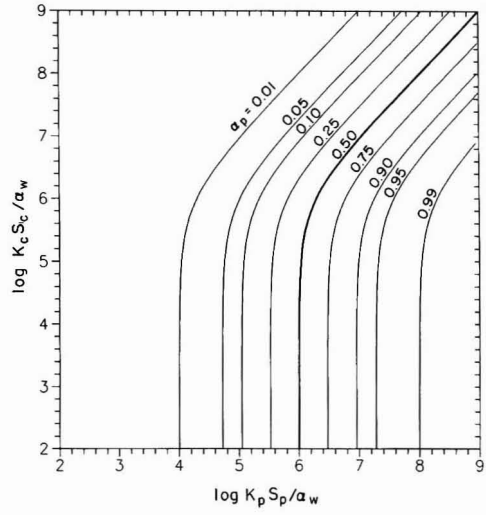

Figure 2. Lines of constant α_p value (isopleths) in the range 0.01–0.99 as functions of log K_pS_p/α_w and log K_cS_c/α_w.

Equations 9–11 are similar to equations given by Gschwend and Wu (*3*), except that those workers made the implicit assumption that α_w will be ~1.0. As noted above, that approximation is appropriate for most surface waters; it will not be valid in systems involving bed sediments and groundwater. Equations 7 and 8 may be used to show that

$$\alpha_d/\alpha_p = 10^6\alpha_w/K_pS_p \quad (12)$$

$$\alpha_d/\alpha_c = 10^6\alpha_w/K_cS_c \quad (13)$$

$$\alpha_c/\alpha_p = K_cS_c/K_pS_p \quad (14)$$

Before proceeding, a few caveats relating to particulate and colloidal material should be mentioned. First, we reemphasize that the *distinction* between material that comprises S_p and that which comprises S_c is always likely to be somewhat operational in nature. Second, particle coagulation and disaggregation can lead to the *exchange* of sorbing mass between S_p and S_c. (For example, very small colloidal particles in a river can coagulate and adhere to larger particles or agglomerations of particles when river water becomes saline, as in an estuary. Alternatively, particle agglomerates can be broken up when exposed to the shear forces in turbulent waters.) Third, we note that since S_p is composed of particles with a range of sizes and chemical compositions, K_p is a composite, *mean sorption constant*. The fact that S_c is composed of both very small particles and truly dissolved humic molecules means that K_c is also a composite, mean sorption constant; the values of K_p and K_c will depend strongly on the natures of the materials making up S_p and S_c, respectively.

While it is important that we understand each of the above three caveats, the fact that they are relevant does not limit the value of the analysis carried out here. Moreover, if it eventually becomes desirable to separate the P and C classes of material into more than just two categories (so that $n_c = 4$ or more), then the types of α values utilized here will be extendable to such cases.

K_pS_p/α_w and K_cS_c/α_w as Variables. Equations 9–11 depend on *five* independent variables, K_p, S_p, K_c, S_c, and α_w. It is therefore not possible to prepare a single two-dimensional plot that shows how a given α value changes as all of these parameters are varied. However, in eqs 9–11, the parameters K_p, S_p, and α_w always appear together as

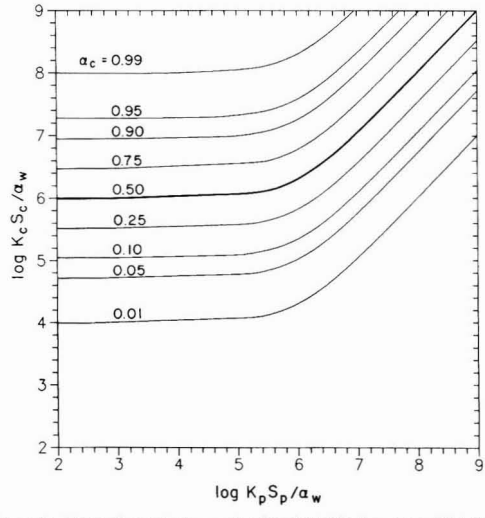

Figure 3. Lines of constant α_c value (isopleths) in the range 0.01–0.99 as functions of log K_pS_p/α_w and log K_cS_c/α_w.

the group K_pS_p/α_w, and the parameters K_c, S_c, and α_w always appear together as K_cS_c/α_w. (Note that K_pS_p/K_cS_c equals the ratio of these two groups.) Thus, K_pS_p/α_w and K_cS_c/α_w provide a very convenient, reduced set of master variables with which to parameterize α_d, α_p, and α_c. Lines for any desired, constant values of α_d, α_p, and α_c (i.e., isopleths) can be easily calculated as functions of these two variables using rearranged versions of eqs 9–11, i.e.

$$K_pS_p/\alpha_w = [1/\alpha_d - 1 - K_cS_c/10^6\alpha_w]10^6 \quad (15)$$

$$K_pS_p/\alpha_w = (10^6 + K_cS_c/\alpha_w)/(1/\alpha_p - 1) \quad (16)$$

$$K_pS_p/\alpha_w = [1/\alpha_c - 1 - 10^6\alpha_w/K_cS_c]K_cS_c/\alpha_w \quad (17)$$

Isopleths for α_d, α_p, and α_c, each ranging between 0.01 and 0.99, have been calculated here and are presented in Figures 1–3, respectively. All of the isopleths are presented together in Figure 4. In order to facilitate examination of these figures, all $\alpha = 0.50$ lines have been drawn as bold lines.

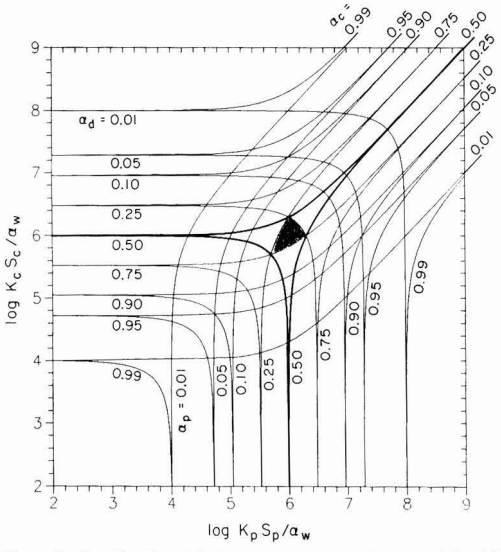

Figure 4. Combined isopleths for α_d, α_p, and α_c in the range 0.01–0.99 as functions of log K_pS_p/α_w and log K_cS_c/α_w. All three α values are simultaneously of similar magnitude in the area bounded by the three isopleths $\alpha_d = \alpha_p = \alpha_c = 0.25$. At the actual center, we have $\alpha_d = \alpha_p = \alpha_c = {}^1/_3$.

Each α_d isopleth in Figure 1 is symmetrical along the line log K_cS_c/α_w = log K_pS_p/α_w because a given change in either K_pS_p/α_w or K_cS_c/α_w will have the same effect on α_d (see eq 9). In Figure 2, in the region where $K_cS_c/\alpha_w \ll 10^6$, the α_p isopleths show essentially no dependence on log K_cS_c/α_w. This may be understood as follows. We reexpress eq 10 as

$$\alpha_p = [1 + (10^6 + K_cS_c/\alpha_w)/(K_pS_p/\alpha_w)]^{-1} \quad (18)$$

When $K_cS_c/\alpha_w \ll 10^6$, the portion of the material of interest that is associated with the C phase is small compared to that in the D phase. Thus, eq 18 becomes

$$\alpha_p \simeq [1 + 10^6\alpha_w/K_pS_p]^{-1} \qquad K_cS_c/\alpha_w \ll 10^6 \quad (19)$$

which is independent of K_cS_c/α_w. As K_cS_c/α_w becomes small relative to both 10^6 *and* K_pS_p/α_w, then the amount of material in the C phase is very small compared to both the D and P phases, and so

$$\alpha_d + \alpha_p \simeq 1 \qquad K_cS_c/\alpha_w \text{ small} \quad (20)$$

Thus for small K_cS_c/α_w, each α_p isopleth in Figure 4 asymptotically approaches the corresponding isopleth for $\alpha_d = 1 - \alpha_p$.

As K_cS_c/α_w approaches and exceeds 10^6, each α_p isopleth in Figure 2 bends over and takes on a slope of +1. This slope takes each isopleth toward increasing log K_pS_p/α_w. This increase is required to maintain α_p constant along the isopleth in the face of increasing partitioning to the C phase. At the same time, partitioning to the D phase becomes increasingly small. Thus, when $K_cS_c/\alpha_w \gg 10^6$, eq 18 becomes

$$\alpha_p \simeq [1 + K_cS_c/K_pS_p]^{-1} \qquad K_cS_c/\alpha_w \gg 10^6 \quad (21)$$

and log K_cS_c/α_w increases linearly with log K_pS_p/α_w along each isopleth. When K_cS_c/α_w and K_pS_p/α_w are both large

$$\alpha_c + \alpha_p \simeq 1 \qquad K_cS_c/\alpha_w \text{ and } K_pS_p/\alpha_w \text{ both large} \quad (22)$$

In the upper right-hand corner of Figure 4, then, each α_p isopleth asymptotically approaches the corresponding isopleth for $\alpha_c = 1 - \alpha_p$.

The α_c isopleths in Figure 3 behave in a manner that is highly analogous to the α_p isopleths in Figure 2, with the roles of colloidal and particulate sorption reversed. In particular, in the region where $K_pS_p/\alpha_w \ll 10^6$, the α_c isopleths are independent of K_pS_p/α_w because

$$\alpha_c \simeq [1 + 10^6\alpha_w/K_cS_c]^{-1} \qquad K_pS_p/\alpha_w \ll 10^6 \quad (23)$$

As K_pS_p/α_w becomes small relative to both 10^6 *and* K_cS_c/α_w, then the amount of material in the P phase is very small and

$$\alpha_d + \alpha_c \simeq 1 \qquad K_pS_p/\alpha_w \text{ small} \quad (24)$$

In Figure 4, when K_pS_p/α_w is small, each α_c isopleth asymptotically approaches the corresponding isopleth for $\alpha_d = 1 - \alpha_c$.

As K_pS_p/α_w approaches and exceeds 10^6, the α_c isopleths in Figure 3 start to bend up and take on a slope of +1. This slope takes each isopleth toward increasing log K_cS_c/α_w. This enables α_c to remain constant along the isopleth in the face of increasing partitioning to the P phase. Relative to that P-phase partitioning, partitioning to the D phase becomes increasingly small. Thus, when $K_pS_p/\alpha_w \gg 10^6$

$$\alpha_c \simeq [1 + K_pS_p/K_cS_c]^{-1} \qquad K_pS_p/\alpha_w \gg 10^6 \quad (25)$$

and log K_cS_c/α_w increases linearly with log K_pS_p/α_w along each α_c isopleth. Once K_cS_c/α_w and K_pS_p/α_w are both large, we again reach the condition given by eq 22.

The region in which *all three* α values are simultaneously of similar magnitude may be identified as the shaded area in Figure 4 that is bounded by the three isopleths, $\alpha_d = 0.25$, $\alpha_p = 0.25$, and $\alpha_c = 0.25$, and centered on the point log $K_pS_p/\alpha_w = 6$, log $K_cS_c/\alpha_w = 6$. At the actual center, we have $\alpha_d = \alpha_p = \alpha_c = {}^1/_3$.

Table I contains the results of example calculations for several different types of surface waters (groundwater systems could just as easily have been examined). The four types of surface water considered are river headwaters, rivers that have received agricultural field runoff, actual field runoff drain channels, and lake waters. Figure 5 illustrates how the corresponding α values for these waters may be viewed as being controlled by the corresponding ranges of the variables K_cS_c/α_w and K_pS_p/α_w. In particular, for each of the four types of water, a range of values for S_p has been assumed. Each of these ranges have been selected from *within* the data ranges currently available in the EPA STORET database (*8*) for a large watershed in eastern Washington state (Yakima River basin). Those ranges are as follows: river headwaters, 1–100 mg/L (50 values); rivers that have received agricultural field runoff, 40–400 mg/L (100 values); agricultural field drain, 10–1000 mg/L (100 values); and lake water, 0.1–20 mg/L (50 values).

Except for the lake waters, the values in the ranges assumed for S_c in Table I have been taken to be one-tenth of the values in the ranges for S_p. For the lake waters, (1) ranges characterized by $S_p = S_c$ have been assumed and (2) the values in the range for S_p have been taken to be one-tenth of the values in the range for S_p in the river headwaters. Thus, the lake water is equivalent to river headwater that has stagnated and undergone sedimentation removal of 90% of its S_p content. For all waters, α_w has been assumed to be equal to 1.0. (Assuming a particle density ρ of 2.65 g/mL, even the agricultural drain water will be characterized by $\alpha_w \geq (1 - (S_p + S_c)/10^6\rho) = 0.999\,75$).

The values of K_p and K_c used in the Table I calculations have been estimated for organic compounds for a range

Table I. Values of α_d, α_p, and α_c for Ranges of log K_pS_p/α_w That Might Occur for Organic Compounds of Varying K_{oc} in River Headwaters, Lake Waters, Downstream of Agriculture, and in an Actual Agricultural Field Drain[a]

log K_{oc}	log K_pS_p/α_w	log K_cS_c/α_w	α_d	α_p	α_c	log K_p	log K_p^{app}	log $K_{p,max}^{app}$
				River, Headwaters[b]				
4	3.40–4.40	2.70–3.70	0.9970–0.9708	0.0025–0.0244	0.0005–0.0049	2.70	2.70–2.70	6.00–5.00
5	4.40–5.40	3.70–4.70	0.9708–0.7685	0.0244–0.1930	0.0049–0.0385	3.70	3.70–3.68	6.00–5.00
6	5.40–6.40	4.70–5.70	0.7685–0.2492	0.1930–0.6259	0.0385–0.1249	4.70	4.68–4.52	6.00–5.00
7	6.40–7.40	5.70–6.70	0.2492–0.0321	0.6259–0.8069	0.1249–0.1612	5.70	5.52–4.92	6.00–5.00
				Lake Water[c]				
4	2.40–3.40	2.70–3.70	0.9992–0.9925	0.0002–0.0025	0.0005–0.0050	2.70	2.70–2.70	6.00–5.00
5	3.40–4.40	3.70–4.70	0.9925–0.9301	0.0025–0.0233	0.0050–0.0466	3.70	3.70–3.68	6.00–5.00
6	4.40–5.40	4.70–5.70	0.9301–0.5710	0.0233–0.1428	0.0466–0.2862	4.70	4.68–4.52	6.00–5.00
7	5.40–6.40	5.70–6.70	0.5710–0.1175	0.1428–0.2938	0.2862–0.5888	5.70	5.52–4.92	6.00–5.00
				River, Downstream of Agriculture[d]				
4	3.65–4.65	2.88–3.88	0.9948–0.9503	0.0044–0.0425	0.0008–0.0072	2.48	2.48–2.48	5.60–4.60
5	4.65–5.65	3.88–4.88	0.9503–0.6568	0.0425–0.2934	0.0072–0.0498	3.48	3.48–3.45	5.60–4.60
6	5.65–6.65	4.88–5.88	0.6568–0.1606	0.2934–0.7175	0.0498–0.1219	4.48	4.45–4.23	5.60–4.60
7	6.65–7.65	5.88–6.88	0.1606–0.0188	0.7175–0.8388	0.1219–0.1424	5.48	5.23–4.55	5.60–4.60
				Agricultural Field Drain[e]				
4	3.78–5.08	3.08–4.38	0.9928–0.8740	0.0060–0.1050	0.0012–0.0209	2.30	2.30–2.29	5.22–3.92
5	4.78–6.08	4.08–5.38	0.9326–0.4095	0.0562–0.4922	0.0112–0.0982	3.30	3.29–3.21	5.22–3.92
6	5.78–7.08	5.08–6.38	0.5805–0.0648	0.3498–0.7796	0.0698–0.1555	4.30	4.25–3.77	5.22–3.92
7	6.78–8.08	6.08–7.38	0.1215–0.0069	0.7323–0.8279	0.1461–0.1651	5.30	4.96–3.90	5.22–3.92

[a] Corresponding ranges for log K_p and log K_p^{app} values are also given; α_w assumed equal to 1.0. Note that the ranges for $K_{p,max}^{app}$ are independent of K_{oc}. [b] S_p = 5–50 mg/L with $(f_{oc})_p$ = 0.05; S_c = 0.5–5 mg/L with $(f_{oc})_c$ = 0.10; x_c = 2.0; S_cx_c/α_w = 1–10 mg/L. [c] S_p = 0.5–5 mg/L with $(f_{oc})_p$ = 0.05; S_c = 0.5–5 mg/L with $(f_{oc})_c$ = 0.10; x_c = 2.0; S_cx_c/α_w = 1–10 mg/L. [d] S_p = 15–150 mg/L with $(f_{oc})_p$ = 0.03; S_c = 1.5–15 mg/L with $(f_{oc})_c$ = 0.05; x_c = 1.67; S_cx_c/α_w = 1–10 mg/L. [e] S_p = 30–600 mg/L with $(f_{oc})_p$ = 0.02; S_c = 3–60 mg/L with $(f_{oc})_c$ = 0.04; x_c = 2.0; S_cx_c/α_w = 1–10 mg/L.

of organic carbon/water partition coefficient (K_{oc}) values. (The partitioning behavior of a range of heavy metals could just as easily have been considered). It has been assumed that, for the organic compounds, the partitioning is "organic carbon based". That is, $K_p = K_{oc}(f_{oc})_p$, and $K_c = K_{oc}(f_{oc})_c$, where $(f_{oc})_p$ is the fraction of organic carbon in the P phase, and $(f_{oc})_c$ is the fraction of organic carbon in the C phase. The values assumed for f_{oc} are given in Table I. It should be noted that river, lake, and field drain waters with properties outside of the ranges considered here are surely possible. For example, for Lake Superior, Baker et al. (*4*) reported $(f_{oc})_p$ values extending as high as ~0.40.

For each type of water in Table I, each K_{oc} value yields a range in values for both K_cS_c/α_w and K_pS_p/α_w. Since the lower limit of each range for K_cS_c/α_w intersects with the lower limit of each range for K_pS_p/α_w, and similarly for the upper limit of each range, in Figure 5 the points between these limits will plot as a straight line for each range. However, this constitutes a rather restrictive view of the conditions that might occur in these types of waters, and so each "range" has been characterized in Figure 5 as a full box. The corners of each box are given by the four possible combinations of the upper and lower limits of the ranges for K_cS_c/α_w and K_pS_p/α_w.

In both examples of river waters as well as in the example agricultural field drain waters, Table I and parts a and b of Figure 5 indicate that the C phase is not as important as the P phase; for these cases, $K_cS_c/\alpha_w < K_pS_p/\alpha_w$ for all K_{oc} values. However, if the value of K_pS_p/α_w is lowered while K_cS_c/α_w is kept constant, any given point in part a or b of Figure 5 is moved horizontally from right to left. As this occurs, α_c and α_d increase, and α_p decreases. If the reduction of K_pS_p/α_w occurs due to the sedimentation removal of suspended particulate matter, these changes will be accompanied by reductions in C_p and C_T; C_d and C_c, however, will remain constant. Given these facts, since the K_pS_p/α_w values in the example lake water are a factor of 10 lower than those in the river headwaters, the K_{oc} boxes in Figure 5b for the lake water are located exactly 1 log unit to the left of those for the river headwaters. This shift is sufficiently extensive to cause the α_c values in the lake water to be quite significant for the compounds with the higher K_{oc} values.

Dependence of the Apparent Partition Coefficient K_p^{app} on K_cS_c/α_w. Recent studies of sorption in surface water systems have considered why partition coefficients measured simply by taking the ratio of c_p to the remaining portion of the concentration tend to decrease as S_p increases. If the remaining concentration is normalized by α_w, and if one assumes that a C phase is not present to any significant extent, one obtains c_d. This result therefore means that the thermodynamic partitioning constant K_p ($=c_p/c_d$) must somehow be influenced by particle/particle interactions (*9*, *10*). Gschwend and Wu (*3*), however, have proposed that this trend is caused by a failure to recognize the importance of C_c. They believe that (1) measuring K_p as described in the first sentence of this paragraph amounts to measuring an *apparent* partition coefficient, denoted here as K_p^{app}, and (2) the magnitude of the artifact increases as S_p increases because S_c tends to increase with S_p.

Using the various α values to express the pertinent parameters, we have

$$K_p^{app} = \frac{\alpha_p C_T 10^6/S_p}{(\alpha_d + \alpha_c)C_T/\alpha_w^{app}} = \frac{\alpha_p 10^6/S_p}{(\alpha_d + \alpha_c)/\alpha_w^{app}} \quad (26)$$

Since

$$K_p = \frac{\alpha_p C_T 10^6/S_p}{\alpha_d C_T/\alpha_w} = \frac{\alpha_p 10^6/S_p}{\alpha_d/\alpha_w} \quad (27)$$

then

$$\frac{K_p^{app}}{K_p} = \frac{\alpha_d(\alpha_w^{app}/\alpha_w)}{\alpha_d + \alpha_c} \quad (28)$$

When the presence of the solid portion of the colloidal phase is not taken into consideration, α_w will be overes-

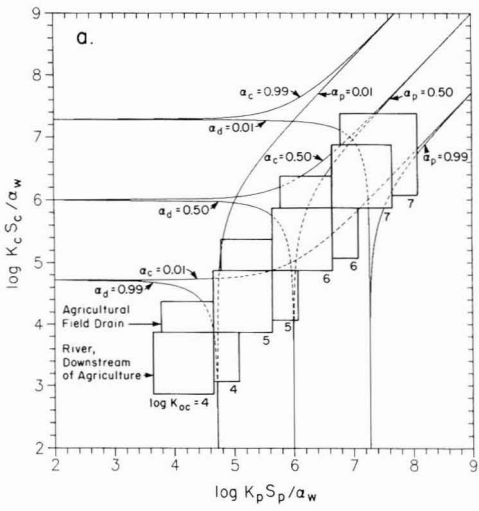

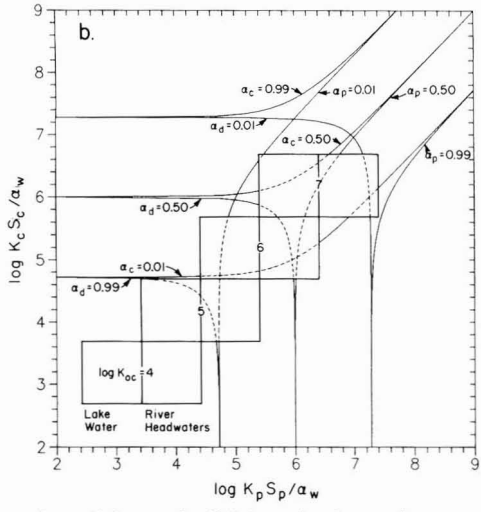

Figure 5. log K_pS_p/α_w vs log K_cS_c/α_w regions for organic compounds with varying log K_{oc} values in example waters. (a) River water downstream of agriculture with S_p = 15–150 mg/L, $(f_{oc})_p$ = 0.03, S_c = 1.5–15 mg/L, and $(f_{oc})_c$ = 0.05; agricultural field drain water with S_p = 30–600 mg/L, $(f_{oc})_p$ = 0.02, S_c = 3–60 mg/L, and $(f_{oc})_c$ = 0.04. (b) River headwaters with S_p = 5–50 mg/L, $(f_{oc})_p$ = 0.05, S_c = 0.5–5 mg/L, $(f_{oc})_c$ = 0.10; lake water with S_p = 0.5–5 mg/L, $(f_{oc})_p$ = 0.05, S_c = 0.5–5 mg/L, and $(f_{oc})_c$ = 0.10.

timated. This apparent value is given as α_w^{app} in eqs 26–28. However, since the colloidal phase will rarely contribute significantly to the volume of an aqueous system, we will almost always have to a very good approximation that $\alpha_w^{app}/\alpha_w \simeq 1$, and so

$$\frac{K_p^{app}}{K_p} \simeq \frac{\alpha_d}{\alpha_d + \alpha_c} = \frac{1}{1 + K_cS_c/10^6\alpha_w} \qquad (29)$$

When $\alpha_w^{app}/\alpha_w \simeq 1$, eq 29 illustrates that K_p^{app}/K_p can only equal 1.0 when when $\alpha_c = 0$. By eq 3, this can only occur when $K_cS_c/\alpha_w = 0$. Thus, for all nonzero values of K_cS_c/α_w, K_p^{app}/K_p will be less than 1.0. The extent to which K_p^{app} is different from K_p is determined by the extent to which the colloidal matter increases the apparent capacity of the "water" to compete with the P phase for the species of interest. Equations 26–29 have the advantage

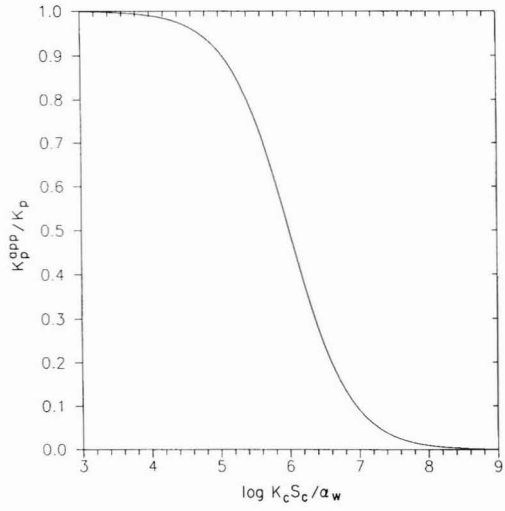

Figure 6. K_p^{app}/K_p as a function of log K_cS_c/α_w.

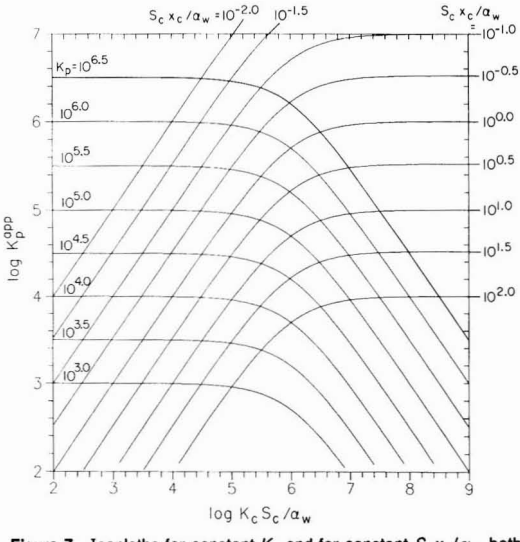

Figure 7. Isopleths for constant K_p and for constant S_cx_c/α_w, both as functions of log K_p^{app} and log K_cS_c/α_w.

that they are expressed in the α format. Equation 29, which is also expressed explicitly in terms of the variable K_cS_c/α_w, is equivalent to an equation given by Gschwend and Wu (*3*).

Figure 6 gives K_p^{app}/K_p as a function of the logarithm of the variable K_cS_c/α_w. Figure 7 gives log K_p^{app} isopleths as a function of log K_cS_c/α_w for a range of K_p values. As discussed above, for low values of K_cS_c/α_w, α_c is small compared to α_d, and so $K_p^{app}/K_p \simeq 1$. As K_cS_c/α_w increases, however, α_c increases, and so both K_p^{app}/K_p and K_p^{app} begin to decrease. Equation 26 indicates that 10^6 is the reference value for judging whether K_cS_c/α_w is "small" or "large". When $K_cS_c/\alpha_w = 10^6$, then $K_p^{app}/K_p = 0.5$. The values of log K_p and log K_p^{app} for the various types of surface water considered in Figure 5 are given in Table I. As required, whenever $K_cS_c/10^6\alpha_w$ approaches and exceeds 10^6, log K_p^{app} becomes significantly less than log K_p.

Independence of K_p^{app} with Respect to K_p when K_cS_c/α_w is Large. In their study of the partitioning of a variety of PCB congeners in lake waters, Baker et al. (*4*)

assumed that K_c might tend to be linearly related to K_p according to

$$K_c = x_c K_p \tag{30}$$

where x_c is a dimensionless proportionality constant. When partitioning to organic carbon controls sorption to the P and C phases, *and* when the carbon in these two phases is *equally sorptive* (i.e., exhibits the same K_{oc} values), then

$$x_c = (f_{oc})_c/(f_{oc})_p \tag{31}$$

Table I gives the x_c values calculated using eq 31 for the different surface water examples considered above.

Equations 29 and 30 yield

$$K_p^{app} = K_p/(1 + K_p S_c x_c/10^6\alpha_w) \tag{32}$$

When $x_c S_c/\alpha_w$ is constant (as in a single specific aqueous system characterized by a compound-to-compound constancy in x_c), the value of K_p^{app} will increase as K_p increases. When $K_c S_c/\alpha_w = K_p S_c x_c/\alpha_w \gg 10^6$

$$K_p^{app} \simeq K_{p,max}^{app} = 10^6\alpha_w/S_c x_c \tag{33}$$

To within the correction embodied in α_w, eq 33 is equivalent to one given by Baker et al. (*4*). Thus, as $K_p S_c x_c/\alpha_w$ increases and rises above 10^6, K_p^{app} approaches a maximum value that is *essentially independent* of K_p. That is, when the amounts of the various species of interest in the D phase are negligible relative to the amounts in the C phase, the partitioning between the P phase and the remainder of the system becomes essentially independent of K_p. The value of $K_{p,max}^{app}$ increases as $S_c x_c/\alpha_w$ decreases because one has to go to more highly sorbing species (larger K_p and K_c) before the lower value of $S_c x_c/\alpha_w$ will allow the C phase to compete with the D phase.

Assuming $\alpha_w \simeq 1$, the ranges for $S_c x_c/\alpha_w$ for the four examples considered above are as follows: river headwater, 1–10; lake water, 1–10; river downstream of agriculture, 2.5–25; and agricultural field drain, 6–120. The corresponding ranges for log $K_{p,max}^{app}$ are given in Table I. It may be noted that the log $K_{p,max}^{app}$ ranges are independent of K_{oc}. They are also independent of $K_p S_p/\alpha_w$, as is brought out clearly by the fact that the ranges are identical for the river headwater and lake water examples. As expected, the larger $x_c K_p S_c/\alpha_w$ becomes, the more log K_p^{app} becomes increasingly close to log $K_{p,max}^{app}$.

These effects may be placed in the simplified variable context as follows. If eq 30 gives the relationship between K_c and K_p for multiple species with a range of K_c and K_p values, then

$$\log K_p = \log K_c S_c/\alpha_w - \log S_c x_c/\alpha_w \tag{34}$$

Based on eqs 29 and 34, we obtain

$$\log K_p^{app} = \log K_c S_c/\alpha_w - \log S_c x_c/\alpha_w - \log (1 + K_c S_c/10^6\alpha_w) \tag{35}$$

Equation 35 may be used to investigate how log K_p^{app} varies with log $K_c S_c/\alpha_w$ for any given constant value of $S_c x_c/\alpha_w$. Accordingly, isopleths are drawn in Figure 7 for $S_c x_c/\alpha_w$ values ranging between 10^{-2} and 10^2. The value of K_p that pertains to any given point on any $S_c x_c/\alpha_w$ isopleth may be deduced from the K_p isopleths also included in that figure.

For $K_c S_c/\alpha_w \ll 10^6$, the $S_c x_c/\alpha_w$ isopleths in Figure 7 cross the K_p isopleths in a regular manner. Under these conditions, by eq 35 we have

$$\log K_p^{app} \simeq \log K_c S_c/\alpha_w - \log S_c x_c/\alpha_w \tag{36}$$

and so along each $S_c x_c/\alpha_w$ isopleth

$$\text{d log } K_p^{app}/(\text{d log } K_c S_c/\alpha_w) \simeq +1 \tag{37}$$

Each unit increase in log K_p^{app} therefore essentially requires a unit increase in log $K_c S_c/\alpha_w$. This is simply a reflection of the fact that we are in the low-$K_c S_c/\alpha_w$ range where the magnitude of the artifact is small, $K_p^{app} \simeq K_p$, and so d log $K_p^{app} \simeq$ d log K_p. Therefore, when both x_c and S_c/α_w are for example constant along a given $S_c x_c/\alpha_w$ isopleth, then by eq 30 we have d log $K_c S_c/\alpha_w$ = dlog K_p, and we obtain eq 37.

For $K_c S_c/\alpha_w \gg 10^6$, eq 35 becomes

$$\log K_p^{app} \simeq \log K_c S_c/\alpha_w - \log S_c x_c/\alpha_w - \log K_c S_c/10^6\alpha_w \tag{38}$$

or

$$\log K_p^{app} \simeq \log 10^6\alpha_w/S_c x_c = K_{p,max}^{app} \tag{39}$$

as expected from eq 33. Thus, for $K_c S_c/\alpha_w \gg 10^6$, along each $S_c x_c/\alpha_w$ isopleth

$$\text{d log } K_p^{app}/(\text{d log } K_c S_c/\alpha_w) \simeq 0 \tag{40}$$

Thus, for each $S_c x_c/\alpha_w$ isopleth in Figure 7, when $K_c S_c/\alpha_w \gg 10^6$, (1) the K_p isopleths for K_p values above some minimal value tend to cross a given $S_c x_c/\alpha_w$ isopleth at a nearly constant K_p^{app} value, and (2) the $S_c x_c/\alpha_w$ isopleth asymptotically approaches the value log 10^6 – log $S_c x_c/\alpha_w$ = log $K_{p,max}^{app}$.

The region wherein $K_c S_c/\alpha_w$ is neither large or small, but is of the same order of magnitude as 10^6, is characterized by a *transition* from K_p^{app} being dependent on K_p, with slope d log $K_p^{app}/(\text{d log } K_c S_c/\alpha_w) \simeq +1$, to independence, with slope ~0.

The fact that 10^6 is the appropriate reference value for judging (1) the relative magnitude of $K_c S_c/\alpha_w$ and (2) the importance of partitioning to the C phase may be reflected in a study of PCB congeners in sediment pore waters (*11*). In that work, a leveling in measured K_p^{app} values was observed for PCB congeners with octanol/water partition coefficient (K_{ow}) values of $>10^6$. Available correlation equations such as (*12*)

$$K_{oc} = 0.411K_{ow} \qquad 20\ °C \tag{41}$$

indicate that a K_{ow} value of $\geq 10^6$ translates into a K_{oc} of $\geq 4 \times 10^5$. For an $(f_{oc})_c$ of ~0.10, we therefore obtain $K_c \geq 4 \times 10^4$. The concentration of the C phase in the sediment pore waters (S_c/α_w^{app}) can be ≥10 mg/L. Since $\alpha_w^{app} \simeq \alpha_w$, under these conditions, we have $K_c S_c/\alpha_w \geq 4 \times 10^5$. Since this order of magnitude estimate of $K_c S_c/\alpha_w$ is quite close to 10^6, it seems likely that Brownawell and Farrington (*11*) were in fact observing the effects of partitioning to a C phase. Factors which might have led to even larger values of this estimate might include (1) greater sorption by the C-phase organic carbon than predicted by eq 41, (2) $(f_{oc})_c$ values greater than 0.10, and/or (3) temperature corrections for K_{oc}. With regard to the first possibility, it may be noted that Means and Wijayaratne (*13*) and Capel (*14*) have found that for hydrophobic organic compounds, C-phase organic carbon can be anywhere from 0.5 to 35 times as sorptive as P-phase organic carbon.

Conclusions

The parameterization developed here using $K_p S_p/\alpha_w$ and $K_c S_c/\alpha_w$ provides a simple approach for viewing the chemistry of species that are subject to partitioning between the dissolved, colloidal, and suspended particulate phases. It allows the nature of this distribution to be

described in a single master diagram (i.e., Figure 4). The dependence of the nature of the dissolved/particulate/colloidal distribution on the S_p and S_c properties of the water and on the K_p and K_c properties of the chemical of interest are readily studied with this diagram. Changes in the distribution caused by individual changes in any of these parameters may be tracked on this diagram. An important example of such a change is the type of decrease in S_p that can occur due to the removal of suspended sediments from surface waters by settling. The simplified parameter approach also allows plots using the variable K_cS_c/α_w to be used in examining the effects of colloidal particulate matter on the apparent partitioning coefficient K_p^{app}.

Glossary

C phase — colloidal phase (nonfilterable particles; includes sorptive dissolved humic type molecules)

c_c — concentration in the colloidal phase (g sorbed/g of dry weight of C phase = $10^6C_c/S_c$)

c_d — concentration in dissolved phase (g/mL of D phase = C_d/α_w)

c_p — concentration in the particulate phase (g sorbed/g of dry weight of P phase = $10^6C_p/S_p$)

C_c — concentration in the colloidal phase per unit volume of total system (g/mL of total system)

C_d — concentration in the dissolved phase per unit volume of total system (g/mL of total system)

C_p — concentration in the particle phase per unit volume of total system (g/mL of total system)

C_T — total concentration per unit volume of total system (g/mL of total system)

D phase — dissolved phase

$(f_{oc})_p$ — fraction of organic carbon in the P phase ($0 \leq (f_{oc})_p \leq 1$, dimensionless)

$(f_{oc})_c$ — fraction of organic carbon in the C phase ($0 \leq (f_{oc})_c \leq 1$, dimensionless)

K_c — partition coefficient between the colloidal and dissolved phases ((g sorbed/g of colloid phase)/(g dissolved/mL water) = c_c/c_d and = $K_{oc}(f_{oc})_c$ if the partitioning is "organic carbon based")

K_{oc} — organic carbon/water partition coefficient ((g sorbed/g of organic carbon)/(g dissolved/mL of water))

K_{ow} — octanol/water partition coefficient ((g in octanol/mL of octanol)/(g dissolved/mL of water))

K_p — partition coefficient between the particle and dissolved phases ((g sorbed/g of particle phase)/(g dissolved/mL of water) = c_p/c_d and = $K_{oc}(f_{oc})_p$ if the partitioning is "organic carbon based")

K_p^{app} — *apparent* (underestimated) value of the partition coefficient K_p as affected by not taking account of partitioning to colloidal phase

$K_{p,max}^{app}$ — maximum possible value of K_p^{app}, independent of K_p, that is possible for given values of α_w, S_c, and x_c

n_c — number of compartments to which partitioning can occur

S_c — mass/volume concentration of solid particulate phase for the overall system (g of dry weight/mL of total system)

S_p — mass/volume concentration of solid particulate phase for the overall system (g of dry weight/mL of total system)

x_c — dimensionless proportionality constant describing relative effectiveness of partitioning to colloidal and particulate phases; when the partitioning is organic carbon based, and when the K_{oc} values for the two phases are equal, then $x_c = (f_{oc})_c/(f_{oc})_p$

P phase — particle phase (suspended, filterable particles, or soil matrix phase in the case of soil/water systems)

Greek

α_c — fraction of C_T that is in colloidal phase (= C_c/C_T, with $0 \leq \alpha_c \leq 1$, dimensionless)

α_d — fraction of C_T that is in dissolved phase (= C_d/C_t, with $0 \leq \alpha_d \leq 1$, dimensionless)

α_p — fraction of C_T that is in particulate phase (= C_p/C_T, with $0 \leq \alpha_p \leq 1$, dimensionless)

α_w — volume fraction of the system occupied by the dissolved phase, with $0 \leq \alpha_w \leq 1$ (dimensionless)

α_w^{app} — *apparent* (underestimated) value of α_w as affected by not taking account of presence of colloidal phase; α_w^{app} will usually be very close to 1.0

ρ — density (g/mL)

Literature Cited

(1) Wershaw, R. L.; Burcar, P. J.; Goldberg, M. C. *Environ. Sci. Technol.* **1969**, *3*, 271.
(2) Carter, C. W.; Suffet, I. H. *Environ. Sci. Technol.* **1982**, *16*, 735.
(3) Gschwend, P. M.; Wu, S.-C. *Environ. Sci. Technol.* **1985**, *19*, 90.
(4) Baker, J. E.; Capel, P. D.; Eisenreich, S. J. *Environ. Sci. Technol.* **1986**, *20*, 1136.
(5) Chiou, C. T.; Malcolm, R. L.; Brinton, T. I.; Kile, D. E. *Environ. Sci. Technol.* **1986**, *20*, 502.
(6) Chiou, C. T.; Kile, D. E.; Brinton, T. I.; Malcolm, R. L.; Leenheer, J. A.; MacCarthy, P. *Environ. Sci. Technol.* **1987**, *21*, 1231.
(7) Pankow, J. F. *Aquatic Chemistry Concepts*; Lewis Publishers: Boca Raton, FL, 1991.
(8) U.S. EPA. STORET data base, Washington, DC.
(9) Ditoro, D. M. *Chemosphere* **1985**, *14*, 1503.
(10) Mackay, D.; Powers, B. *Chemosphere* **1987**, *16*, 745.
(11) Brownawell, B. J.; Farrington, J. W. In *Marine and Estuarine Geochemistry*; Sigleo, A. C., Hattori, A., Eds.; Lewis Publishers: Boca Raton, FL, 1985; Chapter 7, pp 97–120.
(12) Karickhoff, S. W. *Chemosphere* **1981**, *10*, 833.
(13) Means, J. C.; Wijayaratne, R. *Science (Washington, D.C.)* **1982**, *215*, 968.
(14) Capel, P. D. Ph.D. Thesis, University of Minnesota, Minneapolis, MN, 1986.

Received for review June 14, 1991. Accepted July 1, 1991. Work on this project by J.F.P. was supported in part by U.S. Geological Survey Project No. 14-08-0001-G1586.

Environ. Sci. Technol. 1991, 25, 2054–2058

Comparison of Tetrachloromethane Sorption to an Alkylammonium–Clay and an Alkyldiammonium–Clay

James A. Smith*

U.S. Geological Survey, 810 Bear Tavern Road, Suite 206, West Trenton, New Jersey 08628

Peter R. Jaffé

Department of Civil Engineering and Operations Research, Princeton University, Princeton, New Jersey 08544

■ The interlamellar space of Wyoming bentonite (clay) was modified by exchanging either decyltrimethylammonium (DTMA) or decyltrimethyldiammonium (DTMDA) cations for inorganic ions, and tetrachloromethane sorption to the resulting two organoclays from water was studied at 10, 20, and 35 °C. Only one end of the 10-carbon alkyl chain of the DTMA cation is attached to the silica surface of the clay mineral, and tetrachloromethane sorption of DTMA–clay is characterized by isotherm linearity, noncompetitive sorption, weak solute uptake, and a relatively low heat of sorption. Both ends of the 10-carbon chain of the DTMDA cation are attached to the silica surface of the clay mineral, and tetrachloromethane sorption to DTMDA–clay is characterized by nonlinear isotherms, competitive sorption, strong solute uptake, and a relatively high, exothermic heat of sorption that varies as a function of the mass of tetrachloromethane sorbed. Therefore, the attachment of both ends of the alkyl chain to the interlamellar mineral surface appears to change the sorption mechanism from a partition-dominated process to an adsorption-dominated process.

Introduction

Much research in the past 10 years has focused on the mechanism of interaction of nonionic organic contaminants with the natural organic matter of soil in aquatic systems (*1–3*). Part of the difficulty involved in studying this interaction is the well-documented heterogeneous nature of soil and the unknown composition of natural organic matter (*1, 4*). The experimental results and analyses presented in this paper attempt to better define the effect of the molecular structure of organic matter at the mineral–water interface on the sorption of nonionic organic compounds by studying a well-defined solute–organic matter–mineral system composed of tetrachloromethane, alkylammonium or alkyldiammonium cations, and Wyoming bentonite.

Background

Wyoming bentonite (clay) is primarily a Na–montmorillonite, which is a layered silicate that swells when contacted by water. Each layer is composed of an octahedral sheet of the general form $M_{2-3}(OH)_6$ (where M is typically Al^{3+}) between two SiO_4 tetrahedral sheets (*5*). The substitution of Al^{3+} for Si^{4+} in the tetrahedral layer and Mg^{2+} or Zn^{2+} for Al^{3+} in the octahedral layer results in a net negative surface charge on the clay (*6*). The charge imbalance is offset by exchangeable cations such as H^+, Na^+, or Ca^{2+} at the clay surface (*7*). In aqueous solution, large quaternary ammonium organic cations (including alkylammonium and alkyldiammonium cations) readily replace these inorganic cations in the interlamellar space of the clay mineral by ion exchange and are said to be "intercalated" by the clay (*8*). The resulting organic cation substituted clay is called an "organoclay". In the 1950s and 1960s, it was shown that the sorption of vapors of nonionic organic liquids to organoclays was substantially greater than sorption to Na– or Ca–clays (*9–19*), and these results have been summarized elsewhere (*8, 20*). It was determined that the intercalated organic cations act as "props" that hold apart the silicate layers, allowing nonionic organic vapors to be intercalated and sorbed. In the absence of these relatively large organic cations, nonionic organic vapors cannot penetrate the interlamellar space of the expandable clay and sorption is limited to the external surfaces of the clay particles.

More recently, nonionic compound sorption to organoclays from water has been studied (*8, 21–28*). Sorption of nonionic organic compounds to clay modified by the exchange of monovalent quaternary ammonium cations having only small or rigid functional groups (e.g., methyl, ethyl, or benzyl) is characterized by relatively strong solute uptake, isotherm nonlinearity, and competitive sorption (*24, 25, 28*). In addition, the magnitude of solute uptake is not strictly dependent on the solute's aqueous solubility (*24*) and is much greater than the magnitude of solute uptake by natural soil after the data are normalized to account for differences in organic carbon contents (*28*). This behavior is caused by surface adsorption (*24, 25, 28*). By contrast, sorption of nonionic compounds to clay modified with monovalent quaternary ammonium cations having one or more large alkyl functional groups (e.g., 12–18-carbon alkyl chains) is characterized by relatively weak solute uptake, isotherm linearity, and noncompetitive sorption (*21, 27, 28*), in which the magnitude of solute uptake is inversely proportional to the solute's aqueous solubility (*30*) and is comparable to the magnitude of solute uptake by natural soil after the data are normalized to account for differences in organic carbon contents (*28*). This behavior is caused by a partition process (*21, 27, 28*). Therefore, depending on the molecular structure of the organic cation, the modified interlamellar space functions as an adsorbent or a partition medium for the uptake of nonionic organic solutes from water (*21, 24, 25, 28–30*).

This paper compares tetrachloromethane sorption to a clay modified with a monovalent alkylammonium cation and to a clay modified with a divalent alkylammonium cation in order to understand the cause for the two sorption mechanisms (e.g., partition and adsorption) observed previously. Aside from the fundamental objective of defining the mechanistic interaction of organic matter (of known molecular structure) with nonionic organic compounds at the mineral–water interface, this research also has the practical objective of helping to determine the optimum characteristics of an organic cation to be used to modify clay for specific environmental applications. It has been suggested that organoclays can be used as a component of clay liners or slurry walls to prevent contaminant migration (*21*), as a selective sorbent for air contaminant sampling (*31*), or in chromatographic applications (*18*).

 0013-936X/91/0925-2054$02.50/0

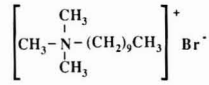

Decyltrimethylammonium (DTMA) bromide

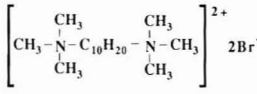

Decyltrimethyldiammonium (DTMDA) bromide

Figure 1. Structural diagrams of an alkylammonium and an alkyldiammonium salt.

Materials and Methods

Wyoming bentonite was obtained from the American Colloid Co. and was used as received. The bentonite contains 3.6% sand, 7.3% silt, and 89.1% clay, and will be referred to as "clay" throughout this paper. Its organic carbon content is 0.1% and its cation-exchange capacity is 78.5 mequiv/100 g. [^{14}C]Tetrachloromethane used in this study has been described previously (*28*). Decyltrimethylammonium (DTMA) bromide, decyltrimethyldiammonium (DTMDA) bromide, and benzene all have chemical purities greater than 98%. Structural diagrams of DTMA and DTMDA bromide are shown in Figure 1.

Combining an alkylammonium or alkyldiammonium cation with an aqueous clay suspension results in strong uptake of the cation by the clay (*28*, *32*, *33*). The resulting alkylammonium– or alkyldiammonium–clay is a unique sorbent that is identified by the cation abbreviation given in Figure 1 followed by "–clay". Therefore, combining decyltrimethylammonium bromide with an aqueous clay suspension creates decyltrimethylammonium–clay or DTMA–clay.

A batch equilibration method was used to quantify tetrachloromethane sorption to the organoclays. For tetrachloromethane sorption to DTMDA–clay at all temperatures, 6 g of clay, 55 mL of water, decyltrimethyldiammonium bromide, and [^{14}C]tetrachloromethane were combined in 50-mL (nominal volume) disposable glass centrifuge tubes with Teflon-lined septum caps. The added mass of decyltrimethyldiammonium bromide was either 0.30, 0.60, or 0.79 g, which corresponds to 30, 61, or 80%, respectively, of the cation-exchange capacity of the clay. These three sorbents are referred to as 30% DTMDA–clay, 61% DTMDA–clay, and 80% DTMDA–clay. The mass of added tetrachloromethane ranged from 7 to 110 mg. For tetrachloromethane sorption to DTMA–clay at all temperatures, 7 g of clay, 55 mL of water, 1.23 g of decyltrimethylammonium bromide (equal to 80% of cation-exchange capacity), and [^{14}C]tetrachloromethane were combined in the above described centrifuge tubes. The mass of added tetrachloromethane ranged from 7 to 65 mg. For each organoclay sorbent, the effect of a competing solute on tetrachloromethane sorption was also studied by adding 35 mg of benzene to each tube. The incubation and centrifugation of the tubes and the scintillation counting of the supernatant have been described previously (*28*).

Three additional centrifuge tubes were handled similarly to the above-described tubes for each sorption isotherm to ensure the quality of the data. Two of these tubes contained water, [^{14}C]tetrachloromethane, either decyltrimethylammonium bromide or decyltrimethyldiammonium bromide, and no clay. These tubes were used to quantify solute losses caused by processes other than sorption to the organoclay. In all cases, solute recovery from these tubes was greater than 94%. The third tube contained water, clay, either decyltrimethylammonium bromide or decyltrimethyldiammonium bromide, and no [^{14}C]tetrachloromethane. This tube was used to quantify the background radiation and to identify whether the glassware, clay, organic cation, or water were contaminated with radioactivity.

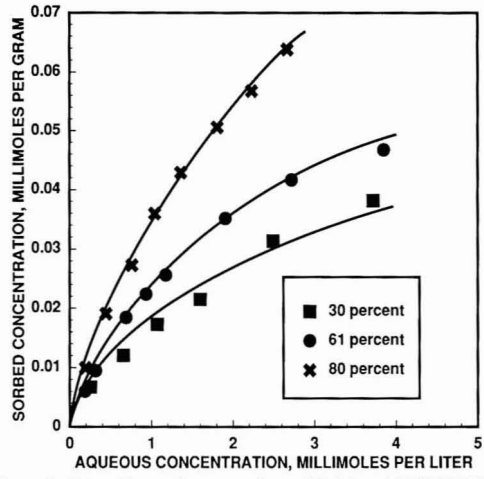

Figure 2. Tetrachloromethane sorption to 30, 61, and 80% DTMDA–clay at 20 °C.

The organic carbon contents of the clay and organoclays were determined in duplicate. The cation-exchange capacity of the clay was determined in quadruplicate. Both analyses were performed by Huffman Laboratories, Golden, CO.

Results

The experimentally measured organic carbon contents of the four sorbents used in this study agree well with theoretical values calculated by assuming that 100% of the added organic cation is retained by the clay. The theoretical organic carbon contents of 30% DTMDA–clay, 61% DTMDA–clay, 80% DTMDA–clay, and 80% DTMA–clay are 2.3, 4.7, 5.8, and 9.0%, respectively, and account for the 0.1% natural organic carbon on the clay. The measured organic carbon contents of these same sorbents are 2.6, 4.5, 5.8, and 9.2%. Comparison of the theoretical and measured organic carbon contents using a one-sided paired t test indicates that the differences between the theoretical and measured values are not statistically significant (p = 0.05).

The isotherms in Figure 2 quantify tetrachloromethane sorption to 30, 61, and 80% DTMDA–clay at 20 °C. The isotherms are distinctly nonlinear and show that tetrachloromethane sorption increases with increased substitution of the DTMDA cation for inorganic cations in the interlamellar space of the clay. All three isotherms in Figure 2 extend to equilibrium aqueous tetrachloromethane concentrations that are approximately 80% of solubility (5.2 mmol/L at 25 °C (*34*)).

Two single-solute and two binary-solute isotherms generated at 20 °C are shown in Figure 3. In both cases, the binary solute is benzene. The upper two isotherms (square symbols) show tetrachloromethane sorption to 80% DTMDA–clay. The isotherms are nonlinear and show competitive sorption. Single- and binary-solute sorption data for 30% DTMDA–clay and 61% DTMDA–clay also exhibited competitive sorption (binary-solute data not

Table I. Freundlich Isotherm Parameters (with 95% Confidence Intervals) and Regression Correlation Coefficients for Tetrachloromethane Sorption to Three Organoclay Sorbents in Both the Presence and Absence of a Binary Solute (Benzene)[a]

sorbent	solute	$1/n$	ln K	corr coeff
30% DTMDA–clay	single	0.64 ± 0.04	−4.20 ± 0.04	0.985
30% DTMDA–clay	binary	0.59 ± 0.18	−4.73 ± 0.18	0.955
61% DTMDA–clay	single	0.68 ± 0.08	−3.84 ± 0.08	0.998
61% DTMDA–clay	binary	0.66 ± 0.14	−4.15 ± 0.12	0.957
80% DTMDA–clay	single	0.71 ± 0.04	−3.41 ± 0.03	0.997
80% DTMDA–clay	binary	0.66 ± 0.11	−3.92 ± 0.10	0.986
80% DTMDA–clay (10 °C)	single	0.71 ± 0.09	−3.31 ± 0.08	0.983
80% DTMDA–clay (35 °C)	single	0.72 ± 0.03	−3.55 ± 0.02	0.999

[a] Sorption measured at 20 °C unless another temperature is specified.

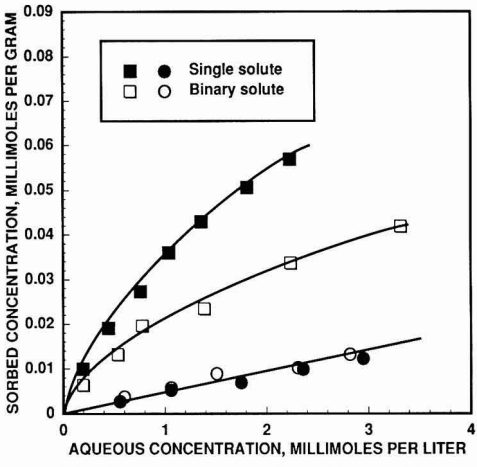

Figure 3. Tetrachloromethane sorption to 80% DTMDA–clay (square symbols) and 80% DTMA–clay (round symbols) at 20 °C. The binary solute is benzene.

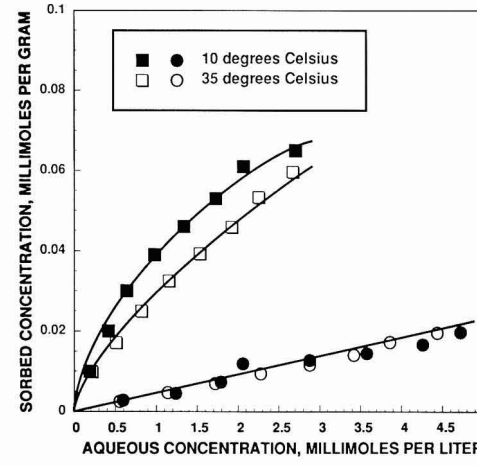

Figure 4. Tetrachloromethane sorption to 80% DTMDA–clay (square symbols) and 80% DTMA–clay (round symbols) at 10 and 35 °C.

shown). The lower two isotherms in Figure 3 show tetrachloromethane sorption to 80% DTMA–clay. The isotherms are linear and show no competitive sorption. Tetrachloromethane uptake by DTMDA–clay is significantly greater than tetrachloromethane uptake by DTMA–clay. This latter result has also been reported for the vapor-phase sorption of organic vapors to alkylammonium- and alkyldiammonium–clays (*17*, *35*).

Figure 4 presents tetrachloromethane sorption isotherms for 80% DTMDA–clay and 80%–DTMA-clay at 10 and 35 °C. Again, tetrachloromethane sorption of DTMDA–clay is characterized by relatively strong solute uptake and nonlinear isotherms relative to tetrachloromethane sorption to DTMA–clay. Increasing the temperature from 10 to 35 °C reduces tetrachloromethane sorption to DTMDA–clay but appears to have little effect on tetrachloromethane sorption to DTMA–clay.

To analyze the experimental data, linear isotherm data (tetrachloromethane sorption to DTMA–clay) and nonlinear isotherm data (tetrachloromethane sorption to DTMDA–clay) were separated for analysis. Linear isotherm data were fit to a one degree of freedom regression model given by

$$C_s = K_d C_e \tag{1}$$

where C_e is the equilibrium aqueous tetrachloromethane concentration (mmol/L), C_s is the equilibrium sorbed tetrachloromethane concentration (mmol/kg), and K_d is the distribution coefficient (L/kg) quantified by the linear regression of C_e and C_s. For the 80% DTMA–clay data in Figure 3 (20 °C), K_d (with a 95% confidence interval) equals 4.5 ± 0.9 L/kg and the logarithm of the organic carbon normalized distribution coefficient (log K_{oc}) equals 1.69 ± 0.08. For the 80% DTMA–clay data in Figure 4 (10 and 35 °C), K_d (with a 95% confidence interval) equals 4.3 ± 0.4 L/kg and the logarithm of the organic carbon normalized distribution coefficient (log K_{oc}) equals 1.68 ± 0.03.

The competitive and noncompetitive sorption data for DTMA–clay at 20 °C were compared with multiple regression analysis using a dummy variable (*36*). This analysis determined that the competitive and noncompetitive isotherm pairs for DTMA–clay (Figure 3) were indistinguishable at a p value of 0.05. In addition, isotherms for tetrachloromethane sorption to DTMA–clay at 10 and 35 °C were also indistinguishable at a p value of 0.05.

Nonlinear sorption data (tetrachloromethane sorption to DTMDA–clay) were fit to the linear form of the Freundlich equation (*37*) given by

$$\ln C_s = \frac{1}{n} \ln C_e + \ln K \tag{2}$$

where $1/n$ and ln K are parameters quantified by the linear regression of ln C_s and ln C_e. The calculated values of $1/n$ and ln K and the regression correlation coefficients for tetrachloromethane sorption DTMDA–clay are given in Table I. The data were also fit to two linear forms of the Langmuir equation. However, the Freundlich equation consistently provided correlation coefficients closest to unity. The competitive and noncompetitive pairs of linearized (eq 2) isotherms for DTMDA–clay at 20 °C were

compared with multiple regression analysis using a dummy variable (*36*). The results indicate that the presence of the binary solute (benzene) reduces tetrachloromethane sorption to DTMDA–clay relative to the single-solute data at a p value of 0.05. In addition, statistical comparison of tetrachloromethane sorption to DTMDA–clay at 10 and 35 °C indicates that increased temperature reduces sorption at a p value of 0.05.

Discussion

Comparison of tetrachloromethane sorption to DTMA– and DTMDA–clay is significant because only a small change in the molecular structure of the organic cation produces dramatic changes in the characteristics of the sorption process. In addition to relatively strong solute uptake, tetrachloromethane sorption to DTMDA–clay exhibits isotherm nonlinearity, competitive sorption, and increased solute uptake at temperatures decreasing from 35 to 10 °C. This behavior is typical of an adsorption interaction. By contrast, tetrachloromethane sorption to DTMA–clay shows relatively weak solute uptake, isotherm linearity, and no competitive sorption. The magnitude of tetrachloromethane sorption to DTMA–clay has no measurable change over the temperature range of 10–35 °C. These results indicate that uptake by the 80% DTMA–clay is caused by solute partition between water and the interlamellar organic phase formed by the conglomeration of the alkyl chains of the DTMA cations.

Isosteric heats of sorption can be calculated from the temperature-dependent isotherm data in Figure 4 by use of the Clausius–Clapeyron relation (*37*) given by

$$\Delta H = \left[\frac{T_1 T_2}{T_1 - T_2}\right] R \ln \left[\frac{C_e^2}{C_e^1}\right] \qquad (3)$$

where ΔH is the isosteric heat of sorption (kcal/mol), R is the gas constant (equal to 0.00199 kcal/mol·K), and C_e^1 and C_e^2 are the equilibrium aqueous concentrations of tetrachloromethane (mmol/L) at temperatures T_1 (308 K) and T_2 (283 K) for a common sorbed tetrachloromethane concentration, C_s. For the linear tetrachloromethane sorption exhibited by DTMA–clay, ΔH is not a function of C_s and is near zero because the 10 and 35 °C isotherms are not statistically different. For the nonlinear tetrachloromethane sorption exhibited by DTMDA–clay, ΔH varies with C_s as shown in Figure 5. Values for ΔH for DTMDA–clay range from −2.0 to −2.6 kcal/mol (exothermic).

Exothermic heats of sorption are requisite for an adsorption process (unless adsorption is very weak) to compensate for losses in entropy. By contrast, low heats of sorption (including endothermic heats) that equal the difference between the molar enthalpies of solution of the solute in the organic and aqueous phases are characteristic of a partition process. Therefore, the heat of sorption data presented in Figures 4 and 5 provide additional thermodynamic evidence that tetrachloromethane sorption of DTMA–clay is caused by solute partition between water and the organic phase formed by the conglomeration of the alkyl chains in the interlamellar space, whereas tetrachloromethane sorption to DTMDA–clay is caused by solute adsorption to the modified interlamellar surfaces of the clay. These observations agree with results reported by Barrer et al. (*13*, *14*, *20*), who measured low heats of sorption (that at times were endothermic) for the uptake of organic vapors by dimethyldioctadecylammonium–montmorillonite (*14*). Uptake of the organic vapors by monomethylammonium–montmorillonite, however, was

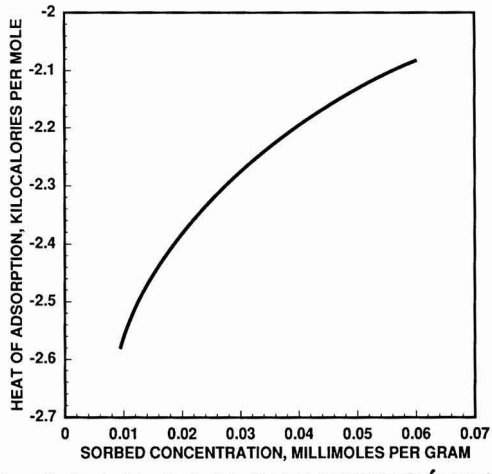

Figure 5. Isosteric heats of adsorption for tetrachloromethane sorption to 80% DTMDA–clay in the temperature range of 10–35 °C.

characterized by strongly exothermic heats of sorption (*13*).

Previous research has shown that the molecular structure of the organic cation retained by the clay influences the mechanism of sorption (*28*). The results presented here explicitly show how the flexibility of the alkyl chain of the organic cation affects the sorption interaction. Because of its diammonium structure, the alkyl chain of the DTMDA cation is attached at both ends to the mineral surface of the clay, which greatly reduces the flexibility of the 10-carbon chain. As a result, this alkyl chain is forced to lie in a flat position (relative to the alkyl chain of the DTMA cation) on the mineral surface. This observation is supported by X-ray diffraction data for dodecyldiammonium–clay (*38*). The rigid, uncharged surface formed by these alkyl chains enhances adsorption of nonionic solutes onto the organic-lined mineral surfaces through London forces and is similar (with regard to sorption mechanism) to the organic surface formed by monoammonium organic cations with small functional groups (e.g., methyl, ethyl, and benzyl). In the absence of organic cations, the mineral surface interacts strongly with water and the adsorption of tetrachloromethane is negligible (*28*). The attachment of only one end of the alkyl chain to the mineral surface (e.g., 80% DTMA–clay) creates an organic partition medium (phase) through the association of the flexible alkyl chains. This association has little effect on the polarity of the clay surface and therefore does not promote significant surface adsorption.

In their most compact form, the long alkyl chains (10–16 carbon atoms) of monovalent organic cations are aligned parallel to the planes of the silicate layers. The increased substitution of the organic cations for inorganic ions causes an increase in the d(001) spacing of the montmorillonite (*21*) and increased bending and overlap of the alkyl chains. The increased "crowding" of the interlamellar space apparently increases both the volume *and* solvency of the organic medium for nonionic solutes. In support of this hypothesis, Boyd et al. (*21*) has reported that K_{om} (organic matter normalized sorption coefficient) values for trichloroethene sorption to hexadecyltrimethylammonium–montmorillonite increase from 50 to 200 as the percent of the clay's exchange sites occupied by the organic cations increases from 35 to 100. Similar results have been reported for benzene (*21*). Also, comparison of the K_{oc} value for tetrachloromethane sorption to 80% DTMA–clay (K_{oc} equal to 48.9) with values reported previously (*28*) for 41%

dodecyltrimethylammonium–, 41% tetradecyltrimethylammonium–, and 41% hexadecyltrimethylammonium–clay (K_{oc} equal to 18.2, 21.9, and 50.1, respectively) shows that the K_{oc} values for these latter three sorbents increase with the length of the alkyl chain, but that the 80% DTMA–clay has a higher K_{oc} value than two of the three sorbents despite its shorter alkyl chain. The high K_{oc} value for 80% DTMA–clay is likely caused by the higher percent substitution of the organic cation onto the clay relative to the other three organoclays. An attempt was made to quantify tetrachloromethane sorption to 41% DTMA–clay but the weak solute uptake prevented precise quantification of the slope of the isotherm. (However, the K_{oc} is estimated to be less than 18.) Therefore, the K_{oc} values for these organoclays appear to increase with the percent substitution of organic cation onto the clay mineral.

It is also useful to compare tetrachloromethane sorption to DTMDA–clay with previous sorption data (*28*) for other small, monoammonium organoclays that exhibited sorption behavior typical of an adsorption process. Specifically, tetrachloromethane sorption to 30 and 61% DTMDA–clay is measurably weaker than tetrachloromethane sorption to 41% tetramethylammonium–, 41% tetraethylammonium–, 41% benzyltrimethylammonium–, and 41% benzyltriethylammonium–clay. The weaker sorption observed by 30 and 61% DTMDA–clay may be caused by bending and overlap of some of the alkyl chains of the diammonium cations, which prevent solute uptake by adsorption in certain localized areas of the interlamellar space. (In some cases, the ends of the alkyl chain of the diammonium cation may be attached to the surfaces of opposing silicate layers.) Therefore, with regard to the alkyl chain of divalent ammonium cations associated with clays, increasing flexibility probably develops as the chain length is increased significantly beyond 10 carbon atoms despite the fact that the alkyl chain is fixed to the mineral surface at both ends.

Acknowledgments

This research was performed by the U.S. Geological Survey in cooperation with the Division of Science and Research of the New Jersey Department of Environmental Protection.

Registry No. CCl_4, 56-23-5; $H(CH_2)_{10}NMe_3$, 15053-09-5; $Me_3N(CH_2)_{10}NMe_3$, 156-74-1; *c*-C_6H_6, 71-43-2.

Literature Cited

(1) Witkowski, P. J.; Smith, J. A.; Fusillo, T. V.; Chiou, C. T. *Geol. Surv. Circ. (U.S.)* **1987**, *No. 993.*
(2) Smith, J. A.; Witkowski, P. J.; Fusillo, T. V. *Geol. Surv. Circ. (U.S.)* **1988**, *No. 1007.*
(3) Smith, J. A.; Witkowski, P. J.; Chiou, C. T. *Rev. Environ. Contam. Toxicol.* **1988**, *103*, 127.
(4) Stevenson, F. J. *Humus Chemistry*; Wiley: New York, 1982.
(5) Theng, B. K. G. *The Chemistry of Clay–Organic Reactions*; Wiley: New York, 1974.
(6) Stumm, W.; Morgan, J. J. *Aquatic Chemistry. An Introduction Emphasizing Chemical Equilibria in Natural Waters*; John Wiley and Sons: New York, 1981.
(7) Worrall, W. E. *Clays: Their Nature, Origin and General Properties*: Transatlantic Arts: New York, 1968.
(8) Smith, J. A.; Tuck, D. M.; Jaffé, P. R.; Mueller, R. T. In *Organic Substances and Sediments in Water*; Baker, R., Ed.; Lewis: Chelsea, MI, 1991.
(9) Barrer, R. M.; Brummer, K. *Trans. Faraday Soc.* **1963**, *59*, 959.
(10) Barrer, R. M.; MacLeod, D. M. *Trans. Faraday Soc.* **1955**, *51*, 1290.
(11) Barrer, R. M.; Hampton, M. G. *Trans. Faraday Soc.* **1957**, *53*, 1462.
(12) Barrer, R. M.; Reay, J. S. S. *Trans. Faraday Soc.* **1957**, *53*, 1253.
(13) Barrer, R. M.; Kelsey, K. E. *Trans. Faraday Soc.* **1961**, *57*, 452.
(14) Barrer, R. M.; Kelsey, K. E. *Trans. Faraday Soc.* **1961**, *57*, 625.
(15) Barrer, R. M.; Perry, G. S. *J. Chem. Soc.* **1961**, 842.
(16) Barrer, R. M.; Perry, G. S. *J. Chem. Soc.* **1961**, 850.
(17) Barrer, R. M.; Millington, A. D. *J. Colloid Interface Sci.* **1967**, *25*, 359.
(18) White, D.; Cowan, C. T. *Trans. Faraday Soc.* **1958**, *54*, 557.
(19) Jurinak, J. J. *Soil Sci. Soc. Am. Proc.* **1957**, *21*, 599.
(20) Barrer, R. M. *Clays Clay Miner.* **1989**, *37*, 385.
(21) Boyd, S. A.; Mortland, M. M.; Chiou, C. T. *Soil Sci. Soc. Am. J.* **1988**, *52*, 652.
(22) Boyd, S. A.; Lee, J.-F.; Mortland, M. M. *Nature* **1988**, *333*, 345.
(23) Lee, J.-F.; Crum, J. R.; Boyd, S. A. *Environ. Sci. Technol.* **1989**, *23*, 1365.
(24) Lee, J.-F.; Mortland, M. M.; Boyd, S. A.; Chiou, C. T. *J. Chem. Soc., Faraday Trans. 1* **1989**, *85*, 2953.
(25) Lee, J.-F.; Mortland, M. M.; Chiou, C. T.; Kile, D. E.; Boyd, S. A. *Clays Clay Miner.* **1990**, *38*, 113.
(26) Wolfe, T. A.; Demirel, T.; Baumann, E. R. *Clays Clay Miner.* **1985**, *33*, 301.
(27) Stul, M. S.; Maes, A.; Uytterhoeven, J. B. *Clays Clay Miner.* **1978**, *26*, 309.
(28) Smith, J. A.; Jaffé, P. R.; Chiou, C. T. *Environ. Sci. Technol.* **1990**, *24*, 1167.
(29) Reference deleted in proof.
(30) Street, G. B.; White, D. *J. Appl. Chem.* **1963**, *13*, 288.
(31) Harper, M.; Purnell, C. J. *Environ. Sci. Technol.* **1990**, *24*, 55.
(32) Giesking, J. E. *Soil Sci.* **1939**, *47*, 1.
(33) Brownawell, B. J.; Chen, H.; Collier, J. M.; Westall, J. C. *Environ. Sci. Technol.* **1990**, *24*, 1234.
(34) Verschueren, K. *Handbook of Environmental Data on Organic Chemicals*; Van Nostrand Reinhold: New York, 1983.
(35) Stul, M. S.; Van Leemput, L.; Rutsaert, M.; Uytterhoeven, J. B. *J. Colloid Interface Sci.* **1983**, *92*, 222.
(36) Kleinbaum, D. G.; Kupper, L. L. *Applied Regression Analysis and Other Multivariable Methods*; Duxbury Press: North Scituate, MA, 1978.
(37) Adamson, J. W. *Physical Chemistry of Surfaces*, 4th ed.; Wiley: New York, 1982.
(38) Wolfe, T. A.; Demirel, T.; Baumann, E. R. *Clays Clay Miner.* **1985**, *33*, 301.

Received for review March 11, 1991. Revised manuscript received May 29, 1991. Accepted July 9, 1991. The use of brand, trade, or product names in this report is for identification purposes only and does not constitute endorsement by the U.S. Geological Survey.

Environ. Sci. Technol. 1991, 25, 2059–2064

Chronology and Sources of Anthropogenic Trace Metals in Sediments from Small, Shallow Arctic Lakes†

Mark H. Hermanson*

Center for Great Lakes Studies, University of Wisconsin—Milwaukee, 600 East Greenfield Avenue, Milwaukee, Wisconsin 53204

■ Fluxes of Pb, Cd, Zn, and Cu are measured in sediment cores from two arctic lakes. One lake is undisturbed by direct human activity, and the other is used for sewage disposal. Sediment layers were analyzed for metals and dated with ^{210}Pb. Sediment focusing was measured by using a ratio of observed to expected ^{137}Cs. Focus-corrected metal fluxes are compared between lakes and show consistent background levels until the 1940s. Following World War II, atmospheric fluxes of Pb, Cd, and Zn increased until the early 1980s when a trend toward lower levels was observed. Atmospheric inputs of anthropogenic trace metals account for no more than 26% of total mass of any of these four metals in sediment. Sewage inputs account for 33% of total Cd mass in sediment, 30% of Zn, and less than 25% of Pb and Cu.

Lake sediments are often used as surrogate measures of changes in the trace metal content of various environmental compartments, including the atmosphere (*1–7*). In areas that are remote from pollutant metal sources, the atmosphere is the only pathway for anthropogenic metals to reach lakes (*8–10*). Sediments are also useful as an archive of changes in point-source metal inputs when the quantity of the nonpoint sources, including the atmosphere, can be measured independently. Under stable conditions, the sediment retains a record of all inputs that can be dated on the basis of the decay of naturally occurring radioisotopes associated with sediment.

The purpose of this investigation is to measure the historical changes in fluxes of Pb, Cd, Zn, and Cu to sediments of two small, shallow arctic lakes. One lake is undisturbed by direct human activity and receives anthropogenic inputs only from the atmosphere. The other lake has been used as a sewage oxidation pond since the late-1960s, so it receives both atmospheric and point-source inputs of metals.

This project is the first to report anthropogenic fluxes of Pb, Cd, Zn, and Cu to arctic lake sediments. A previous investigation (*11*) identified anthropogenic Pb, apparently derived from the atmosphere, in arctic lake sediment, but a flux was not calculated because sedimentation rates and redistribution were not measured. Many previous research efforts have used snow strata or ice cores to measure the historical atmospheric delivery of anthropogenic metals to remote, undisturbed regions of the Arctic (*12–21*). An increase in anthropogenic Pb delivery to the Arctic has been detected this way (*12*), but similar studies have been adversely affected by sample contamination, low concentrations of analytes in the samples, and dating uncertainty.

This report is also among the first to consider the fate of trace metals from human waste in an arctic sewage oxidation pond. The flux of metals in sediment in this type of system is a sign of successful removal of metals from waste. Previous research has focused on removal of oxygen demand and harmful bacteria (*22*) from waste, while more recently, additional attention has been given to metal removal by measuring changes in metal concentrations of pond influents and effluents (*23*).

Various investigators have identified the limitations of interpreting changes of atmospheric chemical flux by use of lake sediment core data (e.g., refs 24 and 25). Successful use of sediment requires that sediment cores be accurately dated, that postdepositional sediment redistribution, or focusing, be measured and factored into the flux, and that the lake system analyzed not have pollutant sources within the drainage basin. The latter requirement is easily reached in the Arctic, where most drainage basins have no pollutant sources. The appearance of anthropogenic metals in arctic lake sediments shows one fate of atmospheric pollutant transport to the Arctic from the midlatitudes, a process known to be very active and one that has been widely investigated (e.g., refs 26 and 27).

Study Area

I collected sediment cores from two lakes on the northern end of Flaherty Island, the largest of the Belcher Islands in southeastern Hudson Bay (see Figure 1). Both lakes are near the Hamlet of Sanikiluaq, NT, Canada, a largely Inuit community with a population at the time of sampling (1983) of ~425.

The largest of the two lakes is known locally as Imitavik. Trace metals were analyzed in three cores, designated as IN-7, IN-9, and IN-10, from the far-northern basin of this lake. This basin has a 25-ha surface area, and a maximum depth of 7.5 m at the site of core IN-10. The lake serves as the water source for the municipal water system in Sanikiluaq. The second lake, known as Annak, is a small, eutrophic lake (surface area 2 ha, maximum depth 4.5 m) used for oxidation of raw domestic sewage from the Hamlet since the late 1960s. One core, designated as A-2, was collected there for metal analysis. The chronology of these cores and the physical characteristics of the lakes are further discussed by Hermanson (*28*).

There are no industrial or agricultural activities in the drainage basins of either Annak or Imitavik, so anthropogenic metal inputs from these sources are not present. The atmosphere is the only pathway for delivery of pollutant metals to Imitavik during the 110-year period between the 1870s and 1980s, the time considered here. Annak is located 2 km west-northwest from Imitavik so both lakes receive the same atmospheric inputs.

The sewage disposal method used in Sanikiluaq since its establishment in 1967 until 1983 was the honey bag system. Human waste was discarded into plastic bags that were collected regularly in the community and dumped into Annak. All other liquid household wastes were discharged on the ground. The natural drainage of the community prevented flow of household wastes into either Imitavik or Annak. Metals found in personal care or other household cleaning products (*29*) were therefore absent from waste discharged to Annak. Bag waste systems also did not include metals leached from plumbing systems in the houses (e.g., ref 30) because piped water was not

* Present address: Academy of Natural Sciences, 1900 Franklin Pkwy., Philadelphia, PA 19103.

† Contribution No. 350, Center for Great Lakes Studies, University of Wisconsin—Milwaukee.

0013-936X/91/0925-2059$02.50/0

Table I. Results of Analysis of Standard Reference Materials 1645 and 2704[a,b]

	Pb		Cd		Zn		Cu	
	mean	SD	mean	SD	mean	SD	mean	SD
			SRM 2704					
certified	161	17	3.45	0.2	438	12	98.6	5.0
this study[c]	157	11	3.56	0.2	450	32	97.2	1.0
			SRM 1645					
certified	714	28	10.2	1.5	1720	169	109	19
this study[c]	734	24	9.9	0.9	1758	12	124	19
Bettinelli et al. (*34*)	739	15	9.1	0.3	1685	45	107	9

[a] All units are micrograms per gram. [b] SD, standard deviation. [c] Values are means of nine individual determinations.

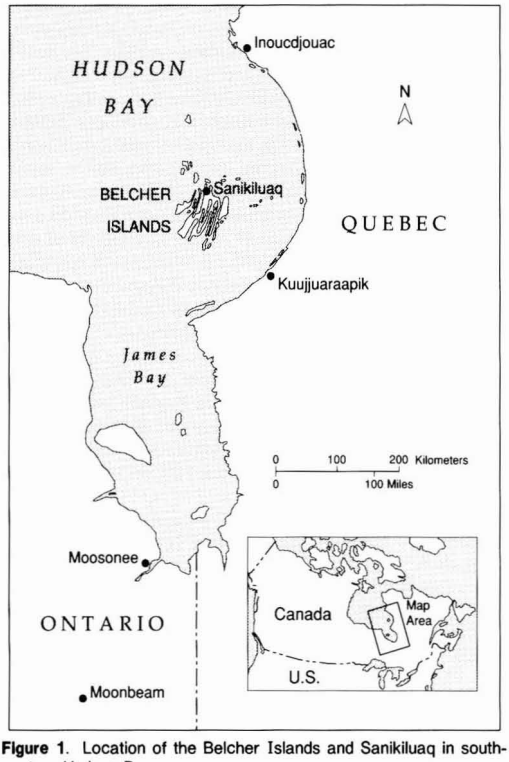

Figure 1. Location of the Belcher Islands and Sanikiluaq in southeastern Hudson Bay.

palatable to most native Hamlet residents. Metals found in bag waste would therefore have originated from exposure of the Hamlet populace to trace metals through ingestion or inhalation.

Methods

Sample Collection. Sediment sampling methods are described by Hermanson (*28*). All cores were collected by the gravity coring method employing 6.7-cm-diameter polybutyrate core liners. They were sectioned at 0.5-cm intervals from the surface to 4-cm depth, at 1-cm intervals from 4 to 20 cm, and 5 cm to the end of each core.

Metal Analysis. Approximately 0.5 g of dried, crushed sediment from each core section was digested in 30 mL of 50% HNO_3 for 4 h at ~100 °C (*31*, *32*). Organic matter was oxidized by five sequential 1-mL additions of 30% H_2O_2 at 30-min intervals. After the final addition of H_2O_2, sample volumes were reduced to ~5 mL. Approximately 25 mL of mixed acid matrix modifier (0.6 N HCl and 3.2 N HNO_3) was added to each sample and heated at 100 °C for 15 min. The solutions were allowed to cool, filtered through No. 42 Whatman filter paper, and volume-adjusted with distilled–deionized water to 100 mL.

Table II. Values of Digestion Blanks and Limits of Detection and Quantitation[a]

	Pb	Cd	Zn	Cu
		Blank Values		
mean	0.0011	0.000015	0.30	0.63
SD	0.00056	0.000016	0.87	0.56
		Limits of Detection		
	0.0028	0.000063	2.9	2.3
		Limits of Quantitation		
	0.0067	0.00018	9.0	6.2

[a] All values in micrograms. Means are based on 15 individual analyses of blank.

Each section of the four cores was analyzed for Pb, Cd, Zn, and Cu. Pb and Cd were analyzed by using a graphite furnace AAS equipped with a square graphite cuvette and a L'vov platform. The low level of matrix interferences introduced during atomization from the platform enabled quantitation by comparison to aqueous standards (*33*). Zn and Cu were analyzed by flame AAS.

The AAS was automatically recalibrated with a calibration blank and a midlevel calibration standard after every eight samples, followed by either a digestion blank or a standard reference material (SRM). Thus, over 27% of the instrumental analysis was devoted to quality control samples.

One blank and one SRM were digested with each group of 14 samples. The SRMs were 1645 (river sediment) or 2704 (Buffalo River sediment) from the National Institute for Science and Technology. Results of the SRM analyses (Table I) are within certified ranges for all elements and compare favorably with values obtained by others using the L'vov platform (*34*).

The limit of detection (LOD) for each metal was computed as the mean value of the blank (X) plus 3 times the standard deviation (σ), while the limit of quantitation (LOQ) for each element was the quantity ($X + 10\sigma$) (*35*). Blank, LOD, and LOQ values appear in Table II.

Dating Analysis and Flux Calculations. Core dating is discussed by Hermanson (*28*). Cores were analyzed for ^{210}Pb and dated by use of the constant rate of supply (CRS) model (*36*). A year was assigned to the top of each sediment layer beginning with 1983 at the top of each core. Sediment porosity (ϕ) was estimated by assuming a solids density of 2.45 g/cm^3. Bulk density (g/cm^3) was calculated as the product of solids density and the quantity ($1 - \phi$). An areal solids burden (g/cm^2) to each core layer was the product of bulk density and thickness of the sediment layer. The areal burden of metal in each layer was computed as the product of the areal solids burden (g/cm^2)

Table III. Years Corresponding to Eras of Individual Imitavik and Annak Sediment Cores

era	IN-7	IN-9	IN-10	A-2
surface	1982–83	1982–83	1980–83	1982–83
Hamlet	1966–83	1966–83	1965–83	1968–83
post-WWII	1946–66	1945–66	1949–65	1946–68
pre-WWII	1902–46	1903–45	1902–49	1897–1946
19th century	1875–1902	1874–1903	1873–1902	1869–97

and the metal concentration ($\mu g/g$). The total burden to several layers divided by the representative number of CRS years yields an average annual flux ($\mu g/cm^2$ per year) over that time period.

Focus Correction. Sedimentation rates measured in Imitavik cores vary by a factor of ~3 because of postdepositional resuspension and redistribution of sediment in parts of the lake. This process, known as sediment focusing, also affects fluxes of metals associated with sediment. The metal flux in cores with redistributed sediment will represent atmospheric deposition to the lake surface if focus correction is used. A common focus correction factor is derived from the inventory of ^{137}Cs in sediment and is measured as a ratio of the total burden of ^{137}Cs in sediment to an estimated total ^{137}Cs fallout at the sampling site (*28*, *37–39*). The ^{137}Cs inventories for these cores are reported elsewhere (*28*). The focus-corrected fluxes of trace metals from a series of cores within a lake should be similar if the background amounts and anthropogenic sources of metals are the same at each coring site.

Historical Flux Comparisons. Average annual focus-corrected fluxes of metals during four different historical periods covering 110 years are used to show changes in metal fluxes to the lakes sampled here. These averages integrate the changes that occur over several years, allowing comparison of cores with different sedimentation rates. The periods vary slightly between cores because of different dating resolution (Table III). In addition, surface fluxes were calculated as the product of mass sedimentation rate (*28*) and the concentrations of metals in the surface sediment layers.

The last quarter of the 19th century, from the early 1870s to ~1900, is the oldest period with quantifiable unsupported ^{210}Pb in Imitavik and Annak sediments and therefore is the oldest period that could be dated. Metal fluxes to Sanikiluaq area lakes during this period are assumed to represent background levels because the metal concentrations in the core sections are not significantly different from each other during that time. None of the cores collected here could be accurately dated before 1870, preventing an earlier Pb flux measurement that may have resulted in a lower background. Greenland ice core data from Murozumi et al. (*12*) show that anthropogenic Pb first appeared after the mid-18th century, in which case a true Pb background would be obtained in sediment layers dated from the early 1700s. Alternatively, Evans and Rigler (*9*) showed the earliest appearance of anthropogenic Pb in lake sediments in northern Quebec to be ~100 years later. These findings suggest that the background Pb fluxes reported here may include some anthropogenic Pb. The anthropogenic Pb fluxes may therefore be conservative.

The pre-WWII era covers the period from ~1900 to the mid-1940s. The use of lead as a gasoline additive began during this period (*12*, *40*) and became the largest source of atmospheric Pb after 1924 (*41*). The post-WWII period covers the late 1940s to the late 1960s and shows the residues of human activity in the Arctic following WWII. Atmospheric transport of trace metals to the Arctic probably increased significantly following WWII. Murozumi et al. (*12*) observed that Pb concentration in Greenland snow strata dated 1946 and later were 3–4 times more concentrated than pre-WWII levels.

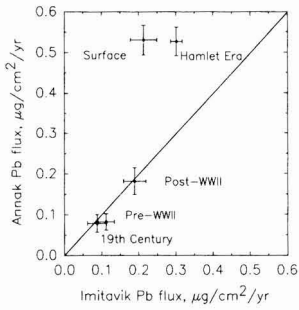

Figure 2. Comparative historical focus-corrected Pb fluxes to Imitavik and Annak sediments. The diagonal is the line of equal flux. Moving up along the diagonal from the 19th century/pre-WWII values represents anthropogenic atmospheric fluxes.

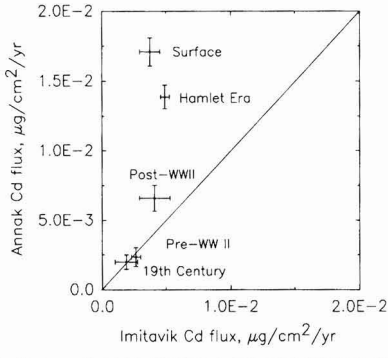

Figure 3. Comparative historical focus-corrected Cd fluxes to Imitavik and Annak. See Figure 2 caption for further explanation.

The most recent flux period covers the years from the establishment of the Hamlet of Sanikiluaq in 1967 to the sampling year (1983). Metal fluxes measured in the two lakes for this era show atmospheric inputs and the increased metal loads in Annak caused by sewage disposal. The surface sediment flux covers the last 1–3 years of this 16-year period, showing trends of the early 1980s.

Measurement of Anthropogenic Source Contributions. Total atmospheric burdens of each metal in Imitavik sediment are measured as the difference between total areal burden and total background burden. In Annak, the anthropogenic burden (sewage + atmospheric) is calculated as in Imitavik. The sewage burden in Annak is the difference between total anthropogenic burden and the atmospheric burden to Imitavik. It is assumed that the background metal fluxes to Imitavik and Annak have not changed during the 110-year period investigated here and that flux amounts in excess of this background are from anthropogenic sources.

Results and Discussion

Changes of Historical Fluxes. Figures 2–5 show the changes in individual metal fluxes occurring between historical periods. The diagonal lines in the figures represent equal flux to both lakes. The 19th century value is the background flux and, with the exception of Cu, is the same in both lakes. Points on the diagonal line above the background level show the anthropogenic contribution by the atmosphere, which is the same to both lakes. The vertical distance that a point lies above the diagonal rep-

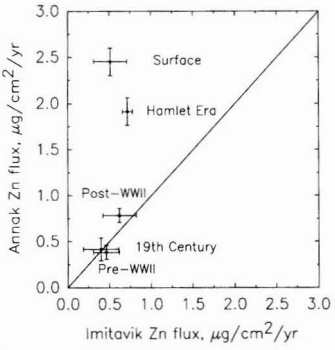

Figure 4. Comparative historical focus-corrected Zn fluxes to Imitavik and Annak. See Figure 2 caption for further explanation.

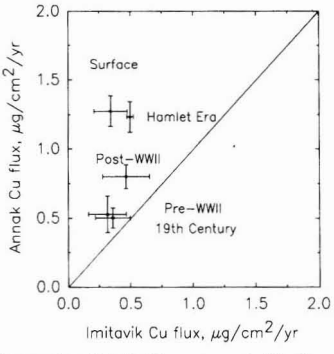

Figure 5. Comparative historical focus-corrected Cu fluxes to Imitavik and Annak. See Figure 2 caption for further explanation.

resents flux to Annak resulting from sewage disposal.

Figure 2 shows that the pre-WWII Pb fluxes to Imitavik and Annak are not significantly different from each other or from background. The post-WWII period Pb flux to both lakes was equal and approximately 2 times greater than background. During the Hamlet era (following 1968), the Pb flux to Imitavik was ~3 times greater than the background amount, while in Annak, the effect of sewage disposal increased the flux to greater than 5 times background. The Pb flux to surface sediment in Imitavik is lower than the Hamlet era flux, while it remains constant in Annak. If atmospheric deposition to the surface sediment has declined, then it appears that inputs from sewage have increased to maintain the constant Pb flux to Annak.

Figure 3 shows that the late-19th century and pre-WWII Cd background fluxes to both lakes are not significantly different. Post-WWII Cd deposition to Imitavik has nearly doubled and has increased even more in Annak. Since sewage disposal to Annak began after 1967, the appearance of greater Cd flux there than in Imitavik during the post-WWII era suggests inaccuracy in sediment dating or postdepositional migration of Cd. Since the excess Cd was probably deposited later, during the Hamlet era, the flux measured during the Hamlet era is probably less than the actual value. As shown, the Hamlet-era Cd flux to Annak is over 6 times greater than background and is 2 times greater than the post-WWII value. The Cd flux to Imitavik during the Hamlet years is again approximately double the background value and not significantly greater than post-WWII. The surface Cd flux is not significantly different from the Hamlet-era flux. In Annak the surface flux is nearly 8 times greater than background and greater than Hamlet-era flux, showing that Cd inputs in recent years are increasing relative to the average for the Hamlet era.

The Zn flux history in Imitavik shows a small atmospheric contribution following WWII. The Hamlet-era Zn flux is greater than background (see Figure 4), but the magnitude of the increase is less than that of Pb and Cd fluxes at that time. The surface Zn flux to Imitavik is roughly the same as the background level, suggesting that the anthropogenic atmospheric contribution to recent sediments is very low. Annak shows large Zn contributions from sewage; the Hamlet-era flux is 5 times background, while the surface flux is even more enriched, showing the same trend observed with Cd.

Cu flux history, shown in Figure 5, differs from the other metals because the background fluxes to the two lakes are different. Cu flux to Imitavik shows little change through these periods. The Hamlet-era flux is significantly greater than pre-WWII, but the amount is small. As with Cd, the post-WWII Cu flux to Annak is higher than expected and, again, may result from dating inaccuracy or postdepositional Cu migration. Sewage disposal during the Hamlet era has led to a Cu flux that is more than double the Annak background value.

The atmospheric flux of each of these four metals increased at some time following WWII. Greater industrial activity in the midlatitudes of North America and Europe or in Arctic regions outside North America during or following the war would contribute to these increases. This result has important application to materials that are transported to the Arctic through the atmosphere and form the Arctic Haze each spring (*26*, *27*).

The total atmospheric anthropogenic burdens of these metals (in $\mu g/cm^2$) are 4.6 for Pb, 0.077 for Cd, 4.0 for Zn, and 6.7 for Cu. The Pb value agrees well with an atmospheric burden of 4.2 $\mu g/cm^2$ measured from a lake in northern Quebec by Evans and Rigler (*9*). Their sampling site was ~420 km east from Sanikiluaq.

Recent fluxes of Pb may have declined, as indicated by the trends of fluxes to surface sediments. This has been observed by investigators outside the Arctic (*5*, *42*) and is attributed to lower metal emissions by industries and by decline in consumption of gasoline with Pb additives during the 1970s (*43*). However, the surface sediment data do not support a long-term trend because only 1–3 years of integrated flux are included in the surface measurements from Imitavik, less than the other historical periods used for comparison. Also, surface sediment in cores IN-7 and IN-9 may have been mixed, which would obscure the record of decreased flux and contribute to the broad error ranges in Imitavik surface fluxes.

Atmospheric Sources. All of the metals analyzed here are considered to be readily transported by the atmosphere (*44*). The relative amounts of anthropogenic metals in Imitavik sediments should then correspond to relative proportions of those metals emitted to the atmosphere from anthropogenic sources, or to atmospheric flux measurements. Estimates of global metal emissions from anthropogenic sources by Nriagu and Pacyna (*43*), Pacyna (*45*), and Galloway et al. (*25*) show ratios of total masses of the four metals of interest here to be Pb > Zn > Cu > Cd. However, relative burdens of anthropogenic trace metals in Imitavik sediment show a pattern of Zn > Pb > Cu > Cd. The latter pattern is similar to the relative amounts of these metals observed in wet deposition to rural and remote areas tabulated by Galloway et al. (*25*).

The fluxes of anthropogenic metals to Imitavik during the Hamlet era are similar to the measured atmospheric deposition at Moonbeam, ON (*46*), ~800 km to the

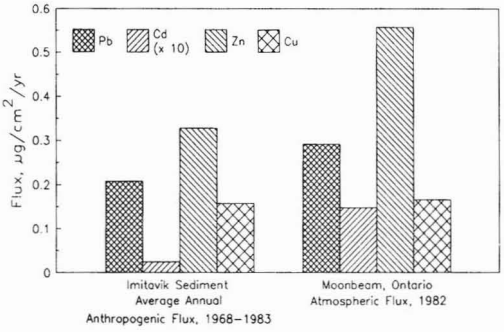

Figure 6. Average annual anthropogenic fluxes of Pb, Cd, Zn, and Cu to Imitavik sediment and atmospheric flux of Pb, Cd, Zn, and Cu to Moonbeam, ON, in 1982 (latter data from ref 46).

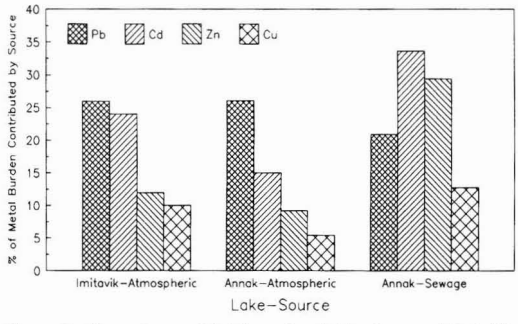

Figure 7. Percentages of total areal metal burdens contributed by atmospheric and sewage sources.

south-southwest (see Figures 1 and 6). The Moonbeam data are only for 1 year and show an unusually high level of Cd in comparison to other sites in Ontario (*46*). However, the similarity of fluxes and the relative values between metals suggest that the source of these metals at both sites is characteristic of the rural/remote type. The Imitavik sediment fluxes are less than the Moonbeam values because of an expected northward decline in wet deposition of metals caused by lower precipitation amounts and lower metal washout in the North (*47*). The Moonbeam flux data may be higher because they also include both anthropogenic and background fluxes from the atmosphere.

Pb is the most anthropogenically enriched of the four metals measured in Imitavik sediment although second to Zn in total pollutant mass (see Figure 7). It has been recognized for many years that Pb compounds used as antiknock additives in gasoline were transported through the atmosphere and appear in lake sediments (*41*). The similarity of historical patterns between gasoline-based Pb consumption in the United States and the anthropogenic Pb in Imitavik sediment suggests that much of the Pb found in the lake sediment may have originated from motor fuel (see Figure 8). A further indication of this relationship is the significantly lower Pb flux to Imitavik surface sediments in comparison with the 1968–1983 period, representing the Hamlet era (see Figure 2). Consumption of gasoline with Pb additives declined sharply during the latter part of this period (*40*).

The other metals analyzed here do not have singular sources to the atmosphere comparable to Pb so that flux histories cannot be associated with any particular sources or events.

The atmosphere is the source of 25% or less of the total sediment burden of these metals in either Imitavik or

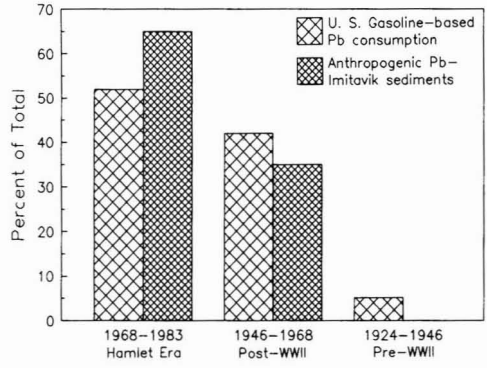

Figure 8. Historical distribution of U.S. gasoline-based Pb consumption and of anthropogenic Pb in Imitavik sediments. The percentages of each source add to 100. Gasoline data are from ref 42.

Annak (see Figure 7). These amounts are significant but are small in comparison to burdens in midlatitude lakes. Sediment analyses of Lake Michigan, for example, show that more than 75% of Pb and Cd and greater than 50% of Zn inputs are from anthropogenic sources (*2*).

Sewage Sources. In comparison with the atmospheric contribution to Annak, sewage from an average population in Sanikiluaq of ~300 persons over 15 years is the source of over twice as much Cd, over 5 times as much Zn, and 40% more copper than the atmosphere (see Figure 7). The Pb contribution from sewage is only ~78% as much as from the atmosphere.

In comparison to the background burdens, Cd is more enriched by sewage dumped into Annak than any of the other metals. Studies of human exposure to metals from ingestion and inhalation show high exposure of the Inuit to Cd. An investigation of Inuit exposure to metals in Greenland showed that Cd dietary intake was 12 times the provisional tolerable weekly intake (PTWI) established by the World Health Organization (*48*). Seal kidney and liver, typical components of the Inuit diet, are concentrated sources of Cd (*49*). Investigations of Greenland Inuit by Hansen (*48*) showed a significant relationship between blood Cd concentrations and cigarette smoking, a habit practiced widely in Sanikiluaq. These results suggest a link between human exposure to Cd and the elevated amounts found in Annak sediments.

Klein et al. (*50*) observed that residential waste from New York City contributed more Cd, Zn, and Cu to treatment plants than any other source, including industries known for large quantities of metal discharge. This result is consistent with the heavy loading of Cd and Zn in Annak from human waste, although residential wastes from New York include metals from household products and plumbing systems.

The elevated metal concentrations in Annak sediments since the beginning of the Hamlet era show that this treatment method is removing some of the metal load in sewage. Since sewage input to Annak is unknown, metal removal efficiency cannot be measured. However, Soniassy and Lemon (*23*) estimated that a serial lagoon treatment system in subarctic Yellowknife, NT, removes 83% of Pb, 90% of Cd and Zn, and 60% of Cu. Lagoon treatment thus can be an effective means of removing metals from sewage in cold environments.

Conclusion

Fluxes of Pb, Cd, Zn, and Cu from the atmosphere to lake sediments in southeastern Hudson Bay increased

following World War II apparently in response to greater emissions to the atmosphere in midlatitudes. The relative amounts of these metals in atmospheric flux are characteristic of rural/remote deposition, and during the last 15 years of record, the actual fluxes are similar to atmospheric deposition in a remote area farther south. The source of these enriched amounts of metals is probably from outside of the North American Arctic. Although the atmosphere has delivered more metals to arctic lakes since World War II, the burdens attributable to the atmosphere are not more than 26% of the total metal burden in sediment of an otherwise undisturbed lake.

Disposal of human waste into a small arctic lake caused large increases in sediment fluxes of all metals measured, although Cd and Zn were most enriched relative to sediment background amounts. Approximately one-third of the total burden of Cd and Zn are attributable to sewage inputs. The deposition of metals from sewage shows that the pond type of waste disposal system is removing some of the metals load from sewage.

Acknowledgments

Several residents of Sanikiluaq, including John Jamieson, Johnny Meeko, and Hamlet administrative officer Lucassie Kittosuk, helped with this work by providing lodging, scuba gear, and temporary laboratory space. J. R. Brozowski helped with sampling work. P. D. Anderson and R. W. Paddock helped with metal analysis. Jane Domier prepared the map. Special thanks to Donn Haglund, who arranged my first visit to the study site and who encouraged later work. This research was conducted under the authority of the Science Advisor of the Northwest Territories, Canada, Scientific Research License 2803.

Registry No. Pb, 7439-92-1; Cd, 7440-43-9; Zn, 7440-66-6; Cu, 7440-50-8.

Literature Cited

(1) Charles, M. J.; Hites, R. A. In *Sources and Fates of Aquatic Pollutants*; Hites, R. A.; Eisenreich, S. J., Eds.; American Chemical Society: Washington, DC, 1987; Chapter 12.
(2) Christensen, E. R.; Chien, N. K. *Environ. Sci. Technol.* **1981**, *15*, 553–558.
(3) Edgington, D. N.; Robbins, J. A. *Environ. Sci. Technol.* **1976**, *10*, 266–274.
(4) Bruland, K. W.; Bertine, K.; Koide, M.; Goldberg, E. D. *Environ. Sci. Technol.* **1974**, *8*, 425–432.
(5) Verta, M.; Tolonen, K.; Simola, H. *Sci. Total Environ.* **1989**, *87/88*, 1–18.
(6) Evans, R. D.; Rigler, F. H. *Environ. Sci. Technol.* **1980**, *14*, 216–218.
(7) Johansson, K. *Water, Air, Soil Pollut.* **1989**, *47*, 441–455.
(8) Nriagu, J. O.; Kemp, A. L. W.; Wong, H. K. T.; Harper, N. *Geochim. Cosmochim. Acta* **1979**, *43*, 247–258.
(9) Evans, R. D.; Rigler, F. H. *Water, Air, Soil Pollut.* **1985**, *24*, 141–151.
(10) Ouellet, M.; Jones, H. G. *Can. J. Earth Sci.* **1984**, *20*, 23–36.
(11) Muller, G.; Barsch, D. *Environ. Technol. Lett.* **1980**, *1*, 131–140.
(12) Murozumi, M.; Chow, T. J.; Patterson, C. *Geochim. Cosmochim. Acta* **1969**, *33*, 1247–1294.
(13) Herron, M. M.; Langway, C. C., Jr.; Weiss, H. V.; Cragin, J. H. *Geochim. Cosmochim. Acta* **1977**, *41*, 915–930.
(14) Wolff, E. W.; Peel, D. A. *Nature* **1985**, *313*, 535–540.
(15) Weiss, H.; Bertine, K.; Koide, M.; Goldberg, E. D. *Geochim. Cosmochim. Acta* **1975**, *39*, 1–10.
(16) Mart, L. *Tellus* **1983**, *35B*, 131–141.
(17) Ross, H. B.; Granat, L. *Tellus* **1986**, *38B*, 27–43.
(18) Davidson, C. I.; Chu, L.; Grimm, T. C.; Nasta, M. A.; Qamoos, M. P. *Atmos. Environ.* **1981**, *15*, 1429–1437.
(19) Boutron, C. *Geochim. Cosmochim. Acta* **1979**, *43*, 1253–1258.
(20) Barrie, L. A.; Vet, R. J. *Atmos. Environ.* **1984**, *18*, 1459–1469.
(21) Gorzelska, K. *Atmos. Environ.* **1989**, *23*, 2729–2737.
(22) Miyamoto, H. K.; Heinke, G. W. *Can. J. Civil Eng.* **1979**, *6*, 324–328.
(23) Soniassy, R. N.; Lemon, R. *Water Sci. Technol.* **1986**, *18*, 129–139.
(24) Nriagu, J. O.; Wong, H. K. T.; Coker, R. D. *Environ. Sci. Technol.* **1982**, *16*, 551–560.
(25) Galloway, J. N.; Thornton, J. D.; Norton, S. A.; Volchok, H. L.; McLean, R. N. A. *Atmos. Environ.* **1982**, *16*, 1677–1700.
(26) Rahn, K. A. *Atmos. Environ.* **1981**, *15*, 1507–1516.
(27) Barrie, L. A.; Hoff, R. M.; Daggupaty, S. M. *Atmos. Environ.* **1981**, *15*, 1407–1419.
(28) Hermanson, M. H. *Geochim. Cosmochim. Acta* **1990**, *54*, 1443–1452.
(29) Stephenson, T. In *Heavy Metals in Wastewater and Sludge Treatment Processes*; Lester, J. N., Ed.; CRC Press: Boca Raton, FL, 1987; Vol. I, Chapter 2.
(30) Samuels, E. R.; Meranger, J. C. *Water Res.* **1984**, *18*, 75–80.
(31) Krishnamurty, K. V.; Shpirt, E.; Reddy, M. M. *At. Absorpt. Newsl.* **1976**, *15*, 68–70.
(32) Katz, S. A.; Jenniss, S. W.; Mount, T.; Tout, R. E.; Chatt, A. *Int. J. Environ. Anal. Chem.* **1981**, *9*, 209–220.
(33) Sturgeon, R. E.; Desaulniers, J. A. H.; Berman, S. S.; Russell, D. S. *Anal. Chim. Acta* **1982**, *134*, 283–291.
(34) Bettinelli, M.; Pastorelli, N.; Baroni, U. *Anal. Chim. Acta* **1986**, *185*, 109–117.
(35) Keith, L. H.; Libby, R. A.; Crummett, W.; Taylor, J. K.; Deegan, J., Jr.; Wentler, G. *Anal. Chem.* **1983**, *55*, 2210–2218.
(36) Appleby, P. G.; Oldfield, F. *Catena* **1978**, *5*, 1–8.
(37) Christensen, E. R.; Bhunia, P. K. *J. Geophys. Res.* **1986**, *91C*, 8559–8571.
(38) Hermanson, M. H.; Christensen, E. R.; Buser, D. J.; Chen, L. M. *J. Great Lakes Res.* **1991**, *17*, 94–108.
(39) Eisenreich, S. J.; Capel, P. D.; Robbins, J. A.; Bourbonniere, R. *Environ. Sci. Technol.* **1989**, *23*, 1116–1126.
(40) Boyle, E. A.; Chapnick, S. D.; Shen, G. T. *J. Geophys. Res.* **1986**, *91C*, 8573–8593.
(41) Nriagu, J. O. *Nature* **1979**, *279*, 409–411.
(42) Rippey, B. *Philos. Trans. R. Soc. London* **1990**, *327B*, 311–317.
(43) Nriagu, J. O.; Pacyna, J. M. *Nature* **1988**, *333*, 134–139.
(44) Lantzy, R. J.; Mackenzie, F. T. *Geochim. Cosmochim. Acta* **1979**, *43*, 511–525.
(45) Pacyna, J. M. In *Toxic Metals in the Atmosphere*; Nriagu, J. O., Davidson, C. I., Eds.; John Wiley & Sons: New York, 1986; Chapter 2.
(46) Chan, W. H.; Chung, D.; Tang, A. J. S. *Acidic Precipitation in Ontario Study. Precipitation Concentration and Wet Deposition Fields of Pollutants in Ontario*, 1982; ARB-142-84-ARSP API-12-84; Ontario Ministry of the Environment: Toronto, ON, Canada, 1984.
(47) Hardy, E. P.; Meyer, M. W.; Allen, J. S.; Alexander, L. T. *Nature* **1968**, *219*, 584–587.
(48) Hansen, J. C. In *Arctic Air Pollution*; Stonehouse, B., Ed.; Cambridge University Press: Cambridge, U.K., 1986; pp 249–257.
(49) Nordstrom, R. J.; Schweinsberg, R. E.; Collins, B. T. *Sci. Total Environ.* **1986**, *48*, 195–212.
(50) Klein, L. A.; Lang, M.; Nash, N.; Kirschner, S. L. *J.—Water Pollut. Control Fed.* **1974**, *46*, 2653–2662.

Received for review February 12, 1991. Revised manuscript received June 17, 1991. Accepted June 28, 1991.

Environ. Sci. Technol. **1991**, *25*, 2065–2070

Kinetics and Transport Parameters for the Fixed-Bed Catalytic Incineration of Volatile Organic Compounds

Albert C. Frost, John E. Sawyer, and Jerry C. Summers

Allied Signal Inc., Tulsa, Oklahoma 74104

Yatish T. Shah* and Carlos G. Dassori

College of Engineering and Applied Sciences, The University of Tulsa, Tulsa, Oklahoma 74104

■ The accurate sizing of a commercial catalytic incinerator from laboratory data requires a comprehensive mathematical model for the reactor. Allied Signal has developed one such model, which is capable of (a) predicting Langmuir–Hinshelwood rate constants and the alumina layer mass-transfer coefficient through a nonlinear regression fitting of the experimental data obtained in a laboratory adiabatic, fixed-bed reactor and (b) sizing a commercial reactor for the desired performance for given sets of kinetic and transport parameters. The model considers axial dispersion of both mass and heat as well as mass-transfer resistance at the gas–solid interface. The mathematical model correlated the experimental data for the conversions of *n*-hexane, *n*-octane, *n*-decane, and *n*-dodecane well over wide ranges of superficial gas velocities, bed depths, temperatures, and inlet concentrations.

Introduction

Catalytic incineration has become a desirable way to control the emission of volatile organic compounds (VOCs). Its relatively low operating temperature requires less fuel and less expensive materials of construction than does thermal incineration.

The proper design of a fixed-bed reactor for catalytic incineration requires the knowledge of kinetic and transport parameters, and an appropriate mathematical description of the reactor behavior. This description has usually been in the form of a simple isothermal model having a single global rate constant (*1*).

A more sophisticated model is presented in this paper that incorporates a Langmuir–Hinshelwood kinetic expression, a bulk film mass-transfer coefficient for the gas flowing around the catalyst pellets, a solid mass-transfer coefficient for any layer of refractory support (e.g., alumina) that may be covering the noble metal, and the dispersion coefficients for the mass and heat along the length of the reactor. The model can also be modified slightly to describe these same rate processes in a monolithic bed.

This model is used to estimate four Langmuir–Hinshelwood constants and the mass-transfer coefficient for the alumina layer covering the platinum from laboratory temperature–conversion data for *n*-hexane, *n*-octane, *n*-decane, and *n*-dodecane. The curves generated by the model using these derived rate constants closely match the experimental curves for conversions over a wide range of space velocities, bed depths, and temperatures. Such a capability makes the model a valuable tool for predicting the performance of commercial reactors.

Mathematical Model

The present model for the fixed-bed reactor containing spherical particles is somewhat similar in character to the one presented by Carberry and Wendel (*2*). It incorporates a different fluid–solid mass-transfer mechanism and uses simpler heat equations, which reduces the number of unknown constants that need to be derived from the data. It makes the following assumptions:

(1) The reactor is operated under adiabatic and steady-state conditions.

(2) There are no radial concentration or temperature gradients.

(3) The axial mass and temperature dispersions are characterized by the usual dispersion coefficients.

(4) The mass-transfer resistance through the gas film surrounding each catalyst particle is characterized by the usual bulk film mass-transfer coefficient. The corresponding heat-transfer resistance is neglected.

(5) The noble metal is deposited on a refractory oxide (e.g., alumina) support as a single film. This film can reside either on the outside surface of the support or at some discrete distance within the support. The mass transfer through the resulting alumina layer is described with a solid mass-transfer coefficient. The corresponding heat-transfer resistance is once again neglected.

(6) The intrinsic reaction rate for the oxidation of the VOCs follows the Langmuir–Hinshelwood kinetic expression. The oxygen concentration is assumed to be in excess and is not explicitly incorporated into the expression.

(7) The heat of reaction for the VOCs and the heat capacity of the gas stream are independent of temperature.

(8) The temperature dependence of the gas flow rate, concentration, and density are governed by the ideal gas law.

(9) The temperature dependence of the bulk film mass-transfer coefficient follows the relationship described by Thoenes and Kramers (*3*).

(10) As shown by Oh et al. (*4*) for an effective diffusion coefficient in an alumina particle, the temperature dependence of the solid mass-transfer coefficient is assumed to be proportional to the absolute temperature raised to the 1.4 power.

Figure 1 illustrates a schematic of the concentration profile across the exterior bulk gas film and the alumina layer that covers the film of noble metal. It is worth noting that while the alumina layer may slow down the rate of a simple first-order reaction, it may actually increase the rate of a Langmuir–Hinshelwood reaction, particularly for the case where the reactant is strongly adsorbed (*5*).

Governing Equations

With the previous assumptions, a differential material balance for the reacting VOC species can be expressed as

$$\frac{d}{dx}\left(D_e \frac{dC}{dx}\right) - \frac{d}{dx}(uC) - k_g a_v (C - C^*_s) = 0 \quad (1)$$

At steady state, the mass-transfer rates can be equated to the rate of reaction as

$$k_g a_v (C - C^*_s) = D_s a'_v / L^* (C^*_s - C_s) = (1 - \epsilon) w r_A \quad (2)$$

*Present address: College of Engineering, Drexel University, Philadelphia, PA 19104.

0013-936X/91/0925-2065$02.50/0

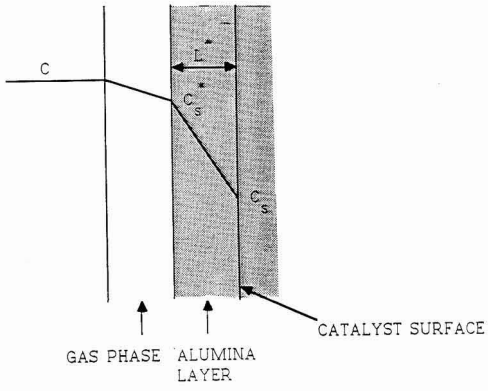

Figure 1. Mass transfer resistances across the bulk gas film and the alumina.

where the intrinsic kinetic reaction rate is expressed by a Langmuir–Hinshelwood equation of the type

$$r_A = \frac{k_\infty \exp(-E/R_gT)C_s}{[1 + k'_\infty \exp(q/R_gT)C_s]^2} \tag{3}$$

Equations 1–3 are subjected to the boundary conditions

$$\text{at } x = 0 \qquad u(C_0 - C) = -D_e\,(dC/dx) \tag{4}$$

$$\text{at } x = L \qquad dC/dx = 0 \tag{5}$$

The differential heat balance for the reactor can be expressed as

$$\frac{d}{dx}\left(\lambda_e \frac{dT}{dx}\right) - \frac{d}{dx}(u\rho c_p T) + (-\Delta H_R)(1 - \epsilon)wr_A = 0 \tag{6}$$

subjected to the boundary conditions

$$\text{at } x = 0 \qquad \rho c_p u(T_0 - T) = -\lambda_e\,(dT/dx) \tag{7}$$

$$\text{at } x = L \qquad (dT/dx) = 0 \tag{8}$$

Finally, the continuity equation leads to

$$(d/dx)(\rho u) = 0 \tag{9}$$

The above equations can be dedimensionalized by using the expressions

$$\bar{C} = (C_0 - C)/C_0 \tag{10}$$

$$\bar{C}_s = (C_0 - C_s)/C_0 \tag{11}$$

$$\bar{C}^*_s = (C_0 - C^*_s)/C_0 \tag{12}$$

$$z = x/L \tag{13}$$

$$\alpha_m = k_g{}^o a_v L/u_0 \tag{14}$$

$$\text{Bi} = D^*_s a'_v L/L^* u_0 \tag{15}$$

$$D^*_s = D_s^{ref}(T/T^{ref})^{1.4} \tag{16}$$

$$\Omega = k'_\infty C_0 \tag{17}$$

$$\text{Da} = (1 - \epsilon)wk_\infty L/u^o \tag{18}$$

$$\gamma = E/R_gT_0 \tag{19}$$

$$\gamma' = q/R_gT_0 \tag{20}$$

$$\theta = (T - T_0)/T_0 \tag{21}$$

$$\beta = (-\Delta H_R)C_0/\rho^0 C_p T_0 \tag{22}$$

$$\text{Pe}_m = u_0 L/D_e \tag{23}$$

$$\bar{r}_A = (1 - \epsilon)wr_A L/C_0 u_0 \tag{24}$$

$$\bar{\rho} = \rho/\rho^o \tag{25}$$

$$\bar{u} = u/u^o \tag{26}$$

$$\text{Pe}_h = \rho^o C_p u^0 L/\lambda_s \tag{27}$$

$$\bar{k}_g = k_g/k^o{}_g \tag{28}$$

$$\bar{D}_s = D_s/D^o{}_s \tag{29}$$

which leads to the dimensionless expressions

$$\frac{1}{\text{Pe}_m}\frac{d}{dz}\left(\frac{d\bar{c}}{dz}\right) + \frac{d}{dz}(\bar{u}(1 - \bar{C})) - \alpha_m \bar{k}_g(\bar{C} - \bar{C}^*_s) = 0 \tag{30}$$

$$\alpha_m \bar{k}_g(\bar{C}^*_s - \bar{C}) = \text{Bi}\bar{D}_s(\bar{C}_s - \bar{C}^*_s) = \bar{r}_A \tag{31}$$

$$\bar{r}_A = \frac{\text{Da}(1 - \bar{C}_s)\exp(-\gamma/(1 + \theta))}{[1 + \Omega(1 - \bar{C}_s)\exp(\gamma'/(1 + \theta))]^2} \tag{32}$$

with the boundary conditions

$$\text{at } z = 0 \qquad (1/\text{Pe}_m)(d\bar{C}/dz) = \bar{u}\bar{C} \tag{33}$$

$$\text{at } z = 1 \qquad d\bar{C}/dz = 0 \tag{34}$$

Similarly, the differential heat balance equation can be expressed as subject to the boundary conditions

$$\frac{1}{\text{Pe}_h}\frac{d}{dz}\left(\frac{d\theta}{dz}\right) - \frac{d}{dz}(\bar{\rho}\bar{u}(1 + \theta)) + \beta\bar{r}_A = 0 \tag{35}$$

$$\text{at } z = 0 \qquad \bar{\rho}\bar{u}\theta = (1/\text{Pe}_h)(d\theta/dz) \tag{36}$$

$$\text{at } z = 0 \qquad d\theta/dz = 0 \tag{37}$$

Finally, the continuity equation can be expressed as

$$(d/dz)(\bar{\rho}\bar{u}) = 0 \tag{38}$$

The temperature dependence of the gas density is based on the ideal gas law. The gas–solid mass-transfer coefficient, the gas viscosity, and the temperature coefficient for the VOC–air diffusivity are calculated from correlations presented by Theones and Kramers (*3*), Reid et al. (*6*), and Benton and Hewitt (*7*), respectively. Mass and heat Peclet numbers for the reaction conditions examined in this study are based on the particle diameter and are estimated to have a value of 2 (*8*). The above equations do not consider the effect of temperature change on the gas-phase concentration. The equations are strictly appropriate only when heat generation and temperature rise are small.

In the present analysis the above described model is fitted to the experimental temperature–conversion data by optimizing tried values for the four rate parameters in the Langmuir–Hinschelwood kinetic expression and for the mass-transfer coefficient for the alumina layer covering the noble metal. IMSL's DBCLSF optimization routine is used to obtain the nonlinear regressive fitting along the entire range of the temperature–conversion curve. This optimization routine relies on IMSL's DBVPFD boundary value problem solver routine to find each of the calculated conversions for each set of reiterated rate constants.

The calculations start with a set of values for the parameters and the system of differential equations is solved by DBVPFD mathematics routine. As a result, the exit conversion that satisfies the boundary conditions is obtained. These results are taken by the mathematics subroutine DBCLSF, which is essentially the implementation of the Marsquordt algorithm, and a better set of param-

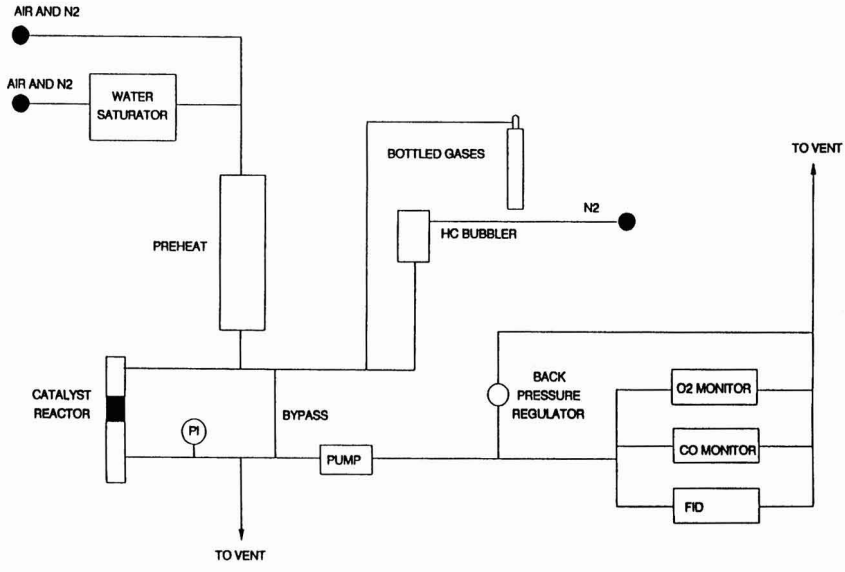

Figure 2. Experimental apparatus.

eters is computed. The process is repeated until no further improvement of the fitting is found. The result is the set of parameters that best fit the data with the predictions of the model.

Once the five rate constants are found in this manner, they can be fed back into the program to determine design parameters for commercial reactors. These design parameters can be either the space velocity required for a new reactor to attain a targeted conversion or the conversion that will result from an existing reactor having a fixed catalyst volume and a fixed volumetric flow rate. The form of the model that solves for the space velocity of a new commercial reactor uses both routines and reiterates in reactor diameter (for a given bed depth) until the prescribed destruction efficiency is achieved. The form of the model that solves for the destruction efficiency of an existing commercial reactor requires only a single pass through the DBVPFD program.

Experimental Section

Reactor System. A schematic of the experimental system is outlined in Figure 2. It shows that metered air and nitrogen streams are passed through water and liquid hydrocarbon saturators, respectively, before they are combined with an additional nitrogen stream to form the inlet feed stream to the reactor. The relative amounts of these streams are such that the combined feed stream has a 50% relative humidity at room temperature and contains 12% oxygen. The total volumetric flow rate is checked with a piston-type flow rate calibrator (Tracor Atlas, Inc.).

The water-saturated air stream and the additional nitrogen stream are passed through a preheater before they are joined by the hydrocarbon-saturated nitrogen stream at the inlet of the reactor. The combined stream then passes down through the catalyst bed (typically 1.0 in. in diameter and 4.0 in. long).

The effluent stream is cooled through a coil before it is split into two parts; one part goes directly to vent and the other to a sample pump that pressurizes it to 6 psig. A small portion of this pressurized stream is fed to the FID, while the rest is passed through a back-pressure regulator and out to vent. This arrangement gives a rapid analytical response and a means of keeping the pressure at the outlet of the reactor to very close to ambient pressure.

Run Procedure. The FID reading for the inlet hydrocarbon concentration is obtained by analyzing the inlet stream as it is bypassed around the reactor. During this time the preheater and reactor are heated to approximately 200 °F. The run starts when the bypassed fluid is directed through the reactor and the temperatures of the preheater and reactor are increased at a rate of 85 °F/h. The temperatures at the top (inlet), wall, and bottom (outlet) of the bed are recorded with the corresponding FID reading at every 25 °F temperature rise. The outlet temperature is adjusted in respect to the inlet temperature to reflect the expected temperature rise resulting from the oxidation of the VOCs, while the wall temperature is maintained at an intermediate temperature. Most of the runs are made at low VOC concentrations and, hence, with temperature rises that are less than 75 °F.

The experimental data were obtained for *n*-hexane, *n*-octane, *n*-decane, and *n*-dodecane with a 2–4-in. catalyst bed, at 15000–45000 h^{-1} GHSVs and in the temperature range of 260 to 750 °F. The inlet concentration was varied from 37 to 234 ppm.

Catalyst. The catalyst was in the form of a 0.12-in.-diameter alumina spheres with the platinum distributed as a sharp Gaussian curve slightly below the outer surface, with a resultant average layer loading of approximately 0.2 wt % platinum. The fresh BET surface area was 100 m^2/g and the fresh pore volume totaled 1.09 mL/g, 69% of which was wider than 1000 Å. It was activated by heating to 1300 °F for 16 h in air that had been saturated with water at room temperature and subsequently subjecting it to a 950 °F, 2000 ppm, 67 vol % propylene/33 vol % propane stream for 4 h.

Results

Figure 3 shows the fits of the mathematical model to the *n*-decane and *n*-dodecane data at 15 000 h^{-1} GHSV. The value for the transport parameter $D_s^{ref}a'_v/L^*$ was determined by applying the model to the experimental data for *n*-dodecane for the conditions where mass transfer is the rate-controlling step. This is at the high-temperature plateau region of the temperature–conversion curve, where the kinetic rate is assumed to be infinitely fast and only

Table I. Derived Rate Constants from Data Shown in Figure 8 (GHSV = 30 000 h^{-1})

component	k_∞, m^3/kg·s	E, kJ/kmol	k'_∞, m^3/kmol	q, kJ/kmol	$D_s^{ref}a'_v/L^*$, s^{-1}
n-C_6	9.2×10^3	2.1×10^4	1.6	4.7×10^4	127.7
n-C_8	6.2×10^4	2.9×10^4	10.0	3.3×10^4	110.4
n-C_{10}	5.2×10^5	3.0×10^4	5.6×10^2	1.7×10^4	96.4
n-C_{12}	1.0×10^7	4.0×10^4	10.0	1.2×10^4	88.0

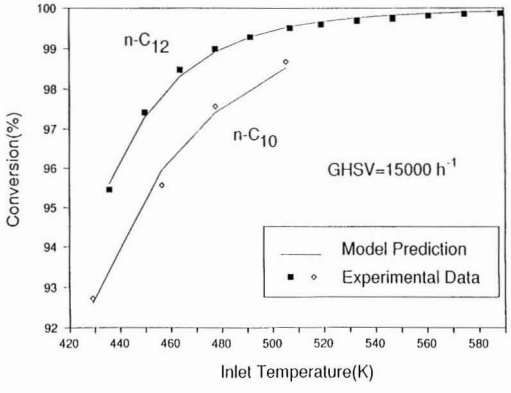

Figure 3. Fit of n-decane and n-dodecane data with model.

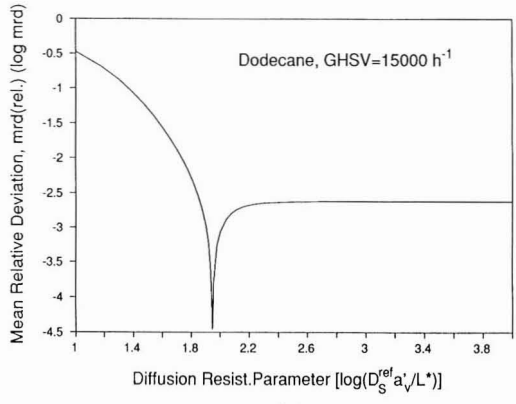

Figure 4. Effects of changing $D_s^{ref}a'_v/L^*$ on predicted minus experimental values.

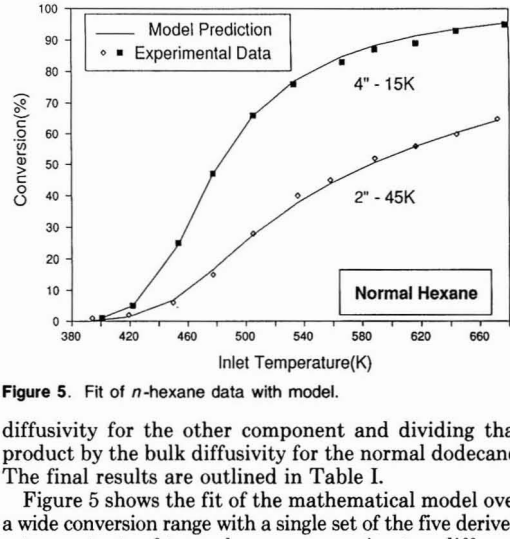

Figure 5. Fit of n-hexane data with model.

the bulk gas film and alumina layer mass-transfer steps control the reaction process. Since the bulk gas film mass-transfer coefficient is estimated from the literature, the alumina layer mass-transfer coefficient is the only unknown in the solution of the mathematical equations.

The value for $D_s^{ref}a'_v/L^*$ obtained in this manner was 88 s^{-1} at 225 °F, which was in good general agreement with a 190 s^{-1}; a value calculated from the effective diffusivity for CO in a Pt/alumina catalyst reported by Oh et al. (*4*). It should be mentioned that $D_s^{ref}a'_v/L^*$ is estimated from a small difference between two large numbers (the predicted conversion minus the experimental conversion) and consequently is sensitive to experimental error. While this experimental error affects the absolute magnitude of $D_s^{ref}a'_v/L^*$, the absolute magnitude has a negligible effect on the fitting of the data below the plateau portion of the temperature–conversion curve.

It is difficult and time consuming to solve for $D_s^{ref}a'_v/L^*$ simultaneously with the four Langmuir–Hinschelwood constants. The reason for this is shown by Figure 4 which plots the absolute value of the mean relative deviation of the fit [(predicted conversion for any assigned value for $D_s^{ref}a'_v/L^*$ − experimental conversion)/(experimental conversion)] as a function of different assigned values for the alumina mass-transfer coefficient for n-dodecane. When this coefficient is set at a value lower than the exact calculated value (indicated by the sharp minimum in Figure 4), it itself is rate limiting and has a pronounced effect on the mean relative deviation. However, when the coefficient is set at a value higher than the calculated value, it quickly loses its rate-determining influence over to the bulk gas film coefficient, and the mean relative deviation starts to level off. This resulting plateau causes an unacceptable large increase in computer time when attempts are made to calculate the alumina mass-transfer coefficient simultaneously with the four Langmuir–Hinshelwood constants.

Since the major component of the diffusion through the alumina layer is believed to be bulk film diffusion through the macropores (*4*), the alumina layer mass-transfer coefficients for the other hydrocarbons were estimated by multiplying the coefficient for the n-dodecane by the bulk diffusivity for the other component and dividing that product by the bulk diffusivity for the normal dodecane. The final results are outlined in Table I.

Figure 5 shows the fit of the mathematical model over a wide conversion range with a single set of the five derived rate constants of two n-hexane runs using two different superficial velocities and two different bed lengths to achieve their two different space velocities. The model matches the data well over the full range of lower conversions (where the two adsorption rate constants in the denominator of the Langmuir–Hinshelwood expression were significant), of intermediate conversions (where all five rate constants were significant), and of higher conversions (where the mass-transfer constants begin to dominate).

Figure 6 shows the effect of bed depth on dispersion for the 15 000 h^{-1} GHSV n-hexane run at 700 °F (corresponding to a 94% conversion). As L/D_b increases, the dispersion model predicts conversion very close to the one predicted by the plug flow model. For shorter beds, the axial dispersion will play a significant role and the dispersion model will predict the conversion considerably lower from the one predicted by the plug flow model. The

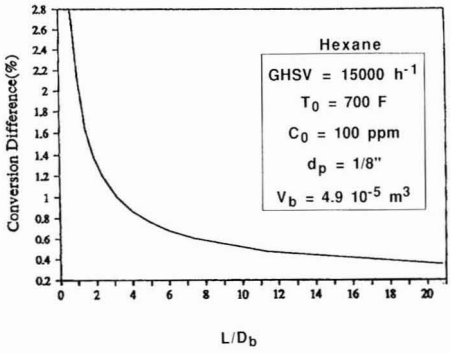

Figure 6. Percentage difference (plug flow to dispersion) in conversion as a function of L/D_b.

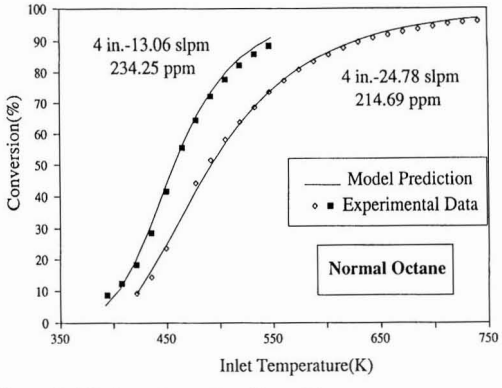

Figure 7. Fit of *n*-octane data with model.

4-in. bed used ($L/D_b = 1$) in this run is shown to have a degree of dispersion that causes the conversion in the experimental bed to be 0.9% lower than that which would result if the bed behaved as an ideal plug flow reactor. If the 3.1-in.[3] bed had a larger diameter and a correspondingly shallower depth, to the point where the bed length to bed diameter ratio was less than 1, the degree of dispersion would have grown exponentially. On the other hand, smaller diameters and correspondingly longer beds would cause the degree of dispersion to go asymptotically toward zero. However, it should be mentioned that even a 0.5% difference in conversions predicted by dispersed flow and plug flow could be significant from a design viewpoint at high conversions, and thus the dispersion coefficients are important components of the mathematical model.

Figure 7 shows the fit of the mathematical model over a wide conversion range with a single set of the five derived rate constants for two *n*-octane runs using two different superficial velocities with the same 4-in. deep bed. Again, the model fits the data well throughout most parts of the two curves.

Figure 8 shows the model data matching for *n*-hexane, *n*-octane, *n*-decane, and *n*-dodecane at 30 000 h^{-1} GHSV. The alumina layer mass-transfer coefficients are obtained from the data of *n*-dodecane in the manner described above, and the four Langmuir–Hinshelwood rate constants, determined from their displayed matches, are listed in Table I. It can be seen that the higher degree of activity shown for the higher molecular weight hydrocarbons in Figure 8 was caused by the orders of magnitude increase in the values for the preexponential term k_∞, with the apparent activation energy E changing only slightly. The

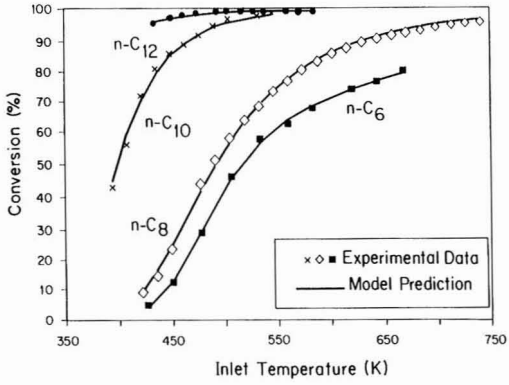

Figure 8. Fit of *n*-hexane, *n*-octane, *n*-decane, and *n*-dodecane data with model at GHSV = 30 000 h^{-1}.

changes in the adsorption constants were less dramatic.

The apparent activation energies (E) listed in Table I were 50–70% lower than the approximately 74 kJ/mol activation energy derived from simple power law rate expressions (*9*, *10*) for alkanes higher than butane. Such discrepancies could be expected in view of the fact that the apparent activation energy in the Langmuir–Hinshelwood equation is separated from the temperature-dependent adsorption effects present in the dnominator, whereas the activation energy in the power law equation incorporates these temperature-dependent adsorption effects.

The adsorption constant present in the denominator of the Langmuir–Hinshelwood equation used in this paper incorporates terms for the adsorption of both the hydrocarbon and oxygen. Consequently, its value by itself has no clear meaning. However, it is worth noting the general agreement between the reported values for the apparent heat of adsorption, q, listed in Table I and the heats of condensation for *n*-hexane and *n*-octane. The lower q values for the *n*-decane and *n*-dodecane may be due to a large experimental error associated with the scarcity of low-temperature, low-conversion data for these two species.

The model described in this article is a predictive model, since it is developed from the first set of principles of mass and energy balances. The fit of the model to the experimental data with two different flow rates through two different bed volumes (see Figure 5), with two different flow rates through the same bed volume (see Figure 7), and with other data at a 15 000 h^{-1} GHSV supports the predictability of the model. Additionally, the rate parameters obtained in this study compare well with the values reported in the literature. The model can be used to design a commercial reactor, as long as the assumptions made in the development of the model are valid. Unfortunately, at the present time we do not have data from a commercial operation to assess the validity of this claim.

Conclusions

The mathematical model developed to extract four Langmuir–Hinschelwood rate constants and an alumina layer mass-transfer coefficient fitted the experimental data well for *n*-hexane, *n*-octane, *n*-decane, and *n*-dodecane over wide ranges of conversions for different bed depths and superficial velocities.

Glossary

a_v	specific interface area, m^{-1}
Bi	defined in eq 15

C	gas-phase reactant concentration in bulk gas, kmol/m^3
$\bar{C}$	dimensionless concentration defined by eq 10
C_0	inlet concentration, kmol/m^3
C_p	heat capacity, kJ/kg·K
C_s	gas-phase reactant concentration at the active catalyst film, kmol/m^3
$\bar{C}_s$	dimensionless concentration defined by eq 11
$\bar{C}^*_s$	dimensionless concentration defined by eq 12
d_p	diameter of catalyst particle, m
Da	dimensionless parameter defined by eq 18
D_b	diameter of catalyst bed, m
D_0	axial dispersion coefficient for mass, m^2/s
D_s^{ref}	reference constant in eq 16
D_s	effective diffusion coefficient in alumina layer, m^2/s
$\bar{D}^*_s$	dimensionless parameter defined by eq 16
D	apparent energy of activation, kJ/mol
$-\Delta H_R$	heat of reaction, kJ/kmol
K'_∞	frequency factor, m^3/kmol
k_∞	frequency factor, m^3/kg·cal·s
k_g	gas-phase mass-transfer coefficient, m/s
$\bar{k}_g$	dimensionless gas-phase mass-transfer coefficient defined by eq 28
k^o_g	gas-phase mass-transfer coefficient for inlet gas, m/s
L	reactor length, m
L^*	alumina layer thickness, m
Pe_h	Peclet number defined in eq 27
Pe_m	Peclet number defined in eq 23
q	apparent heat of adsorption, kJ/kmol
R_g	universal gas constant, 8.313 kJ/kmol·K
r_A	rate of reaction, kmol/g·cal·s
$\bar{r}_A$	dimensionless parameter defined by eq 24
T	temperature, K
T_0	inlet bed temperature, K
T^{ref}	reference temperature, K, in eq 16
u	superficial gas velocity, m/s
u_0	superficial velocity of inlet feed gas, m/s
$\bar{u}$	dimensionless velocity, defined by eq 26
v_b	volume of catalyst bed, m^3
x	axial direction, m
z	dimensionless axial direction defined by eq 13
IMSL	mathematics library for Fortran subroutine for mathematical applications
DBS-LSF, DBV-PFD	two subroutines of the above mentioned library
GHSV	gas hourly space velocity
VOC	volatile organic compound

Greek Characters

α_m	dimensionless parameter defined in eq 14
β	dimensionless parameter defined in eq 22
γ'	dimensionless parameter defined in eq 19
γ	dimensionless parameter defined in eq 20
ϵ	bed voidage, dimensionless
λ_s	axial dispersion coefficient for heat, kJ/m^2-s
ρ	density, kg/m^3
$\bar{\rho}$	dimensionless density as defined by eq 25
ρ_0	density of inlet feed gas, kg/m^3
θ	dimensionless temperature defined by eq 21
ω	active catalyst loading of noble metal, kg/m^3 of catalyst
Ω	parameter defined in eq 17

Registry No. n-C_6, 110-54-3; n-C_8, 111-65-9; n-C_{10}, 124-18-5; n-C_{12}, 112-40-3.

Literature Cited

(1) Chen, J.; Heck, R.; Burns, K. Commercial Development of Oxidation Catalyst for Gas Turbine Cogeneration Applications. Presented at the 82nd Annual Meeting and Exhibition, Air and Waste Management Association, Anaheim, CA, 1989.

(2) Carberry, J. J.; Wendel, M. M. A Computer Model of the Fixed Bed Catalytic Reactor: The Adiabatic and Quasi-adiabatic Cases. *AIChE J.* **1963**, *9*(1), 139.

(3) Thoenes, D.; Kramers, H. Mass Transfer from Spheres in Various Regular Packings to a Flowing Fluid. *Chem. Eng. Sci.* **1958**, *8*, 271.

(4) Oh, S. H.; Baron, K.; Sloan, E. M. Effects of Catalyst Particle Size on Multiple Steady States. *J. Catal.* **1979**, *59*, 272.

(5) Morbidelli, M.; Servida, A. Optimal Catalyst Activity Profiles in Pellets. 2. The influence of External Mass Transfer Resistance. *Ind. Eng. Chem. Fundam.* **1982**, *21*, 278.

(6) Reid, R. C.; Prausnitz, J. M.; Poling, B. E. *The Properties of Gases and Liquids*, 2nd ed.; McGraw-Hill: New York, 1987.

(7) Benton, C.; Hewitt, L. *Prediction of Fluid Properties*, 1st ed.; Plenum Press: New York, 1985.

(8) Froment, G.; Hofmann, H. In *Chemical Reaction and Reaction Engineering*; Carberry, J. J., Varma, A. M., Eds.; Dekker: New York, 1987; pp 391–392.

(9) Yu Yao, Y. F. Oxidation of Alkanes over Noble Metal Catalysts. *Ind. Eng. Chem. & EC Proc. Res. Dev.* **1980**, *19*, 293.

(10) Schwartz, A.; Holbrook, L. L.; Wise, H. Catalytic Oxidation Studies with Platinum and Palladium. *J. Catal.* **1971**, *21*, 199.

Received for review May 13, 1991. Accepted July 1, 1991.

Environ. Sci. Technol. 1991, 25, 2071–2075

Kinetic Study of SO_2 Reaction with Dolomite

Sanjeev Tambe,[†] K. Lal Gauri,*[,†] Suhan Li,[†] and W. Geoffrey Cobourn[‡]

Department of Geology and Department of Mechanical Engineering, University of Louisville, Louisville, Kentucky 40292

■ In today's industrialized environments, sulfur dioxide, to the exclusion of other pollutant gases, is the main cause of chemical deterioration of building materials such as marble, limestone, and dolomite. This paper gives the results of an experimental study of the reaction of laurel dolomite, a coarsely crystalline variety of dolomite, with sulfur dioxide. With the progress of reaction it was found that a gypsum–epsomite crust grows outward due to a continuous supply of Ca and Mg ions from an increasingly greater depth inside the stone. Therefore, the rate data were analyzed by following a shrinking unreacted core model using first- and fractional-order (0.5) kinetic rate constants. These two reaction orders fit the experimental data equally well for the initial phase of the reaction, but the fractional rate constant, 0.19 $mmol^{0.5}$ $cm^{-0.5}$ h^{-1}, gives the best fit to the overall experimental data.

Introduction

The deterioration of building stone due to the air pollutants sulfur and nitrogen oxides is of increasing concern because these pollutants adversely affect the appearance and life of building materials. SO_2 and NO_2 react with carbonate rocks to form sulfates and nitrates, which, due to their solubility in water, may be drained away or, if protected from the rain, may form unsightly crusts that eventually exfoliate. The analysis of crusts upon naturally weathered carbonate rocks and experimental studies on combined SO_2 and NO_2 reactions reveal that the crusts are largely made of sulfates while only trace quantities of nitrate are present (*1–3*).

A substantial amount of literature on the reactivity and kinetics of the reaction of SO_2 with carbonate rocks is available (*4–9*). Recently, Kulshreshtha et al. (*10*) and Gauri et al. (*11*) conducted experimental studies involving the exposure of different types of marble to 10 and 300 ppm SO_2 atmospheres. The rate constants thus determined have proved useful in estimating the extent of damage to marble in ambient SO_2 concentrations found in industrial environments. The damage was expressed as the thickness of the product crust ($CaSO_4 \cdot 2H_2O$) at the surfaces of structures protected from rain or for surfaces exposed to rain as the amount of erosion.

In this paper we describe the results of experiments on SO_2 reaction with a dolomite [$CaMg(CO_3)_2$], laurel dolomite, which is a coarsely crystalline and highly porous variety of dolomite rock. Further, this dolomite is stoichiometrically balanced; i.e., the proportions of Ca and Mg are nearly equal (*12*). However, this dolomite has certain occluded minerals, including gypsum in the amount of nearly 1% by weight. This quantity of gypsum was subtracted from the reaction rate calculations. X-ray diffraction analysis of a 120-year-old sample of dolomite from Louisville and that of samples reacted in the laboratory reveals that the reaction of SO_2 with dolomite takes place according to the equation

$$CaMg(CO_3)_2 + 2SO_2 \xrightarrow{H_2O,\ O_2} CaSO_4 \cdot 2H_2O + MgSO_4 \cdot 7H_2O + 2CO_2 \quad (1)$$

Experiments were conducted employing sulfur dioxide concentrations in the range 8–21 ppm. The kinetics of the reaction was established by fitting the shrinking unreacted core model (*13–15*) to the rate data. Also, analytical solutions for model equations for the reacted mass of dolomite and the crust thickness were obtained.

Experimental Methods and Materials

Dolomite slabs were exposed to humid atmospheres containing SO_2. The details of the experimental setup used in the present study are given in Kulshreshtha et al. (*10*). Dolomite slabs (2.8 cm × 1.6 cm × 0.3 cm) were cut, uniformly polished with 400-grit silicon-carbide powder, cleaned in an ultrasonic bath, and exposed to a given test atmosphere.

The dimensions of the slab were measured accurately with a vernier caliper. An atmosphere containing SO_2 was generated by passing air through a humidifier and then over a permeation tube. The airflow rates were adjusted properly so as to obtain the desired SO_2 concentration in the reaction chamber, where the specimens under study were suspended. To maintain 100% relative humidity, a prerequisite to the performance of rapid reaction, water was placed at the bottom of the reaction chamber, a modified 10-L desiccator. This simulates a frequently occurring condition outdoor, where the stone is coated with a thin film of condensed moisture. Prior to exposing the dolomite samples to SO_2, the water at the bottom of the chamber was equilibrated with the partial pressure of SO_2 in the test atmosphere. At any given time no more than 30 samples were present in the chamber.

Each dolomite sample was weighed before exposure. At irregular intervals, two or three samples were removed from the chamber and immediately immersed in 100 mL of deionized water to dissolve the reaction product. For long exposures, the slabs were washed two to three times to ensure that the entire reaction product had been removed. These washings were analyzed for calcium, magnesium, and sulfate ions. The amounts of Ca and Mg were determined by atomic absorption spectrophotometry, and the amount of sulfate was determined by a turbidimetric method using UV/vis spectroscopy. The permeation tube was weighed before and after the end of each run to estimate the total amount of SO_2 passed through the reaction chamber. The amount of SO_2 was also monitored by a sulfur dioxide analyzer manufactured by Columbia Scientific Instruments.

For the calculation of the reaction rate, 20 samples were selected from a total of 50 exposed. The selection was based upon a close match of mass of the reaction product [gypsum ($CaSO_4 \cdot 2H_2O$) and epsomite ($MgSO_4 \cdot 7H_2O$)] calculated through various methods, namely, from Ca + Mg ions, from SO_4 ions, and from the gravimetric weight loss of the leached samples. For the selected samples, the mean and standard deviation values fall in the ranges of 3.46–508.77 and 0.27–12.62 mg, respectively; higher standard deviation values (>5) were encountered for only two samples with long exposure times (>400 h).

Mechanism of Formation and Measurement of Thickness of Crust

Figure 1 shows the profile of a reacted sample in cross section. Three horizons, namely, crust, leached zone, and

[†] Department of Geology.
[‡] Department of Mechanical Engineering.

0013-936X/91/0925-2071$02.50/0

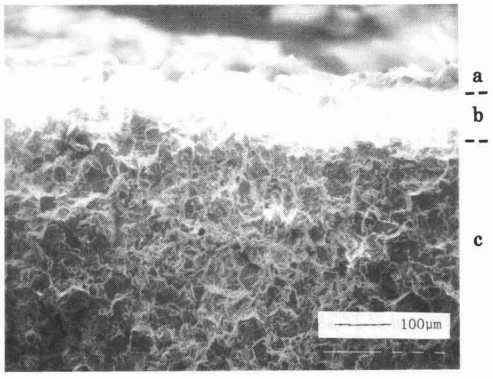

Figure 1. Profile of a sectioned dolomite specimen exposed to 14.05 ppm SO_2 atmosphere for 410 h, showing crust (a), leached zone (b), and unreacted dolomite core (c).

the unaltered dolomite, are seen. The crust, a continuous layer of gypsum crystals, lies above the original slab surface. Underlying the crust is the cavernous leached zone, which must have provided the Ca and Mg ions that reacted with SO_2 at the surface to form the gypsum and epsomite. Epsomite is absent from the crust due to its deliquescent property. Figure 2 shows schematically the mechanism of formation of crust upon dolomite.

Skoulikidis and Charalambous (*16*), in their studies on the sulfur dioxide reaction with calcite ($CaCO_3$), found that the calcium ions near the solid surface diffuse outward and react with SO_2. They explained this phenomenon on the combined basis of a galvanic cell model and solid-state diffusion. Our studies on dolomite corroborate that explanation.

The thickness of the reacted dolomite (δ_d) was calculated by dividing the reacted volume, obtained from the weight loss of reacted sample when immersed in deionized water, by the surface area of the sample. This thickness was converted to equivalent product crust thickness (δ_p) by multiplying it by the ratio of the molar volume of product (gypsum plus epsomite) to that of dolomite. The following equation summarizes this calculation:

$$\delta_p = \frac{(W_1 - W_2)}{A_s \rho_d} \frac{M_p \rho_d}{M_d \rho_p} \qquad (2)$$

Where W_1, W_2, and A_s denote the sample weight before exposure, sample weight after the reaction product is leached, and external surface area, respectively. ρ_d and ρ_p denote densities of dolomite (2.6593 g/mL as determined by pycnometer and mercury porosimeter) and reaction products, respectively. The term $M_p\rho_d/M_d\rho_p$ represents the ratio of the molar volumes of reaction product $CaSO_4{\cdot}2H_2O + MgSO_4{\cdot}7.H_2O$ and dolomite and has a value of 3.187.

Application of the Shrinking Unreacted Core Model to the Decay of Dolomite

The shrinking unreacted core model is directly applicable to the dolomite–SO_2 reaction. In this model, the reaction front, in terms of the supply of Ca and Mg ions (thereby the mass loss of parent dolomite) uniformly moves inside the solid with progress of reaction. This results in the reduction of the unreacted part of the solid.

The presented model assumes that the pore diffusion resistance is negligible. This assumption is based upon the fact that the observed reaction rate is small due to the low reaction temperature (*17*). Also, the reaction rate remains

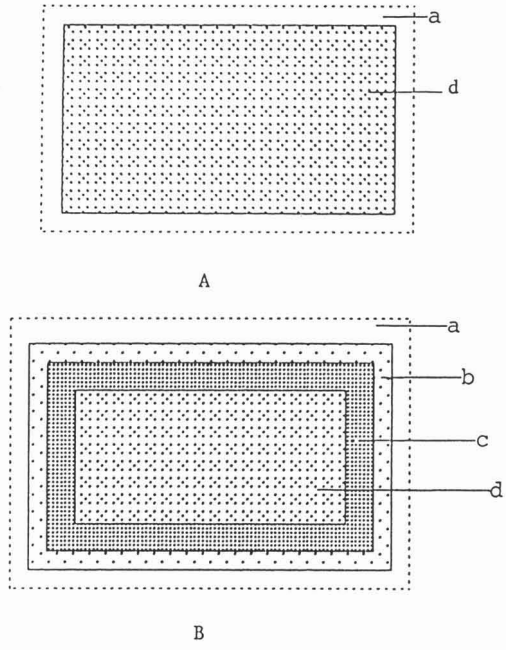

Figure 2. Schematic diagram for unreacted (A) and reacted dolomite specimen (B), showing gas film (a), crust (b), leached zone (c), and unreacted dolomite core (d).

essentially constant throughout the reaction period, indicating that the pore diffusional resistance was not operative.

In the event that the progress of reaction is affected by chemical reaction and external mass-transfer resistances, the contributions of these processes must be simultaneously considered. Consequently, the overall reaction rate, assuming pseudo steady state, is equal to the interfacial chemical reaction and to that of external mass transfer. The mass balance equation can then be written as (*13–15*)

$$(1/A_s)(dN_d/dt) = bk_s C_s^p \qquad (3a)$$

$$= h_d(C_b - C_s) \qquad (3b)$$

Where A_s is the surface area of the sample, N_d denotes the number of millimoles of dolomite reacted in time t (h), b is the ratio of the stoichiometric coefficient of dolomite to SO_2 (0.5), k_s is the surface reaction rate constant, C_b and C_s are the bulk and surface concentrations (mmol/cm^3) of sulfur dioxide, respectively, p is the reaction order, and h_d is the gas-phase mass-transfer coefficient. Equation 3a can be integrated to obtain

$$N_d = bA_s k_s C_s^p t \qquad (4)$$

To obtain an expression for the thickness, we note that the derivative term of eq 3 can be modified to represent the thickness of the reaction product, i.e., the crust buildup on the slab surface. From eq 2, the reacted number of moles of dolomite (N_d) is given by

$$N_d = \rho_d \upsilon_d / M_d = \rho'_d \upsilon_d \qquad (5)$$

where M_d, ρ'_d, and υ_d respectively denote molecular weight, molar density, and reacted volume of dolomite.

Since υ_d/A_s is equal to the thickness of dolomite reacted (δ_d), eq 3a after substitution and rearrangement becomes

$$d\delta_d/dt = (M_d/\rho_d) b k_s C_s^p \qquad (6)$$

Table I. Mass-Transfer Coefficients and Other Related Data[a]

run no.	equiv diameter (d_p), cm	SO_2 conc, bulk (C_b), ppm	SO_2 conc, surface (C_s), ppm	flow rate, mL/min	N_{Re}	mass-transfer coeff (h_d), cm/h
1	2.072	14.05	11.15	700	0.3436	549
2	2.072	20.88	17.19	350	0.1718	524
3	2.072	8.00	5.89	800	0.3927	555
4	2.130	14.12	11.18	800	0.4037	541

[a] $N_{Sh} = 1.134$; $\rho_g = 1.2047 \times 10^{-3}$ g/cm^3.

Integration of eq 6, assuming k_s is essentially constant with respect to time, yields the equation giving the equivalent reacted thickness of the dolomite as

$$\delta_d = (M_d/\rho d) b k_s C_s^p t \quad (7)$$

In order to apply eq 4 or 7 to obtain k_s, it is essential to determine the surface concentration of sulfur dioxide, C_s. For this, eq 3b can be rearranged

$$C_s = \frac{dC_d/dt + h_d A_s C_b}{h_d A_s} \quad (8)$$

wherein the mass-transfer coefficient, h_d, can be obtained from the definition of the Sherwood number as

$$h_d = D_{ab} N_{Sh}/d_p \quad (9)$$

The mass-transfer coefficient (h_d) for each run was estimated (*18*) from the knowledge of the binary diffusion coefficient (D_{ab}) of the air–SO_2 system, the Sherwood number (N_{Sh}), and the equivalent diameter (d_p) of the dolomite slab (*19*). The binary diffusion coefficient (0.1336 cm^2/s) and Sherwood number were estimated using the Chapman–Enskog equation and the Rantz–Marshall correlation, respectively.

The correlation for laminar flow, which is valid over Reynolds number range 0–200, is as follows:

$$N_{Sh} = 2.0 + 0.6 N_{Re}^{0.5} N_{Sc}^{0.33} \quad (10)$$

wherein N_{Re} and N_{Sc} denote Reynolds and Schmidt dimensionless numbers. The Reynolds number is proportional to the ratio of inertial to viscous effects and the Schmidt number is the ratio of molecular momentum diffusivity to molecular mass diffusivity. Their values have been obtained using the definitions

$$N_{Re} = d_p G \rho_g/\mu \qquad N_{Sc} = \mu/\rho_g D_{ab} \quad (11)$$

The notations G, μ, and ρ_g respectively represent linear fluid velocity (cm/s), viscosity, and density of humid air. The value of μ as found from the viscosity tables is equal to a 0.000 182 7 (g cm^{-1} s^{-1}) at 293 K.

The values of C_s were estimated by fitting the experimental data to eq 8 with utilization of an optimization subroutine. Table I lists the values of the mass-transfer coefficients and surface concentrations thus obtained for each of the conducted runs.

Evaluation of Surface Rate Constant, k_s

The N_d versus time data for individual runs were interpolated using the Spline interpolation technique, and the reaction rate was calculated using a second-order finite difference approximation. Data consisting of the derivatives and surface concentration of SO_2 (obtained from eq 8) for all the runs were combined. This single set of data was fitted to eq 3a using a multivariable regression subroutine to obtain unique values of reaction order with respect to SO_2 and the rate constant k_s (Figure 3a). Their magnitudes are $p = 0.498$ (~0.5) and $k_s = 0.19$ mmol$^{0.5}$ cm$^{-0.5}$ h^{-1}.

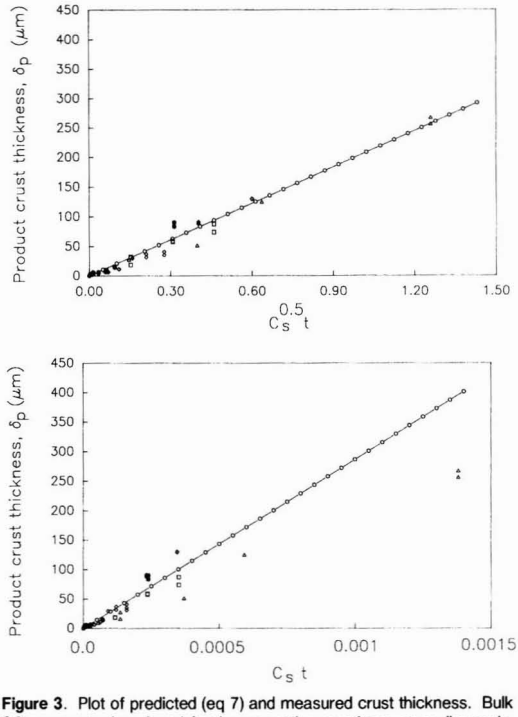

Figure 3. Plot of predicted (eq 7) and measured crust thickness. Bulk SO_2 concentrations (ppm) for the respective reactions: open diamonds, 8; filled circles, 14.05; open squares, 14.12; open triangles, 20.88. Panels a (top) and b (bottom) half- and first-order models, respectively.

Our earlier studies on the SO_2 reaction with marble (*10*) showed that the reaction order with respect to SO_2 is 1. As a trial, therefore, we fitted our experimental data to a first-order rate model (Figure 3b) in addition to the 0.5 order, as indicated by Figure 3a. The rate constant value thus obtained is 280 cm/h. As reported in the section on methods, 20 samples were selected for the estimation of model parameters. Nevertheless, parts a and b of Figure 3 show all the generated experimental data points. The standard deviation and correlation coefficient values for predicted and measured values of crust thickness for reaction order $p = 0.5$ are 13.18 μm and 0.98 and for $p = 1$ they are 35.52 μm and 0.95, respectively. The smaller value of the standard deviation in the case of reaction order 0.5 indicates that the fit in this case is better. However, the first-order rate constant expresses more accurately the rate of decay of dolomite in outdoor environments, as discussed in the following section.

Results and Discussion

A primary aim of our reaction rate studies on stone is to determine rate constants from experimental work so that the reactivity of such stone can be predicted for

outdoor exposures in a variety of industrial environments. The criteria for comparison of outdoor weathering and experimental reactions are the thickness of the crust and the degree of surface erosion.

Correlating field and experimental studies, earlier we (*11*) developed rate constants for the decay of marble. There it was possible to compare predicted results with actual values of the crust thickness and the amount of erosion for even century-old structures because the crusts were yet intact and the marble contained weathering-resistant silicate minerals which projected above the receded marble surface. In the case of the dolomite in question, weathering-resistant minerals are absent and the crust falls off rather rapidly after it has formed, as explained below.

In dolomite, we found that the reaction rate is nearly constant through the entire period of exposure of specimens in the laboratory and we expect the same in the case of outdoor weathering. Theoretically, therefore, a relatively much greater crust thickness will be built upon the dolomite surface in a few years than in the case of marble, where after an initial few micron thick crust is formed under kinetic control, the remaining crust is built up very slowly through diffusion-controlled reaction.

The overall constant reaction rate in dolomite, and not its reduction during advanced exposure as in marble, appears to be a result of the formation of the mineral epsomite as one of the reaction products. The deliquescence point, i.e., the relative humidity at which epsomite goes into solution, is 88.3% at 20 °C (*20*). As a result, epsomite is frequently able to convert the ambient moisture into liquid water. Our experimental samples showed that after nearly 150 h of reaction, when an adequate quantity of epsomite has formed, water droplets begin to appear at the surface of the specimens. This water film allows the reaction to continue at an essentially constant pace allowing for a thicker crust to develop on experimental specimens. In the outdoor conditions, however, the frequent fluctuation of relative humidity above and below the deliquescence point of epsomite generates crystallization pressure in the crust, fragmenting it before a large thickness can form.

In previous studies with marble, the rate constant calculated on the basis of 10 ppm SO_2 concentrations predicted the outdoor thickness of gypsum crust reasonably well. Therefore, to compare our theoretical results with actual circumstances, we examined naturally dislodged peels from the dolomite facade of a 120-year-old local church. We determined (*21*) that the crust fell off after a nearly 40 μm thick layer was formed. According to the reaction rate determined by us, this crust, in the prevailing outdoor SO_2 concentrations of 0.01–0.04 ppm, was formed in 9–38 years. Unfortunately, not enough recently installed samples could be found in the field in order to verify the model.

The calculation of this time to obtain the observed 40-μm-thick crust was based upon the first-order rate model and not the half-order model that, as given earlier, fitted the experimental data better. Application of the half-order rate model generated 40 μm in 7–13 months, a thickness not observed anywhere on field materials. It may be postulated then that epsomite, once again, by enhancing the reactivity somewhat in the later phase of the reaction makes the half-order rate model fit the experimental data better and that for the purpose of extrapolation to low atmospheric SO_2 concentrations the first-order rate model may have to be used.

Further, the stream velocities used in our experiments, due to the low permeation rates of the SO_2 source, were often lower than those experienced outdoors. Therefore, the estimated gas-phase mass-transfer coefficient in our system ($\simeq$0.15 cm/s) is lower than in an urban atmosphere, in which turbulent flow conditions typically prevail. Reported values, determined outdoors experimentally, are in the range 0.5–10.0 cm/s (*22*). This factor may have given us the outdoor conversion value that is probably somewhat lower than the real value. This explanation suggests that, in the absence of criteria for verification, any prediction of the rate of weathering will only be approximate.

Conclusion

We have simulated the outdoor weathering of dolomite by reacting it in the laboratory with SO_2 concentrations between 8 and 21 ppm. The experimental data were modeled using the shrinking unreacted core model. Even though the experimental data on reactivity fit the half-order rate model better, the first-order rate model expresses more accurately the weathering of dolomite in outdoor conditions.

Acknowledgments

We thankfully acknowledge the assistance of Profs. Dermot Collins and Raul Miranda for their useful suggestions during the presented modeling work. Prof. John Sinai assisted us in writing the manuscript.

Glossary

A_s	surface area of the slab (cm^2)
b	stoichiometric constant of dolomite
C_b	bulk concentration of SO_2 ($mmol/cm^3$)
C_d	concentration of dolomite (mmol)
C_s	surface concentration of SO_2 ($mmol/cm^3$)
d_p	diameter of slab, assuming spherical geometry (cm)
D_{ab}	binary diffusion coefficient of air–SO_2 (cm^2/s)
G	linear fluid velocity (cm/h)
h_d	mass-transfer coefficient (cm/h)
k_s	surface rate constant [for 0.5 order ($mmol^{0.5}$ $cm^{-0.5}$ h^{-1}) and for first order (cm/h)]
M_d	molecular weight of dolomite
N_d	mass of the reacted solid (mmol)
p	reaction order with respect to sulfur dioxide
v_d	reacted volume (cm^3)
W_1	weight of the dolomite slab before exposure to SO_2 atmosphere (g)
W_2	weight of the dolomite slab after exposure to SO_2 atmosphere (g)

Greek Letters

δ_d	thickness of reacted solid (cm)
δ_p	product crust thickness (cm)
ρ_d	density of dolomite (g/cm^3)
ρ'_d	molar density of dolomite ($mmol/cm^3$)

Registry No. SO_2, 7446-09-5; dolomite, 16389-88-1; gypsum, 13397-24-5; epsomite, 14457-55-7.

Literature Cited

(1) Gauri, K. L.; Holdren, G. C. *Environ. Sci. Technol.* **1981**, *15*, 385–390.
(2) Livingston, R. A. The role of nitrogen oxides in the deterioration of carbonate stones. *Proceedings, Fifth Congress on Deterioration and Conservation of Stone*; Lausanne, Switzerland, 1985; pp 509–516.
(3) Johansson, L. G.; Lindqvist, O.; Mangio, R. E. *Durabil. Build. Mater.* **1988**, *5*, 439–449.
(4) Borgwardt, R. H. *Environ. Sci. Technol.* **1970**, *4*, 59–63.
(5) Borgwardt, R. H.; Harvey, R. D. *Environ. Sci. Technol.* **1972**, *6*, 350–360.
(6) Hartman, M.; Coughlin, R. W. *Ind. Eng. Chem. Proc. Design Dev.* **1978**, *22*, 411–419.

(7) Bhatia, S. K.; Perlmutter, D. D. *AIChE J.* **1981**, *27*, 226–234.
(8) Stouffer, M. R.; Yoon, H.; Burke, F. P. *Ind. Eng. Chem. Res.* **1989**, *28*, 20–27.
(9) Alvfors, P.; Svedberg, G. *Chem. Eng. Sci.* **1988**, *43*, 1183–1193.
(10) Kulshreshtha, N. P.; Punuru, A. R.; Gauri, K. L. *J. Mater. Civ. Eng.* **1989**, *1*, 60–72.
(11) Gauri, K. L.; Kulshreshtha, N. P.; Punuru, A. R.; Chowdhury, A. N. *J. Mater. Civ. Eng.* **1989**, *1*, 73–85.
(12) Blatt, H.; Middleton, G.; Murray, R. *Origin of Sedimentary Rocks*, 2nd ed.; Prentice-Hall: Englewood Cliffs, NJ, 1980; p 510.
(13) Carberry, J. J. *Chemical and Catalytic Reaction Engineering*, 1st ed.; McGraw Hill: New York, 1976; p 20.
(14) Levenspiel, O. *Chemical Reaction Engineering*, 2nd ed.; Wiley: New York, 1972; p 367.
(15) Szekely, J.; Evans, J. W.; Sohn, H. Y. *Gas–Solid Reactions*, 1st ed.; Academic Press: New York, 1976; p 70.
(16) Skoulikidis, Th.; Charalambous, D. *Br. Corros. J.* **1981**, *16*, 70–77.
(17) Szekely, J.; Evans, J. W.; Sohn, H. Y. *Gas–Solid Reactions*, 1st ed.; Academic Press: New York, 1976; pp 234–239.
(18) Szekely, J.; Evans, J. W.; Sohn, H. Y. *Gas–Solid Reactions*, 1st ed.; Academic Press: New York, 1976; pp 21–22.
(19) Smith, J. M. *Chemical Reaction Engineering*, 3rd ed.; McGraw-Hill: New York, 1981; p 395.
(20) Arnold, A.; Zehnder, K. In *The Conservation of Monuments in the Mediterranean Basin*; Zezza, F., Ed.; Proceedings, 1st International Symposium at Bari, 1989; pp 30–58.
(21) Gauri, K. L.; Tambe, S. S.; Caner-Saltik, E. N. *Environ. Geol. Water Sci.*, in press.
(22) Garland, J. A. *Atmos. Environ.* **1978**, *12*, 349–362.

Received for review March 4, 1991. Revised manuscript received July 11, 1991. Accepted July 12, 1991. This research was funded by the Samuel H. Kress Foundation and the National Science Foundation under Grant BCS-8918935 to K.L.G. We are indebted to our colleagues and these organizations for their support.

Determination of Bacterial Collision Efficiencies in a Rotating Disk System

Robert E. Martin,[†,‡] Linda M. Hanna,*[,†,§] and Edward J. Bouwer[∥]

Department of Environmental Health Sciences and Department of Geography and Environmental Engineering, The Johns Hopkins University, 615 North Wolfe Street, Baltimore, Maryland 21205

■ The objective of this work was to determine the probability of attachment of *Pseudomonas aeruginosa* to glass surfaces for a range of concentrations of a 1:1 electrolyte. This parameter, referred to as the collision efficiency, was determined by depositing cells on a rotating glass disk. Collision efficiencies ranged from 0.000 83 to 0.41 for NaCl concentrations from 10^{-6} to 10^{-1} M, respectively, and supported the argument that the deposition of *P. aeruginosa* can be limited by interaction of similarly charged electric double layers. It was also shown that transport of cells to the disk surface was comparable to that of similar-sized polystyrene latex particles, although results for both were inconsistent with theory in that the deposition decreased with increasing distance from the center of the disk. The most likely explanation was nonuniform transport of particles to the rotating disk surface arising from lateral migration.

Introduction

The movement of bacteria in porous media is important for understanding mobility of pathogens and for implementation of bioremediation measures that enhance pollutant biodegradation by the addition of nutrients and/or acclimated bacteria. An important determinant of the extent of microbial movement in porous media is the interaction between the bacteria and solid surfaces, particularly the quantity of bacteria that attach under various solution conditions. Although numerous studies of bacterial attachment have given some indication of factors relevant to attachment, they have failed to quantitate the probability that a cell will attach to a surface with which it collides. This probability is often referred to as the collision efficiency, or simply α. One of the advantages of this parameter is that it is independent of the rate of transport of cells to a surface and can therefore be used to predict deposition rates in any system for which particle transport can be predicted. The success of this approach, however, is contingent on the availability of an experimental system for reliable determinations of the collision efficiency.

This paper presents the results of collision efficiency determinations for bacteria evaluated in a rotating disk system. The system consisted of a rotating shaft to which a glass disk was attached and then immersed in aqueous solutions of different electrolyte concentrations. The study was undertaken to obtain collision efficiences to be used in modeling the deposition of cells in a porous medium. Observed particle deposition was also compared to predictions of particle transport models in a rotating disk system. The observations did not conform to expectations and suggest that lateral migration needs to be included in the particle transport models.

Approach

The collision efficiency, α, is defined as the ratio of the rate at which cells attach to a surface to the rate at which cells come into contact with the surface. Purely empirical, semiempirical, and purely theoretical approaches to estimating α can be distinguished. The first case entails experimental determination of both the rate of particle transport to the surface and the rate of attachment; the second consists of measuring the rate of attachment and calculating the rate of transport; the third involves calculation of both on the basis of fundamental properties of the system. At the present time, theories of particle–surface interactions in aqueous media have not proved to be accurate in quantifying α for relatively stable particles. The availability of particle transport models for selected systems, however, makes the semiempirical approach an attractive possibility since it entails half the experimental effort of the fully empirical alternative. Nonetheless, reliability of the models remains to be verified.

[†] Department of Environmental Health Sciences.
[‡] Present address: Lyonnaise des Eaux—Dumez, 72 Avenue de la Liberte', 92000 Nanterre, France.
[§] Present address: BCM Engineers, One Plymouth Meeting, Plymouth Meeting, PA 19462.
[∥] Department of Geography and Environmental Engineering, Charles and 34th Sts., Baltimore, MD 21218.

0013-936X/91/0925-2075$02.50/0

The choice of systems which lend themselves to theoretical calculation of particle transport as well as experimental measurement of attachment is rather restricted, parallel plate channels and rotating disks being two examples for which both types of studies have been published (*1–4*). The data validating transport models for these systems have been limited to submicron nonbiological particles. It has not been demonstrated that they adequately describe the behavior of particles the size of bacteria and larger (e.g., protozooan cysts). One goal of the experiments reported here was to test the applicability of particle transport models for the rotating disk system to bacteria, which is necessary for a semiempirical approach to evaluate the collision efficiency. The procedure adopted here to measure cell transport to the surface was analogous to that used by others to test particle transport theories (*1, 3, 5*). Since bacteria are negatively charged, their accumulation on a positively charged surface in a given time should reflect their rate of transport to the surface (i.e., it is assumed that the collision efficiency is 1). To estimate rates of particle transport in this work, glass surfaces were coated with a cationic water-insoluble polymer. The results were used both for calculating collision efficiencies using a fully empiric approach and for evaluating particle transport models to assess the feasibility of the semiempiric approach.

The rotating disk was selected in part because the transport of cells to the surface can be readily controlled and experimentally measured. It is also very sensitive; the lower sensitivity limit for measurement of deposition by direct counting depends only on the total area counted and the amount of extraneous deposition associated with manipulations of the disk and particle suspensions. A third advantage of the system is that fluid flows toward the disk such that the flux of particles to the surface is relatively high. Experiments with bacteria can be of short duration and still yield significant numbers of deposited cells. Complications associated with growth and die-away over longer periods can thus be avoided. The final major advantage is that the flow in this system is well-defined. Cochran (*6*) provided an exact solution for the fluid velocity and others have since developed models for the deposition of Brownian and non-Brownian particles (*2, 4, 7–9*).

One feature common to all models for both molecular and particulate mass transport to a rotating disk is that deposition is predicted to be uniform over the surface of the disk. This property of the system is a consequence of the axial symmetry of the flow toward the disk and the fact that the axial component of the fluid velocity is independent of radial position. On the other hand, the velocity parallel to the surface, and hence the surface shear stress, increases linearly with radial position. The potential for fluid shear to prevent attachment of particles colliding with a surface has been suggested by several investigators (*10–12*). It could also influence particle transport, however, by generating migration of particles across streamlines (*13*). This effect has not been incorporated in any particle transport model. If present, lateral migration, also referred to as hydrodynamic lift, would be expected to result in a radial dependence of the particle transport rate toward the disk surface. Deposition was therefore examined as a function of radial position in this study.

Collision efficiencies for *Pseudomonas aeruginosa* depositing on glass surfaces were calculated from measured rates of attachment to glass surfaces (disks) under a range of electrolyte conditions, and empiric determinations of particle transport rates in the rotating disk system. The collision efficiency depends on properties of both the bacterial and disk surfaces and on solution conditions (*14*). Only the latter was varied in this investigation, however. Collision efficiencies for five concentrations of sodium chloride ranging from 10^{-6} to 10^{-1} M were based on observations of 30 disks representing three replicates for both glass and polymer-coated glass surfaces at each salt concentration. Supplementary investigations using polystyrene latex spheres were conducted to further examine the observed radial dependency of deposition.

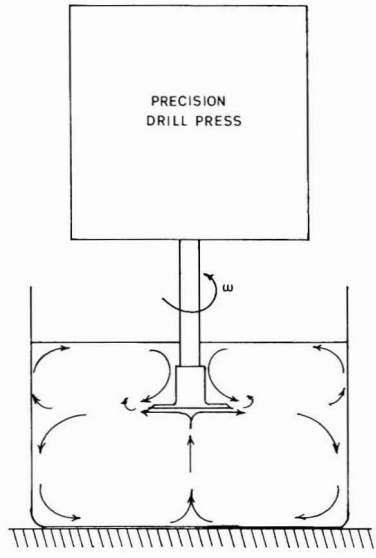

Figure 1. Schematic of rotating disk system showing approximate flow pattern as visualized by dye injection.

Materials and Methods

All water used for glassware washing and solution preparation was triple glass distilled, deionized, and sterilized by filtration through a Filterite 0.2-μm cartridge filter (Brunswick Technetics, Timonium, MD).

System Design. The rotating disk apparatus used for the bulk of experiments consisted of a circular glass coverslip fixed to the end of a shaft driven by a precision drill press (Servo Products Company, Pasadena, CA) and rotating in a particle suspension contained in an 800-mL beaker (Figure 1). The coverslips were 22 mm in diameter and held tightly in a machined recess at the end of the shaft by a small amount of vacuum grease at the end of the shaft. Consequently, the glass surface exposed to the suspension did not come in contact with the vacuum grease, which would alter its hydrophobicity. Because of the close tolerances and the short duration of the experiments, contamination of the aqueous phase was assumed negligible. Observations of particles deposited on coverslips were restricted to a circular area ~20.6 mm in diameter.

Theoretical design considerations as given by Riddiford (*15*) were respected in the construction and operation of the apparatus. The maximum disk Reynolds number for any experiment was 11 300, based on the coverslip radius and a rotational speed, ω, of 83.8 rad/s (83.8 s^{-1}), well within the limit of 200 000 for laminar flow (*15*).

Investigations under conditions of very low particle flux to the disk required that background deposition due to manipulations of the disk during exposure and rinsing be reduced to an absolute minimum. This led to the devel-

opment of an improved chamber and procedure permitting both exposure and rinsing steps to be accomplished without the disk surface breaking the air–water interface (*16*).

Disk Surfaces. Glass coverslips used as deposition surfaces were cleaned by soaking in hot 10 g/L Alconox detergent solution (Fisher Scientific, Pittsburgh, PA) for at least 2 h, rinsing three times with water, soaking in 5 N nitric acid for at least 12 h, and then finishing with a thorough rinse with sterile water.

To obtain a positively charged surface in water, clean glass coverslips were coated with a copolymer (2-VPS) containing 70% 2-vinylpyridine and 30% styrene (Polysciences, Inc., Warrington, PA) by a method based on the falling level technique described by Revell and Agar (*17*). Details are provided elsewhere (*16*). Several investigators have used similar polymer-coated surfaces and reported ζ potentials calculated from electroosmotic and streaming potential measurements ranging from +15 to +72 mV (*1*, *3*).

Bacteria. The *P. aeruginosa* culture used in this study was an ATCC strain originally obtained from The Johns Hopkins Hospital Department of Clinical Microbiology (Baltimore, MD). Cells were maintained on nutrient agar slants and transferred to fresh media every 4–6 weeks. Cultures for experimental use were grown for ~20 h in a water bath shaker at 37 °C in 250-mL Erlenmeyer flasks containing 100 mL of tryptone yeast extract (TYE) broth (10 g/L tryptone, 8 g/L NaCl, and 1 g/L yeast extract). These conditions yielded a bacterial suspension containing $\sim 5 \times 10^9$ CFU/mL.

Motility was always observed and aggregates were never seen in wet mounts of 20-h cultures observed under phase-contrast microscopy. Negative staining with India ink as described by Norris and Swain (*18*) failed to reveal capsules on cells from 20-h cultures. Examination of cells grown under these conditions by transmission electron microscopy revealed that the cells did have single polar flagella, as is characteristic of the species *P. aeruginosa*, but did not possess fimbriae. Singlet cells ranged from 1.1 to 1.9 μm in length and from 0.66 to 0.75 μm in diameter.

For deposition experiments, cells were washed three times by centrifugation at 3600*g* for ~7 min and resuspended in a 10^{-4} M sodium chloride solution. The short centrifugation time and low salt concentration resulted in a loose pellet that was easily resuspended. After the last wash, the pellet was resuspended in a volume of 30 mL, giving a concentrated stock suspension containing $\sim 10^{10}$ cells/mL. The final suspension was prepared in the beaker of the rotating disk apparatus by adding a 5-mL aliquot of the stock suspension to 500 mL of the appropriate salt solution while the disk was rotating. The concentration of cells in the suspension for each disk was determined by the direct count method described below and ranged between 10^7 and 10^8 cells per milliliter. Motility was also checked in each suspension by direct observation of wet mounts. Although difficult to quantify, it typically appeared that ~50% of the cells were motile. Some loss of motility relative to the original culture could be expected as a result of the washing procedure, which may have caused removal of flagella.

Various electrolyte concentrations were obtained by adding sodium chloride to sterile water. The final concentrations of NaCl added were 10^{-6}, 10^{-4}, 10^{-3}, 10^{-2}, and 10^{-1} M. The pH of these unbuffered solutions varied between 5 and 6.

Polystyrene Latex Particles. The supplementary investigations on particle transport using polystyrene latex spheres initially involved depositing 1.62-μm-diameter spheres with sulfate and hydroxyl surface functional groups on polymer surfaces of 2-vinylpyridine–styrene (2-VPS). The spheres were obtained from Interfacial Dynamics Corp. (Portland, OR) and were manufactured by a surfactant-free process. Information provided by Interfacial Dynamics Corp. indicated the spheres were hydrophobic with 1–10 charge groups per 2000 Å^2, the pK_a of the sulfate group was less than 2, and the density of the particles was 1.055 g/cm^3 at 20 °C. In the pH range of these experiments (pH 5–6), the spheres carried a negative charge.

For the lowest rotational speed of 5.15 s^{-1}, 1.0-μm particles with amino surface functional groups (Polysciences, Inc.) were deposited on clean glass surfaces. Although limited information on these particles was available, they were assumed to be positively charged in the pH range of these experiments. The major advantage to this system was that deposition in the absence of an electrostatic barrier could be tested without the inconvenience associated with polymer coating of glass coverslips.

Suspensions of latex particles were prepared by diluting the concentrated stock in sterile water. Particle number concentrations ranged between 10^7 and 10^8 particles per milliliter for all experiments.

Suspended Particle Enumeration. All microscopy for particle enumeration was carried out with a Nikon Optiphot microscope equipped for phase contrast and epifluorescence microscopy (Nikon, Inc., Garden City, NY). Suspended bacteria were enumerated by an acridine orange direct count procedure based on ASTM standard test method D 4455–85 (Enumeration of Aquatic Bacteria by Epifluorescence Microscopy Counting Procedure).

Samples of latex suspensions were filtered through 0.45-μm mixed cellulose ester membrane filters, which were clarified by acetone vapor (Acetone Vaporiser, Model No. VAP 100, Casella London, Ltd., London, England), and counted under phase-contrast microscopy at 400× magnification.

Exposure Procedure. To avoid depositing bacteria on the disk surface during immersion, 5 mL of a concentrated cell suspension was added by pipet as the disk rotated. The stream was directed toward the shaft in the portion of the beaker above the plane of the disk; this allowed the maximum time for mixing before bacteria reached the disk surface. The rotational speed for experiments with *P. aeruginosa* was 31.4 s^{-1} (300 rpm, Re = 4240). For the glass surfaces, the exposure time was 20 min, while for the 2-VPS, times ranged from 5 to 15 min.

After exposure, the disk was stopped and removed from the suspension by slowly lowering the beaker. The residual drop hanging from the disk surface was drawn off with the corner of a tissue. The disk was then rinsed by rotation at the same speed for 30 s in a particle-free solution of the same chemical composition as the test suspension. Following the rinse, the disk was again removed from the beaker as described above. Specimens with deposited bacteria were then lowered into a 0.1 g/L solution of acridine orange and allowed to stain for 5 min.

Experiments with polystyrene latex particles were conducted at rotational speeds of 5.15, 10.5, 31.4, and 83.8 s^{-1} (50, 100, 300, and 800 rpm). For the latter three cases, 1.62-μm spheres with sulfate functional groups were deposited on 2-VPS surfaces. The procedure was similar to that for the bacteria. The trial at the lowest speed was carried out with 1.0-μm amino-modified spheres and a glass surface, using the modified chamber mentioned above. Exposure times for the latex particles ranged from 5 to 15 min.

Deposited Particle Enumeration. Singlet particles attached to a disk surface were counted as a function of radial position. A special device was constructed to facilitate rotation of coverslips on an x–y translating stage. Counting was performed at 400× magnification using, for the most part, phase contrast. Cells were often difficult to distinguish on the coated disks, however, and the use of epifluorescence permitted clear identification. Singlet cells in the area bounded by a Porton graticule (1.5×10^4 μm^2) were counted in 10 fields in each of 10 concentric zones at 1–10 mm from the center. For the latex particles, a zone at 0.5 mm from the center was added and field sizes of 1.5×10^4 μm^2 were counted; 16 fields were counted in each zone. The trial conducted at a rotational speed of 5.15 s^{-1} represented the single exception in that the entire field of view (8.6×10^4 μm^2) was counted because of the relatively small number of deposited particles.

Data Analysis

Local deposition rates, $R(r)$, expressed as particles deposited per unit time and evaluated as a function of radial position, r, were calculated for each of the concentric counting zones on the basis of the average count for the zone, $\bar{n}_i(r)$, the area of the field, A_c (typically 1.5×10^4 μm^2), and the exposure time, t, such that

$$R(r) = \bar{n}(r)A_z(r)/A_c t$$

where $A_z(r)$ is the total area in the counting zone of average radius r ($2\pi r\, dr$).

In order to account for differences in cell concentrations and exposure times between different trials, local deposition rates were divided by the particle flow rate, $R_o(r)$, toward the counting zone, i.e., in the axial direction. This quantity, $R_o(r)$, was calculated from the measured concentration of particles in suspension, N, the projected area of the counting zone, $A_z(r)$, and the theoretical axial fluid velocity far from the disk, where it asymptotically approaches a value of $0.886(\nu\omega)^{1/2}$ (*4*). $R_o(r)$ is therefore given by

$$R_o(r) = 0.886(\nu\omega)^{1/2}NA_z(r)$$

Since the ratio of $R(r)$ to $R_o(r)$ represents the fraction of particles flowing toward the disk that actually deposit, i.e., that are "collected" by the disk, it is referred to as a local collection efficiency, $I(r)$. The total collection efficiency, I_t, for each trial was obtained by dividing the sum of local deposition rates for all counting zones by the predicted total particle flow rate toward the disk whereby

$$I_t = \sum_j R(r)/\sum_j R_o(r)$$

Assuming that the collision efficiency was 1 in the case of oppositely charged particles and surfaces, the rate of deposition on the 2-VPS surface was used as an empirical estimate of the rate at which particles were transported to the disk. Collision efficiencies for the deposition of cells on glass were therefore calculated by dividing the total collection efficiency for deposition on glass by that for deposition on 2-VPS, with differences between trials in particle concentrations and exposure times being taken into account by the use of collection efficiencies. This approach in determining the collision efficiency was therefore fully empirical.

Results

Effect of NaCl Concentration on Deposition. The variation in total collection efficiency with salt concentration for the deposition of *P. aeruginosa* on both glass and 2-vinylpyridine–styrene (2-VPS) surfaces is shown in Figure 2. The bars show the negative logarithm of the average values for three replicate disks for each surface and salt concentration. For glass surfaces, the collection efficiency increased by 2 orders of magnitude with increasing salt concentration, ranging from 1.2×10^{-8} for virtually no salt added (10^{-6} M) to a maximum of 2.7×10^{-6} for 10^{-2} M salt.

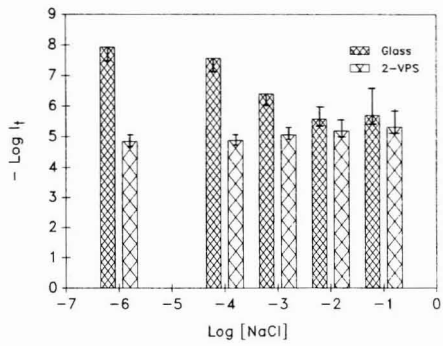

Figure 2. Variation with salt concentration in the negative logarithm of the mean total collection efficiency for *P. aeruginosa* deposition on glass and 2-VPS surfaces in the rotating disk system. The error bars show the logarithm of the mean plus and minus one standard deviation where greater than zero.

Table I. Effect of NaCl Concentration on the Collision Efficiency for *P. aeruginosa* Deposition on Glass

[NaCl], M	α	[NaCl], M	α
10^{-6}	8.3×10^{-4}	10^{-2}	4.1×10^{-1}
10^{-4}	2.1×10^{-3}	10^{-1}	4.1×10^{-1}
10^{-3}	4.6×10^{-2}		

In contrast to the glass surfaces, the highest collection efficiencies for the 2-VPS surfaces were obtained at the lowest salt concentrations and the range of values were much smaller. The maximum shown in Figure 2 was 1.4×10^{-5}, obtained at 10^{-6} M NaCl, while the minimum was 5×10^{-6} at 10^{-1} M NaCl.

Collision Efficiency. Estimates of the collision efficiency for the deposition of *P. aeruginosa* on glass for the different electrolyte conditions were obtained by dividing the total collection efficiency observed for glass by that observed for the 2-VPS surface. Values ranged from 8.3×10^{-4} to 4.1×10^{-1} for NaCl concentrations from 10^{-6} to 10^{-1} M (Table I). The collision efficiency calculations clearly show the following: (1) a nearly 3 order of magnitude difference in α for the range of NaCl concentrations from 10^{-6} to 10^{-1} M, (2) the absence of an effect of changing salt concentration above 10^{-2} M NaCl, (3) the failure of the collision efficiency to attain a value of 1, and (4) the presence of intermediate values for NaCl concentrations between 10^{-6} and 10^{-2} M.

Variation in Collection Efficiency with Radial Position. Evaluation of the local collection efficiency revealed a radial dependence (Figure 3). In the figure, the data for *P. aeruginosa* deposition on 2-VPS at 10^{-6} and 10^{-4} M NaCl were combined since the efficiencies were similar. Each point thus represents the average of values for a given radial position from six disks. The collection efficiency decreased by 1 order of magnitude as the radial position increased from 1 to 10 mm. The error bars show one standard deviation and include the variability in counts and among disks. A similar trend was observed for cells deposited on glass. The horizontal lines in this plot represent the total collection efficiency predicted by the trajectory model of Spielman and Fitzpatrick (*4*) for 0.7-

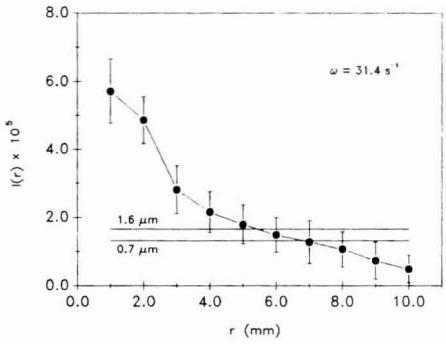

Figure 3. Variation with radial position in the local collection efficiency for *P. aeruginosa* deposition on 2-VPS surfaces in the rotating disk system. The means shown are based on data for 10^{-6} and 10^{-4} M NaCl (six disks). The error bars show one standard deviation. The horizontal lines indicate levels predicted by the trajectory model of Spielman and Fitzpatrick (*4*) for 1.6- and 0.7-μm spheres of specific gravity 1.1.

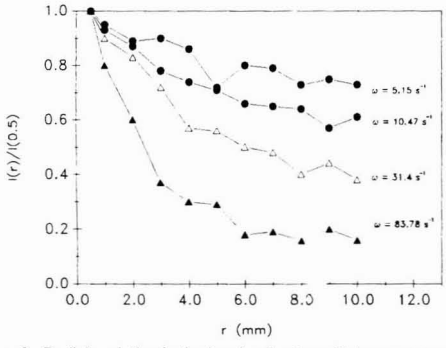

Figure 4. Radial variation in the local collection efficiency normalized with respect to the maximum value for polystyrene latex spheres depositing on disks rotating at various speeds. The medium was distilled water. For $\omega = 5.15$ s^{-1}, 1.0-μm amino-modified spheres and a glass disk were used. For all other speeds, 1.62-μm sulfated spheres and 2-VPS-coated disks were used.

and 1.6-μm spheres. If the radial variation were overlooked, the comparison between the empirical and predicted total collection efficiency might be considered either very good or off by 1 order of magnitude, depending on the random selection of counting fields.

Similar experiments using polystyrene latex spheres also revealed a radial dependence. Local collection efficiencies for various disk rotation speeds, normalized with respect to the maximum value, are presented in Figure 4. For all speeds, the collection efficiency for polystyrene latex spheres decreased with increasing distance from the center of the disk in a pattern similar to that shown for *P. aeruginosa*. A more rapid decrease with radial position was observed as the rotational speed increased from 5.15 to 83.8 s^{-1}.

The distributions for the 1.62-μm latex spheres and *P. aeruginosa* deposited on 2-VPS surfaces obtained at a rotational speed of 31.4 rad/s are compared in Figure 5. The results for the bacteria are based on the data for 10^{-6} and 10^{-4} M NaCl as in Figure 3. Since the rate of decline in the local collection efficiency was similar for both particles, the effect cannot be attributed to particular mechanisms of bacterial attachment. For example, it is not likely that attachment was limited by the time required for bacterial synthesis and extrusion of cementing polymers.

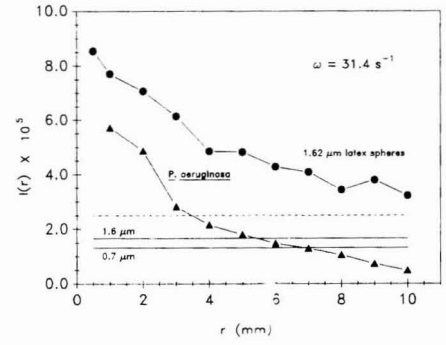

Figure 5. Comparison of radial distributions in the local collection efficiency for 1.62-μm sulfated polystyrene latex spheres (as in Figure 4) and *P. aeruginosa*, 0.7 × 1.6 μm rod-shaped bacteria (as in Figure 3), both deposited on 2-VPS surfaces in the rotating disk system at a rotational speed of 31.4 s^{-1}. The dashed line shows the trajectory model prediction for the latex particles, assuming specific gravity 1.05. The solid lines are the predicted values for 1.6- and 0.7-μm spheres of specific gravity 1.1.

Discussion

Effect of NaCl Concentration. The trend observed here for bacteria depositing on glass was qualitatively consistent with the theory of double-layer interaction. That is, the repulsive electrical interaction energy should decrease with increasing ionic strength for a given particle–surface separation distance thereby permitting the dominance of attractive interactions such as van der Waals forces and an increase in deposition. Abbott et al. (*19*) obtained similar results for the deposition of *Streptococcus mutans* in a rotating disk system. Other investigators, using various experimental systems, have observed increasing levels of attached cells with increasing ionic strength up to 0.01–0.1 M (*20–23*).

While the results shown in Figure 2 suggested a trend of decreasing collection efficiency on 2-VPS with increasing salt concentration, the experimental variability prevents any firm conclusion. Bowen and Epstein (*1*) attributed such an apparent increase in deposition rates at low ionic strength for oppositely charged particles and surfaces to increased attractive double-layer interactions. Recent work by Elimelech (*24*) provides additional support for this hypothesis. Another possibility for the trend in Figure 2 is steric stabilization as the ionic strength is increased. At high ionic strength, adsorbed polyelectrolytes, such as bacterial polymers, can have a configuration that extends further from the solid surface (*25*) and can give rise to a strong repulsive interaction energy.

The comparison of deposition on the 2-VPS and glass surfaces at low salt concentration as well as the effect of increasing salt concentration provided strong evidence that electrostatic forces can have a dominating influence on the deposition of *P. aeruginosa* at NaCl concentrations below 10^{-2} M. Above this concentration, however, collection efficiencies for the two surfaces became comparable, differing by a factor of ~2. This relatively small difference may have been due to attractive hydrophobic interactions, the polymer-coated surface being considerably more hydrophobic than the glass. Such interactions could involve proteins present in the flagella or the outer membrane of the cells. It is also possible that despite compression of the electrical double layers under these electrolyte conditions, repulsive electrostatic interactions at small separation decreased the probability of attachment to the glass surfaces. Finally, trace quantities of organics in the aqueous phase carried over from the original *P. aeruginosa*

culture may have contributed to the effect by altering the surface charge and surface free energy of the glass and 2-VPS surfaces (*26*, *27*).

Collision Efficiency. Although the collection efficiencies discussed above are convenient for analyzing the results of this study, only the trends and not the numbers can be extrapolated to other systems of different hydrodynamic properties. The collision efficiencies reported in Table I, however, represent probabilities of attachment regardless of the particle transport conditions. A subsequent paper will describe their use in modeling the deposition of bacteria under similar solution conditions in a model porous medium consisting of glass beads.

One important implication of these results is that any discussion of mechanisms of bacterial attachment must take into account the relevant solution conditions. Thus, in seawater, for example, in which electric double layers are not diffuse, short-range hydrophobic interactions could play a more important role in attachment than they would in ultrapure water systems characterized by very low ionic strength and, hence, extended electric double layers.

There is currently a great deal of interest in the movement of bacteria in groundwater, in relation to both traditional concerns about microbial pollution and recent schemes for biological remediation of contaminated groundwater. Typical ionic strengths for groundwaters range from 10^{-3} to 10^{-2} M (*28*), with often significant concentrations of divalent cations. The collision efficiencies determined in this work varied by 1 order of magnitude over this range, showing the need to consider specific solution conditions when dealing with bacterial attachment in aquifers.

Comparison with Particle Deposition Models. As shown in Figure 3, predicted collection efficiences based on the trajectory model of Spielman and Fitzpatrick (*4*) and observed values were within 1 order of magnitude for *P. aeruginosa* at a rotational speed of 31.4 s^{-1}, despite the radial variation. This extent of quantitative agreement was probably only fortuitous, however. The trials with latex particles at a rotational speed of 5.15 s^{-1} yielded levels 4 times higher than predicted values while at 83.8 s^{-1} observed levels were 10 times lower than predicted. This may have been due to fluid shear effects, which are discussed below.

Because of the radial dependency of deposition, the results were not qualitatively consistent with the model's prediction of uniform deposition. Possible explanations, including experimental artifact, have been discussed in detail elsewhere (*16*), the most likely being nonuniform transport of particles to the disk surface arising from lateral migration. This phenomenon, also referred to as hydrodynamic lift, is the translation of particles across streamlines in a shear flow and results from the effects of fluid inertia on particle motion (*13*). Particle transport models in the neighborhood of a rotating disk do not include lateral migration since the description of particle motion is based on the assumption that fluid inertia is negligible. Studies of particles in shear flow have demonstrated, however, that migration can occur even at low particle Reynolds number. The phenomenon has been invoked to explain the tendency of red blood cells to concentrate at a finite distance from the capillary walls (*29*).

Theoretical and experimental work reviewed by Brenner (*13*) has indicated that the migration velocity depends on the relative velocity of particle and fluid, the particle size, and the shear rate. Work by Saffman (*30*) showed that, for a small rigid sphere moving in a uniform simple shear flow, if the particle lags behind the fluid, then migration occurs toward streamlines of higher velocity. If the particle moves faster than the fluid, migration is in the opposite direction. In a rotating disk system, lateral migration of particles across streamlines may result in particles moving across the limiting trajectory (*4*). Depending on the direction of the axial component, lateral migration across the limiting trajectory may either increase or decrease the number of particles transported to the disk. Because both the tangential and radial velocity gradient which give rise to migration are radially dependent, the magnitude of the migration velocity across streamlines should similarly be radially dependent.

An analysis of particle motion close to the disk lends credence to the hypothesis that lateral migration influences particle transport in the rotating disk system. Although the flow is three dimensional with axial, radial, and tangential components, it is sufficient to consider only the tangential component of the fluid velocity in the region close to the disk since this approaches the disk velocity while the axial and radial components decrease to zero at the disk surface (*31*). To a first approximation, the tangential velocity increases linearly with increasing radial position as well as with decreasing distance from the surface. Since the velocity of a particle close to the surface would be less than that of the fluid as a result of wall effects (*32*), the essential factors giving rise to migration would be present, i.e., a nonzero particle velocity relative to the fluid (slip velocity) and shear flow. Furthermore, because both the particle slip velocity and the magnitude of the velocity gradient depend on the radial and axial coordinates, the migration velocity would not be uniform. The rate of particle transport to the disk would therefore depend on radial position.

Several other studies of particle deposition employing a rotating disk have given no indication of nonuniform deposition (*3*, *33*, *34*). Indeed, Hull and Kitchener (*3*) plainly stated that for negatively charged particles and positively charged surfaces the deposition was uniform. This conclusion was based on counts made in four different areas of the disk, which may not have been sufficient to reveal radial variation. In all of these studies, the particle diameter did not exceed 0.45 μm. In the Masters Thesis of Toppan (*35*), however, the observation of higher levels of deposition toward the center of the disk for 8-μm polystyrene latex particles was reported. The effect was not systematically studied, however, and no effort was made to explain the radial dependence. Since the migration velocity depends on particle size, it is possible that the effect was negligible for the studies employing submicron particles.

With regard to understanding the transport of bacteria, many vegetative cells are smaller than 1 μm in size, and starved cells less than 0.4 μm in diameter have been observed (*36*, *37*). Further investigation of lateral migration for submicron particles under various hydrodynamic conditions is needed to clarify the significance of the phenomenon in situations such as the transport of bacteria in groundwater.

To quantify the migration for purposes of determining particle transport to the surface of the rotating disk, the shear stress resulting from the radially dependent tangential and radial velocity components must be considered and is currently being developed. For the purposes of this study, the vector sums of the radial and tangential velocities were used to evaluate the shear stress at the surface of the disk. In Figure 6, the normalized local collection efficiencies for 1.62-μm latex spheres have been plotted

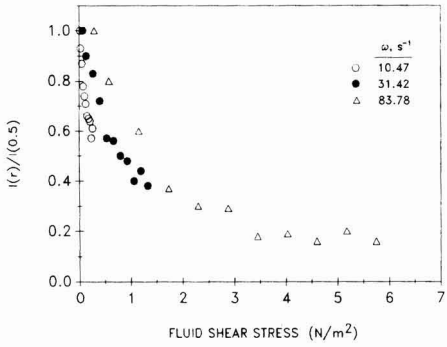

Figure 6. Combined data for 1.62-μm polystyrene latex spheres showing variation in the local collection efficiency normalized with respect to the maximum value of the tangential fluid shear stress at the disk surface. The shear stress was determined from the vector sum of the tangential and radial velocity components, assuming the resultant velocity gradient was linear.

as a function of the shear stress (τ) at the surface. The shear stress was determined from the vector sum of the velocities by assuming a linear velocity profile. The interesting observation that emerges is that for rotational speeds of 10.5, 31.4, and 83.8 s^{-1}, the variation in the local collection efficiency with shear stress is very similar with rapid decreases occurring at low levels of shear (<1 N/m^2). Furthermore, there appears to be no characteristic value of shear that might correspond to a mean strength of particle–surface interaction.

It should be noted that nonuniform deposition has also been reported by Varennes and van de Ven (*12*) for deposition of 3-μm polystyrene particles on glass surfaces in an impinging jet system. Theoretical considerations lead to the expectation of uniform deposition in this axially symmetric system in which the fluid shear at the surface increases linearly with distance from the stagnation point. The authors found that deposition rates and total accumulation decreased with radial position. Qualitatively, the radial distribution was quite similar to that observed in this work. It also showed a more rapid decline as the Reynolds number increased. The explanation offered by the authors implied that a finite time for bond formation is required and that there is insufficient contact time in a high-shear environment. Similar arguments have been advanced to explain the effect of shear on bacterial attachment in capillaries (*10*, *11*). Considering the plot in Figure 6, however, this explanation would imply in the present case that the kinetics of bond formation vary over a wide range and that there is no clearly identifiable contact time sufficient for all particle–surface encounters to result in bond formation. This does not seem likely for oppositely charged particles and surfaces.

Conclusions

Because of their widespread significance in natural and engineered systems, particle–surface interactions remain a topic of active theoretical and experimental investigation. From a practical standpoint, the rotating disk system has provided a fully empirical approach to determining particle collision efficiencies provided that deposition is evaluated as a function of distance from the disk center. Because of the radial dependence of particle deposition, a semiempirical approach to determining collision efficiencies based on theoretical modeling of particle transport to the disk surface is not yet feasible. It is likely that this effect was due to lateral migration, and its incorporation into particle deposition models for the rotating disk is under study at the present time. The results of this study show that the effect can be significant for particles as small as 1 μm in diameter and at levels of fluid shear stress below 0.5 N/m^2. Models for other systems such as parallel plate channels and impinging jets should also be reexamined to determine the importance of migration.

Despite the lack of a satisfactory particle deposition model, the rotating disk system described in this study has been used successfully to demonstrate an increase in collision efficiency with increasing salt concentration for *P. aeruginosa* depositing on glass. Values ranged from 8.3 $\times 10^{-4}$ to 0.41 for NaCl concentrations from 10^{-6} to 10^{-1} M. These results confirm the importance of electrostatic forces in the attachment of bacteria to surfaces.

Glossary

A_c	area counted in field (1.5 $\times 10^4$ μm^2 except as noted)
A_d	total area of disk (3.5 $\times 10^{-4}$ m^2)
$A_z(r)$	total area in counting zone of average radius r ($2\pi r$ dr)
$I(r)$	local collection efficiency
I_t	total collection efficiency
N	concentration of suspended particles
$\tilde{n}(r)$	average of particles counted in zone at r
$R(r)$	local deposition rate in area $A_z(r)$
$R_o(r)$	rate of particle flow far from disk toward counting zone
t	exposure time
α	collision efficiency
ω	rotational speed in radians per second (s^{-1})

Literature Cited

(1) Bowen, B. D.; Epstein, N. *J. Colloid Interface Sci.* **1979**, *72*, 81–97.
(2) Dabros, T.; Adamczyk, Z.; Czarneck, J. *J. Colloid Interface Sci.* **1977**, *62*, 529–541.
(3) Hull, M.; Kitchener, J. A. *Trans. Faraday Soc.* **1969**, *65*, 3093–3104.
(4) Spielman, L. A.; Fitzpatrick, J. A. *J. Colloid Interface Sci.* **1973**, *42*, 607–623.
(5) Tobiason, J. E.; O'Melia, C. R. *J.—Am. Water Works Assoc.* **1988**, *80*, 54–64.
(6) Cochran, W. G. *Proc. Cambridge Philos. Soc.* **1934**, *30*, 365–375.
(7) Levich, V. G. *Physico-chemical Hydrodynamics*; Prentice-Hall, Inc.: Englewood Cliffs, NJ, 1962.
(8) Ruckenstein, E.; Prieve, D. C. *J. Chem. Soc., Faraday Trans. 2* **1974**, *69*, 1522–1536.
(9) Spielman, L. A.; Cukor, P. M. *J. Colloid Interface Sci.* **1973**, *43*, 51–65.
(10) Powell, M. S.; Slater, N. G. K. *Biotechnol. Bioeng.* **1983**, *25*, 891–900.
(11) Rutter, P.; Leech, R. *J. Gen. Microbiol.* **1980**, *120*, 301–307.
(12) Varennes, S.; van de Ven, T. G. M. *PCH, Physico Chem. Hydrodyn.* **1987**, *9*, 537–539.
(13) Brenner, H. *Adv. Chem. Eng.* **1966**, *6*, 287–438.
(14) O'Melia, C. R. *Environ. Sci. Technol.* **1980**, *14*, 1052–1060.
(15) Riddiford, A. C. *Adv. Electrochem. Electrochem. Eng.* **1966**, *4*, 47–116.
(16) Martin, R. E. Ph.D. Dissertation, The Johns Hopkins University, Baltimore, MD, 1990.
(17) Revell, R. S. M.; Agar, A. W. *Br. J. Appl. Phys.* **1955**, *6*, 23–25.
(18) Norris, J. R.; Swain, H. *Methods in Microbiology*; Norris, J. R., Ribbons, D. W., Eds.; Academic Press: New York, 1971; Vol. 5A, pp 105–134.
(19) Abbott, A.; Rutter, P. R.; Berkeley, R. C. W. *J. Gen. Microbiol.* **1983**, *129*, 439–445.
(20) Gordon, A. S.; Millero, F. J. *Appl. Environ. Microbiol.* **1984**, *47*, 495–499.
(21) Marshall, K. C.; Stout, R.; Mitchell, R. *J. Gen. Microbiol.* **1971**, *68*, 337–348.

(22) Rutter, P. R.; Abbott, A. *J. Gen. Microbiol.* **1978**, *105*, 219–226.
(23) Stanley, P. M. *Can. J. Microbiol.* **1983**, *29*, 1493–1499.
(24) Elimelech, M. Ph.D. Dissertation, The Johns Hopkins University, Baltimore, MD, 1990.
(25) Yokoyama, A.; Srinivasan, K. R.; Fogler, H. S. *Langmuir* **1989**, *5*, 534–538.
(26) Bitton, G.; Marshall, K. C. *Adsorption of Microorganisms to Surfaces*; Wiley Interscience: New York, 1980; pp 59–104.
(27) Neihof, R.; Loeb, G. *J. Mar. Res.* **1974**, *32*, 5–12.
(28) Stumm, W.; Morgan, J. *Aquatic Chemistry*; John Willy and Sons: New York, 1981; pp 534–548.
(29) Segre, G.; Silberberg, A. *J. Fluid Mech.* **1962**, *14*, 136–157.
(30) Saffman, P. G. *J. Fluid Mech.* **1965**, *22*, 385–400.
(31) Schlichting, H. *Boundary Layer Theory*, 4th ed.; McGraw Hill Book Co., Inc.: New York, 1960; pp 102–107 (translated by J. Kestin).
(32) Goldman, A. J.; Cox, R. G.; Brenner, H. *Chem. Eng. Sci.* **1967**, *22*, 653–660.
(33) Clint, G. E.; Clint, J. H.; Corkill, J. M.; Walker, T. *J. Colloid Interface Sci.* **1973**, *44*, 121–132.
(34) Marshall, J. K.; Kitchener, J. A. *J. Colloid Interface Sci.* **1966**, *22*, 342–351.
(35) Toppan, W. C. An experimental investigation of particle capture by the rotating disk (with application to water and wastewater treatment). Masters Thesis, Clarkson College of Technology, Potsdam, NY, 1973.
(36) Kjelleberg, S.; Hermansson, M. *Appl. Environ. Microbiol.* **1984**, *48*, 497–503.
(37) Novitsky, J. A.; Morita, R. Y. *Appl. Environ. Microbiol.* **1977**, *33*, 635–641.

Received for review December 13, 1990. Accepted July 1, 1991. This research was supported by the U.S. Geological Survey (Project 14-08-0001-G1284) and by the National Science Foundation (Grant ECE-8451060 Presidential Young Investigator Award). R.E.M. also gratefully acknowledges the support of the Washington Chapter of the ARCS foundation.

Experimental Investigation and Review of the "Solids Concentration" Effect in Adsorption Studies

James P. McKinley* and Everett A. Jenne

Pacific Northwest Laboratory, Richland, Washington 99352

■ Abundant literature references suggest that unit adsorption (i.e., mass of adsorbate sorbed per unit mass of adsorbent) declines as the mass of available adsorbent per unit volume increases. Adsorption of cadmium by iron oxyhydroxide was experimentally quantified at pH 7.00 for equilibrium aqueous cadmium of 0.025–22000 nM and for suspended iron oxyhydroxide concentrations of 0.5–50 mmol/L. For the full range of solids concentrations, over all equilibrium cadmium concentrations, adsorption was approximated by a single Freundlich isotherm. An exception to this was slightly *increased* unit adsorption at high relative solids or low relative aqueous concentrations, which were inversely related. Examination of published accounts of the "solids concentration" effect—excluding those which are admittedly caused by experimental artifacts—revealed either inappropriate experimental design or errors of data interpretation.

Introduction

During groundwater transport of a dissolved metal from a point source, adsorption incrementally reduces the concentration along the flow path, and the quantity of adsorbate removed from solution declines accordingly. The equilibrium dissolved concentration at any point is a function of the following: the solid-phase surface area per unit volume of the aqueous phase; the adsorption site density per unit area of the adsorbent; the binding strength, or affinity, of the adsorbate–adsorbent pair; and the total amount of dissolved adsorbate available for interaction with the adsorbent surface. The mathematical relationships between these quantities must be known to understand and model the transport process successfully. The effective surface site density per unit volume of the aqueous phase, for example, may be taken to be a direct function of the solid-phase surface area. Contrary to this assumption, however, are experimental results indicating that the quantity of a metal adsorbed per unit quantity of adsorbent ("unit adsorption") decreases significantly with increasing mass of adsorbent per unit volume, e.g., as summarized by Honeyman and Santschi (*1*). This decrease in unit adsorption has been termed the "solids concentration" effect. If real, this effect would require scaling of surface complexation constants, defined in dilute suspensions, to the greater effective sediment concentrations encountered in the field.

Some observations of the solids concentration effect may be explained by experimental procedure. These causes may be grouped into five classes: (1) adsorption by "nonsettling" colloids that remain suspended in the aqueous phase after centrifugation or filtration (*2–6*); (2) competition for adsorbate by complexing agents (particularly organic carbon) desorbed from the adsorbent (*4–8*); (3) implicit adsorbate competition (*8, 9*); (4) increased solids aggregation (e.g., flocculation) to produce a net decrease in readily available adsorption sites (*3, 10–15*); and (5) extraneous chemical reactions such as sulfide mineral dissolution or metal oxyhydroxide precipitation (*2*), or the presence of bacteria (*16*) that produce changes in system composition, pH, or E_h.

The results of a number of investigations show decreased adsorption with increasing solids concentration that cannot be accounted for by experimental artifacts. In these investigations, adsorption may be expressed as the quantity adsorbed per unit quantity of adsorbent (unit adsorption) or as the fractional partitioning of adsorbent to the solid phase when normalized to the quantity of adsorbent present (K_d). Among the most direct observations are those of Di Toro et al. (*17*), who reported a decrease in unit adsorption. Other investigations of a variety of solutes report that K_d decline as solids concentration increases (*3, 5, 18*). More recently, Honeyman and Santschi (*1*) and Honeyman et al. (*19*) have attempted to generalize the effect to show that K_d values for six adsorbates on various adsorbents tend to decrease with increasing solids concentration (C_p). Substances for which adsorption apparently declined with increasing C_p include inorganic and organic adsorbates in freshwater and marine sediments, quartz, clays and clay minerals, and digested sewage sludge (*3, 4, 17, 18*). It seems unlikely that experimental artifacts could explain widespread agreement of a C_p effect for so diverse a set of adsorbates, adsorbents, and investigators.

 0013-936X/91/0925-2082$02.50/0

In contrast to the above, researchers investigating a variety of adsorbates and adsorbents have failed to observe a significant solids concentration effect. These investigations include manganese adsorption by $CaCO_3$ (*20*), copper and lead adsorption by hydrous ferric hydroxide (*21*), calcium and zinc adsorption by ferrihydrite (*22*), and adsorption of chromate by a variety of natural solids (*23*).

The interrelationship of parameters determining the equilibrium dissolved concentration of adsorbate may, in part, explain these disparate results. It has been previously noted that unit adsorption increases with solids concentration at fixed total metal concentration and constant pH, analogous to the titration of a metal cation with a dissolved complexing ligand (*24*, *25*) or of anions with positive complexing solid ligands (*26*). In this paper, we detail an experimental investigation of the solids concentration effect, review the results of other investigations, and conclude that prior observations and models of the solids effect for cationic metals may be in error.

Theoretical Model. The surface complexation model represents the hydroxylated solid (adsorbent) surface by a general hydrolyzed species (*27*), [e.g., $\equiv FeOH^0$ ($\equiv$Fe may represent any solid inorganic substrate)]. The substrate interacts amphoterically with its coexistent solution (*28*):

$$\equiv FeOH_2^+ = \equiv FeOH^0 + H_s^+ \quad (1)$$

$$\equiv FeOH^0 = \equiv FeO^- + H_s^+ \quad (2)$$

where the subscript s indicates proximity to the surface. Equations 1 and 2 have associated "intrinsic" acidity constants that use the Boltzman distribution to relate H_s^+ to the bulk solution concentration via an electrostatic term (*29*):

$$K_{a1}^{int} = [\equiv FeOH^0][H^+] \exp(-e\psi_o/kT)/[\equiv FeOH_2^+] \quad (3)$$

$$K_{a2}^{int} = [\equiv FeO^-][H^+] \exp(-e\psi_o/kT)/[\equiv FeOH^0] \quad (4)$$

where ψ_o is the surface electrostatic potential (μV). The reaction of a dissolved cation with an $\equiv FeOH^0$ site may be represented by an analogous equation (*30*):

$$\equiv FeOH^0 + M^{2+} = \equiv FeO\text{–}M^+ + H^+ \quad (5)$$

By analogy with aqueous-phase reactions

$$K_{ads} = [\equiv FeO\text{–}M^+][H^+]/[\equiv FeOH^0][M^{2+}] \quad (6)$$

where concentrations are in moles per liter. This expression for K_{ads} includes the following assumptions: (1) the activity coefficients for H^+ and Cd^{2+} in a medium of fixed ionic strength are constant and can be included in K_{ads}; (2) the ratio of activity coefficients for the surface species $\equiv FeO\text{–}Cd^+$ and $\equiv FeOH^0$ is near unity (*31*); (3) at constant pH (a nominal condition), the electrostatic term [as specified in Davis and Leckie (*30*)] is constant and included in K_{ads}. Two further specifications are sufficient to describe the adsorptive process. First, the mass-balance relationships for adsorbent and adsorbate

$$[\equiv FeOH]_t = [\equiv FeOH^0] + [\equiv FeO^-] + [\equiv FeOH_2^+] + [\equiv FeO\text{–}Cd^+] \quad (7)$$

$$[Cd]_t = [Cd]_e + [\equiv FeO\text{–}Cd^+] \quad (8)$$

where $[Cd]_t$ and $[Cd]_e$ are total cadmium and equilibrium aqueous cadmium concentrations, respectively. The system of interest may usually be constructed so that $[\equiv FeO^-]$ and $[\equiv FeOH_2^+]$ are negligible; otherwise, they may be calculated from eqs 5 and 6. Second, the definition of the adsorption maximum as the fraction of adsorbent that is surface active

$$A_{max} = [\equiv FeOH]_t/[Fe]_t \quad (9)$$

where $[Fe]_t$ is the total moles or mass of iron in the system, and A_{max} is the fraction of $[Fe]_t$ that could accept M^{2+} at saturation. Substitution of eq 6 into 7 and rearrangement yields an equation in the form of the Langmuir isotherm, implicitly including eq 9:

$$[\equiv FeO\text{–}M^+]/[Fe]_t = ([\equiv FeOH]_t/[Fe]_t)(K_{ads}/[H^+])[M^{2+}]/(1 + (K_{ads}/[H^+])[M^{2+}]) \quad (10)$$

On a logarithmic isotherm plot of unit adsorption ($[Cd]_a$; moles of Cd/mole of Fe) versus $[Cd]_e$, suspensions with low M^{2+} to $[Fe]_t$ ratios exhibit unit slope (i.e., Langmuirian behavior).

Experimental data often do not behave as predicted by eq 10, but fit the empirical Freundlich isotherm, which may be expressed

$$[\equiv FeO\text{–}M^+]/[Fe]_t = K_{ads}[M^{2+}]^{1/n} \quad (11)$$

where K and n are constants. When $n = 1$, the Freundlich isotherm is operationally similar to the Langmuir isotherm. Unlike the Langmuir isotherm, the Freundlich isotherm does not have a limiting adsorbed concentration. When $n > 1$, a logarithmic isotherm plot will have less than unit slope, so that at higher $[Cd]_e$, fractionally less adsorbate will have been removed from solution.

Equations 10 and 11 indicate that an equilibrium state is determined by either the total adsorbate or adsorbent present, when the other is held constant. However, in experimental systems, the nonequivalence of constant adsorbate and adsorbent has been frequently reported. Various explanations are evaluated in the Discussion.

Experimental Procedure

Experiments were conducted at $[Fe]_t$ of 0.0005, 0.001, 0.005, 0.01, and 0.05 mol/L. Fresh iron oxyhydroxide was prepared from ferric nitrate for each experiment in a 500-mL jacketed stir vessel under an inert nitrogen atmosphere at 25 °C (±0.1 °C). Sodium nitrate was added as necessary to yield a final ionic strength of 0.1 M. Iron oxyhydroxide was precipitated by titration with 1.0 M carbonate-free sodium hydroxide to a final pH of 7.2 (±0.05). Since iron oxyhydroxide is not a thermodynamically stable phase, a new preparation was made and aged for a uniform period of 16 h at pH 7.2 before each experiment. The experiments were conducted in a nitrogen atmosphere.

Amounts of solutions and suspensions were quantified by weight. By use of a volumetric pipet, 0.1 mL of ^{109}Cd-bearing, pH-neutral, standard solution at eight cadmium concentrations, spanning a concentration range of 1×10^{-6} to 3×10^{-3} M, was added in duplicate to polycarbonate centrifuge tubes. A 10-mL aliquot of iron oxyhydroxide suspension at pH 7.2 was added to each tube. Tubes were capped and shaken for 4 h and then centrifuged. A 1.0-mL aliquot of supernatant was removed to a scintillation vial; the activity of ^{109}Cd was determined by liquid scintillation counting. Samples were processed sequentially with blanks and standards during each experiment, and the concentration of cadmium in each standard solution was confirmed by inductively coupled plasma atomic emission spectroscopy. The pH of the unstirred supernatant in each sample tube was determined immediately after removal of the scintillation volume by using a combination electrode under a nitrogen atmosphere. Equilibration with the electrode required 20–30 min.

Results

Overall results are presented in Table I. The log–log isotherm for all results, in logarithmic terms of eq 11, is

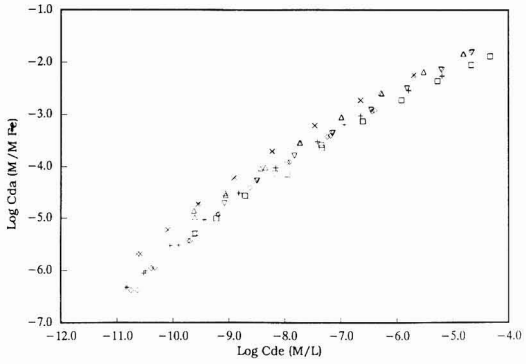

Figure 1. Combined adsorption isotherms, uncorrected for the effects of pH. Experiments were conducted in duplicate. Total iron: ▽, 0.0005 mol/L; △ and □, 0.001 mol/L; ×, 0.005 mol/L; +, 0.01 mol/L; ◇, 0.05 mol/L.

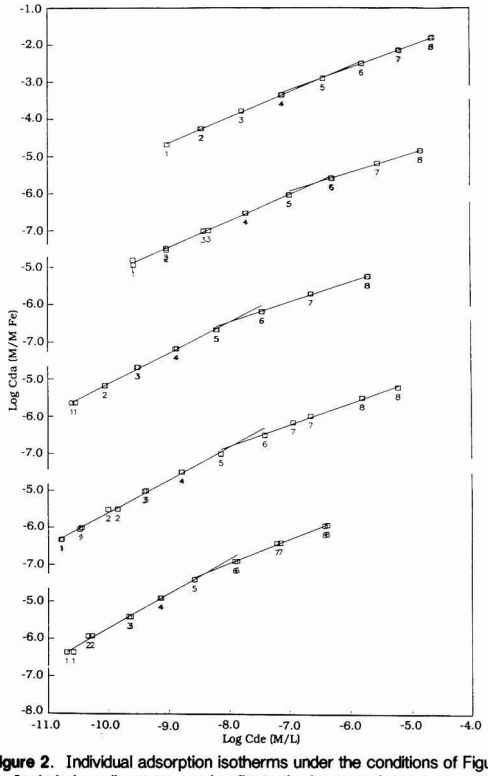

Figure 2. Individual adsorption isotherms under the conditions of Figure 1. Included are linear regression fits to the lower and upper segments of each isotherm.

presented as Figure 1. The results from different experiments vary over approximately three-quarters of a log unit in the dependent variable ($[Cd]_a$) at any given $[Cd]_e$ but do not vary in a systematic manner with adsorbent concentration.

Each isotherm is seen to be curvilinear (Figure 2). In a manner analogous to that of Benjamin and Leckie (*32*), each isotherm may be approximated by two intersecting straight-line segments, which are also plotted in Figure 2. The point of intersection for the two line segments was determined by simultaneously solving the regression-line pair for each isotherm. Intersection concentrations of $[Cd]_e$ are listed along with line-segment slopes in Table I.

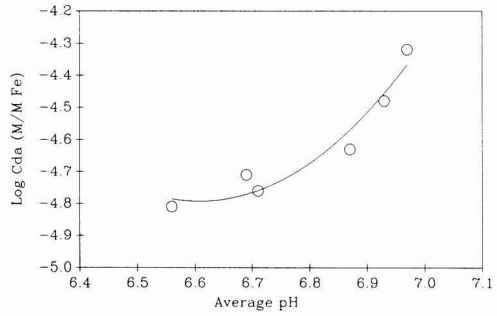

Figure 3. Effect of average pH on cadmium adsorption at $[Cd]_e$ of 1×10^{-9} M. Regression line is defined by the equation log $[Cd]_a$ = 137.2 − 42.98pH + 3.25pH^2.

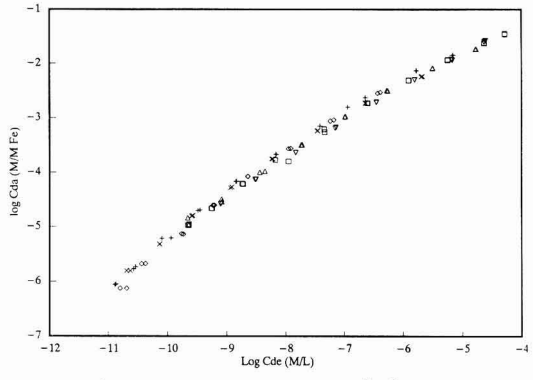

Figure 4. Combined adsorption isotherm at $[Fe]_t$ of 0.0005–0.05 mol/L, corrected to a uniform pH of 7.00.

Base addition and pH buffers were considered to be possible sources of error in sorption experiments, so pH was not adjusted during equilibration. Inspection of Table I shows that the final pH in all experiments deviated from the initial value of 7.2, held by titration during aging, by as much as −0.6 unit. The effects of pH variation on adsorption were empirically corrected as follows. The amount of Cd^{2+} that would be adsorbed at 1 nM $[Cd]_e$ was estimated from interpolation of the appropriate line segment in Figure 2. A graph of this calculated $[Cd]_a$ against the average pH for each experiment shows a strong correlation (Figure 3), but there is no correlation between $[Fe]_t$ and pH. From the regression of the data shown in Figure 3, a pH correction value (the departure of the regression line from its value at pH 7.00) was determined for each experiment that would approximate the unit adsorption results at $[Cd]_e$ of 1 nM of dissolved concentration for an otherwise identical experiment at pH 7.00. Since adjustments in pH affect the Y intercept only (pH may be incorporated into K_{ads} of eq 11 as it is in eq 10), and since the equilibrated pH of each isotherm is less than 7.00, this value may be applied to individual values of $[Cd]_a$. This incremental value, given as $[Cd]_{a,corr}$ in Table I, was added to each value for cadmium adsorbed to produce equivalent log–log isotherms for all data at pH 7.00 (Figure 4). All data are now essentially collinear (i.e., they express a single isotherm) over a range in $[Fe]_t$ of 0.0005–0.05 mol/L.

Discussion

Experimental results show that, as $[Fe]_t$ increases, the slope of the low-$[Cd]_e$ segment of each isotherm is steeper and the $[Cd]_e$ at which the apparent inflection between segments occurs is lower (see Figure 2 and Table I). In-

Table I. Experimental Results[a]

	experiment					
	1	2	3	4	5	6
$[Fe]_t$	0.0005	0.001	0.001	0.005	0.01	0.05
pH	6.87	6.56	6.93	6.97	6.69	6.71
SD pH	0.14	0.14	0.15	0.10	0.10	0.08
$[Cd]_{a,corr}$	0.48	0.47	0.46	0.16	0.07	0.27
M_1	0.68	0.82	0.71	0.82	0.87	0.93
M_2	0.59	0.57	0.50	0.54	0.56	0.65
$[Cd]_{e,int}$	6.44	7.75	6.54	7.98	7.94	8.43

	experiment											
	1		2		3		4		5		6	
$[Cd]_s$	$[Cd]_a$	$[Cd]_e$	$[Cd]_a$	$[Cd]_e$	$[Cd]_a$	$[Cd]_e$	$[Cd]_a$	$[Cd]_e$	$[Cd]_a$	$[Cd]_e$	$[Cd]_a$	$[Cd]_e$
5.97	4.70	9.05	4.99	9.21	4.84	9.60	5.67	10.60	6.00	10.50	6.37	10.6
5.51	4.26	8.47	4.56	8.69	4.51	9.04	5.21	10.10	5.51	10.00	5.94	10.4
5.01	3.79	7.81	4.13	8.15	4.01	8.33	4.71	9.52	5.02	9.43	5.42	9.67
4.51	3.34	7.12	3.58	7.33	3.54	7.70	4.22	8.90	4.50	8.80	4.92	9.18
4.00	2.91	6.44	3.13	6.60	3.05	6.98	3.70	8.19	4.02	8.14	4.41	8.61
3.50	2.49	5.81	2.72	5.91	2.60	6.25	3.21	7.45	3.52	7.40	3.91	7.93
3.01	2.15	5.18	2.36	5.26	2.19	5.51	2.72	6.62	3.19	6.93	3.41	7.17
2.52	1.82	4.66	2.06	4.66	1.84	4.79	2.25	5.69	2.54	5.78	2.92	6.38

[a] Cadmium was added in variable but known concentrations to suspensions with fixed $[Fe]_t$; $[Cd]_a$, adsorbed (M Cd/M Fe); $[Cd]_e$, final dissolved cadmium concentration; $[Cd]_s$, cadmium standard concentration; pH, average (arithmetic) pH; $[Fe]_t$, total iron in moles per liter; $[Cd]_{a,corr}$, incremental adjustment (additive) to bring the isotherm into equivalence at pH 7.00; M_1, M_2, slopes of individual isotherm line segments; $[Cd]_{e,int}$, $[Cd]_e$ at intersection of M_1 and M_2 segments. All cadmium concentrations are pCd.

creased slope indicates a greater affinity of dissolved metal for the solid surface, so this behavior cannot be the result of decreased unit adsorption at increasing $[Fe]_t$. The changes in slope may be accounted for by the multiple-site adsorption theory (*32*) and/or "the surface precipitation" model (*27*).

According to Benjamin and Leckie (*32*), who examined the adsorption of cadmium to iron oxyhydroxide, sites with relatively high affinities for adsorbate dominated the adsorption reaction at low adsorbate concentrations, to the degree that fractional adsorption was independent of the amount of adsorbate available to the adsorbent. In this circumstance, $[Cd]_a$ was linearly proportional to $[Cd]_e$ (i.e., Langmuirian behavior was observed). At higher $[Cd]_e$, $[Cd]_a$ was a function of both total adsorbent and adsorbate, the two quantities being inversely proportional in their effect. In other words, where adsorbate was present in an amount greater than could be accommodated solely by the adsorbent's high-affinity sites, multiple-site adsorption occurred and a Freundlich isotherm could describe the behavior of the overall system. Multiple-site theory can thus explain the division of each isotherm into segments (shifting from Langmuir to Freundlich behavior).

The surface precipitation model (*27*) treats the curvilinear isotherm as the expression of a chemical continuum between adsorption due to surface complexation reactions (the Langmuir portion of the isotherm) and heterogeneous precipitation of a solid phase of the adsorbate. The common observation that a system exhibiting Freundlich behavior has no apparent adsorption maximum is considered to be the result of a solid solution of the adsorbate with the adsorbent phase. The transition from Langmuir (surface complexation) behavior to Freundlich (surface precipitation) behavior need not be abrupt; the increase in slope, at increasing $[Fe]_t$, of the low-$[Cd]_e$ segment of each adsorption isotherm in Figure 2 and, conversely, of the low-$[Cd]_e$ portion of the combined isotherm in Figure 4 may be the manifestation of a more purely adsorptive relationship between cadmium and the iron oxyhydroxide surface.

The experimental data presented here lead to the conclusion that a higher $[Fe]_t$ yields increased, not decreased, unit adsorption. In a qualitative evaluation of varying $[Cd]_t$ and $[Fe]_t$, Benjamin and Leckie (*32*) made repeated measurements of the adsorption edge both in systems in which $[Cd]_t$ varied, while $[Fe]_t$ remained constant, and in systems where the converse was true. As $[Fe]_t$ was increased, at constant $[Cd]_t$, the adsorption edge shifted to a lower pH value. Conversely, as total cadmium increased at constant $[Fe]_t$, the adsorption edge shifted to higher pH values. These findings are in accord with eqs 10 and 11 and the experimental results shown in Figure 2. At fixed pH, the amount of available adsorbent bears a constant relationship to total adsorbate. This relationship is reflected quantitatively in the single isotherm of Figure 4. As the concentration of solids increases, there is no decrease in adsorption at a given $[Cd]_e$. These observations directly contradict the body of literature that concludes that decreased unit adsorption occurs at elevated solids concentration.

Particle Interaction Model. Di Toro et al. (*17*) used elaborate experimental procedures to rule out artifact effects [i.e., desorption of complexing ligands, increased implicit adsorbate concentrations, and flocculation (or aggregation) of particles]. Nevertheless, they found that the adsorption of nickel onto montmorillonite at an aqueous concentration of 35 mg/L declined from 840 to 50 μg/g at solids concentrations of 30 and 1000 mg/L, respectively. This general relationship was said to be "independent of both sorbate [Ni and Co] and sorbent [unpurified, commercially available montmorillonite and crushed quartz]" (ref 17, p 59), over the entire range of solids concentrations examined.

To explain the dramatic decremental effect of C_p on unit adsorption, a kinetic particle interaction model was constructed (*33*). In this model, equilibrium is established between adsorbed and dissolved quantities of adsorbate when the magnitude of adsorptive and desorptive flux is equal. The underlying assumption of the model is that desorption is affected by collision, or some other interaction, between particles, and that the magnitude of this effect is proportional to the solids concentration. Di Toro et al. (*17*) adjusted the value of K_{ads} to account for increased solids concentration by inclusion of an effective

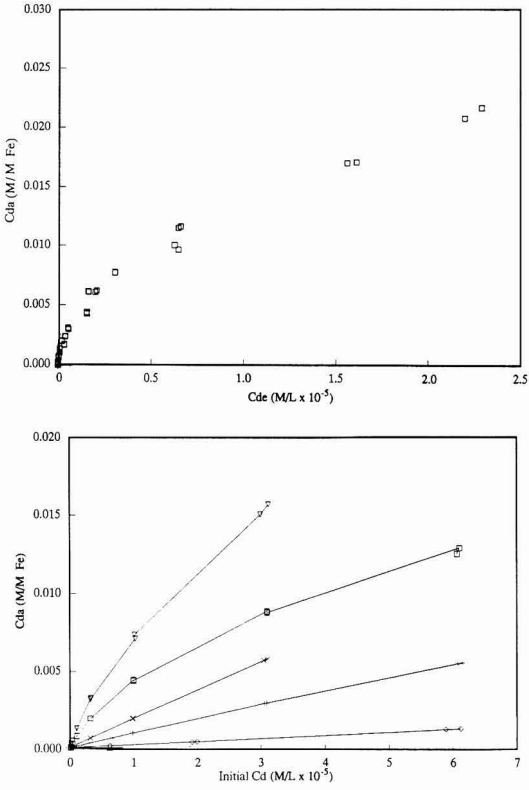

Figure 5. (A, top) Single linear-scale isotherm for all experimental data. (B, bottom) Incorrect depiction of adsorption using initial rather than equilibrium ($[Cd]_e$) adsorbate concentrations. Total Fe: ▽, 0.0005 mol/L; △ and □, 0.001 mol/L; ×, 0.005 mol/L; +, 0.01 mol/L; ◇, 0.05 mol/L.

adsorption constant K_{ads}' [expressed in the notation adopted in this paper, but otherwise identical with eq 5 of Di Toro et al. (*17*)]:

$$K_{ads}' = K_{ads}/[1 + C_p(K_{ads}/C)] \quad (12)$$

where C_p represents the mass of any adsorbent per liter and C is a correction factor. The value of C, which ranged from 0.68 to 0.91, was said to be "essentially constant for the experiments presented" (ref 17, p 60). Each C_p resulted in a distinct isotherm whose intercept was zero adsorbed metal at zero aqueous concentration, but whose slope was determined by eq 12.

Our data, collected over a wide range in $[Fe]_t$ and $[Cd]_e$, exhibited a curvilinear log–log isotherm (see Figure 4) and yielded an approximately constant K_{ads} (eq 6). Figure 5A is a linear-scale isotherm of our experimental data. The trend of adsorbed metal per unit solids concentration is curvilinear (because the axes are not logarithmic), but a 100-fold change in solids concentration is nevertheless described by a single value for K_{ads}. However, if the $[Cd]_a$ data presented in Figure 5A and Table I are plotted against *initial* aqueous concentration of Cd (Figure 5B), rather than $[Cd]_e$, the results are consistent with those reported for the particle interaction model. In this case, each solids concentration results in a distinct isotherm of characteristic average slope. This plot is *not* a valid demonstration of the effect of solids concentration on unit adsorption since K_{ads} must be calculated by using final (not initial) adsorbate concentration.

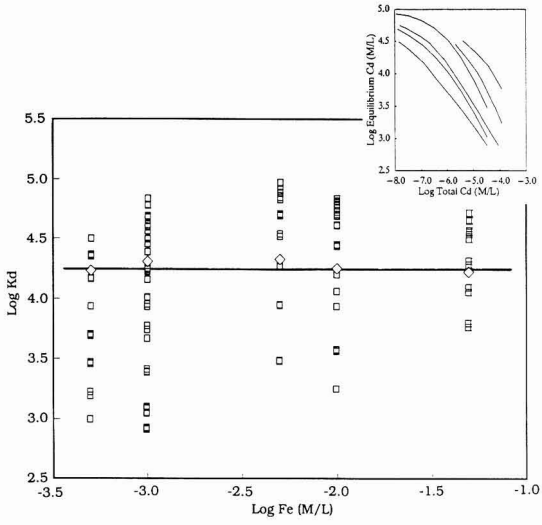

Figure 6. Dependence of K_d on particle concentration, C_p, for individual data points at 100-fold variations of $[Fe]_t$ (□) and at fixed $[Cd]_e$ (1×10^{-8} mol/L) for each C_p (◇), and for all C_p at mean K_{ads} and $1/n$ (line). For each C_p, $[Cd]_t$ increases toward lower K_d. The inset shows the dependence of K_d on $[Cd]_t$ at fixed $[Fe]_t$ values. All data are plotted without pH correction.

Variation of K_d with Solids Concentration. In published plots of K_d versus C_p, K_d is often reported to vary inversely with solids concentration (*3, 5, 18*). Consider the expression for K_d, expressed in our terminology:

$$K_d = [\equiv FeO\text{–}M^+]/[M^{2+}]C_p \quad (13)$$

where C_p is proportional to $[\equiv FeOH^0]$ (by eq 9) in units of moles or mass per liter, M^{2+} is the equilibrium concentration of the adsorbate in moles per liter, and K_d is identical with K_{ads} of eq 6 with units of volume per mass or moles, again assuming that pH is constant and that the ratio of activity constants is unity.

The value of K_d, computed for all of our data, is plotted against $[Fe]_t$ in Figure 6. Note that each experiment was conducted at constant $[Fe]_t$, while $[Cd]_t$ was varied. For each $[Fe]_t$ value, K_d declines as $[Cd]_t$ increases. Experimental data may be used with eq 11 to express a line (i.e., an isotherm), if the value of one of three variables ($[\equiv FeO\text{–}M^+]$, $[M^{2+}]$, $[Fe]_t$) is fixed. If all three variables are computationally unconstrained, the value of K_d is, likewise, not constrained to a meaningful value.

If C_p is to be treated as a variable, then K_d has a valid definition only at constant $[M^{2+}]$ (or $[Cd]_e$ in our experiments). This is because the exponential term in the Freundlich isotherm, which was shown above to affect the distribution of the adsorbate, is not explicitly recognized in eq 13. Calculated K_d values at a fixed $[Cd]_e$ (arbitrarily fixed at 1×10^{-8} mol/L) for each (constant $[Fe]_t$) experiment are included in Figure 6. Also indicated by a horizontal line is the average K_d, computed by regression to determine K_{ads} and $1/n$ for all experiments included in Figure 4. In both cases, K_d is constant (within experimental error for computations from individual experiments) over the entire 100-fold range of C_p. In contrast, the dependence of K_d, calculated according to eq 13, on $[Cd]_t$ is shown in inset in Figure 6; for each experimentally fixed value of $[Fe]_t$, K_d declines as $[Cd]_t$ rises. Finally, the interdependence between K_d, pH, and adsorption density ($[Cd]_a$) must be recognized. Intercomparison of K_d's is valid at equal pH or at equivalent (pH-corrected) $[Cd]_a$.

Conclusions

Direct experimental investigation of adsorption at varying solids concentration under appropriately controlled conditions shows that $[Cd]_a$ is constant at constant pH and equilibrium adsorbate concentrations. The increased unit adsorption at higher solids concentrations is attributed to the greater concentration of high energy sites. Reported decreases in unit adsorption with increasing C_p are apparently the result of experimental artifacts or of incorrect data reduction. Plots similar to those illustrating the particle interaction model (*33*) may be produced from data conforming to a Freundlich isotherm by misapplication of adsorption parameters during data reduction. Observed decreases in K_d at elevated C_p are directly related to specific aspects of experimental design and may not be mathematically manipulated to reproduce observed Freundlich or Langmuirian isotherms.

Registry No. Cd, 7440-43-9; iron oxyhydroxide, 11115-92-7.

Literature Cited

(1) Honeyman, B. D.; Santschi, P. H. *Environ. Sci. Technol.* **1988**, *22*, 862–871.
(2) Ames, L. L.; McGarrah, J. E., Basalt-Radionuclide Distribution Coefficient Determinations. PNL-3146; Pacific Northwest Laboratory, Richland, WA, 1980.
(3) Li, Y.-H.; Burkhardt, L.; Buchholtz, M.; O'Hara, P.; Santschi, P. H. *Geochim. Cosmochim. Acta* **1984**, *48*, 2011–2019.
(4) Gschwend, P. M.; Wu, S.-C. *Environ. Sci. Technol.* **1985**, *19*, 90–96.
(5) Voice, T. C.; Rice, C. P.; Weber, W. J. *Environ. Sci. Technol.* **1983**, *17*, 513–517.
(6) Voice, T. C.; Weber, W. J. *Environ. Sci. Technol.* **1985**, *19*, 789–796.
(7) Gschwend, P. M.; Reynonds, M. D. *J. Contam. Hydrol.* **1987**, *1*, 309–327.
(8) Higgo, J. J. W.; Rees, L. V. C. *Environ. Sci. Technol.* **1986**, *20*, 483–490.
(9) Curl, R. L.; Keioleian, G. A. *Environ. Sci. Technol.* **1984**, *18*, 916–922.
(10) Grover, R. J.; Hance, R. J. *Soil Sci.* **1970**, *109*, 136–138.
(11) Chang, C. C. Y.; Davis, J. A.; Kuwabara, J. S. *Estuarine, Coastal, Shelf Sci.* **1987**, *24*, 419–424.
(12) Santschi, P. H. *Limnol. Oceanogr.* **1988**, *33*, 848–866.
(13) Nyfeller, U. P.; Li, Y.-H.; Santschi, P. H. *Geochem. Cosmochim. Acta* **1984**, *48*, 1513–1522.
(14) Yasunaga, T.; Ikeda, T. In *Geochemical Processes at Mineral Surfaces*; Davis, J. A.; Hayes, K. F., Eds.; ACS Symposium Series 323; American Chemical Society: Washington, DC, 1986; Chapter 12.
(15) Hayes, J. A.; Leckie, K. F. In *Geochemical Processes at Mineral Surfaces*; Davis, J. A., Hayes, K. F., Eds.; ACS Symposium Series 323; American Chemical Society: Washington, DC, 1986; Chapter 7.
(16) Avotins, P. V.; Jenne, E. A. *J. Environ. Qual.* **1975**, *4*, 515–519.
(17) Di Toro, D. B.; Mahony, J. D.; Kirchgraber, P. R.; O'Byrne, A. L.; Pasquale, L. R.; Piccirilli, D. C. *Environ. Sci. Technol.* **1986**, *20*, 55–61.
(18) O'Connor, D. J.; Connolly, J. P. *Water Res.* **1980**, *14*, 1517–1521.
(19) Honeyman, B. D.; Balistrieri, L. S.; Murry, J. W. *Deep-Sea Res.* **1988**, *35*, 227–246.
(20) McBride, M. B. *J. Am. Soc. Soil Sci.* **1979**, *43*, 693–698.
(21) Swallow, K. C.; Hume, D. N.; Morel, F. M. M. *Environ. Sci. Technol.* **1980**, *14*, 1326–1331.
(22) Kinniburgh, D. G.; Barker, J. A.; Whitfield, M. *J. Colloid Interface Sci.* **1983**, *95*, 370–384.
(23) Zachara, J. M.; Ainsworth, C. C.; Cowan, C. E.; Resch, C. T. *J. Am. Soc. Soil Sci.* **1989**, *53*, 418–428.
(24) Lion, L. W.; Altman, R. S.; Leckie, J. O. *Environ. Sci. Technol.* **1982**, *16*, 660–666.
(25) Hirsch, D.; Nir, S.; Banin, A. *J. Am. Soc. Soil Sci.* **1989**, *53*, 716–721.
(26) Goldberg, S.; Glaubig, R. A. *J. Am. Soc. Soil Sci.* **1985**, *49*, 779–783.
(27) Farley, K. J.; Dzombak, D. A.; Morel, F. M. M. *J. Colloid Interface Sci.* **1985**, *106*, 226–242.
(28) Parks, G. A.; DeBruyn, P. L. *J. Phys. Chem.* **1962**, *66*, 967–973.
(29) Davis, J. A.; James, R. O.; Leckie, J. O. *J. Colloid Interface Sci.* **1978**, *63*, 480–499.
(30) Davis, J. A.; Leckie, J. O. *J. Colloid Interface Sci.* **1978**, *67*, 90–107.
(31) Chan, D.; Perram, J. W.; White, L. R.; Healey, T. W. *J. Chem. Soc., Faraday Trans. 1* **1975**, *71*, 1046–1057.
(32) Benjamin, M.; Leckie, J. O. *J. Colloid Interface Sci.* **1981**, *79*, 209–221.
(33) Di Toro, D. M. *Chemosphere* **1985**, *14*, 1503–1538.

Received for review May 1, 1990. Revised manuscript received January 22, 1991. Accepted March 19, 1991. This research was supported by the U.S. Environmental Protection Agency under the U.S. Department of Energy (DOE) Contract DE-AC06-76RLO 1830 under a Related Services Agreement, Interagency Agreement DW 89932714-01-0. Pacific Northwest Laboratory is operated for DOE by Battelle Memorial Institute. Although the research described in this article has been funded wholly or in part by the U.S. Environmental Protection Agency (EPA), it has not been subjected to EPA review and therefore does not necessarily reflect the views of EPA and no official endorsement should be inferred.

Environ. Sci. Technol. 1991, 25, 2088–2095

Bacteriophage Adsorption during Transport through Porous Media: Chemical Perturbations and Reversibility

Roger C. Bales,* Stephen R. Hinkle,† Thomas W. Kroeger,‡ and Kristen Stocking§

Department of Hydrology and Water Resources, University of Arizona, Tucson, Arizona 85721

Charles P. Gerba

Department of Microbiology and Immunology, University of Arizona, Tucson, Arizona 85721

■ In a series of seven column experiments, attachment of the bacteriophage PRD-1 and MS-2 to silica beads at pH's 5.0–5.5 was at least partially reversible; however, release of attached phage was slow and breakthrough curves exhibited significant tailing. Rate coefficients for attachment and detachment were on the order of 10^{-4} and 10^{-6}–10^{-4} s^{-1}, respectively. Corresponding time scales were hours for attachment and days for detachment. The sticking efficiency (α) for phage attachment was near 0.01. The rate of phage release was enhanced by raising pH and introducing surface-active chemical species, illustrating the importance of chemical perturbations in promoting biocolloid transport. In a series of batch experiments, MS-2 adsorbed strongly to a hydrophobic surface, octadecyltrichlorosilane-bonded silica, at both pH's 5 and 7. Adsorption to the unbonded silica at pH 5 was linear, but was 2.5 (with Ca^{2+}) to 0.25% (without Ca^{2+}) of that to the bonded surface. Neither MS-2 nor PRD-1 adsorbed to unbonded silica at pH 7. Hydrophobic effects appear to be important for adsorption of even relatively hydrophilic biocolloids.

Introduction

The fate of viruses in groundwater is governed by attachment to immobile substrates, generally referred to as adsorption, and by inactivation (*1*). In a study of over 100 groundwater samples, Yates et al. (*2*) found temperature to be the only measured water characteristic significantly correlated with viral inactivation. Gerba (*3*) cited extensive evidence to the effect that sorbed viruses are generally protected from inactivation relative to free viruses.

Several factors contribute to the adhesion of viruses and other colloids to soil particles, including electrostatic attraction and repulsion, van der Waals forces, covalent–ionic interactions, hydrogen bonding, and hydrophobic effects. Murray and Parks (*4*) showed that free energies for adsorption of poliovirus to a variety of metal oxides corresponded well with potentials predicted by electrostatic theory. Both chemical and electrostatic interactions could be important in observations that divalent cations were more effective than monovalent cations in promoting adsorption of poliovirus to membrane filters (*5*).

Reported virus adsorption and transport experiments have generally not involved well-characterized surfaces, but have focused on specific soils or groundwater media (*6–11*). These results, while quantitative, have failed to give general insight into how chemical properties of the virus, collector, and aqueous solution control attachment and release. In addition, the reversibility of virus adsorption has been studied for only a few cases (*4*). While several mathematical models are available for describing transport of viruses and other colloids in soil and groundwater (*1*), all lack data for validation.

The research described in this paper is part of our ongoing studies of virus attachment and transport in natural waters. Our first objective was to determine the effect of pH on the attachment of MS-2 and PRD-1 to well-characterized silica and hydrophobic surfaces. We chose MS-2, PRD-1, and silica as their surface chemical properties are well-known, offering the potential to determine the factors controlling the degree of adsorption. We examined the importance of Ca^{2+} concentration and temperature in influencing MS-2 adsorption on silica at one pH. A second objective was to demonstrate the reversibility of bacteriophage adsorption and to determine the effect of chemical perturbations on the rates of desorption. Our third objective was to test equilibrium, first-order, and two-site colloid transport models using the quantitative data and parameter estimates developed for the chemical conditions studied.

Materials and Methods

Batch Experiment Procedures. A set of pH 5 and pH 7 batch experiments using silica and surface-modified silica was undertaken to determine the role of pH and hydrophobicity in MS-2 adsorption. Adsorption isotherms were run at 4 °C in order to minimize viral inactivation. A set of pH 5 batch experiments was also done at 24 °C to investigate the effect of temperature under one set of conditions.

Experiments consisted of placing 0.75 g of unbonded or 0.100 g of hydrophobic bonded silica (Min-u-sil 30, PGS, Berkeley Springs, WV) in sterilized 4-mL glass vials with Teflon cap inserts. Phage stock was diluted in buffer to the desired titer and 2-mL aliquots were pipeted into silica-containing vials and silica-free control vials. Vials were hand-mixed and placed on a rotating Labquake Shaker (Labindustries, Berkeley, CA) at 12 rpm. One set of vials was assayed to give starting values. After 60 (unbonded) and 90 (bonded) min, vials were centrifuged at 3500 rpm and 1-mL aliquots of the supernatant removed for assay. Concentrations were corrected for inactivation and isotherms plotted. The pH of each vial was measured following an experiment; samples that varied more than 0.05 pH unit from the set pH were discarded.

Vials, caps, and inserts were autoclaved for 20 min after each experiment and then cleaned by soaking vials and inserts in RBS-35 detergent (Pierce Chemical Co., Rockford, IL) for 24 h followed by rinsing and soaking in distilled water for 2 h. Vials were sterilized by baking for 30 min at 300 °C; caps and inserts were autoclaved for 20 min.

In four sets of experiments, mean phage removals (± sample standard deviation) in sets of vials shaken for 30, 60, and 90 min were 97.7 ± 1.7, 99.3 ± 0.4, and 97.9 ± 1.3%, respectively. As there was no statistically significant difference in adsorption at the three times, subsequent

† Present address: USGS, Water Resources Division, 10615 SE Cherry Blossom Dr., Portland, OR 97216.

‡ Present address: STS Consultants, Ltd., 11425 W. Lake Park Dr., Milwaukee, WI 53224.

§ Present address: Stearns & Wheler, One Remington Park Dr., Cazenovia, NY 13035.

 0013-936X/91/0925-2088$02.50/0

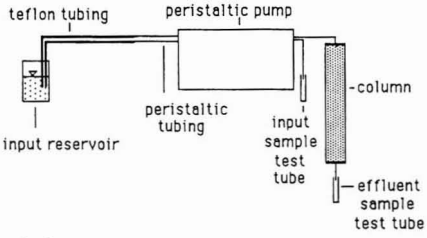

Figure 1. Column experimental setup.

experiments had a contact time of 60 min.

Column Experiment Procedures. Four continuous-flow column experiments were conducted with the bacteriophage PRD-1 at pH's 5.5 and 7.0 and three with MS-2 at pH 5. Experiments were done at 4 °C using a 15 cm × 0.9 cm i.d. precision-bore glass chromatography column (Spectrum Medical Industries, Inc., Los Angeles, CA) packed with 45–90-μm glass beads. Buffers and phage were stored in glass reservoirs and fed through the column by a peristaltic pump (Ismatec, Cole Parmer Instrument Co., Chicago, IL). Column fittings were Teflon, and Teflon tubing was used everywhere in the system except for a length of Tygon tubing in the pump. Phage were pumped through the peristaltic tubing for a minimum of 1 (MS-2) or 18 h (PRD-1) prior to beginning an experiment to reduce subsequent tubing losses. Columns were packed with new beads for each experiment by the tap and fill method (*12*). After columns were flooded from the bottom to remove air, a minimum of 40 pore volumes of the buffer was passed through the column prior to introducing bacteriophage to the column.

In order to take column inlet samples throughout an experiment without disrupting the flow, a parallel feed tubing was set up (Figure 1). Feed-reservoir titers (from 0.9 to 3.9 × 10^5 plaque-forming units (PFU) mL^{-1}) remained constant during an experiment, within analytical uncertainty. Inlet and outlet samples were collected in sterile glass test tubes for 10–20 min and assayed the same day. Desorption solutions were fed to the column with separate, uncontaminated tubing.

Outlet pH's were within 0.06 pH unit of the target values, with the exception of the pH 8 and pH 9 Tween-80 detergent and beef extract eluent phases of experiment 7, when pH's dropped from 8.00 to 7.86, and from 9.00 to 8.81. Few phage were eluted with these solutions, however.

Flow rates, monitored continuously, remained fairly steady; occasional excursions by as much as ±9.5% were quickly reset to target values. Column pore volumes were determined by flooding with 0.01 M NaCl overnight and then introducing a 0.03 M NaCl solution and monitoring outflow conductivity. When outlet conductivity became constant, 0.01 M NaCl was again introduced at the top of the column and conductivity monitored. Pore volumes calculated by conservative tracer breakthrough were greater than those calculated by weighing empty and filled columns by as much as 4.6%. This difference may be due in part to variability in bead specific gravity, reported by the manufacturer to be 2.45–2.50 g cm^{-3}; we used 2.475 g cm^{-3}.

Materials and Chemicals. Sodium phosphate was used to buffer pH, with Ca added as $CaCl_2$. In experiments 1 and 2 (pH 7.0), 0.08 M NaCl was added to raise ionic strength. Stock solutions of beef extract and Tween 80 detergent were made by adding deionized water to beef extract V (Becton Dickinson and Co., Cockeysville, MD) and polyoxyethylene (20) sorbitan monooleate (Tween 80) (J. T. Baker, Inc., Phillipsburg, NJ) to give 1.0 or 2.5% solutions. These solutions were autoclaved for 20 min and cooled to 4 °C, and the buffer was made with Na_2HPO_4.

Tris-buffered saline solution was prepared by dissolving 63.2 g of Trisma base (Sigma Chemical Co., St. Louis, MO), 163.6 g of NaCl, 7.46 g of KCl, and 1.13 g of Na_2HPO_4 in 1600 mL of distilled water. To make experimental Tris solutions, 32 mL of this saline solution was added to 368 mL of distilled water; the mixture autoclaved for 20 min and distributed with a sterile Cornwall pipet in 2.7-mL aliquots into sterile glass test tubes that were then capped with sterile rubber stoppers and stored at 4 °C.

Trypticase soy broth (TSB) host medium was prepared by dissolving 30 g of Tryptic soy broth powder (Gibco Laboratories, Madison, WI; Difco Laboratories, Detroit, MI) in 1 L of distilled water. Aliquots (3 and 100 mL) of TSB were then dispensed into glass test tubes and Erlenmeyer flasks, respectively; these were capped, autoclaved for 20 min, and stored at 4 °C.

Trypticase soy agar (TSA) overlay medium was prepared by dissolving 30 g of TSA powder and 10 g of Bactoagar (Difco Laboratories, Detroit, MI) in 1 L of distilled water. Three-milliliter aliquots were delivered into 14-mL glass test tubes; these were then capped, autoclaved for 20 min, and stored at 4 °C. TSA plates for phage growth and assay were prepared by dissolving 40 g of TSA in 1 L of distilled water, autoclaving the solution for 20 min, cooling it to 50 °C, and dispensing in 10-mL aliquots into sterile, 100 mm × 15 mm plastic Petri dishes. TSA plates were cooled overnight and stored at 4 °C in their original plastic bags.

Bacteriophage and Assays. Bacteriophage MS-2 is an icosahedral phage with a diameter of 26.0–26.6 nm (*13*) and pH_{iep} of 3.9 (*14*). The surface of MS-2 contains hydrophobic and hydrophilic portions (*14*). MS-2 (ATCC 15597 B-1) was obtained from the University of Arizona Department of Microbiology and Immunology culture collection. Bacteriophage PRD-1 is an icosahedral lipid phage with a diameter of 62 nm (*15*). PRD-1 was obtained from JuiCheng Hsieh (Department of Microbiology and Immunology, College of Medicine, University of Arizona, Tucson, AZ).

Coliphage MS-2 was grown and assayed in *Escherichia coli* (ATCC 15597) and PRD-1 in *Salmonella typhimurium* LT2. Both were assayed by the plaque-forming-unit method described by Adams (*16*). Phage stocks were prepared by covering infected host bacterial lawns with 5–10 mL of Tris-buffered saline solution for 2 h at room temperature. The buffer was then poured from the Petri dishes and collected in 250-mL centrifuge bottles. The eluent solutions were centrifuged at 10 000 rpm for 10 min and removed, leaving behind and agar pellet. Bacterial fragments were removed by filtration through a 0.45-μm membrane filter (Millipore Corp., Bedford, MA). The phage solution was then purified by ultracentrifugation for 2 (MS-2) or 1.5 h (PRD-1) at 25 000 rpm. The phage pellet was resuspended in Tris buffer by pipeting action and the concentrated phage removed and diluted to 10 mL with Tris buffer. Phage titers between 10^{11} and 10^{13} pfu mL^{-1} were obtained. For microelectrophoretic experiments, PRD-1 was further purified in a sucrose gradient. Concentrated PRD-1 stock was placed at the top of a set of filter-sterilized sucrose solutions with bands made of 20, 10, and 5% sucrose by weight in deionized water. The gradients were placed in a ultracentrifuge for 105 min at 45 000 rpm, after which the pellet was resuspended in 1 mL of buffer. A titer of approximately 10^{12} pfu mL^{-1} resulted.

Samples to be assayed were sequentially diluted with Tris (or phosphate buffer) to appropriate concentrations,

usually 100–300 pfu mL^{-1}, by pipeting 0.3 mL of diluent into 2.7 mL of Tris (or phosphate buffer) and vortexing the mixture for 5 s. One milliliter of host culture and 0.1 mL of the diluted sample were added to each of two to six overlay media tubes, the solutions vortexed for 5 s, and the contents poured onto TSA plates and allowed to solidify for 15–30 min. The plates were incubated overnight and individual plaques counted with a C-100 automatic plaque counter (New Brunswick Scientific Co., New Brunswick, NJ).

Silica Sorbents. The silica for batch experiments (Min-u-sil 30, PGS) was first washed by placing 60 g of Min-u-sil and 200 mL of 0.1 M NH_4OH in each of four 250-mL Teflon centrifuge bottles. The bottles were shaken for 5 min and centrifuged for 5 min at 5000 rpm. Supernatants were discarded, and the process was repeated with 200 mL of 1.0 M HCl, then with 200 mL of 0.5 M HCl, and finally with eight rinses of deionized water. The final rinse pH was ~5. The silica was then transferred to a glass beaker, covered with a glass watchglass, and oven-dried at 100 °C.

To prepare organosilane-modified silica, 100 g of the cleaned Min-u-sil was suspended in 150 mL of deionized water, 0.125 mL of octadecyltrichlorosilane added, and the resultant solution stirred with an eye-shaped magnetic stir bar for 2 h. The mixture was dried at 110 °C for 24 h, at which time 50 g of the bonded Min-u-sil was washed with 150 mL of pentane. The mixture was centrifuged, the pentane discarded, and the procedure repeated with another pentane rinse, two methanol rinses, two rinses in 1 M HCl, and seven deionized water rinses, at which point the supernatant was at a pH of ~5. The bonded Min-u-sil was oven-dried in a glass beaker. In order to maintain control experimental conditions, unbonded silica used in batch experiments for comparison with the bonded silica was subjected to the same additional rinsing as the bonded silica. All silicas were stored in sterile glass jars with ground-glass or solid PTFE stoppers.

The silicas for column experiments, Spheriglass 2530 beads (Potters Industries, Inc., Hasbrouck Heights, NJ), were washed to remove soluble oxides of calcium and sodium and other impurities from the surfaces. Beads were cleaned by first rinsing with distilled water, with NH_4OH, and then with deionized water until the rinse water pH dropped below 11. Beads were then refluxed in 2 M HCl for 4 h, rinsed in deionized water, and refluxed in fresh 2 M HCl for 2 h more; this second refluxing was repeated a third time with fresh HCl. The beads were next rinsed in deionized water until the rinse water pH rose above pH 4 and then refluxed in deionized water for 1 h. This last step was needed as electrophoretic mobility measured on beads following the acid refluxing was slow to reach a constant value. Last, the beads were rinsed in deionized water and oven-dried overnight at 200 °C.

Surface area, determined by single-point N_2 adsorption on a Model QS-10 Quantasorb Sorption System (Quantachrome Corp., New York), was 2.0 $m^2\ g^{-1}$ for unbonded and 1.7 $m^2\ g^{-1}$ for bonded Min-u-sil and 0.060–0.066 $m^2\ g^{-1}$ for beads.

Bonded and unbonded silica were analyzed for organic carbon by elemental pyrolysis (Desert Analytics, Tucson, AZ). The mass-fraction organic carbon (f_{oc}) for unbonded Min-u-sil was 0.000 04; for bonded silica it was 0.000 18. Assuming a silanol surface site density of 4.6 nm^{-2} (*17*) and the manufacturer's reported size distribution, this corresponds to a surface coverage of 0.065. The mass-fraction organic carbon for both batches of beads was 0.000 02; the instrument error for measurements was ±0.000 05.

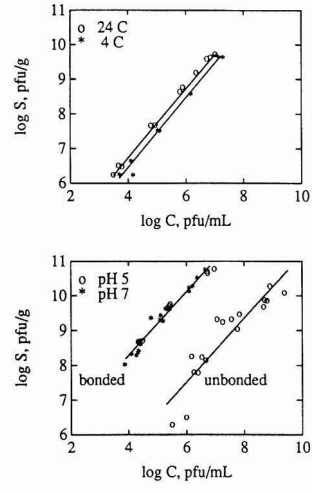

Figure 2. Batch experiment isotherms for MS-2 adsorption in (a, top) calcium phosphate buffer at pH 5 at two temperatures with unbonded silica and (b, bottom) calcium-free phosphate buffer at pH's 5 and 7 at 4 °C with bonded and unbonded silica. Each point is from a single vial and blank.

Electrophoretic mobility was measured using a Rank Brothers (Cambridge, England) Mark II microelectrophoresis apparatus equipped with a flat cell and platinum electrodes. A measurement was made by timing at least five particles at each polarity (constant voltage) at each stationary level. Reported mobility is the average velocity divided by the voltage gradient. The large beads used in experiments settled out of the field of view before measurements could be made. Smaller beads (Spheriglass 2900; ≤53 μm) were washed by the same process as the larger beads and measurements made on the nonsettling fraction. For phage measurements, a cylindrical cell and a He–Ne laser (Scientifica-Cook, Ltd., London, England) were used. Purified PRD-1 was suspended in calcium phosphate buffer (10^{-4} M Ca) to give approximately 1.5 × 10^{10} pfu mL^{-1}.

Results

Batch Experiments. Isotherms for MS-2 adsorption to Min-u-sil in calcium phosphate buffer (Figure 2a) were linear, with the partition coefficient [$(pfu_{sorbed}/g_{sorbent})/(pfu_{water}/mL_{water}) = S/C = K_p$] for the 24 °C isotherm (K_p = 580 $cm^3\ g^{-1}$) twice that for the 4 °C isotherm (K_p = 270 $cm^3\ g^{-1}$). Standard errors were 30 for each. Freundlich isotherm ($C = KS^n$) exponents for the respective experiments were 0.99 and 1.01.

In calcium-free phosphate buffer, MS-2 adsorbed to unbonded Min-u-sil at pH 5 but did not adsorb at pH 7; it adsorbed to bonded Min-u-sil at both pH 5 and pH 7 (Figure 2b). A one-way, completely random analysis of variance (ANOVA) (Costat Statistical Software, CoHort Software, Berkeley, CA) with C as the variate showed the variation between the pH's 5 and 7 bonded silica to be not statistically significant (P = 0.25). MS-2 adsorption to bonded Min-u-sil was 400 times greater than to unbonded Min-u-sil. Fitting a Freundlich isotherm to the bonded and unbonded silica isotherms gave K's of 41 000 and 100, respectively, with r^2 values of 0.97 and 0.84; values of n were 0.92 in each case. Linear isotherm partition coefficients (K_p) were 8300 and 6.6 $cm^3\ g^{-1}$, respectively, with r^2 values of 0.90 and 0.53; respective standard errors were 800 and 0.6.

Table I. Equilibrium Model Fits to Data

exp[a]	u, cm s^{-1}	C_0, pfu mL^{-1}	fitted parameters R^b	fitted parameters P	ssq[c]	K_{pl}, cm^3 g^{-1}	D, cm^2 s^{-1}
			MS-2 Experiments at pH 5.0 and 4 °C				
1 ads	0.0037	2.62×10^4	2.71 ± 0.10	4.51 ± 0.78	0.1571	0.376	0.0127
1 des	0.0037		0.81 ± 0.02	109 ± 47	0.0956		0.00053
2 ads	0.0037	3.49×10^4	1.55 ± 0.06	6.47 ± 1.43	0.1087	0.121	0.0089
2 des	0.0037		0.645 ± 0.016	7.37 ± 1.18	0.0181		0.00778
3 ads	0.0035	1.59×10^4	2.91 ± 0.16	1.79 ± 0.37	0.1101	0.420	0.0295
3 des	0.0035		0.964 ± 0.016	326 ± 202	0.1354		0.00016
			PRD-1 Experiments at pH 7.0 and 4 °C				
4 ads	0.0057	1.05×10^5	1.00 ± 0.02	192 ± 107	0.0650		3.1×10^{-5}
5 ads	0.0039	9.15×10^4	1.02 ± 0.01	221 ± 99	0.0505		2.7×10^{-5}

[a] Adsorption (ads) and desorption (des) parts of breakthrough curves listed separately. [b] Parameter estimate ± standard error. [c] Sum of squared errors.

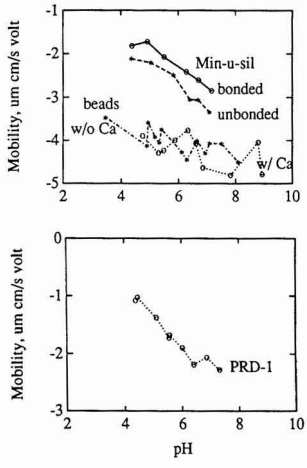

Figure 3. (a, top) Mobility of Min-u-sil as a function of pH in calcium-free phosphate buffer and of silica beads as a function of pH in phosphate buffer, both with 10^{-4} M calcium (O) and without calcium (•). (b, bottom) Mobility of PRD-1 as a function of pH in phosphate buffer with 10^{-4} M calcium.

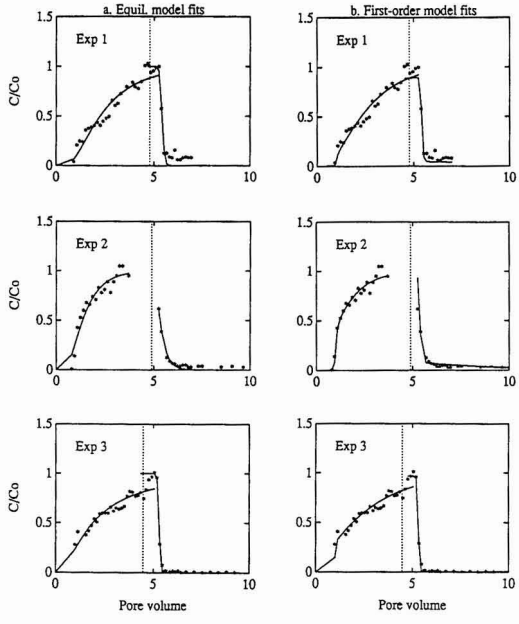

Figure 4. Breakthrough curves for experiments 1–3 with MS-2 at pH 5.0. Experimental conditions are given in Table I. *Pulse* values (number of pore volumes of feed solution containing phage) were 4.6, 4.7, and 4.3 for experiments 1–3, respectively (vertical dotted lines). (a, left) Data with equilibrium model fits; parameters given in Table I. (b, right) First-order model fits; parameters given in Table II. Vertical dotted lines indicate points at which column input conditions were changed.

At pH 5 and 4 °C, adsorption to unbonded silica was on the order of 10-fold or more greater with (Figure 2a) versus without (Figure 2b) Ca^{2+}, suggesting either a charge-neutralization or cation-bridging role for the ion. Both unbonded and bonded Min-u-sil are negatively charged in the pH range studied (Figure 3a), with bonded silica being slightly less negative than unbonded silica.

Column Experiments. Experiments 1–3 (MS-2, pH 5.0) show a slowly rising breakthrough curve to C/C_0 of 1.0 after 4.5–5.0 pore volumes (Figure 4). The jaggedness of the curve is due to the variability of the plaque assay procedure. Replicate assays of a sample differed by an average of 25%. The first phage were detected after 0.9–1.0 pore volume had passed through the column. There was bacteriophage retention in the column, as C/C_0 = 0.5 occurred after 2.2, 1.4, and 2.0 pore volumes in experiments 1–3, respectively. It is thought that the earlier breakthrough of the bacteriophage front in experiment 2 was due to not fully flushing phage from experiment 1 out of the column; new packing was used for each subsequent experiment. All three experiments showed steep declines in C/C_0 ~1 pore volume after the feed was switched to the bacteriophage-free solution. The fractions of bacteriophage recovered in desorption were 0.85 and 0.69 in experiments 1 and 3, respectively; these include perturbations after 10 pore volumes, which were not shown on Figure 4. Slow desorption apparently contributed to the fractions being less than 1.0. Uncertainty in the plaque assay, especially for short-term peaks, could also be a factor. The second MS-2 experiment was carried out without changing column packing, so mass balance was not calculated.

After 20 pore volumes of desorption at pH 5 in experiment 3, C/C_0 dropped below 0.01; switching to a pH 7.0 Ca-free buffer resulted in a small peak of C/C_0 = 0.06 (not shown). After 4 days (158 pore volumes) of desorption in experiment 2 at pH 5.0, changing the buffer pH to 7.0 resulted in an outlet pulse with C/C_0 = 0.14.

PRD-1 did not adsorb at pH 7.0 (experiments 4 and 5, Figure 5 and Table I) for either the 64- (0.0057 cm s^{-1}) or 94-min (0.0037 cm s^{-1}) residence time. PRD-1 adsorbed slowly at pH 5.5 (experiments 6 and 7, Figure 6), but did not reach C/C_0 = 1.0; upon switching to bacteriophage-free

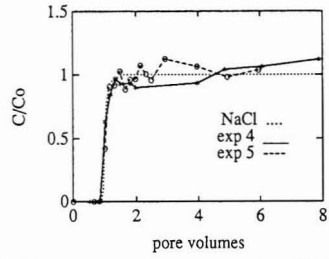

Figure 5. Breakthrough curve for experiments 4 and 5 with PRD-1 and conservative salt tracer; pH 7.0 Experimental conditions are given in Table I.

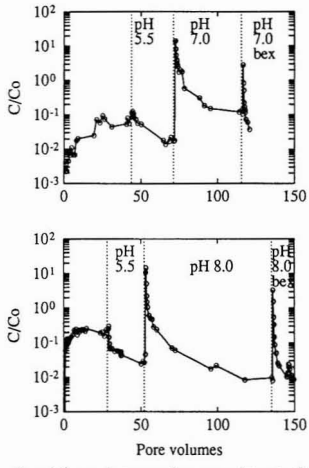

Figure 6. Breakthrough curve for experiments 6 and 7 with PRD-1: (a, top) adsorption at pH 5.5 in phosphate buffer with 10^{-4} M Ca^{2+}, u = 0.0039 cm s^{-1}; $C_0 = 2.15 \times 10^5$ pfu mL^{-1}; (b, bottom) adsorption at pH 5.5 in phosphate buffer with 10^{-6} M Ca^{2+}, u = 0.0039 cm s^{-1}; $C_0 = 3.89 \times 10^5$ pfu mL^{-1}. See text for explanation of desorption sequences, which began after 44 and 28 pore volumes of input *pulse* (number of pore volumes of feed solution containing phage) in experiments 6 and 7, respectively. Vertical dotted lines indicate points at which column input conditions were changed.

buffer the phage slowly desorbed. PRD-1 is negatively charged at pH's 4.5–7.5 in a phosphate buffer in the presence of 10^{-4} M Ca^{2+} (Figure 3b).

In experiment 6, there was little desorption with calcium phosphate buffer at pH 5.5, but a pulse with $C/C_0 = 14$ occurred upon switching to a calcium-free pH 7.0 phosphate eluent. A smaller but significant pulse occurred upon switching to a pH 7.0 calcium-free buffer with 1% beef extract. The beef extract addition provided two chemical changes, a higher ionic strength and introduction of organic, largely protein, molecules. Mass balance calculations indicate that 82% of the sorbed phage was eluted during desorption (including perturbations). The unaccounted-for bacteriophage were apparently either resistant to desorption or were inactivated. Phage were still detaching after 77 pore volumes of desorption.

There was little desorption in experiment 7 with calcium phosphate buffer at pH 5.5 (pore volumes 28–36), or with calcium-free phosphate buffer at pH 5.5 (pore volumes 36–52). A change from pH 5.5 to 8.0 eluent produced a large bacteriophage pulse, suggesting that changes in pH rather than changes in calcium concentration were responsible for the large desorption pulse seen in experiment 3. Only small pulses were observed in subsequent desorption steps with (i) calcium-free buffer at pH 8 with 1.0% Tween 80 detergent (a surfactant) and 2.5% beef extract and (ii) desorption with the same mixture at pH 9. After 135 pore volumes of desorption, 76% of the adsorbed phage was eluted.

Discussion

Interpretation of Chemical Effects. The greater MS-2 adsorption to bonded silica is apparently due largely to hydrophobic factors rather than any surface charge reduction from bonded carbon chains reducing the total number of silanol sites. Note that the difference in surface charge of the bonded silica at pH's 5 and 7 is greater than the difference in surface charge between bonded and unbonded silica at pH 5 (Figure 3a). The greater MS-2 adsorption to unbonded silica at pH 5 versus pH 7 is consistent with electrostatic repulsion being important in that the surface charges of both the colloid and the immobile surfaces are nearer zero at lower pH. Thus MS-2, which is relatively nonadsorbing in sandy soil (*11*), should be retained in soil with an appreciable organic matter content.

Other indications of the importance of surface hydrophobicity come from batch experiments with the bacteriophage ΦX-174 and five different soils in which there was a correlation between adsorption and soil organic carbon content (*18*). Farrah et al. (*19*) observed that at pH 9, antichaotropic salts, which act to increase the structure of water, retarded or prevented elution of poliovirus from membrane filters. Chaotropic salts, which disrupt the structure of water, antagonized the effects of antichaotropic salts at pH 9. At pH 4 neither salt had any effect. It was concluded that electrostatic interactions dominate poliovirus adsorption to membrane filters at pH 4, but that hydrophobic interactions dominate at pH 9. Similar results were also found with bacteriophage MS-2 (*20*).

MS-2 adsorption to unbonded silica is apparently endothermic, and the temperature effect was opposite that expected for ion adsorption. Hydrophobic interactions are more stable at higher temperatures (*21*); if sorption was partially driven by a partitioning of hydrophobic portions of phage onto silica surfaces by exclusion from water, sorption could increase with temperature. We have not observed this behavior for sorption of hydrophobic molecules onto the same bonded surfaces, however (*22*). Zittle (*23*) cited evidence that proteins tend to sorb to a greater extent at higher temperatures than they do at lower temperatures. He noted that the processes of protein unfolding is endothermic and suggested that protein sorption may involve such unfolding on surfaces. If virus adsorption involves the unfolding of surficial protein groups, virus uptake should increase with increases in temperature. In that case, our temperature results would be important for virus and bacteria transport but would not be applicable to abiotic colloids. Different rates of adsorption at 4 and 24 °C could also contribute to the observed temperature dependence. Zittle (*23*) noted that the rate of protein adsorption is faster at higher temperatures. It is possible that experimental variability could have masked nonequilibrium in the time curves, creating a situation in which kinetics resulted in more sorption at 24 °C than at 4 °C. However, that seems unlikely given the small changes at later times and the time scales observed in the column experiments.

Results of the column experiments are also consistent with electrostatic repulsion being important. Strong adsorption at low pH and no adsorption at higher pH is expected where both the colloids and immobile surface have low pH_{iep}'s (isoelectric pH's). The desorption of MS-2 and PRD-1 with an increase in pH is also consistent with the greater repulsion further away from the pH_{iep}. However, the small pulses that followed pH changes suggested

that complete desorption requires significant chemical perturbations.

There was greater MS-2 adsorption to unbonded silica with versus without Ca present; adsorption of PRD-1 was also lower in experiment 7 as compared with 6 (10^{-6} versus 10^{-4} M). Assuming a bead density of 2.5 g cm^{-3} and a mean bead diameter of 2 μm, the surface area of the beads is estimated to be 1.2 m^2 g^{-1}. Assuming a 100 mg L^{-1} suspension and 4.6 silanol groups/nm^2 of silica suggests that the concentration of surface silanol groups was 10^{-6} M. Thus, sufficient Ca^{2+} was present at both 10^{-6} and 10^{-4} M to influence phage adsorption. These are consistent with Mix (*24*), who proposed that cations may act as complexing agents in attachment, forming salt bridges between viruses and surfaces.

Modeling and Kinetic Influences. We fit experimental breakthrough curves to three different one-dimensional advection–dispersion models (equilibrium, first-order kinetic, and two-site kinetic models) in order to estimate the magnitude of adsorption and time scales for reaching equilibrium. Governing equations for the most general model used, one-dimensional transport in a porous media with two types of adsorption sites, one of which is kinetically limited, have been given by various investigators (*25*, *26*):

$$\theta \frac{\partial C}{\partial t} + \phi \frac{\partial S_1}{\partial t} + \phi \frac{\partial S_2}{\partial t} = \theta D \frac{\partial^2 C}{\partial z^2} - u\theta \frac{\partial C}{\partial z} \quad (1)$$

$$S_1 = K_{p1} C \quad (2)$$

$$\phi \frac{\partial S_2}{\partial t} = \theta k_1 C - \phi k_2 S_2 \quad (3)$$

where C is the bacteriophage (or solute) concentration in the aqueous phase; S_1 and S_2 are the bound concentrations for fast and kinetically limited sites, respectively; θ is porosity; ϕ is the dry bulk density of the solid material; D is the longitudinal dispersion coefficient; u is the average interstitial velocity; k_1 is a pseudo-first-order rate coefficient (s^{-1}) for attachment, which depends on the bacteriophage's (solute's) molecular diffusion coefficient and the sticking efficiency (i.e., net energy of interaction between phage and silica); and k_2 is a pseudo-first-order detachment rate coefficient, which also depends on the energy of phage–surface interaction. These rate coefficients do not depend on the surface site concentration, as only a very small fraction of the surface was covered by adsorbed phage. Equation 1 expresses the total change in concentration with time due to advection, dispersion, attachment, and detachment. Equation 2 expresses the linear adsorption equilibrium for the fast (type 1, equilibrium) adsorption sites. K_{p1} and $\theta k_1/\phi k_2$ are the equilibrium partition coefficients for the type 1 and type 2 sites, respectively. Letting $K_{p2} = \theta k_1/\phi k_2$, the overall, total equilibrium partition coefficient for $t \to \infty$ is $K_{p1} + K_{p2}$. Type 1 sites could correspond to colloids held near the surface in a secondary minimum of the potential energy of interaction, with little or no energy barrier for detachment. In eq 3, the change in bacteriophage concentration bound to type 2 sites with time is the difference between the attachment and detachment rates.

It is often useful to express the four model parameters in dimensionless terms. The total partition coefficient, $K_{p1} + K_{p2}$ is related to the retardation factor:

$$R = 1 + \frac{\phi(K_{p1} + K_{p2})}{\theta} = 1 + \frac{\phi K_{p1}}{\theta} + \frac{k_1}{k_2} \quad (4)$$

The Peclet number

$$P = Lu/D \quad (5)$$

indicates the time scale for dispersion divided by the residence time in the system. The dimensionless mass-transfer coefficient is a Damkohler number (*27*, *28*):

$$\omega = \frac{\text{physical time scale}}{\text{chemical time scale}} = \frac{L/u}{1/k_1} = \frac{k_1 L}{u} \quad (6)$$

where L is the length of the column. When $\omega > 100$, local equilibrium applies, and as ω drops below about 0.1–0.5, adsorption is too slow to observe and the solute appears to be conservative. A fourth parameter, β, related to the ratio of equilibrium to total adsorption, can be defined by

$$\beta = \frac{\theta + \phi K_{p1}}{\theta + \phi K_{p1} + \theta k_1/k_2} = 1 - \frac{k_1}{k_2 R} = 1 - \frac{\omega u}{k_2 L R} \quad (7)$$

For no type 1 sites, a three-parameter ($K_{p1} = 0$; $\beta = 1/R$) model (first-order model) can be used. For no type 2 sites ($\beta = 1/R$ and $\omega \geq 100$), a two-parameter equilibrium model results. Parameter values were estimated using the nonlinear-least-squares curve-fitting routine of van Genuchten (*29*), with constant-flux lower boundary condition. Applying the equilibrium model to three NaCl breakthrough curves accompanying experiments 1–3, we found dispersion to be linearly related to pore-water velocity (D of 4.8×10^{-5}, 8.7×10^{-5}, and 18.0×10^{-5} cm^2 s^{-1} for velocities of 0.0014, 0.0030, and 0.0058 cm s^{-1}, respectively):

$$D = 0.0303u + 1.92 \times 10^{-6} \quad (r^2 = 0.99) \quad (8)$$

Fitting the *adsorption* portion of the MS-2 breakthrough curves with the equilibrium model gave good fits (low sum of squared errors) but apparent dispersion values ~150-fold higher than for the salt tracer, indicating nonequilibrium behavior (Table I and Figures 4 and 5). There was adsorption of MS-2 to the glass beads; fitted R's ranged from 1.6 to 2.9. The *desorption* portions of the same three breakthrough curves gave dispersion values nearly the same as for the salt tracer; however, the desorption curve R values were less than 1. The apparent R can be less than 1.0 if there is colloid exclusion from a part of the pore volume, i.e., the pore volume for colloid transport is smaller than the pore volume for salt transport; that is not plausible for our system. These two results—small D and $R \leq 1$—are an artifact of fitting a slow-desorption breakthrough curve with an equilibrium model; they suggest that the time scale for desorption was slower than those for sorption, and for flow through the column. From experiments 4 and 5 (PRD-1), which had no adsorption ($R = 1.0$), D estimated from an equilibrium model fit averaged 2.9×10^{-5} cm s^{-1} for a velocity of 0.0039 cm s^{-1} (Table I and Figure 6). This dispersion value is in the same range as that of the salt tracer; there was apparently no additional dispersion associated with PRD-1 in the absence of adsorption. The fitted Peclet number of 210 for PRD-1 was used for subsequent analysis of experiments 6 and 7. A corresponding Peclet number of 470—based on its smaller size—was used for MS-2 in later analyses to separate the effects of slow adsorption and desorption from dispersion. Bales et al. (*11*) obtained D values of (1.4–1.7) $\times 10^{-2}$ cm^2 s^{-1} in soil column experiments with MS-2 at velocities of 0.01 cm s^{-1}. Using a Peclet number based on the mean grain size for their heterogeneous soils, ~1.5 mm, suggests that dispersion was similar to that observed in our PRD-1 experiments (Figure 7).

Further modeling efforts concentrated on determining a range of values for k_1 and k_2, the attachment and detachment rate coefficients, respectively. Adsorption and desorption portions of the curves were modeled separately

Table II. First-Order and Two-Site Model Fits to Data

exp[a]	fitted parameters[b] R^c	ω^c	β^c	ssq[d]	$K_{p1} + K_{p2}$, $cm^3\ g^{-1}$	k_1, s^{-1}	k_2, s^{-1}	α
			First-Order Model: MS-2 Experiments at pH 5.0 and 4 °C					
1 ads	2.66 ± 0.07	2.16 ± 0.23		0.1270	0.365	5.33×10^{-4}	3.21×10^{-4}	1.1×10^{-2}
1 des		0.160 ± 0.043		0.0928		3.95×10^{-5}	2.38×10^{-5}	8×10^{-4}
2 ads	1.62 ± 0.05	0.871 ± 0.014		0.0547	0.136	2.15×10^{-4}	3.47×10^{-4}	4×10^{-3}
2 des		0.132 ± 0.037		0.1045		3.26×10^{-5}	5.25×10^{-5}	7×10^{-4}
3 ads	2.72 ± 0.09	1.20 ± 0.12		0.1041	0.378	2.80×10^{-4}	1.63×10^{-4}	6×10^{-3}
3 des		0.0348 ± 0.0120		0.0092		8.12×10^{-6}	4.72×10^{-6}	2×10^{-4}
			First-Order Model: PRD-1 Experiments at pH 5.5 and 4 °C					
6 ads	210 ± 42	4.53 ± 0.40		0.0063	46	1.18×10^{-3}	5.64×10^{-6}	1.3×10^{-2}
6 des		2.16 ± 0.40		0.0088		5.62×10^{-4}	2.69×10^{-6}	6×10^{-3}
7 ads	115 ± 22	2.08 ± 0.08		0.0513	26	5.41×10^{-4}	4.74×10^{-6}	6×10^{-3}
7 des		0.11 ± 0.01		0.0027		2.86×10^{-5}	2.51×10^{-7}	3×10^{-4}
			Two-Site Model: PRD-1 Experiments at pH 5.5 and 4 °C					
6 ads	230 ± 51	4.30 ± 0.41	0.0080 ± 0.0039	0.0060	50	11.2×10^{-4}	4.90×10^{-6}	1.3×10^{-1}
6 des		0.82 ± 11.43	0.0028 ± 0.0425	0.0083		2.13×10^{-4}	9.34×10^{-7}	2×10^{-3}
7 ads	118 ± 24	2.07 ± 0.08	0.0089 ± 0.0018	0.0501	26	5.38×10^{-4}	4.60×10^{-6}	6×10^{-3}
7 des		2.34 ± 0.17	0.0050 ± 0.0004	0.0029		6.08×10^{-4}	5.18×10^{-6}	7×10^{-3}

[a] Adsorption (ads) and desorption (des) parts of breakthrough curves listed separately. [b] Peclet number fixed at 210 for PRD-1 and 470 for MS-2. [c] Parameter estimate ± standard error. [d] Sum of squared errors.

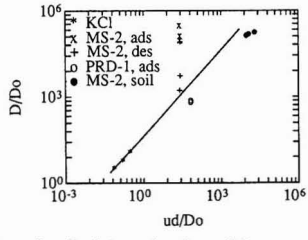

Figure 7. Dispersion Peclet number for salt tracer and virus breakthrough curves; from equilibrium model fits, Table I. D_0 is the molecular diffusion coefficient and d is the bead diameter.

because of poor performance of the fitting algorithm when given both parts of the breakthrough curves to model as a unit, due in part to the lack of complete mass balance. Note that the *adsorption* portion of the breakthrough curve refers to the part during which bacteriophage-containing solution was fed to the column; the *desorption* portion refers to the second part, in which phage-free buffer was fed to the column. The first-order model gave good fits (low sum of squared errors) to the MS-2 breakthrough curves (Figure 4), with R values nearly the same as from the equilibrium model fits (Table II). The low ω values indicate nonequilibrium conditions, with k_1 and k_2 values on the order of (0.3–3.0) × 10^{-4} s. Time scales for equilibration (k_i^{-1}) are thus on the order of several hours.

For the PRD-1 experiments, the unusually high bacteriophage concentrations eluted with the first pore volume of desorption were removed from the data set; it is thought that the high values were caused by jarring of the virus tubing during the changeover from virus-containing tubing to virus-free tubing. The first-order and two-site models provided essentially the same parameter estimates and equally good fits for experiment 6 adsorption and desorption curves (Figure 8), as indicated by the sum of square errors (ssq). The ω values for PRD-1 are in the same range as for MS-2, but the R values are nearly 100-fold higher. Time scales for reaching equilibrium are thus on the order of 1 h for adsorption and several days for desorption. The low β values for the two-site-model fit indicate that bonding to type 1 (fast) sites contributes little to the total adsorption. That is, $K_{p1} \ll K_{p2}$ for both MS-2 and PRD-1.

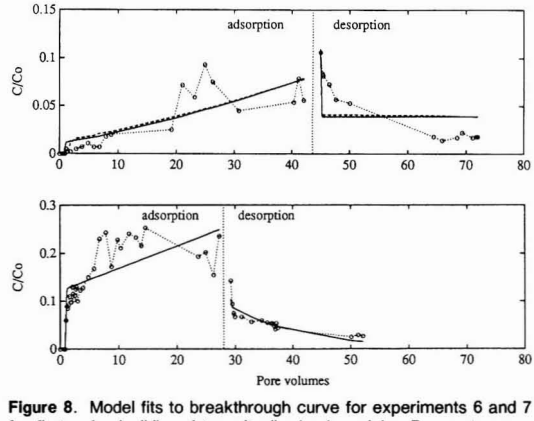

Figure 8. Model fits to breakthrough curve for experiments 6 and 7 for first-order (solid) and two-site (broken) models. Parameters are given in Table II.

Physical and chemical factors influencing the magnitude of k_1 can be described separately following the single-collector model used to describe particle removal in water filtration (*30*). The single-collector removal efficiency, η, is defined as

$$\eta = \frac{\text{rate at which particles strike a collector}}{\text{rate at which particles approach a collector}} \quad (9)$$

and the sticking efficiency, α, is defined as

$$\alpha = \frac{\text{rate at which particles stick to a collector}}{\text{rate at which particles strike a collector}} \quad (10)$$

Particles are removed from a unit volume of fluid at the rate k_1C and thus are removed by (stick to) a single collector at the rate $k_1C(\pi\theta d^3/6(1-\theta))$, where the quantity in parentheses is the volume of fluid associated with a single, spherical collector of diameter d. The rate at which particles approach this volume is $\theta u C(\pi d^2/4)$, giving

$$\eta\alpha = (2/3)(k_1 d/u)[1/(1-\theta)] \quad (11)$$

For the bacteriophage-sized colloids, Brownian diffusion is the primary mechanism for particle transport to the collector, and $\eta = 4Pe^{-2/3}$, where Pe is a Peclet number. Substituting, $\eta = 0.9[\mu d_p d u/\bar{k}T]^{-2/3}$, where μ is fluid viscosity, d_p is the bacteriophage diameter, $\bar{k}$ is the Boltzmann

constant, and T is temperature. α values estimated from first-order-model k_1's from the adsorption portions of the breakthrough curves range from 4×10^{-3} to 1.3×10^{-2}, averaging 7×10^{-3} for MS-2 and 1×10^{-2} for PRD-1. Values from k_1's estimated from the desorption portions of the breakthrough curves were 3–10-fold lower.

The partition coefficients for MS-2 adsorption to Min-u-sil at pH 5.5 and to silica beads at pH 5.0 were ~700-fold different, 270 versus 0.36 $cm^3\ g^{-1}$, which is significantly greater than their 30-fold differences in surface areas. These small, but significant, different densities suggest that adsorption is not site limited. If kinetics control the adsorption density, as indicated by the column experiments, batch experiments that are significantly longer than 1 h are needed. Respective batch and column adsorption densities for $C_0 = 3 \times 10^4$ pfu mL^{-1}, typical of the column experiments, are calculated to be 500 and 17 pfu cm^{-2}. As residence times in the batch and column experiments were similar, differences in the sorbents rather than kinetics were probably responsible for sorption differences. Burge and Enkiri (*18*) reported a partition coefficient of 160 $cm^3\ g^{-1}$ for bacteriophage ΦX-174 sorption to a silt loam (f_{oc} of 0.0238) in batch experiments conducted at pH 6.2; the large partition coefficient may be due in part to the large surface area of the sample, 150 $m^2\ g^{-1}$. The estimated partition coefficient for PRD-1 in our experiments is also large, especially for bacteriophage adsorption to an inorganic surface with a relatively small surface area. This suggests that sorption of PRD-1, a lipid phage, may be largely due to hydrophobic factors.

Conclusions

MS-2 and PRD-1 adsorption in silica bead columns at flow rates of ~0.004 cm s^{-1}—somewhat fast for groundwater velocities—is at least partially reversible, but both adsorption and desorption are kinetically controlled. Thus, one expects nonequilibrium conditions to prevail in some natural systems. The greater adsorbing PRD-1 did not reach equilibrium for the flow rates used. The strong kinetic effect, evidenced in the slow rising limbs and the long tailing limbs of the breakthrough curves, is important because significant errors can result from the application of equilibrium sorption parameters to nonequilibrium situations.

MS-2 adsorption to unbonded silica at pH 5.5 was linear over several orders of magnitude. Neither MS-2 nor PRD-1 adsorbed to silica at pH 7.0, where electrostatic repulsion was important. At pH 5.5, where electrostatic repulsion was less important, PRD-1 adsorption was much greater than for MS-2. Hydrophobic factors are thought to be responsible for this difference; PRD-1's larger size would make the hydrophobic effect greater for it than for MS-2. Hydrophobic factors are thought to be responsible for this difference; PRD-1's larger size would make the hydrophobic effect greater for it than for MS-2. In general, hydrophobic effects are important in adsorption of both MS-2 and PRD-1 to the model surfaces studied and may be orders of magnitude more important than electrostatic forces in soil.

Our results suggest that chemical perturbations such as changes in pH may cause more desorption of colloids than would occur over long periods at constant pH. On the other hand, slow desorption under steady-state conditions could result in long-term release of viruses into groundwater. Observed time scales for desorption—i.e., order of magnitude changes in bound phage—were ~1 day.

Literature Cited

(1) Yates, M. V.; Yates, S. R.; Wagner, J.; Gerba, C. P. *J. Contam. Hydrol.* **1987**, *1*, 329–345.
(2) Yates, M. V.; Gerba, C. P.; Kelley, L. M. *Appl. Environ. Microbiol.* **1985**, *49*, 778–781.
(3) Gerba, C. P. *Adv. Appl. Microbiol.* **1984**, *30*, 133–168.
(4) Murray, J. P.; Parks, G. A. In *Particulates in Water*; Kavanaugh, M. C., Leckie, J. O., Eds.; Advances in Chemistry Series 189; American Chemical Society: Washington, DC, 1980; pp 97–133.
(5) Wallis, C.; Melnick, J. L. *J. Virol.* **1967**, *1*, 472–477.
(6) Duboise, S. M.; Moore, B. E.; Sagik, B. P. *Appl. Environ. Microbiol.* **1976**, *31*, 536–543.
(7) Goyal, S. M.; Gerba, C. P. *Appl. Environ. Microbiol.* **1979**, *38*, 241–247.
(8) Lry, E. F.; Vaughn, J. M.; Penello, W. F. *Appl. Environ. Microbiol.* **1980**, *40*, 1032–1038.
(9) Gerba, C. P.; Goyal, S. M.; Cech, I.; Bogdan, G. F. *Environ. Sci. Technol.* **1981**, *15*, 940–944.
(10) Vaughn, J. M.; Lry, E. F.; Beckman, C. A.; Thomas, M. Z. *Appl. Environ. Microbiol.* **1981**, *41*, 139–147.
(11) Bales, R. C.; Gerba, C. P.; Grondin, G. H.; Jensen, S. L. *Appl. Environ. Microbiol.* **1989**, *55*, 2061–2067.
(12) Snyder, L. R.; Kirkland, J. J. *Introduction to Modern Liquid Chromatography*, 2nd ed.; Wiley: New York, 1979; p 863.
(13) VanDuin, J. In *The Bacteriophages*, 1st ed.; Calendar, R., Ed.; Plenum Press: New York, 1988; Vol. 1, pp 117–167.
(14) Zerda, K. S. Ph.D. Dissertation, Department of Virology and Epidemiology, Baylor College of Medicine, Houston, TX, 1982.
(15) Olsen, R. H.; Siak, J.; Gray, R. *J. Virol.* **1974**, *14*, 689–699.
(16) Adams, M. H. *Bacteriophages*; Interscience Publishers: New York, 1959.
(17) Iler, R. K. *The Chemistry of Silica*; Wiley: New York, 1979; pp 866.
(18) Burge, W. D.; Enkiri, N. K. *J. Environ. Qual.* **1978**, *7*, 73–76.
(19) Farrah, S.; Shah, D. O.; Ingram, L. O. *Proc. Natl. Acad. Sci. U.S.A.* **1981**, *78*, 1229–1232.
(20) Farrah, S. *Appl. Environ. Microbiol.* **1982**, *43*, 659–663.
(21) Kauzmann, W. *Adv. Protein Chem.* **1959**, *14*, 1–63.
(22) Bales, R. C.; Szecsody, J. E. In *Chemical Modeling in Aqueous Systems II*; Melchior, D. C., Bassett, R. L., Eds.; ACS Symposium Series 416; American Chemical Society: Washington, DC, 1990; pp 526–538.
(23) Zittle, C. A. *Adv. Enzymol.* **1953**, *44*, 319–374.
(24) Mix, T. W. *Dev. Ind. Microbiol.* **1974**, *15*, 136–142.
(25) Cameron, D.; Klute, A. *Water Resour. Res.* **1977**, *13*, 183–188.
(26) Rao, P. S. C.; Davidson, J.; Jessup, R.; Selim, H. *J. Soil Sci. Soc. Am.* **1979**, *43*, 22–28.
(27) Valocchi, A. *Water Resour. Res.* **1985**, *21*, 808–820.
(28) Bahr, J.; Rubin, J. *Water Resour. Res.* **1987**, *25*, 438–452.
(29) VanGenuchten, M. Th. Research Report 119, U.S. Salinity Laboratory, Riverside, CA, 1981.
(30) OMelia, C. R. *Environ. Sci. Technol.* **1980**, *14*, 1052–1060.

Received for review April 1, 1991. Revised manuscript received July 8, 1991. Accepted July 11, 1991. This researrch was supported in part by a grant awarded under Section 105 of the Water Resources Research Act of 1984, administered by the U.S. Geological Survey.

CORRESPONDENCE

Comment on "Speciation of Airborne Nickel in Occupational Exposures"

SIR: We agree with Wong and Wu that airborne nickel must be speciated to assess any nickel-related occupational health hazards (*1*). We were also pleased to see data on occupational exposures to nickel appear in the literature. However, we do not think their proposed procedure for determining soluble, metallic, and oxidic nickel is generally applicable to workplaces where nickel is present. We also wish they had provided more information on the operations being carried out and on the nickel species being handled near each sampling site.

Our concern for their speciation method is based on more than 10 years of work to develop, refine, and test a protocol for separating airborne nickel in the workplace into four different groups: soluble, sulfidic, metallic, and oxidic. The protocol, based on sequential selective leaches, was successfully tested on three industrial dusts in an international interlaboratory program (*2*).

First, there can be no argument with using an aqueous leach to determine soluble nickel. However, we believe Wong and Wu should not have used glass fiber filters in connection with this assay. They found decreased concentrations of soluble nickel and increased concentrations of oxidic nickel when using a glass fiber filter compared with using a cellulose ester membrane. They attempted to explain these differences in terms of sampling periods of different length, different pore sizes of the filters, and different size distributions (which were not determined) of the three nickel species. We believe the explanation for their observations is much simpler.

Every glass fiber filter that we have examined has an alkaline surface. We have found as much as 240 μequiv of alkali/g of filter for some makes. This alkalinity can convert some or all of the soluble normal nickel salts collected on the filter into insoluble basic nickel salts. Less nickel dissolves from the basic salts during the subsequent water leach, resulting in an underestimate of soluble nickel. The remaining basic salt dissolves during the hydrochloric acid leach, leading to an overestimate of the oxidic nickel.

To provide experimental support for our belief, we found that Gelman type A/E filters available in our laboratory contained a natural surface alkalinity of 32 μequiv/g. We spiked two such filters with 10 μg of Ni as $NiCl_2$, dried them at ambient temperature, and then leached them in water. We recovered only 65 and 68% of the total nickel. The remainder would report as oxidic nickel. This outcome agrees with results we obtained on other glass fiber filters and report elsewhere (*2*). *Glass fiber filters should not be used when attempting to determine the soluble nickel content of airborne dust.*

Wong and Wu may find this hard to believe in view of the 100% recovery of soluble nickel they reported for the same glass fiber filters in their method validation study (*3*). We can think of three possible explanations for the high recovery: (1) the filter was water leached before the added soluble nickel could react with the filter's surface alkalinity; (2) the soluble nickel was added on top of and absorbed by the additions of nickel-containing silica already on the filter and hence did not contact the filter; (3) commercial standard metal salt solutions such as the one used by Wong and Wu are likely to contain between 2 and 5% free acid as stabilizers. This amount of acid could easily have eliminated the surface alkalinity of the glass fiber filter.

Second, Wong and Wu's method for determining metallic nickel relies on a *physical separation* based on magnetic properties. This approach may have been suitable for the workplace they studied, but in many workplaces, metallic nickel will not exist as discrete, homogeneous particles. For example, oxide fume from high-temperature furnaces often contains a metallic core while metallic dust from reducing operations could well have cores of unreduced oxide. If the oxidic nickel took the form of a magnetic nickel-bearing spinel, it would all report as metallic nickel. Thus, Wong and Wu's method is likely to overestimate the amount of metallic nickel and underestimate the amount of oxidic nickel. Our speciation protocol employs a selective leach for the metallic nickel phase. If that phase is completely encapsulated by an oxidic phase, our method would underestimate the amount of metallic nickel and overestimate the amount of oxidic nickel. However, we do not think this happens very often with dusts fine enough to remain airborne.

Third, we think Wong and Wu have underestimated the refractory nature of oxidic nickel found in many workplaces. Its dissolution in dilute single acids like the 18.5% HCl they used is often incomplete. Sodium peroxide fusion or digestion with fuming perchloric acid are the only ways we know to ensure the complete dissolution of any type of oxidic nickel, including refractory oxides produced at high temperatures.

Since we believe speciation of airborne nickel is essential for meaningful assessment of workplace hazards, we must caution readers of ES&T that the speciation method of Wong and Wu is of limited applicability. One would have to know in advance the microscopic nature of the dust of interest to know whether their method could be relied upon. We believe we have developed a method for speciation that, while not foolproof, is better suited for general application.

Registry No. Ni, 7440-02-0.

Literature Cited

(1) Wong, J. L.; Wu, T.-G. *Environ. Sci. Technol.* **1991**, *25*, 306–309.
(2) Zatka, V. J.; Warner, J. S.; Maskery, D. *Environ. Sci. Technol.*, in press.
(3) Wu, T.-G.; Wong, J. L. *Anal. Chim. Acta* **1990**, *235*, 457–460.

Vladimir J. Zatka, J. Stuart Warner*

Inco Limited
P.O. Box 44 Royal Trust Tower
Toronto-Dominion Centre
Toronto, Ontario, Canada M5K 1N4

 0013-936X/91/0925-2096$02.50/0

SIR: The correspondence by Zatka and Warner referring to our paper (*1*) shows the complexity in the study of occupational exposures to nickel. In the paper, we report findings of speciation of airborne nickel inside a building used for manufacturing specialized nickel products. This paper was not intended to propose a generally applicable procedure for nickel analysis.

Their concern about the alkaline surface of glass fiber filter is based on a special experiment: "We spiked two such filters with 10 μg of Ni as $NiCl_2$ [solution], dried them at ambient temperature, and then leached them in water". They recovered only ~65% of the total nickel due to Ni^{2+} ion reacting with glass alklai at the water–fiber interface. However, this is not the situation with our air sampling, where the Ni^{2+} particulates were trapped by the filter membrane in the solid state, the filter membranes stored in a desiccator, and then the air particulates sonicated into dionized water of pH 5.7. It is only in the last step that the filter membrane contacts water, and at that point the glass alkaline surface is more likely quenched by H^+ in water than by the solid Ni^{2+} particles being drawn into water. We have found no evidence of loss of Ni^{2+} in validating the nickel speciation scheme for our air filter samples. It should be noted that this paper does not advocate using glass filters. We have made a statistical comparison of air sample data obtained from two types of air monitoring systems: one with a glass fiber membrane and the other with a cellulose ester membrane; both are in regular use and approved by OSHA for the nickel manufacturing building. Our observations are consistent with significant heterogeneity in airborne nickel concentrations and nickel species, but further study is necessary to develop the proper air sampling technique for determining nickel exposure profiles.

The second concern is about separation based on the magnetic property of Ni^0. They suggest that (a) this approach may have been suitable for the workplace we studied, (b) the magnetic separation is likely to overestimate the amount of metallic nickel in some workplaces, and (c) their leaching method may underestimate the amount of metallic nickel when it is encapsulated by an oxidic phase. Thus, it is important to interpret the analytical data obtained within the framework of calibration. We have described such calibration in our previous paper dealing with development of the new nickel speciation method (*2*).

The third concern is about our use of 18.5% HCl to dissolve oxidic nickel. They suggest that "sodium peroxide fusion and digestion with fuming perchloric acid are the only ways...to ensure the complete dissolution of any type of oxidic nickel". Below we have compared the nickel determinations of Nickel Oxide on Silica, a manufactured product, digested with the two acids. From 18.5% HCl, six separate experiments gave Ni of 44.2, 44.4, 44.6, 44.9, 44.1, and 44.5%, mean 44.5%, coefficient of variation 0.7%. From 70% $HClO_4$, four determinations of the same nickel product gave Ni of 42.0, 42.9, 42.3, and 42.9%, mean 42.5%, coefficient of variation 1.1%. These results do not support the contention that perchloric acid dissolution is a better method or that we have underestimated the refractory nature of oxidic nickel by using 18.5% HCl. In sample preparations, our experience is that perchloric acid is necessary for digesting hair samples but not for dissolving air samples. The procedure for evaporation of nonvolatile $HClO_4$ is much more tedious (careful heating to avoid spattering) and time consuming (four times longer) than evaporation of the volatile HCl.

Registry No. Ni, 7440-02-0.

Literature Cited

(1) Wong, J. L.; Wu, T.-G. *Environ. Sci. Technol.* **1991**, *25*, 306–309.
(2) Wu, T.-G.; Wong, J. L. *Anal. Chim. Acta* **1990**, *235*, 457–460.

John L. Wong,* Ting-Guo Wu

Department of Chemistry
University of Louisville
Louisville, Kentucky 40292

0013-936X/91/0925-2097$02.50/0

ES&T INDEX

1991
Volume 25, Numbers 1–12

Refer to the list below to determine in which issue an entry appears.

Front Section Index

Front Section Author Index

BR = book review
E = editorial
F = feature
L = letter
P = precis
RF = regulatory focus
S = series
V = view

AUTHOR INDEX TO VOLUME 25, 1991

KEYWORD INDEX TO VOLUME 25, 1991

ENVIRONMENTAL SCIENCE & TECHNOLOGY

ES&T

VOLUME 25, 1991
ESTHAG (1–12) 1–2116
ISSN 0013-936X

The Same Fate Awaits Anyone Who Can't Detect Pesticides Quickly.

Pesticides can kill more than insects, weeds and fungi. They can kill your bottom line. Particularly if your facility takes days or weeks to conduct pesticide tests. EnviroGard™ immunoassay-based test kits provide results in just 7 minutes (1–2 hours for plate kits). Test for aldicarb, benomyl, triazines and 6 other compounds. Results compare favorably with gas chromatography (chart), mass spectrometry and HPLC. But at $20 per test, there's no comparison when it comes to price. Order these easy-to-use kits, or get a video and brochure by calling Millipore at 800-225-1380 (in MA: 617-275-9200). MILLIPORE

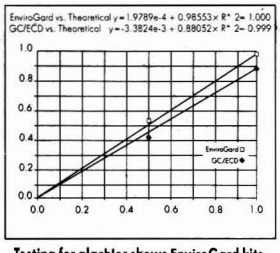

Testing for alachlor shows EnviroGard kits correlate strongly with traditional tests.

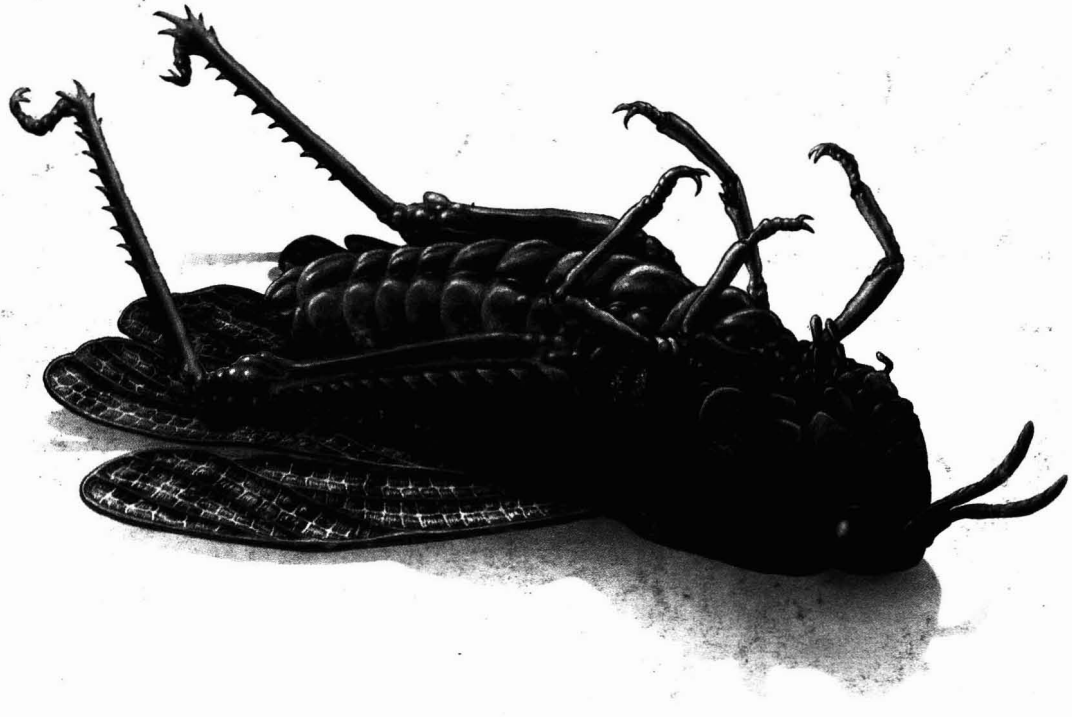

CIRCLE 2 ON READER SERVICE CARD